NASA CR-134482

MDC G4798

STUDY OF THERMODYNAMIC VENT AND SCREEN BAFFLE INTEGRATION FOR ORBITAL STORAGE AND TRANSFER OF LIQUID HYDROGEN

Final Report
August 1973

by E. C. Cady

MCDONNELL DOUGLAS ASTRONAUTICS COMPANY
5301 BOLSA AVENUE
HUNTINGTON BEACH, CALIFORNIA 92647

prepared for

NATIONAL AERONAUTICS AND SPACE ADMINISTRATION

NASA Lewis Research Center
Contract NAS 3-15846

1. Report No.	2. Government Accession No.	3. Recipient's Catalog No.
NASA CR-134482		

4. Title and Subtitle	5. Report Date
STUDY OF THERMODYNAMIC VENT AND SCREEN BAFFLE INTEGRATION FOR ORBITAL STORAGE AND TRANSFER OF LIQUID HYDROGEN	August 1973
	6. Performing Organization Code
7. Author(s)	8. Performing Organization Report No.
E. C. Cady	MDC G-4798
9. Performing Organization Name and Address	10. Work Unit No.
McDonnell Douglas Astronautics Company 5301 Bolsa Avenue Huntington Beach, California 92647	11. Contract or Grant No. NAS 3-15846
12. Sponsoring Agency Name and Address	13. Type of Report and Period Covered
NASA Lewis Research Center Cleveland, Ohio	Final 7/1/72 to 7/31/73
	14. Sponsoring Agency Code

15. Supplementary Notes

Project Manager, John C. Aydelott, NASA Lewis Research Center, Cleveland, Ohio

16. Abstract

A comprehensive analytical and experimental program was performed to determine the feasibility of integrating an internal thermodynamic vent system and a full wall-screen liner for the orbital storage and transfer of liquid hydrogen (LH_2). Ten screens were selected from a comprehensive screen survey. The experimental study determined the screen bubble point, flow-through pressure loss, and pressure loss along rectangular channels lined with screen on one side, for the 10 screens using LH_2 saturated at 34.5 N/cm^2 (50 psia). The correlated experimental data were used in an analysis to determine the optimum system characteristics in terms of minimum weight for 6 tanks ranging from 141.6 m^3 (5,000 ft^3) to 1.416 m^3 (50 ft^3) for orbital storage times of 30 and 300 days.

17. Key Words (Suggested by Author(s))	18. Distribution Statement
LIQUID HYDROGEN PROPELLANT ACQUISITION ORBITAL STORAGE SCREEN CHARACTERISTICS THERMODYNAMIC VENT	

19. Security Classification (of this report)	20. Security Classification (of this page)	21. No. of Pages	22. Price*
Unclassified	Unclassified	206	

*For sale by the National Technical Information Service, Springfield, Virginia 22151

PREFACE

This report was prepared by McDonnell Douglas Astronautics Company under Contract NAS 3-15846. The contract is administered by the National Aeronautics and Space Administration, Lewis Research Center, Cleveland, Ohio. The NASA Project Manager for the contract is Mr. John C. Aydelott. This is the final report on the contract, and it summarizes the technical effort from 1 July 1972 to 31 July 1973. The contributions of J. N. Castle and Dr. J. B. Blackmon of MDAC to this report are gratefully acknowledged.

CONTENTS

FIGURES

TABLES

SYMBOLS

A, B	Experimentally determined constants
a	Screen surface area to unit volume ratio (1/m)
A	Area (m^2)
b	Screen thickness (m)
C	Constant
D	Diameter (m)
e	Roughness dimension (m)
Eu	Euler Number, $\Delta P\, 2g_c/\rho V^2$
f	Friction factor, $\dfrac{H_f\, 2\, g_c}{\frac{L}{D_h} V^2}$, $\dfrac{H\, \epsilon^2\, D\, g_c}{V^2\, Qb}$
g	Acceleration level (g's)
g_c	Gravitational constant (9.806m/sec^2)
h	Heat transfer coefficient (Joule/m^2-sec-°K)
H	Head loss (m)
J	Energy conversion factor, 0.102 kg-m/Joule
K	Thermal conductivity (Joule/m-sec-°K)
L	Length (m)
ℓ	Insulation thickness (m)
n	Rotational Speed - RPM
N	Number of insulation layer-pairs
N_s	Pump specific speed
$\overline{N}$	Layer density (layer-pairs/m)
P	Power (watts)

ΔP	Pressure loss (N/m^2)
$\dot{q}$	Heat flux ($watts/m^2$)
Q	Screen tortuosity factor (1.0 for square weave, 1.3 for Dutch weave)
$\dot{Q}$	Volumetric flowrate (m^3/sec)
r	Radius (m)
R, KR	Outer and inner annulus radii (m)
R	Reynolds number, $\frac{\rho V D_h}{\mu}$, $\frac{\rho V}{\mu a^2 D}$
s	Annulus spacing, channel height, (m)
S	Screen solidity (fraction of closed area)
t	Time (sec)
t, t'	Wall thickness (m)
T	Temperature (°K)
u, v	Flow velocity (m/sec)
V	Fluid approach velocity (m/sec)
w	Channel width (m)
$\dot{W}$	Weight flowrate (kg/sec)
W	Weight (kg)
X	Thickness (m)
α, β	Experimentally determined constants
ϵ	Screen void fraction
η	Efficiency
θ	Spherical angle (radians)
μ_a	Screen absolute micron rating
μ	Viscosity ($N\text{-}sec/m^2$)
ν	Kinematic viscosity (m^2/sec)

ξ	Pump geometry coefficient
ρ	Density (kg/m^3)
σ	Surface tension (Dynes/cm), Stefan-Boltzmann constant
ϕ	Pump flow coefficient, spherical angle (radians)
ϕ'	Constant in equation (1)
ψ	Pump head coefficient
Ω	Pump rotational speed (radians/sec)

Subscripts

a	Annulus
C	Cold
d	Dynamic
eff	Effective
f	Frictional, fluid
F	Foam
g	Hydrostatic
h	Hydraulic
H	Hot
I	Insulation
r	In r-direction
s	Through the screen, standpipe
T	Tank
TUBE	Tube
ϕ	In ϕ -direction
θ	In θ -direction

STUDY OF THERMODYNAMIC VENT AND SCREEN BAFFLE INTEGRATION FOR ORBITAL STORAGE AND TRANSFER OF LIQUID HYDROGEN

By E. C. Cady
McDonnell Douglas Astronautics Company

SUMMARY

A comprehensive analytical and experimental program was performed to determine the feasibility and desirability of integrating an internal thermodynamic vent system (TVS) and a full wall-screen liner (WSL) for the orbital storage and transfer of liquid hydrogen (LH_2). First, the conceptual design of the tankage system was determined, then a comprehensive survey of screens for use in the WSL was performed. Ten screens, spanning a wide range of weaves and retention performance (bubble point), were selected for analytical and experimental study. The experimental study determined the screen bubble point, flow-through pressure loss, and screen roughness-induced pressure loss along rectangular channels lined with screen on one side, for the 10 selected screens, using LH_2 saturated at 34.5 N/cm^2 (50 psia). The screen bubble-point and flow-through pressure loss data agreed well with previously determined data. The channel pressure loss data were unique and were correlated with friction factor and Reynolds number using a roughness parameter based on screen wire diameter.

The experimental data were used in an analysis to determine the flow and performance characteristics of the WSL annulus during low-gravity LH_2 outflow. The TVS pump system was optimized for pumping characteristics and minimum weight. These analyses were combined to determine the optimum integrated system in terms of minimum weight. The optimum system characteristics were determined and system fluid-dynamic feasibility was established for six tanks ranging from 141.6 m^3 (5,000 ft^3) to 1.416 m^3 (50 ft^3) for orbital storage times of 30 and 300 days, and for several TVS and LH_2 transfer flowrates.

INTRODUCTION

Future space systems will require feed systems capable of in-orbit storage, expulsion, and resupply of cryogens in a controllable and predictable manner. Various concepts have been proposed to accomplish in-orbit transfer of fluids using surface tension principles. Some of these concepts have been evaluated to a limited extent. For example, during small-scale experiments conducted on Apollo 14 (ref. 1), a flow model using a relatively simple perforated annular baffle successfully controlled fluid behavior during low-gravity transfer. However, to achieve similar success with liquid hydrogen (LH_2) during orbital storage and transfer, the heat transfer to the stored LH_2 must be controlled.

A number of techniques have been proposed to achieve the required thermal control. One concept uses a dual-screen liner, and is designed to hold the LH_2 off the tank wall to limit the heat transfer (ref. 2). This approach entails complexity in construction and relies on passive, g-dependent thermal control which has not been demonstrated in low gravity. Active systems for thermal control, based on thermodynamic venting phase conversion, have been extensively developed under NASA contracts (refs. 2 and 3). These thermodynamic vent systems use a pump-mixer to obtain fluid-dynamic and heat-transfer processes that are not significantly g-dependent, and have been satisfactorily demonstrated in extensive ground tests.

Proper integration of this proven low-gravity venting and thermal control system with a single-wall screen liner for liquid acquisition could provide a simply constructed, reliable, and proven solution to low-gravity LH_2 storage and outflow. Further, optimization of the thermodynamic vent system and single-wall screen liner configuration and flow characteristics could provide thermal and fluid dynamic control in the LH_2 tank during inflow. Inflow control problems were studied by MDAC during Project THERMO (ref. 4) and were found to be critical for most in-orbit resupply systems.

The overall system concept studied is shown schematically in Figure 1. The system consists of two major components: a single-screen complete wall liner and a pump-driven thermodynamic vent system. The annulus between the screen and the tank wall remains full of LH_2 at all times and serves two functions. First, it provides liquid communication from the outflow line to the bulk LH_2 in the tank, which, although its orientation in the tank is unknown, will certainly be in contact with the tank wall because of the wetting characteristics of LH_2. This communication allows outflow and LH_2 transfer in low gravity. Second, the annulus provides a flow path for pumped LH_2 which will absorb tank incident heating, flow through the standpipe, and reject the absorbed heat to the thermodynamic vent system.

To determine the important characteristics of this integrated thermodynamic vent and screen system, a three-task study was conducted. In Task 1, details of the system configuration were determined, all available screens were surveyed, and pertinent data compiled, and then 10 different screens were selected for use in the next two tasks. In Task 2, important characteristics of the 10 selected screens, such as bubble point, flow-through

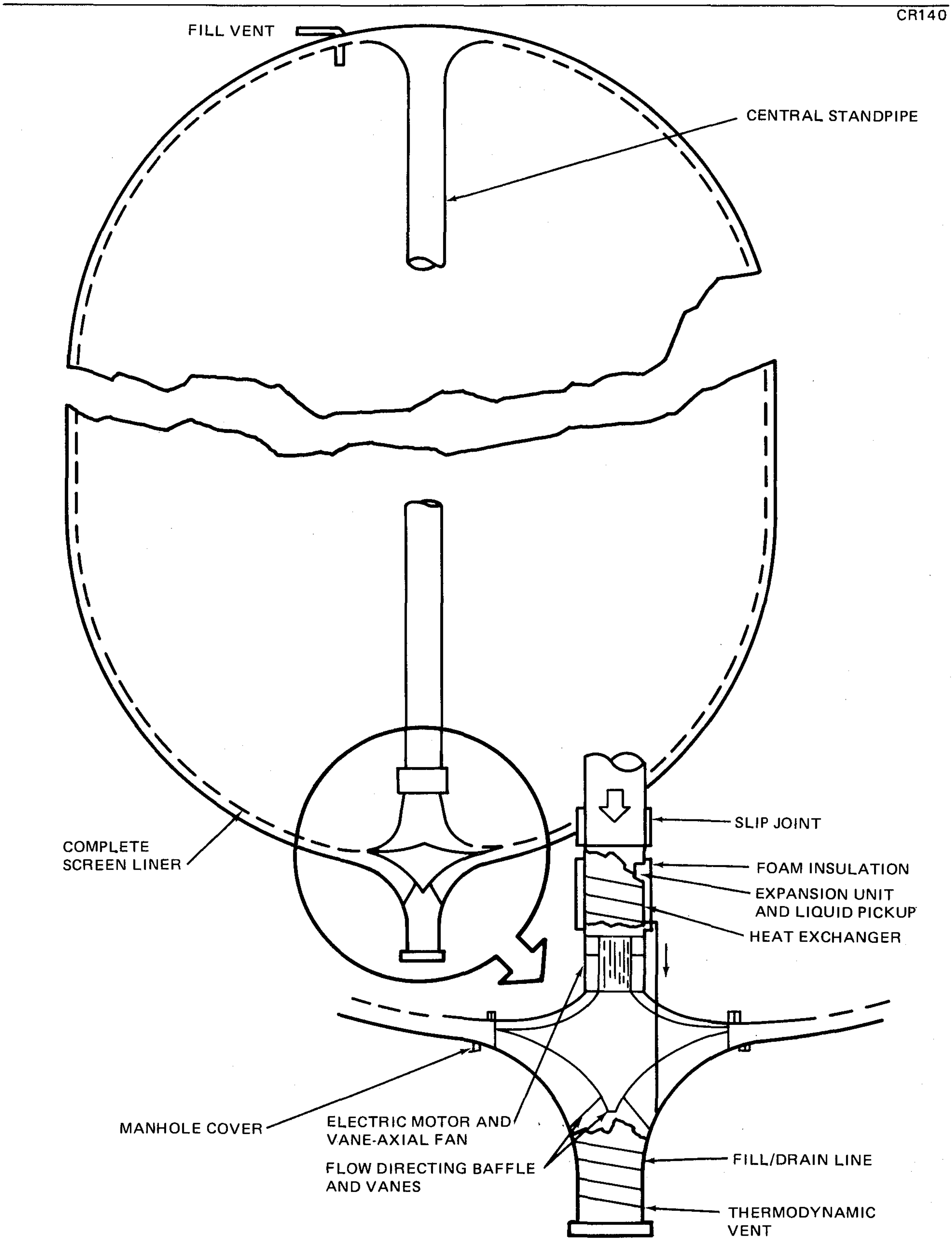

Figure 1. Conceptual Tankage Design

loss, and channel-flow loss were experimentally determined using LH_2 saturated at 34.5 N/cm^2 (50 psia). In Task 3, the Task 2 experimental data were used in a theoretical analysis to determine the optimum system characteristics in terms of minimum weight for storage times of 30 and 300 days in orbit.

CONCEPTUAL DESIGN AND SCREEN SELECTION

Tankage Design Characteristics

Six basic tank sizes and configurations were evaluated throughout the study. The characteristics of these tanks are shown in Table I. The annulus gaps which give residual volumes of 1% to 5% of the tank volume were basic parameters used both in the Task 2 experimental work and in the Task 3 analysis. Referring to Figure 1, details of the system are shown which are common to all of the tanks studied. The thermodynamic vent system (TVS) is mounted on a manhole to allow removal. A slipjoint in the central standpipe facilitates TVS removal and allows use of different materials for the standpipe (the tank and screen liner are assumed to be type 304 stainless steel). Because of the very low head requirements for the TVS pump, an axial flow type of pump, driven by an electric motor was chosen, and shown together with vanes to direct the TVS flow into the annulus gap. Solid baffles are used at each end of the standpipe to direct the TVS flow and the outflow or incoming flow from or into the annulus gap. The TVS vent flow is boiled in a heat exchanger tube bonded to the outside of the standpipe to minimize standpipe pressure drop. The TVS vent flow is used to cool the inflow line, and some of the TVS flow is directed through the inflow baffle to eliminate a hot spot at the inflow line. The detailed operation of the system is described in the section on Analytical Evaluation of the Tankage System.

Screen Survey

The screen used in the wall-screen liner (WSL) will have an important effect on the design of the integrated system. In surveying screen materials for possible application in the WSL, the important characteristics are screen weave, bubble point, and pressure drop for flow through the screen. The bubble point is defined as that pressure, or head, which can be supported by the vapor-liquid interface in the pores of the screen before vapor bubbles break through into the liquid, or "breakdown" occurs. The supported head, H, at a g-level, g, for cryogenic propellants (zero contact angle) has been shown to be:

$$H = \frac{\phi' \sigma}{g \rho D} \tag{1}$$

where $\phi' = 4$ for circular pores of diameter, D, (ref. 5). To properly evaluate equation (1), the fluid properties of surface tension, σ, and density, ρ, must be accurately specified. The latest data on LH_2 surface tension from the National Bureau of Standards (NBS) (ref. 6) indicate a variation with temperature as shown in Figure 2. Accepted data on LH_2 density from the NBS (ref. 7) is shown in Figure 3. Equation (1) is plotted in Figure 4 for 10.1 N/cm^2 (14.7 psia) and 34.5 N/cm^2 (50 psia) saturated LH_2 properties for three specified g-levels, 10^{-1}, 10^{-2}, and 10^{-3} g's. Superimposed on the plot (extrapolated to 0.1 g's for convenience) are LH_2 bubble-point test data

TABLE I. - TANKAGE SYSTEM CHARACTERISTICS

Volume, m^3 (ft^3)	L/D	Dia, m(ft)	Length, m(ft)	Area m^2 (ft^2)	Gap width-cm (in.) for residual of				
					1%	2%	3%	4%	5%
141.6 (5,000)	4	3.66 (12.02)	14.65 (48.06)	168.5 (1,814)	0.84 (0.33)	1.68 (0.66)	2.52 (0.99)	3.35 (1.32)	4.19 (1.65)
14.16 (500)	4	1.70 (5.58)	6.80 (22.31)	36.3 (391)	0.38 (0.15)	0.79 (0.31)	1.17 (0.46)	1.55 (0.61)	1.96 (0.77)
14.16 (500)	2	2.21 (7.25)	4.42 (14.50)	30.8 (331)	0.46 (0.18)	0.92 (0.36)	1.37 (0.54)	1.85 (0.73)	2.31 (0.91)
14.16 (500)	1	3.00 (9.85)	3.00 (9.85)	28.3 (305)	0.51 (0.20)	0.99 (0.39)	1.50 (0.59)	2.01 (0.79)	2.52 (0.99)
1.416 (50)	2	1.03 (3.37)	2.06 (6.74)	6.6 (71.2)	0.213 (0.084)	0.427 (0.168)	0.643 (0.253)	0.856 (0.337)	1.069 (0.421)
1.416 (50)	1	1.39 (4.57)	1.39 (4.57)	6.1 (65.6)	0.231 (0.091)	0.465 (0.183)	0.696 (0.274)	0.930 (0.366)	1.161 (0.457)

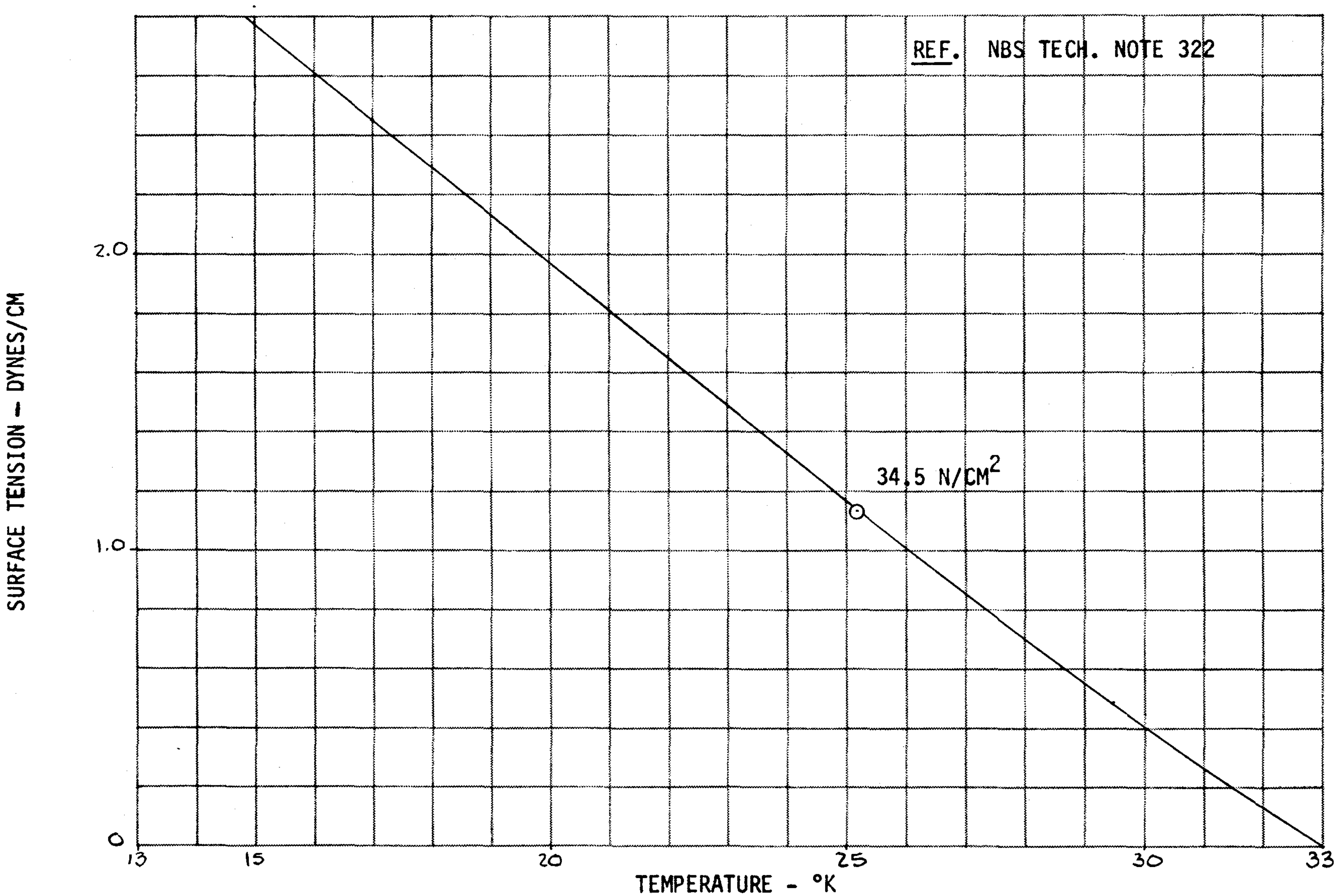

Figure 2. Surface Tension of Para-hydrogen

CR

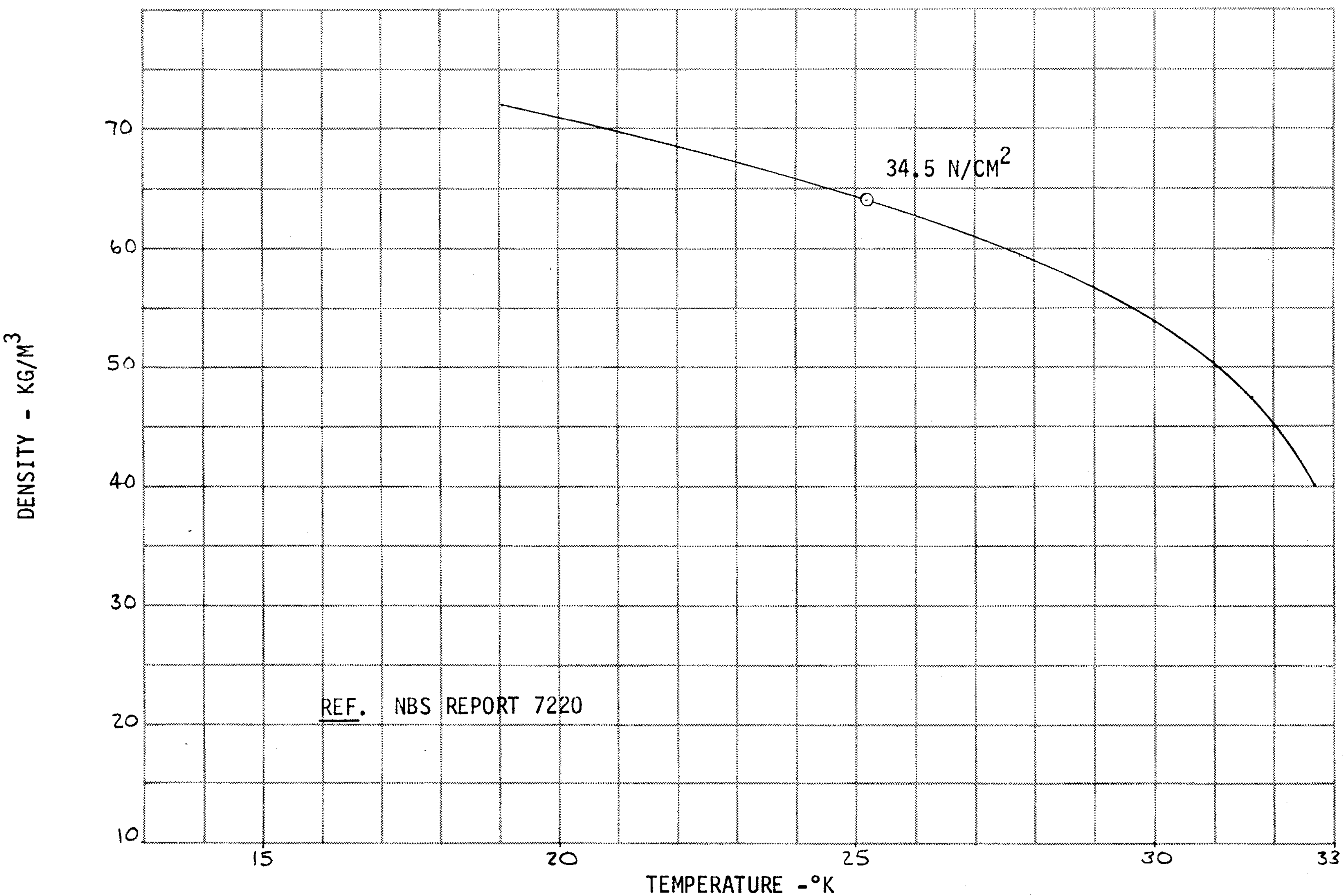

Figure 3. Density of Saturated Liquid Para-hydrogen

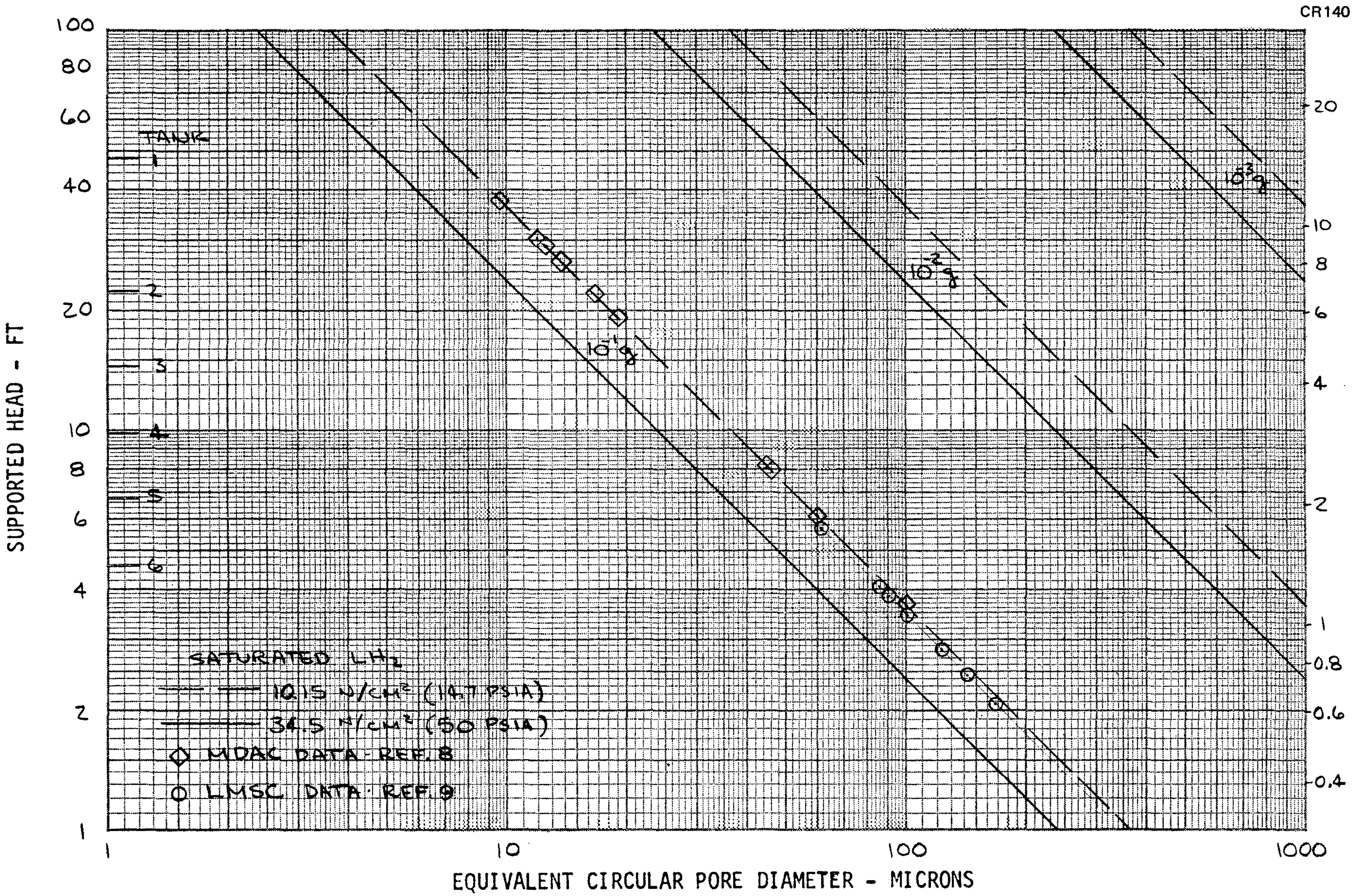

Figure 4. LH_2 Static Head Retention Versus Pore Diameter

(taken in 1 g) of various screens, as summarized in Table II. The only LH_2 bubble-point test data known prior to the experimental work performed in this study were determined by MDAC (ref. 8) and Lockheed Missiles & Space Co. (LMSC) (ref. 9). The equivalent circular pore size, D, in microns which satisfies equation (1) with $\phi' = 4$ and the experimental H is shown in Table II for each screen. Also shown, are the screen manufacturer's absolute micron rating for each screen. For the Dutch weave material, the absolute rating is determined experimentally, usually by filtering a slurry of glass beads; the largest bead passed by the screen determines the absolute rating. For square-weave screens, the absolute rating is determined analytically as the largest inscribed circle in the weave pore.

To determine the anticipated LH_2 retention height from the manufacturers absolute rating (in the absence of bubble point data) for a particular screen, the absolute rating pore diameter was used in equation (1) and ϕ' was determined, based on the experimental LH_2 retention data. The equivalent ϕ' is close to 3 (rather than 4), with a deviation of generally less than 10% (see Table II and Figure 5). Therefore, for fine mesh screens in LH_2, the bubble point can be expressed as

$$H = \frac{3\sigma}{g \rho \mu_a} \tag{2}$$

where μ_a is the absolute rated pore diameter.

The pressure drop for flow through a screen can be described in terms of friction factor, f, and Reynolds number, R, in the manner of Armour and Cannon (ref. 10). The correlation is

$$f = \frac{\alpha}{R} + \beta \tag{3}$$

where $R = \dfrac{\rho V}{\mu a^2 D}$, $f = \dfrac{\Delta P \epsilon^2 D g_c}{Q b \rho V^2}$, α and β are experimentally determined constants (see symbols) and Q is a tortuosity factor (1.0 for square weave screens, 1.3 for Dutch weave screens), while viscosity, μ, and density, ρ are fluid characteristics, and V is the fluid approach velocity to the screen.

For the laminar flow regime, where R is small, β is generally much smaller than α/R and can be ignored, resulting in $f = \frac{\alpha}{R}$; substitution of f and R gives:

$$\frac{\Delta P \epsilon^2 D g_c}{Q b \rho V^2} = \alpha \frac{\mu a^2 D}{\rho V}$$

TABLE II. - SCREEN BUBBLE POINT DATA

Mesh	1-G LH_2 Bubble-Point m (ft)	Source	Experimental equivalent circular pore size, (microns)	Manufacturer's rated absolute pore size, (microns)		ϕ'	Deviation from ϕ' = 3.0, %
450 x 2,750	1.151 (3.775)	MDAC	9.6	7	a, b, c*	2.92	- 2.7
325 x 2,300	0.933 (3.06)	MDAC	12.0	10	a, b, c	3.33	+ 11.0
	0.884 (2.90)	MDAC	12.5			3.20	+ 6.7
325 x 1,900	>.805 (>2.64)	MDAC	13.7	-		-	
250 x 1,370	>.666 (>2.185)	MDAC	16.6	12.5	a, b, c	3.01	+ 0.3
200 x 1,400	0.582 (1.91)	MDAC	19	14	a, c	2.95	- 1.7
				15	b	3.16	+ 5.3
165 x 800	0.25 (0.82)	MDAC	44.5	35	b	3.15	+ 5.0
				37	d	3.32	+ 10.7
200 x 600	0.244 (0.80)	MDAC	46	30	b, d	2.61	- 13.0
				40	e	3.48	+ 16.0
80 x 700	>.247 (>0.81)	MDAC	45	35	b	3.11	+ 3.7
				40	a, c	3.56	+ 18.7
325 x 325	0.186 (0.61)	MDAC	60	45	b	3.0	0
	0.173 (0.566)	LMSC	61.5	50.8	f	3.3	+ 10.0
50 x 250	0.123 (0.405)	LMSC	86	64	f	2.98	- 0.7
	0.112 (0.367)	MDAC	100	65	d	2.60	- 13.3
200 x 200	0.117 (0.384)	LMSC	90	73.6	f	3.27	+ 9.0
	0.104 (0.342)	LMSC	101	73.6	f	2.92	- 2.3
	0.112 (0.367)	MDAC	100	75.0	b	3.0	0
150 x 150	0.0866 (0.284)	LMSC	122	100.4	f	3.3	+ 10.0
30 x 160	0.0750 (0.246)	LMSC	142	100	b, f	2.82	- 6.0
				120	d	3.38	+ 12.7
24 x 110	0.0634 (0.208)	LMSC	168	138	f	3.28	+ 9.3

*a. Kressilk b. Wintec c. Cambridge d. Jelliff e. Capital Westward f. LMSC

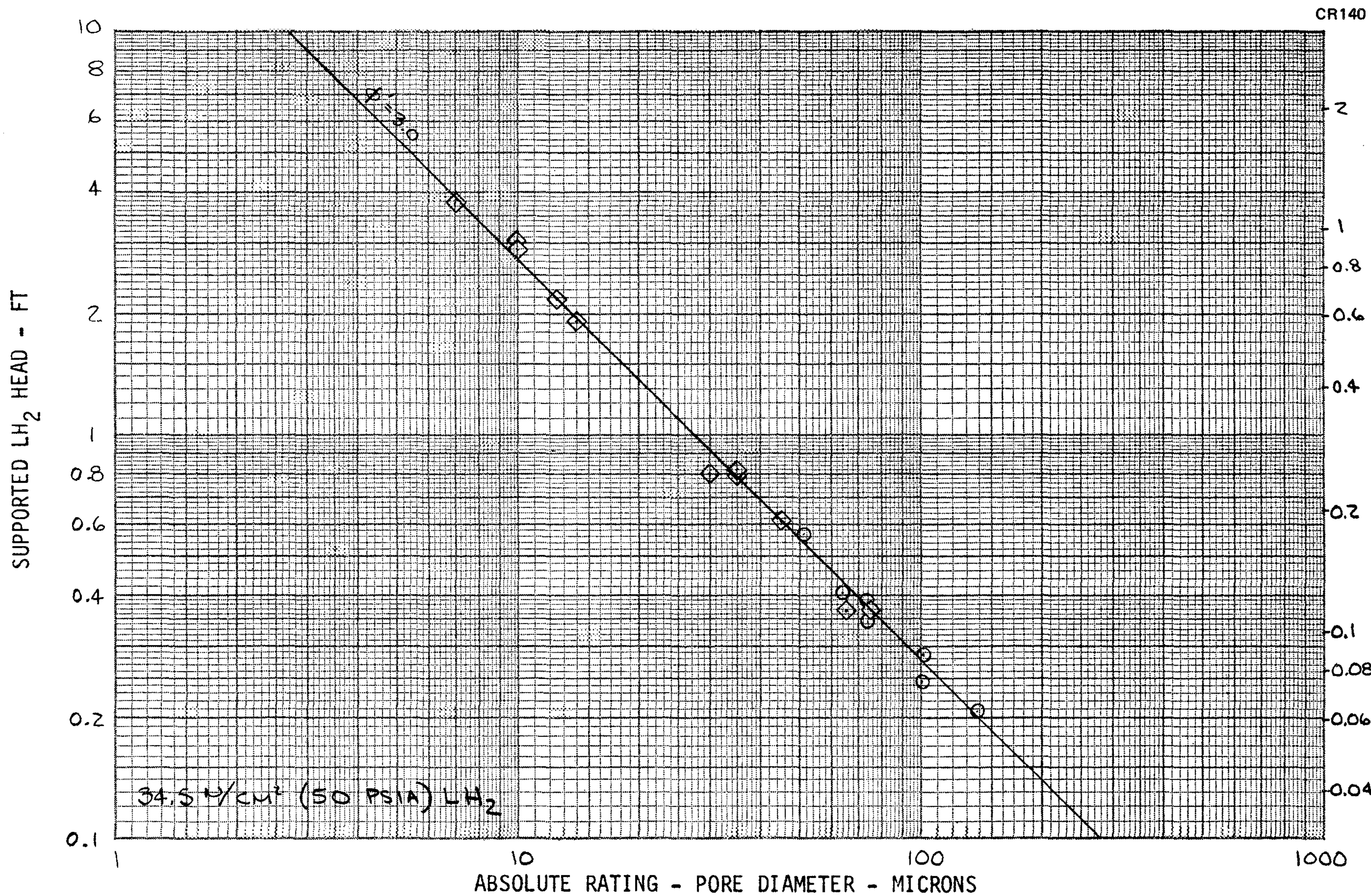

Figure 5. LH_2 Head Versus Rated Pore Diameter for $\phi' = 3.0$

or

$$\Delta P = \alpha \left[\frac{Q\ b\ a^2}{\epsilon^2}\right] \frac{\mu V}{g_c} \tag{4}$$

The term in parentheses is a function of screen configuration, wire size, weave, etc. and is a direct indication of screen flow loss for laminar flow. Similarly, for turbulent flow, with R large, α/R is much smaller than β, and

$$f = \frac{\Delta P\ \epsilon^2\ D\ g_c}{Q\ b\ \rho V^2} = \beta$$

or

$$\Delta P = \beta \left[\frac{Q\ b}{\epsilon^2\ D}\right] \frac{\rho V^2}{g_c} \tag{5}$$

Again, the term in parentheses indicates the magnitude of the pressure loss for turbulent flow.

The screen survey performed determined the important dimensional and geometric qualities of the screens, together with the flow-loss indicators specified by equations (4) and (5). The survey was limited to screen materials with application to aerospace needs, and thus started with 20-mesh ($\sim$1,000 micron pore size) screens. (There are hundreds of meshes coarser than 20 mesh, made by dozens of suppliers, which are not included in the survey.)

It should be noted that screen nomenclature is based on English Engineering units, (e.g. mesh count in wires per inch, wire gage diameters in inches, etc.) and no attempt was made to convert the screen survey or nomenclature to the Systéme International (SI) units because of the likelihood of confusion. Conversion factors for the reader's convenience are included in the results of the screen survey shown in Appendix A. The screens are organized as to weave: square, twilled square, plain Dutch, reverse plain Dutch, and twilled Dutch. Only woven screens are included; sintered or calendered mesh are not shown (see Appendix A for wire-cloth terminology). The principal suppliers of the full spectrum of screens are tabulated (although there are many other suppliers for some of the common screens) and coded in the survey. Most of the screens shown can be made from any metallic material which can be supplied as wire; all the screens shown are available in stainless steel. The weights and costs given are for stainless steel; for other materials, the weights and costs can be found from the supplier. Only representative (and approximate) costs are shown, since the costs do not increase appreciably until the very fine micronic sizes are encountered. For the Dutch weave screens, the manufacturer's rated absolute pore size in microns is shown (if known). The twilled Dutch screens shown on the third page of Appendix A are all the products of the Unique Wire Weaving Co. Inc. and are the only micronic grade of twilled Dutch screens woven in the USA (all others are imported, generally from Germany, Switzerland, or Japan). The wire diameters used for weaving these screens are considered as proprietary information by Unique Wire Weaving, Inc. and, therefore, the geometric data and flow loss parameters are not shown, although the absolute screen ratings, based on alcohol bubble-point tests, are shown. It will be noted that the cost of these screens is two to four times that of similar imported screens.

All of the screens shown in the survey, in stainless steel, are available from stock except the finest twilled Dutch meshes. All are also available, in virtually any material, on special order. The overall screen size, width, and length varies between meshes and manufacturers and should be checked on an individual basis with the supplier.

Screen Selection

Figure 4, shown previously, indicated the range of experimental LH_2-tested pore sizes (bubble points) for screens, together with the largest tank dimension for the six tanks specified (see Table I). To facilitate the Task 3 analysis, a realistic spectrum of pore diameters were chosen.

Two observations are apparent from Figure 4: first, if 0.1 g is the only selection criteria, then the circular pore diameter need not exceed the range of 10μ to 50μ (a span of less than an order-of-magnitude); second, based on previous LH_2 data, there is a data gap from 20μ to 40μ.

To obtain a pore size spectrum that will assure adequate coverage of the conditions of the Task 3 analysis, it was recommended that an acceleration range of 0.1 g to 0.01 g be used as the screen selection criterion - giving a pore size range of 10μ to 500μ. This range allowed selection of different weaves as well as coverage of the complete range of interest for the Task 3 analysis.

Selection of screens in this pore size range which will give the best potential performance makes it necessary to obtain screens with the maximum ratio of bubble-point-to-flow-loss pressure drop for a given bubble point. Since the bubble point varies as $1/\mu_a$ [see equation (2)] and the laminar flow loss varies as $\alpha\left[\frac{Q\ b\ a^2}{\epsilon^2}\right]$, the performance ratio can be computed for each screen, as shown plotted versus $1/\mu_a$ in Figure 6. This figure, together with other selection criteria, such as cost, enabled the selection of the higher performance screens for use in this program. Based solely on Figure 6, the screens selected would have included the following: 450 x 2,750, 325 x 2,300, 850 x 850, 635 x 635, 500 x 500, 165 x 800, 325 x 325, 50 x 250, 150 x 150, and 24 x 110 mesh. However, the 450 x 2,750, 850 x 850, and 635 x 635 screens have many practical problems associated with their use. These screens are very expensive (about $1,400/m^2$) and it is difficult to obtain large areas of screen with consistent performance, i.e., without flaws or bubble point reduction over the entire sheet. The 850 x 850 and 635 x 635 mesh are woven of extremely fine wire and are very flimsy; it is difficult to visualize an actual WSL constructed of

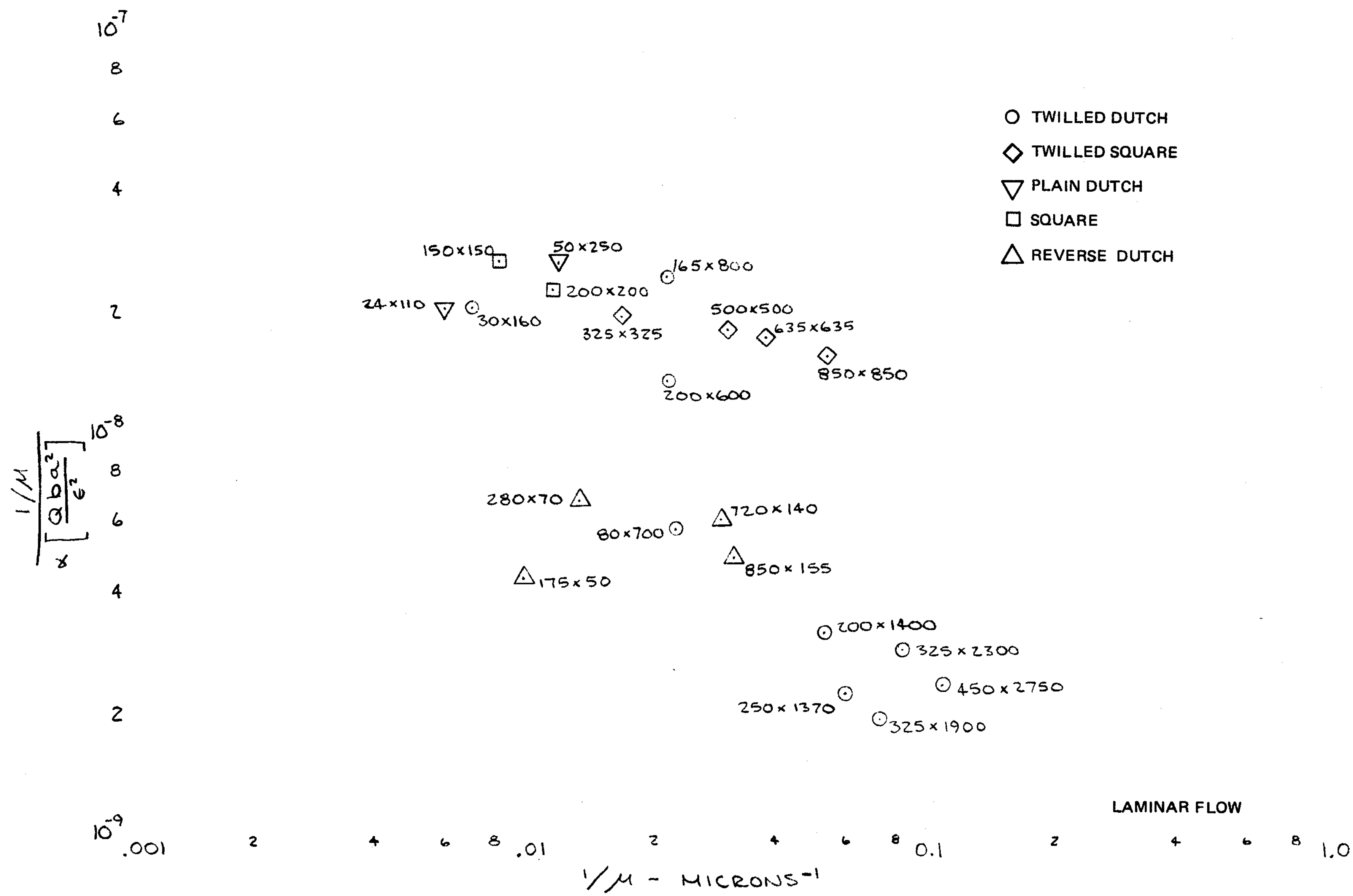

Figure 6. Bubble-Point Flow Loss Ratio Parameter versus Bubble Point

such flimsy material, and capable of tank installation in a reliable fashion. Finally, bubble-point data in LH_2 were not available for the 850 x 850 and 635 x 635 mesh, so that it was not certain that these screens would fill the gap in Figure 4 between 20μ and 40μ.

Therefore the 450 x 2,750, 850 x 850, and 635 x 635 screens were not selected. Rather, the 200 x 1,400 mesh and the 720 x 140 reverse Dutch were used together with the 500 x 500 mesh. This gave two distinctly different weaves with about the same bubble point for Task 2 evaluation. The final screen selection to cover the entire range from 10μ to 500μ with samples of every type of weave and in a cost-effective fashion is shown in Table III.

TABLE III. - FINAL SELECTION OF SCREENS

Mesh	Wire diameter, in.	Weave	Experimental circular pore size, microns	Source	Approximate cost $/m^2$
325 x 2,300	0.0015/0.001	Twilled Dutch	12	TET/Kressilk	405
200 x 1,400	0.0028/0.0016	Twilled Dutch	19	Gerard Daniel	161
500 x 500	0.001	Twilled Square	34[a]	TET/Kressilk	389
720 x 140	0.0014/0.0043	Reverse Dutch	35.1	TET/Kressilk	116
165 x 800	0.0029/0.002	Twilled Dutch	44.5	Gerard Daniel	129
50 x 250	0.0055/0.0045	Plain Dutch	86	Gerard Daniel	55
150 x 150	0.0026	Square	138	Jelliff	55
24 x 110	0.015/0.0105	Plain Dutch	168	TET/Kressilk	40
60 x 60	0.0075	Square	310[a]	Jelliff	35
40 x 40	0.01	Square	510[a]	Jelliff	31

[a]Estimated

DETERMINATION OF SCREEN CHARACTERISTICS

Bubble-Point Determination

Screen samples were procured from the sources of the selected screens shown in Table III. The samples ranged from 0.3 m to 0.46 m by 1.22 m (12 to 18 in. by 48 in.) with the shute wires in the long direction. All experimental test specimens were fabricated from the single sample of each screen. The bubble-point specimens were 3-cm circles and the flow-through specimens were 6.5-cm circles cut from the same general area of the screen sample.

The bubble-point and flow-through specimens only were cleaned, using cleaning procedures developed especially for this study after consultation with Wintec, Inc., a leading firm in the fields of filter fabrication, cleaning of filter materials, and handling of fine-mesh screens. It was determined that the polyurethane adhesive which would be used to fasten the bubble-point specimen to the holding fixture was not compatible with long-term exposure to trichloroethylene, detergent, water, or isopropyl alcohol. MDAC experience showed no problems with the adhesive during short term isopropyl alcohol bubble-point tests. However, it was decided to limit the screen cleaning material to Freon PCA with which the polyurethane adhesive is compatible.

It was determined that the adhesive was unaffected by sonic cleaning in Freon PCA, and that there was no requirement for a particle count following cleaning for the bubble-point specimens. Since the flow-through specimens are oriented to the LH_2 flow with the finest screen upstream, particle counts served no purpose because particles can go through the coarser downstream screens. The final NASA-approved screen cleaning procedure is shown in Table IV. The screen bubble-point specimens were precleaned in nitric acid (step 1 in Table IV), bonded to the specimen holders with EC3901 primer (3M Company) and Sta-Bond U-135 polyurethane adhesive per the bonding procedures of (Appendix A, ref. 11), then air-cured for 24 hours, and followed by an oven-cure at 71°C (160°F) for 24 hours. The specimens were bubble-point checked using ACS Reagent Grade isopropyl alcohol and helium, and then cleaned per the remaining steps of the procedure of Table IV. The bubble-point specimens (stainless steel elbows with the screen samples bonded to them) were arranged as shown in Figure 7 and suspended within a 0.17-m^3 (45-gallon) LH_2 Dewar. The 10 samples were mounted so that they were visible through windows at the bottom of the Dewar.

An LH_2-level scale, indexed to the center of the bottom row of samples, was used to provide LH_2 head corrections to the individual bubble points, depending on where breakdown occurred. A 1389-Ω (ice point) platinum resistance temperature sensor was used to obtain the proper LH_2 temperature of 25.2°K (45.4°R), corresponding to saturation at 34.5 N/cm^2 (50 psia), in the vicinity of the samples. Dewar pressure control maintained the proper saturation conditions. Pressurization of the bubble-point specimens with gaseous hydrogen was accomplished through individual needle valves in the pressurization manifold.

TABLE IV. - SCREEN CLEANING PROCEDURE

NOTE: All liquids and gases to be filtered through 0.45 micron membrane filter.

1. Soak test item in pure nitric acid for 10 minutes minimum.

2. Soak test item in Freon PCA for 15 minutes minimum.

3. Drain Freon and immerse test item in a beaker of fresh Freon PCA and expose to an ultrasonic field of 16 to 20 Hz and a minimum intensity of 0.5 watts per square cm of tank bottom of a period of 3 to 4 minutes.

4. Rinse with Freon PCA for 1/2 to 1 minute.

5. Repeat steps 3 and 4.

6. Purge dry with 0.45 micron filtered GN_2.

7. Package in clean Nylon 6 film.

8. Overbag in 6 mil polyethylene.

Installation of the Dewar into the LH_2 facility is shown in Figure 8. The Dewar was filled to about 0.1 m (4 in.) above the screen specimens (see Figure 7) and allowed to saturate at 34.5 N/cm^2 (50 psia). The LH_2 temperature in the vicinity of the screen samples was controlled to 25.2 ± 0.03°K (45.4 ± 0.05°R) by controlling the Dewar pressure. The LH_2 was allowed to boil down to about 1/2 cm above the top row of screen specimens to minimize head effects on bubble point. The appropriate valve in the pressurization manifold was opened, and GH_2 was slowly bled to the sample through the GH_2 metering valve. The gas pressure behind the sample was slowly increased and monitored by a Merriam 150-mm manometer and a precision hook gauge (Microtector) until bubbles appeared, as viewed through the viewports. The LH_2 level and the point of bubble emergence on the sample were recorded.

The primary bubble-point pressure measurements were made with the Microtector, which after several trials, gave repeatable results within less than 0.025-mm H_2O. The 150-mm manometer reading was also recorded, as a backup, and agreed with the Microtector value within less than 0.5-mm H_2O. Following the LH_2 bubble-point tests, the screen samples were again bubble-point checked with ACS Reagent Grade isopropyl alcohol. The surface tension of the alcohol used for the bubble-point tests was measured with a DeNuoy tensiometer. The average of several trials gave a value of 23.8 dynes/cm at 22.2°C (72°F), which is somewhat in excess of the standard value. It is possible that water absorption by the rather hygroscopic alcohol caused the surface tension increase. The alcohol and LH_2 bubble-point data (corrected for head effect) are summarized in Table V. The alcohol data are shown corrected to the standard isopropanol surface tension value of 21.15 dynes/cm at 25°C (77°F), and also expressed in meters of 34.5 N/cm^2 (feet of 50 psia) LH_2, using the properties given in Reference 6.

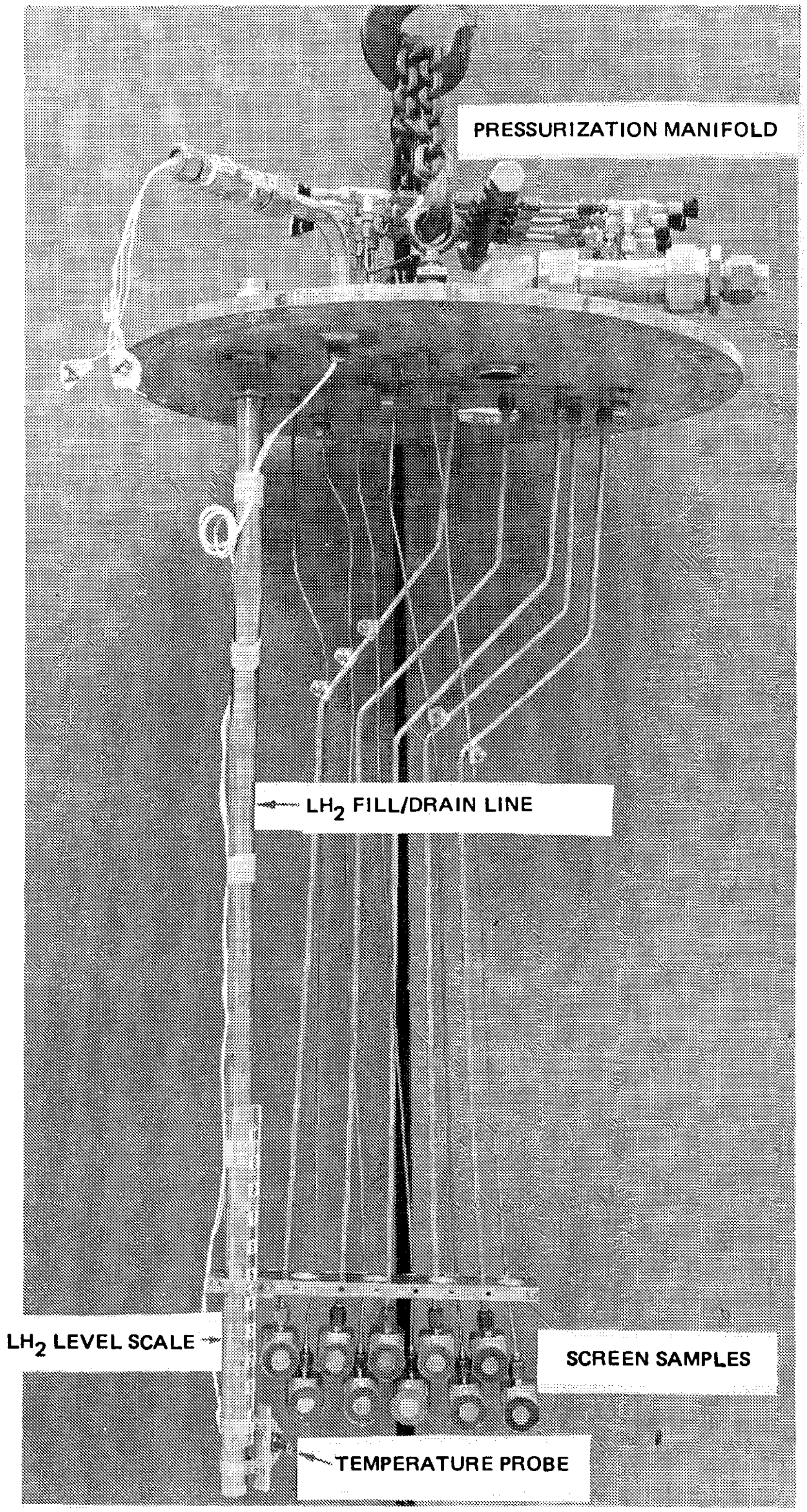

Figure 7. Bubble Point Test Apparatus

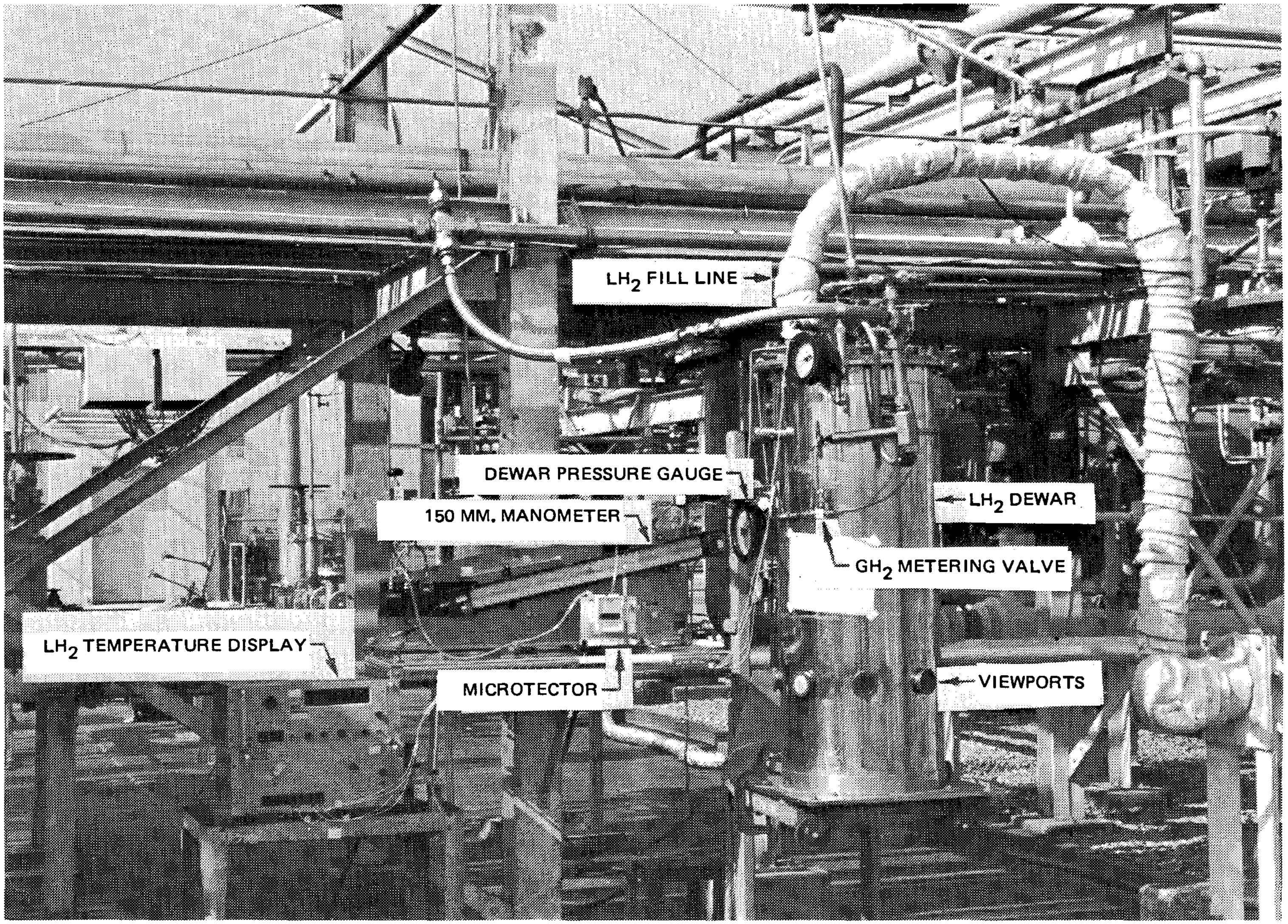

Figure 8. LH_2 Bubble Point Test Setup

TABLE V. - ALCOHOL AND 34.5 N/cm^2 (50 psia) LH_2 BUBBLE-POINT TEST DATA

Screen (wire dia)	Pre LH_2 test alcohol data		Post LH_2 test alcohol data		LH_2 data	D	ϕ'
	Measured bubble point in inches H_2O (standard)	Predicted bubble point in meters of 34.5 N/cm^2 (feet of 50 psia) LH_2	Measured bubble point in inches H_2O (standard)	Predicted bubble point in meters of 34.5 N/cm^2 (feet of 50 psia) LH_2	Bubble point in meters of 34.5 N/cm^2 (feet of 50 psia) LH_2	Manufacturer's Rated Absolute pore size (microns)	
325 x 2,300 (0.0015/0.001)	23.90	0.5090 (1.670)	21.60	0.4602 (1.510)	0.4815 (1.580)	10	2.66
200 x 1,400 (0.0028/0.0016)	16.55	0.3523 (1.156)	16.51	0.3517 (1.154)	0.3377 (1.108)	14	2.60
500 x 500 (0.001)	7.73	0.1646 (0.540)	7.75	0.1652 (0.542)	(0.1704)[a] 0.146[b] ((0.559)[a] 0.479[b])	25.4	(2.39)[a] 2.05[b]
720 x 140 (0.0014/0.0043)	7.82	0.1664 (0.546)	7.82	0.1664 (0.546)	0.1767 (0.580)	26	2.53
165 x 800 (0.0029/0.0020)	6.70	0.1426 (0.468)	6.75	0.1436 (0.471)	0.1228 (0.403)	36	2.44
50 x 250 (0.0055/0.0045)	3.45	0.07346 (0.241)	3.38	0.0719 (0.236)	0.0682 (0.224)	65	2.45
150 x 150 (0.0026)	2.25	0.0480 (0.1575)	2.26	0.04816 (0.1580)	0.0460 (0.1510)	103	2.62
24 x 110 (0.015/0.0105)	1.685	0.0359 (0.1178)	1.695	0.03612 (0.1185)	0.0336 (0.1105)	155	2.88
60 x 60 (0.0075)	0.998	0.02121 (0.0696)	0.996	0.02118 (0.0695)	0.0230 (0.0754)	233	2.95
40 x 40 (0.010)	0.620	0.01323 (0.0434)	0.625	0.01332 (0.0437)	0.0170 (0.0559)	381	3.58

[a] General breakdown

[b] Single wire breakdown

The actual LH_2 bubble-point data are compared to the predicted value based on the alcohol data in Figure 9, and to the absolute screen pore size rating in Figure 10. From Figure 9, the only sample that showed a difference in the pre-LH_2 test and post-test alcohol data was the 325 x 2, 300 screen, and this unexplained difference was less than 10%.

The 500 x 500 twilled square screen exhibited anomalous behavior in the LH_2 bubble-point tests. Bubble retention failure occurred at a lower value than expected, and was confined to a single horizontal wire location, which would be easily seen with the naked eye. This single wire location was not the failure point in either the pre- or post-test alcohol bubble-point check, where failure occurred about 1 cm above the horizontal wire location (which could still be seen, but was not a failure point until general screen breakdown was induced). During the LH_2 tests, general screen breakdown occurred at a value closer to that predicted (see Table V). The reason for this anomaly may be that the 500 x 500 screen is extremely flimsy, and cryogenic contraction may have somehow caused the wire location to open.

The 40 x 40 square weave screen also showed anomalous behavior in the LH_2 tests by exhibiting a much higher bubble point than predicted from the alcohol data. As can be seen from Table V, this screen has a very small bubble-point value in LH_2, and thus the effects of all sources of error (such as instrument zero shift, head contribution, etc.) are magnified, even though great care was taken to acquire accurate data.

Many careful repetitions of the bubble-point measurements, with instrument zero rechecks between them, were made with the 40 x 40 screen, with the same unexplained result. It was thought that the vertical orientation of the screen might have influenced the bubble-point value, so during the post-test alcohol checks, the 40 x 40 screen and the 60 x 60 screen were also alcohol tested in a horizontal orientation facing upwards. The bubble-points in both orientations were virtually identical, and in fact the horizontal orientation had a higher bubble-point by about 5% for both screens. (This can perhaps be explained by gas interface distortion due to buoyancy just before bubble-through which would tend to decrease the bubble point in the vertical orientation.)

The superior bubble-point performance of the 40 x 40 screen is also evident in Figure 10, compared to the other screens. The line in Figure 10 is for a $\phi' = 2.6$ in the bubble-point equation (1).

$$H = \frac{\phi' \sigma}{g \rho D}$$

where D is the manufacturer's rated absolute pore size (inscribed circle of the largest pore in the screen). The value of ϕ' is 4.0 for circular pores, however, in general, the value of ϕ' is degraded for Dutch twill and square weave screens which have triangular and square pores, respectively. In previous bubble-point work with saturated LH_2 at 10.1 N/cm^2 (14.7 psia) Table II), ϕ' was found to be more nearly equal to 3.0, while for our tests the value of ϕ' is 13% lower. It is perhaps coincidental that the heat of vaporization at 34.5 N/cm^2 (50 psia) is 10% lower than that at 10.1 N/cm^2 (14.7 psia),

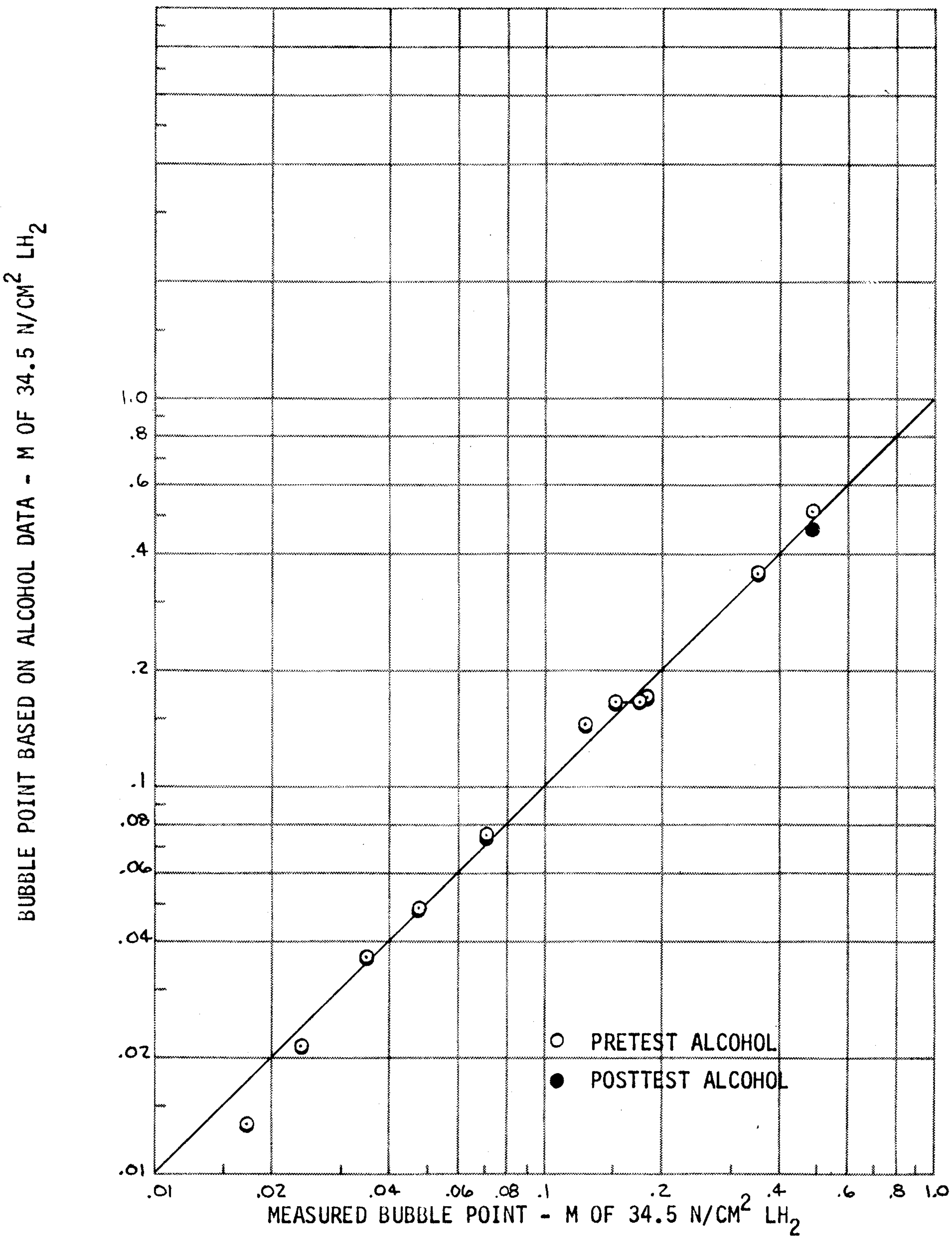

Figure 9. Comparison of Alcohol Extrapolation and Measured LH_2 Bubble Point

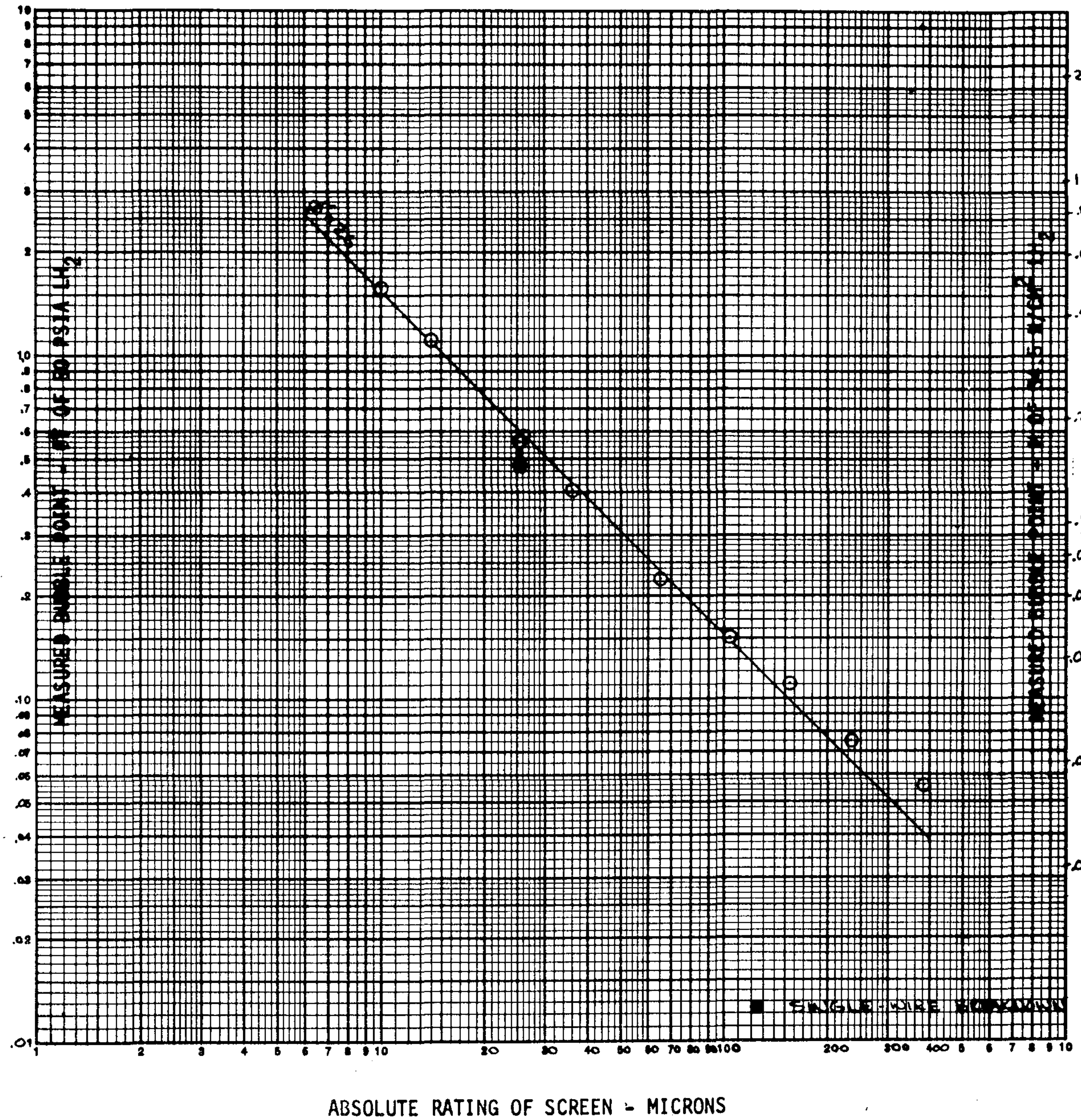

Figure 10. LH_2 Bubble Point Versus Absolute Screen Rating

but heat transfer to saturated liquids may have a noticeable effect on bubble point. It was noticed during bubble-point testing that lights, directed through the viewports onto the screens, caused fine bubbles to emanate from the screens, especially the fine meshes. Therefore, all bubble-point observations were made with rather dim available light which fortunately was adequate for viewing. From Figure 10, all of the screens follow the ϕ' line rather well, except for the three coarsest screens, which gave higher performance and ϕ' values closer to 3.0 (see Table V). It may be significant that the wires which make up the three coarsest screens have cross-sectional (heat conduction) areas at least nine times that of the finer screens. This, combined with fewer wire joint or pore nucleation sources, may contribute to reducing the effects of heat transfer, if any, resulting in increased performance. In any event, it would be accurate or conservative to use the ϕ' value of 2.6 in the bubble-point equation for a functional description of bubble-point, based on the manufacturer's absolute rating for screens in 34.5 N/cm^2 (50 psia) saturated LH_2.

Flow Test Apparatus Design and Fabrication

To characterize the screen flow-through loss and channel flow loss parameters, all 10 screens had to be tested at several flow-through rates and, for the channel flow loss tests, at several flowrates and channel spacings. This required obtaining literally hundreds of data points and design of a test apparatus to efficiently determine these data accurately but with minimum apparatus modifications represented a significant challenge. A schematic representation of the apparatus is shown in Figure 11. The basic channel flow apparatus was a box formed of a number of channels in series, as shown. A movable partition lined with screen formed one side of two channels in series, so that one partition position gave data on two annulus spacings. The LH_2 flow entered through a long entrance tube and manifold to minimize entrance effects. The flow-through specimens were integrated into this inlet line and provided flow-through loss data simultaneously with the channel loss data. The entire apparatus was installed in a large insulated pipe which served as a pressure vessel for the 34.5 N/cm^2 (50 psia) LH_2. The LH_2, after leaving the channel box, flooded the interior of the pipe and provided thermal isolation before leaving the pipe through the back pressure system. The initial design problem was to place the screens in channels with gaps that were representative of the tank application of these screens, so that the data obtained would be usable in the Task 3 analysis without excessive extrapolation. The tankage systems specified are shown in Table VI, with the annulus gap for each tank for an annular residual of 1% to 5% of tank volume shown. In all cases, the apparatus gap range was chosen to span the annulus gap range shown. From the static retention analysis described previously for the six tanks over a range of 0.1 to 0.01 g's, the required screen bubble point in microns for static retention of the head imposed by the largest tank dimension, L, for 34.5 N/cm^2 (50 psia) LH_2 is shown. Finally, the screens selected for each channel pass are shown in the last column. The finest screen, 325 x 2,300, was used with the finest static retention requirement. For direct ΔP comparison between twilled Dutch and twilled square weaves, the 500 x 500, which has the same shute wire diameter (assumed to be an independent variable for pressure

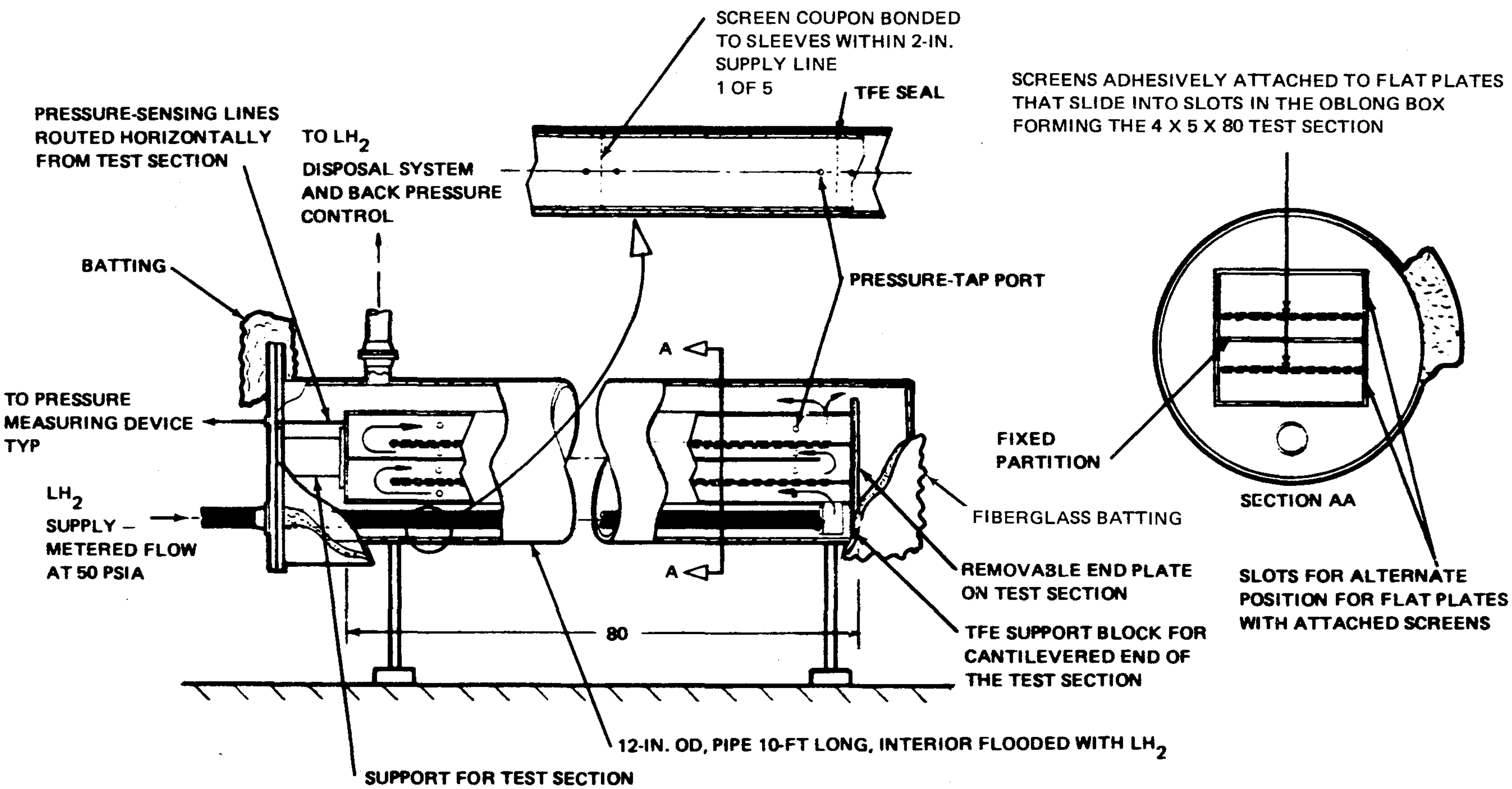

Figure 11. Flow-Loss Test Apparatus

TABLE VI. - SCREEN/CHANNEL GAP SELECTION RATIONALE

Tank no.	Vol m^3 (ft^3)	L/D	L m(ft)	Annulus 1%-5% gap, cm (in.)	Planned channel gap, cm (in.)	Configuration	Static retention microns		Screens bubble-point, microns Shute wire diameter, in.	
							0.1g	0.01g		
1	141.6 (5,000)	4	14.65 (48)	0.84-4.19 (0.33-1.65)	1.02-3.465 (0.4-1.364)	2	5	50	325 x 2,300 12 0.001	500 x 500 34 0.001
2	14.16 (500)	4	6.80 (22.3)	0.38-1.96 (0.15-0.77)	0.38-1.91 (0.15-0.75)	1	10	100	200 x 1,400 19 0.0016	740 x 140 35.1 0.0043
3	14.16 (500)	2	4.42 (14.5)	0.46-2.31 (0.18-0.91)	0.51-2.54 (0.20-1.0)	2	16	160	165 x 800 44.5 0.002	150 x 150 122 0.0026
4	14.16 (500)	1	3.00 (9.9)	0.51-2.52 (0.20-0.99)	0.51-2.54 (0.20-1.0)	1	24	240	50 x 250 86 0.0045	60 x 60 310 0.0075
5	1.416 (50)	2	2.06 (6.7)	0.213-1.069 (0.084-0.421)	0.254-1.27 (0.10-0.50)	1	35	350	24 x 110 168 0.0105	40 x 40 510 0.010
6	1.416 (50)	1	1.39 (4.6)	0.231-1.161 (0.091-0.457)			53	530		

loss), was also used in the same channel. The next finest screen, 200 x 1,400, was in the channel with the next finest static retention requirement; for direct pressure loss comparison, a reverse Dutch weave was used. The coarsest mesh, 40 x 40, was used in the channel with the coarsest static retention requirement. A plain Dutch weave (24 x 110) of nearly the same wire diameter was used in the same channel for the pressure loss comparison. The remaining four screens were placed in the remaining channels in generally increasing micron size. The configurations 1 and 2 noted in Table VI are shown schematically in Figures 12 and 13, with only the vertical dimensions approximately to scale. Configuration 1 had six passes and six screens mounted as shown in the channels, plus the six Dutch weave screen flow-through specimens. Configuration 2 had fixed partition A (see Figure 12) removed to give the large gaps necessary for the 325 x 2,300 and 500 x 500 screens. The remaining two screens were mounted in the channels of Configuration 2, along with the four square weave flow-through specimens. The channel flow test matrix is shown in Table VII. The as-built channel spacing and planned volumetric flowrates are shown. The actual flowrate obtained during testing varied continuously but approximated the values given in Table VII.

The apparatus was made with all-welded construction. The critical design problem was to configure the sides of the apparatus to provide the close tolerances required on the channel height over the 2.26-m (89-in.) -long apparatus. Machining the grooves was rejected because of problems of extreme length and alignment, and requirements for thick material which leads to potential welding problems and warpage. Instead, the grooves were accurately rolled into the thin 0.5-mm (0.020-in.) material. This minimized the heating necessary for welding and minimized weld damage and warpage. Some difficulty in rolling caused by work-hardening resulted in the as-built channel gaps being somewhat different from the planned gaps (Tables VI and VII). A large number of static pressure sensing taps were used to determine the pressure loss along the channel. The pressure taps were arranged to provide data in both screen sample partition positions. The length between the pressure taps was arranged to give three length values (e.g., 1 to 2, 2 to 3, and 1 to 3), which allowed a check on the linearity of pressure loss with length. The pressure taps were situated alternately on opposite sides of the apparatus to avoid interference and allow full use of the pressure-vessel flange for external routing of pressure sensing lines. The pressure taps were also arranged to give a channel entrance L/D ratio of at least 5 to allow flow smoothing leaving the entrance manifold and the 180 degree "mitered" bends. The entrance manifold contained vanes to equally distribute the flow from the entrance line to the apparatus. The assembled flow loss test apparatus is shown in Figure 14. The pressure sensing lines were routed horizontally (to avoid head errors), passed through the pressure vessel flange, and terminated in the needle-valve pressure-tap panel. The principal pressure instruments used were a pair of Dwyer "microtector" electronic hook gauges with a range of 0 to 5.08 cm (0 to 2 in.) of H_2O and a sensitivity of 0.001 cm (0.0005 in.) of H_2O. A Merriam 0 to 76-cm (0 to 30 in.) of H_2O manometer was also used for the higher pressure loss measurements. A complete pressure loss analysis through the entire flow apparatus was performed to determine the necessary flowhead and ensure that at the nominal flowrates (Table VII) the pressure drops would be within the range of the

TABLE VII. - CHANNEL FLOW TEST MATRIX

Channel Width = 12.5 cm (4.94 in.)

Screen	Actual channel spacing depth		Approximate equivalent annulus gap, %	Channel length, cm (in.)	Flow Rate, m^3/sec (gpm)
	cm	in.			
40 x 40	0.455	0.179	1.95	33 66 99	0.001, 0.0015, 0.002
	0.554	0.218	2.4	(13 26 39)	(16, 24, 32)
	1.034	0.407	4.5		
	1.133	0.446	4.9		
24 x 110	0.457	0.180	2.0		
	0.531	0.209	2.3		
	1.011	0.398	4.4		
	1.085	0.427	4.7		
720 x 140	0.622	0.245	1.6		
	0.747	0.294	1.95		
	1.514	0.596	4.0		
	1.638	0.645	4.3		
200 x 1,400	0.635	0.250	1.7		
	0.762	0.300	2.0		
	1.499	0.590	3.9		
	1.626	0.640	4.3		
60 x 60	0.587	0.231	1.15		
	1.252	0.493	2.5		
	1.948	0.767	3.8		
	2.614	1.029	5.1		
50 x 250	0.589	0.232	1.15		
	1.234	0.486	2.4		
	1.963	0.773	3.9		0.001, 0.0015, 0.002
	2.609	1.027	5.1		(16, 24, 32)
150 x 150	0.612	0.241	1.35		0.003, 0.0035, 0.004
	1.278	0.503	2.8		(48, 56, 64)
	1.974	0.777	4.3		
	2.639	1.039	5.8		
165 x 800	0.610	0.240	1.35		
	1.255	0.494	2.7		
	1.984	0.781	4.3	33 66 99	
	3.629	1.035	5.75	(13 26 39)	
500 x 500	1.090	0.429	1.3	99 132 198)	
	1.643	0.647	1.95	(39 52 78)	
	(2.890)[a]	(1.138)[a]	3.45		
	(3.444)	(1.356)	4.1		
325 x 2,300	(1.090)	(0.429)	1.3		
	(1.643)	(0.647)	1.95		
	2.890	1.138	3.45	99 132 198	0.003, 0.0035, 0.004
	3.444	1.356	4.1	(39 52 78)	(48, 56, 64)

Parentheses indicate optional measurement if required

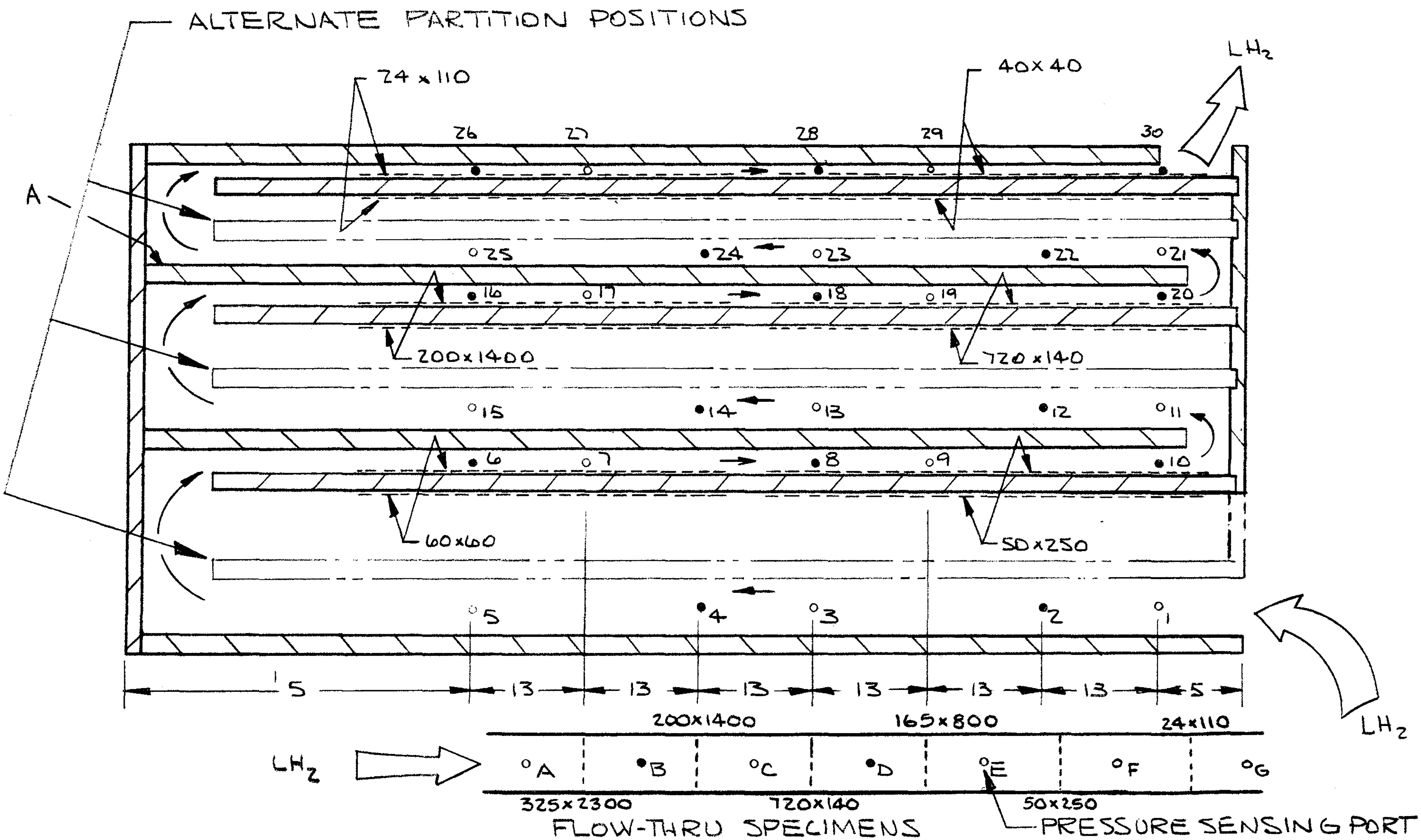

Figure 12. Configuration One Flow Apparatus (Vertical Dimensions Approximately to Scale)

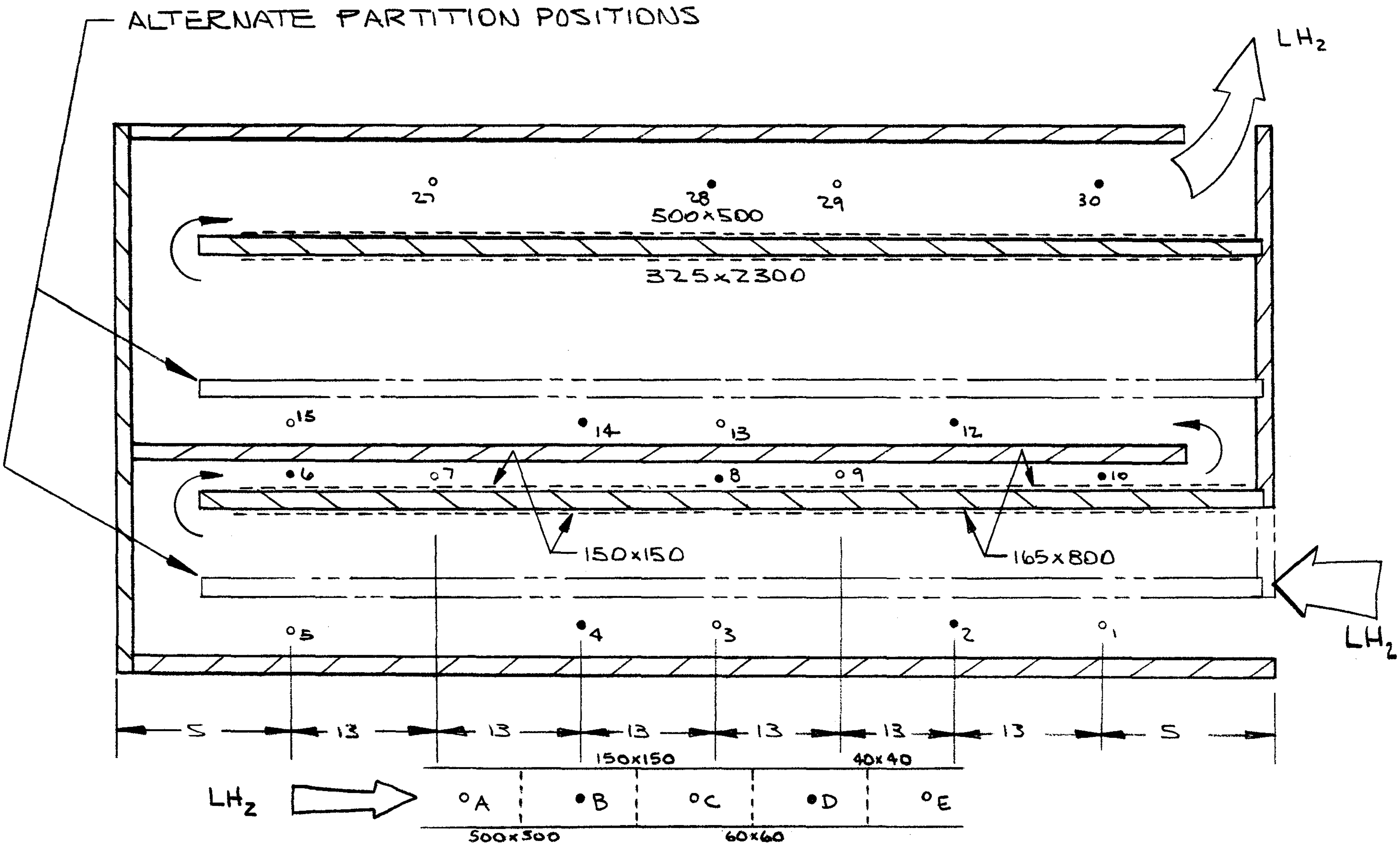

Figure 13. Configuration Two Flow Apparatus (Vertical Dimensions Approximately to Scale)

CR 140

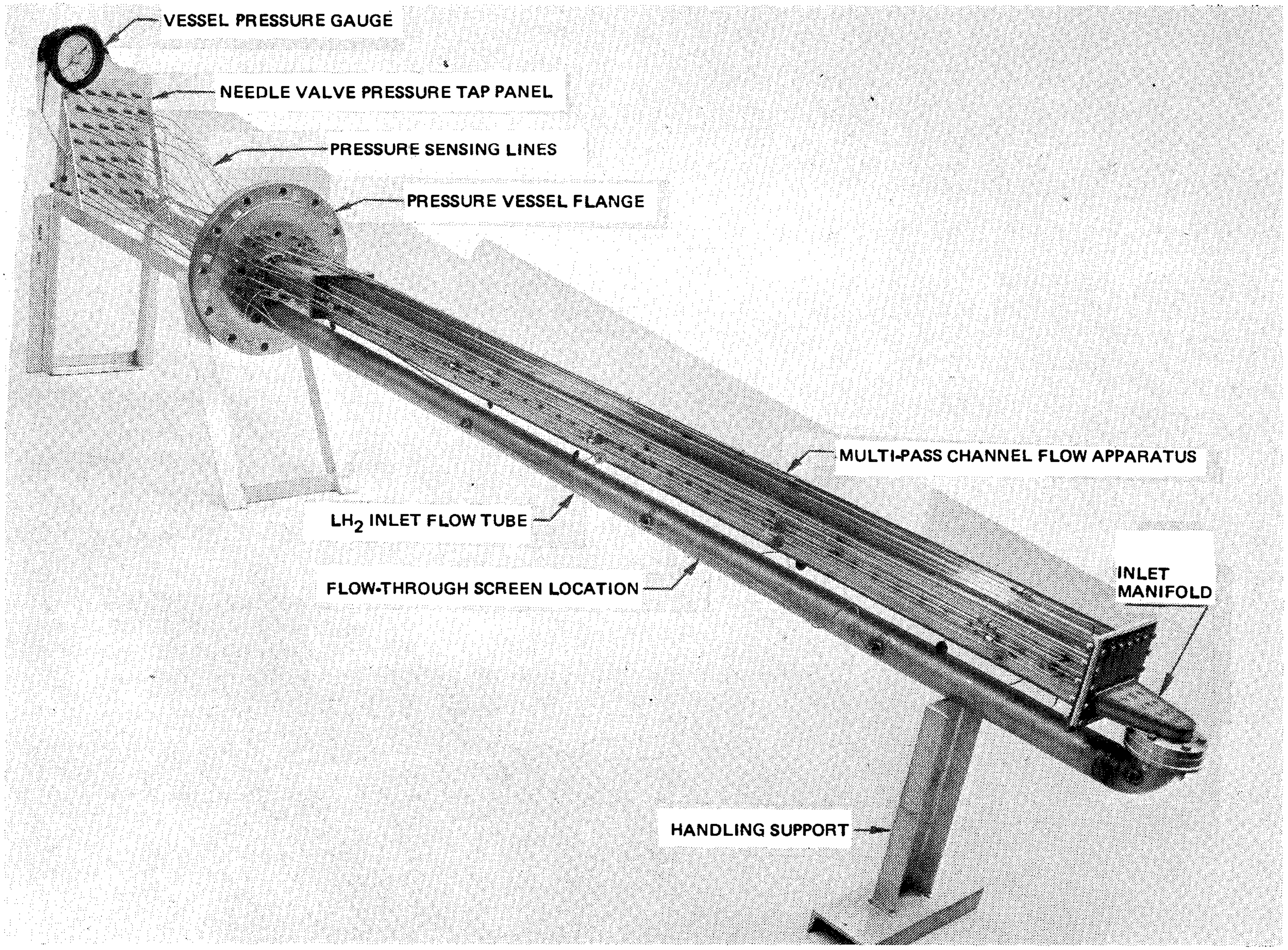

Figure 14. LH_2 Flow Loss Test Apparatus

instrumentation, and more important, was in the appropriate range for later use of the data in the Task 3 analysis. The flow-loss test apparatus was inserted in the pressure vessel and installed in the MDAC LH_2 test facility as shown in Figure 15. The LH_2 was allowed to saturate in the storage tank at 34.5 N/cm^2 (50 psia) prior to use. During testing, LH_2 at 34.5 N/cm^2 (50 psia) flowed through a 10-micron filter, through the inlet control valve, the flowmeter, and the specimens in the apparatus. The flow then emptied into the pressure vessel where it provided thermal shielding of the specimens and was exhausted through another control valve into a 3.79-m^3 (1000-gallon) catch tank. When the catch tank was full, testing was halted and the LH_2 was returned to the storage tank for reuse. Two previously anticipated problems were encountered: there was some difficulty in obtaining single phase LH_2 flow through the specimens. This was overcome by increasing the storage tank pressure by up to 3.5 N/cm^2 (5 psi). In addition, it was found that a minimum of about 0.001 m^3/sec (16 gpm) of LH_2 flow was required to ensure single-phase flow through the specimens. The presence of two-phase flow was detected by low pressure drop across the screens, and by cyclic surging of the screen pressure drop. The flowrate was determined using a turbine type flowmeter, and the LH_2 temperature entering and leaving the apparatus was determined using platinum resistance sensors. These data, together with time, were recorded on a digital data paper tape system. The time was also manually recorded together with the pressure-drop data for later correlation with the paper-tape data.

Screen Flow-Through Test Results

The screen flow-through specimens were welded between stainless-steel washers, and sealed between spacers in the LH_2 inlet line to the flow test apparatus. The screen area exposed to the flow was 23 cm^2 (3.56 in.^{2}) and was the same as the inside area of the flow passage. The entrance section in the inlet line up to the first specimen was 1.4 m (55 in.) long (L/D = 26) which is believed adequate for inlet flow smoothing. The pressure drop across the screen, H, was determined in inches of H_2O and converted to meters of saturated LH_2 at 34.5 N/cm^2 (50 psia). The flowrate together with the screen (flow passage) area determined the fluid approach velocity, V, in m/sec. As described in the section on Screen Survey, the pressure drop for flow through a screen can be described in terms of a friction factor, f, and a Reynold's number, R, in the manner of Armour and Cannon (ref. 10). The correlation is

$$f = \frac{\alpha}{R} + \beta \tag{6}$$

where

$$f = \frac{H \epsilon^2 D g_c}{V^2 Q b}$$

and

$$R = \frac{\rho V}{\mu a^2 D}$$

CR 140

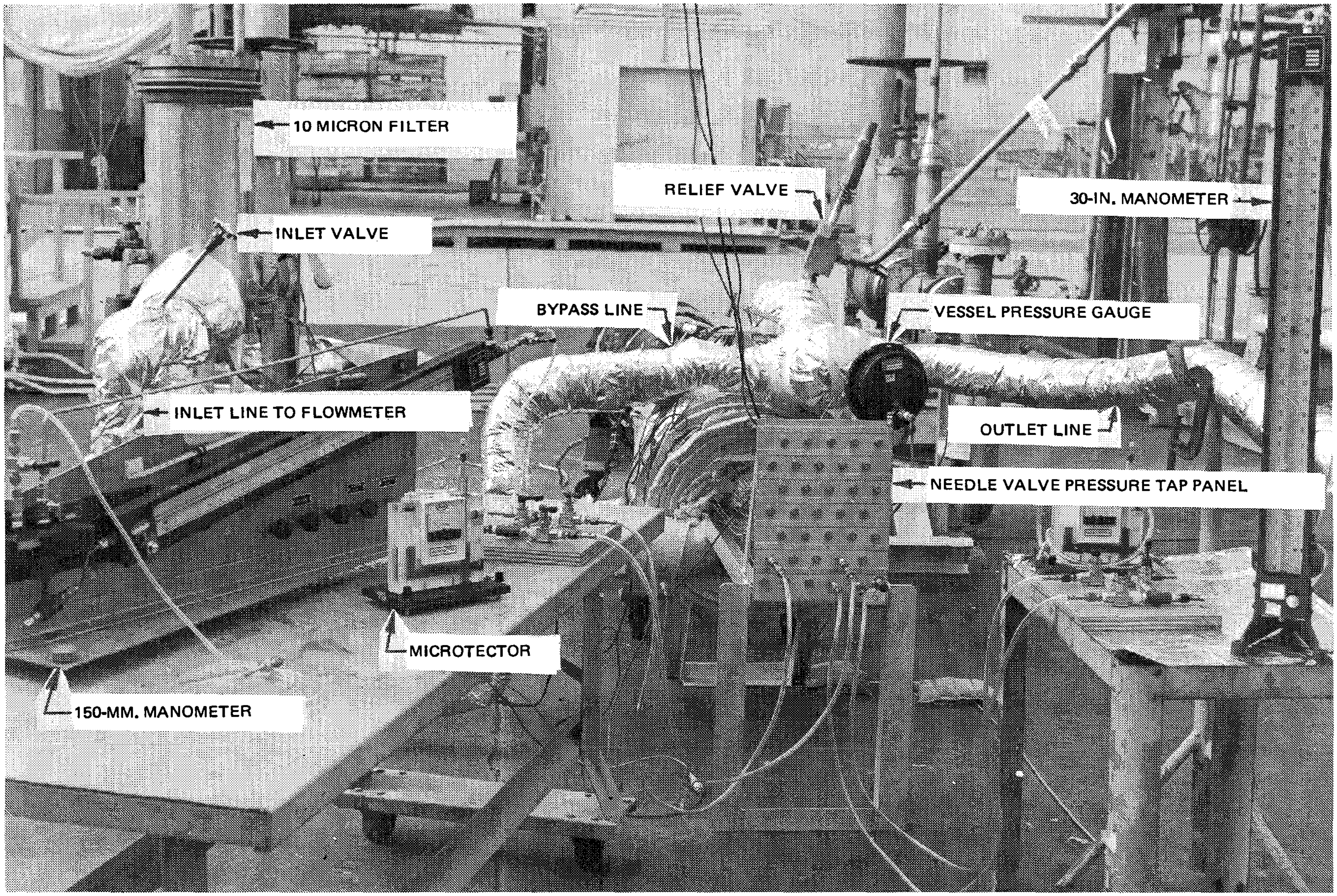

Figure 15. LH_2 Flow Loss Test Setup

(See Symbols) and α and β are experimentally determined constants.

Substitution of f and R gives the following expression relating pressure drop, H, and fluid approach velocity, V:

$$H = \alpha\left[\frac{Qba^2}{\epsilon^2 g_c \rho}\right]\mu V + \beta\left[\frac{Qb}{\epsilon^2 D g_c}\right] V^2$$

$$H = AV + BV^2 \tag{7}$$

From equations (6) and (7), it can be seen that in the laminar flow regime (small V and R), f is essentially only a function of R, and H depends essentially only on V, while in the turbulent flow regime, f is essentially constant, and H essentially depends only on V^2. For the LH_2 tests, a minimum flowrate of about 0.001 m^3/sec (16 gpm) was required to maintain good quality LH_2 in the apparatus. This, together with the low viscosity and (relatively) high density of the LH_2, resulted in the LH_2 test data being in the turbulent Reynold's number regime only. To evaluate the functional constants in the laminar regime, additional tests were made with both the channel apparatus and with another flow apparatus used for the Reference 12 flow-loss tests, using ambient gaseous nitrogen as the flow medium. The relevant screen characteristics and the experimentally determined α, β, A and B for the 10 selected screens are shown in Table VIII. The data, plotted in Armour and Cannon form, are shown in Appendix B for all screens, with typical examples shown in Figures 16 and 17.

Figure 16 shows the available data for the 325 x 2, 300 screen, including gas data from the MDAC-MSFC contract NAS8-27685 (ref. 12) which agree with our data rather well. Water test data from Kressilk (ref. 13) and Wintec Corp. (ref. 14) are also shown, together with the generalized Armour and Cannon correlation for all screens, which overpredicts the friction factor and thus the pressure loss for this screen by 170 percent.

Also shown in Appendix B are data from all other known sources, i.e., GDA (ref. 15), MDAC IRAD (ref. 16), NAR (ref. 17), and MDAC-MSFC contract NAS8-27685 (ref. 18). These data have been normalized to agree with the geometric characteristics of our screens (especially specified pore diameter) as shown in Table VIII.

The correlations for the square weave screens are all shown in Figure 17, which exhibits a number of interesting aspects. First, in the laminar regime, all four screens are reasonably well represented by a single correlation value of α. Second, in the turbulent regime, assuming one-dimensional

TABLE VIII. - FLOW LOSS CORRELATION

Screen	D, m (ft)	a, 1/m (1/ft)	b, m (ft)	ϵ	Armour and Cannon Form $f = \frac{\alpha}{R} + \beta$		$H = AV + BV^2$			
							H in m of 34.5 N/cm^2 LH^2 V in m/sec		H in ft of 50 psia LH_2 V in ft/sec	
					α	β	A	B	A	B
325 x 2,300	0.000005 (0.0000164)	110,235 (33,598)	0.000089 (0.000292)	0.245	3.2	0.19	1.14	0.6919	1.14	2.27
200 x 1,400	0.000010 (0.0000328)	65,390 (19,930)	0.0001524 (0.0005)	0.248	4.2	0.20	0.885	0.6126	0.885	2.01
720 x 140	0.000015 (0.0000492)	32,954 (10,044)	0.0001804 (0.000592)	0.514	11.0	0.47	0.162	0.2627	0.162	0.862
165 x 800	0.000025 (0.000082)	41,360 (12,606)	0.0001753 (0.000575)	0.426	3.3	0.17	0.108	0.0805	0.108	0.264
50 x 250	0.00005 (0.000164)	13,075 (3,985)	0.000369 (0.00121)	0.611	13.5	0.26	0.045	0.0631	0.045	0.207
24 x 110	0.000115 (0.000377)	5,889 (1,795)	0.000914 (0.003)	0.572	8.61	0.52	0.0165	0.1554	0.0165	0.51
500 x 500	0.0000254 (0.0000833)	65,495 (19,962)	0.0000509 (0.000167)	0.584	5.7	0.65 (0.77)[a]	0.0554	0.03298 (0.04267)[a]	0.0554	0.1082 (0.140)[a]
150 x 150	0.000103 (0.000339)	19,916 ((6,070)	0.000132 (0.000433)	0.671	5.7	0.50 (0.50)[a]	0.0101	0.01347 (0.01347)[a]	0.0101	0.0442 (0.0442)[a]
60 x 60	0.000233 (0.000764)	(8,137) (2,480)	0.000381 (0.00125)	0.612	5.7	0.40 (0.61)[a]	0.00585	0.01820 (0.02761)[a]	0.00585	0.0597 (0.0906)[a]
40 x 40	0.000381 (0.00125)	5,328 (1,624)	0.000509 (0.00167)	0.662	5.7	0.60 (0.52)[a]	0.00287	0.01728 (0.01497)[a]	0.00287	0.0567 (0.0491)[a]
Armour and Cannon (Reference 10)					8.61	0.52				

[a]Based on $Eu = \left(\frac{S}{1 - S}\right)^2$

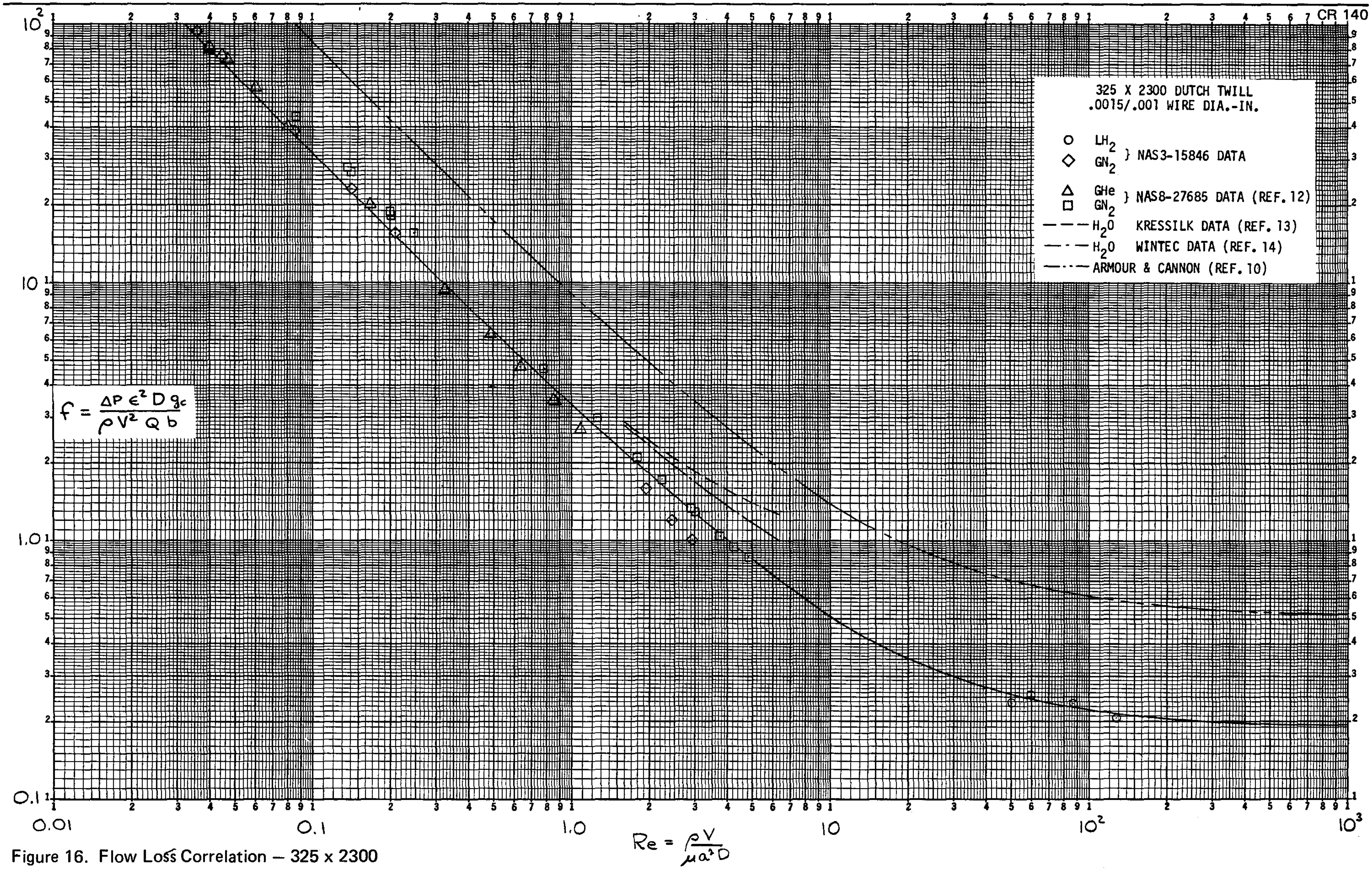

Figure 16. Flow Loss Correlation – 325 x 2300

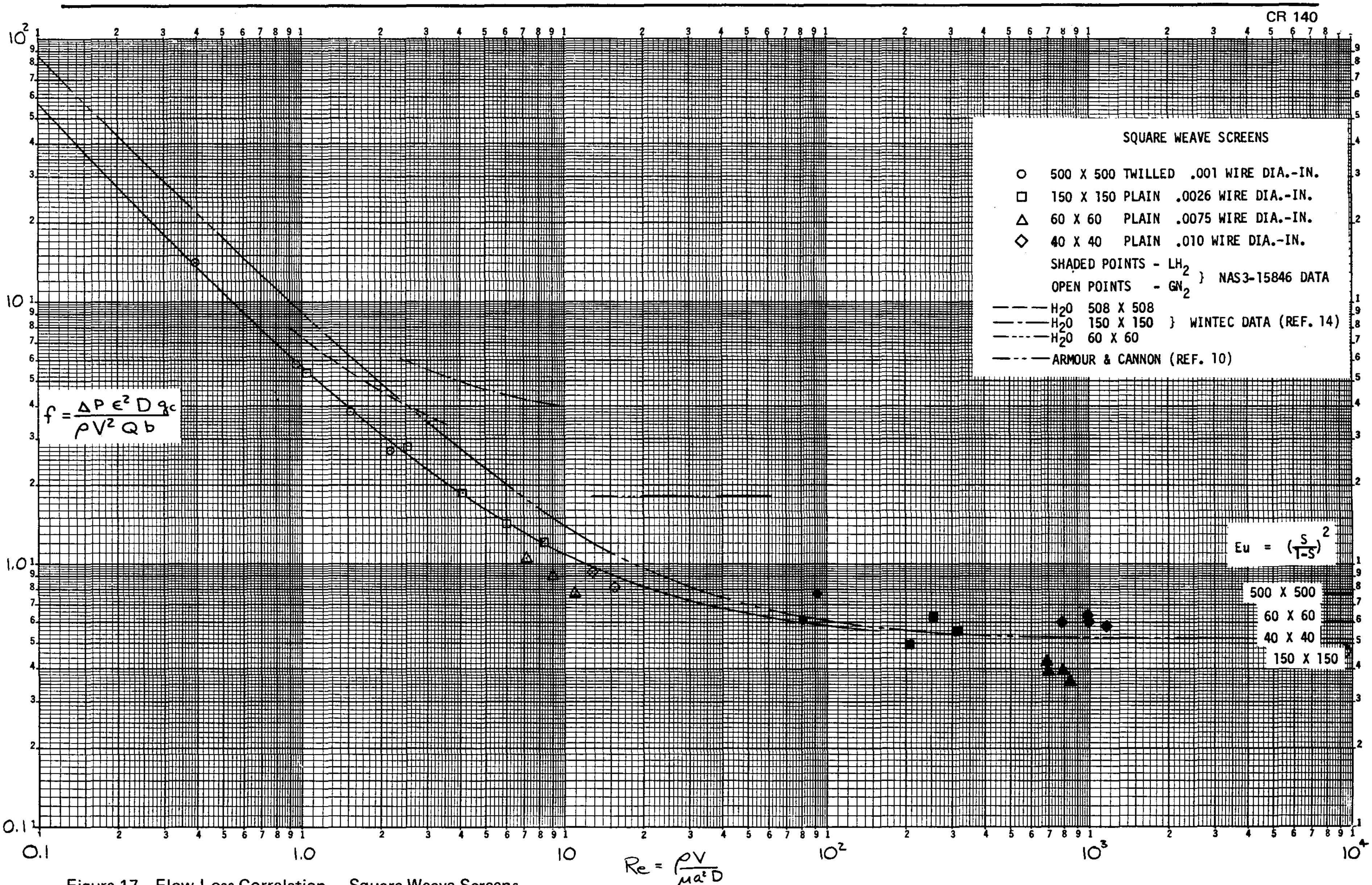

Figure 17. Flow Loss Correlation – Square Weave Screens

incompressible flow with a sudden expansion, a potential flow analysis which balances momentum loss with pressure recovery behind the screen (ref. 19) results in the expression:

$$Eu = \left(\frac{S}{1 - S}\right)^2 \tag{8}$$

where the Euler No. $Eu = \Delta P\ 2g_c/\rho V^2$, and S is the screen solidity (fraction of closed area). This is equivalent to a constant friction factor where

$$f = \frac{Eu}{2}\ \frac{\epsilon^2 D}{Qb} = \left(\frac{S}{1 - S}\right)^2 \frac{\epsilon^2 D}{2Qb} = \beta \tag{9}$$

which is a function only of screen geometric characteristics.

The value of β and B based on equation (9) for our four square-weave screens is shown in Table VIII. There is reasonably good agreement for all of the screens, with the 40 x 40 screen value being perhaps a little high, and the 60 x 60 screen value being a little low. Shown for comparison is Wintec Corp. water data which shows very poor agreement, especially in the turbulent regime. The Wintec equation for the 60 x 60 screen has only the turbulent component which gives an equivalent f of 1.82. Evaluation of the equivalent f for the ten 60 x 60 screens included in our screen survey (Appendix A) indicates that the equivalent f should be in the range of 0.275 to 1.07. This illustrates the potential unreliability of much available screen pressure loss data.

The data for pressure loss, in meters of 34.5 N/cm^2 LH_2 ($\rho = 64.08\ kg/m^3$) versus approach velocity in meters/sec are shown in Figure 18. The lines shown are equation (7), based on the α and β of equation (6) and shown in Table VIII for each of the 10 screens. The deviation of some of the data for the correlation indicates the desirability of obtaining the correlation over the entire laminar-turbulent flow regime based on dimensionless parameters such as f and R, rather than simply on pressure drop versus velocity data. It is believed that the correlations described in Table VIII adequately describe the screen flow-loss characteristics over the entire flow spectrum.

Channel Flow Test Results

The channel-flow screen specimens were screen samples 0.125 m by 1.0 m (5 in. by 40 in.) (with the shute wires in the long direction of flow) bonded to stainless steel backup plates with the same polyurethane adhesive used for bonding of the bubble-point specimens. The adhesive was used sparingly and wiped from the top surface of the screens to ensure that the screens would exhibit the necessary roughness due to the weave. The complete matrix of test conditions shown in Table VII was performed.

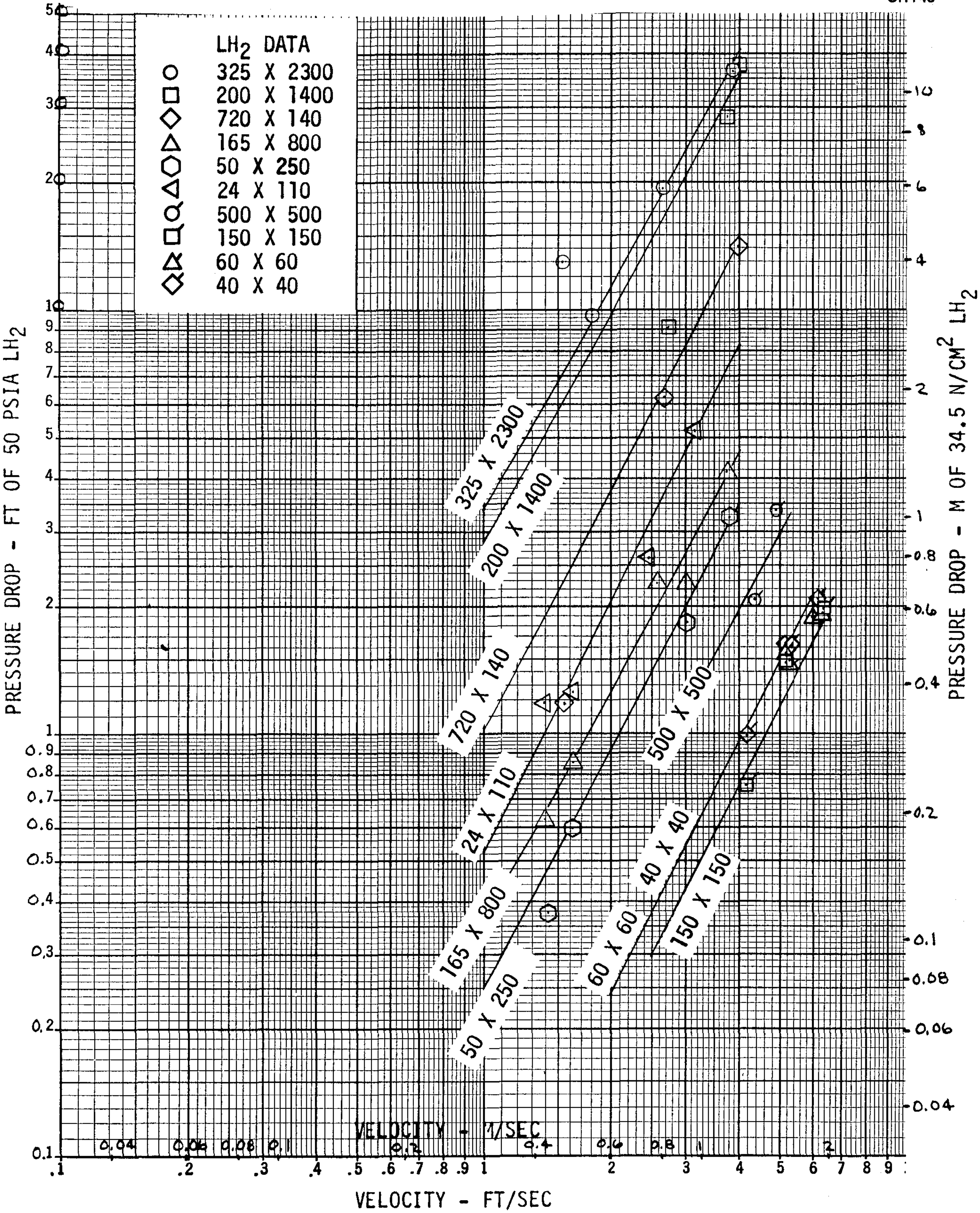

Figure 18. Flow Loss Correlation — Pressure Drop Versus Velocity

The data, plotted as head loss in meters of 34.5 N/cm^2 LH_2 versus channel flow velocity in meters/sec with length (L) over channel height (s) as a parameter, are shown in Appendix B for all 10 screens, with a typical example shown in Figure 19. As anticipated in test planning, the pressure drop was linear with length: in Figure 19, the plain symbols are for the 33 cm (13-inch) length, the primed symbols are for 66 cm (26-inch), and the double-primed symbols for the 99 cm (39-inch) length. Because the channel flow lies in the turbulent regime, the pressure drop varies essentially as the channel flow velocity squared, as shown by the slope of the lines on Figure 19. In general, the pressure drop increases with increasing L/s, but extreme channel height values cause jumps in the L/s correlation because of the effect of channel height on friction factor (Fig. 19).

To evaluate this effect and define the important physical factors influencing the channel flow, a dimensionless analysis of the channel flow, in the manner of Moody (ref. 20) was performed. In pipe flow, the friction factor is defined by the Darcy formula (see Symbols):

$$f = \frac{H_f}{\frac{L}{D_h}\frac{V^2}{2g_c}} = \frac{H_f D_h w^2 s^2 2g_c}{L \dot{Q}^2} \tag{10}$$

and at ordinary velocities f is a function only of Reynolds number, R, and a roughness parameter, e/D_h, where

$$R = \frac{\rho V D_h}{\mu} = \frac{V D_h}{\nu} \tag{11}$$

and e is a linear dimension representative of the absolute roughness of the surface. For non-circular pipes, D_h in e/D_h and equations (10) and (11) is the hydraulic diameter defined as four times the flow area divided by the wetted perimeter, or, for a rectangular channel of width w and height s,

$$D_h = 2\frac{ws}{w + s} \tag{12}$$

In Reference 20, Moody presents a graph giving the relationship between f, R, and e/D_h. The pipe flow is characterized by four flow regimes: in the laminar flow regime, the flow loss correlation is of the form

$$f = \frac{C}{R} \tag{13}$$

and the roughness has no effect on the flow, which is dominated by viscous effects. At a critical R of 2,000 to 4,000, ordinary laminar pipe flow makes a rather abrupt transition to turbulent flow. In this critical region, the f is

CR140

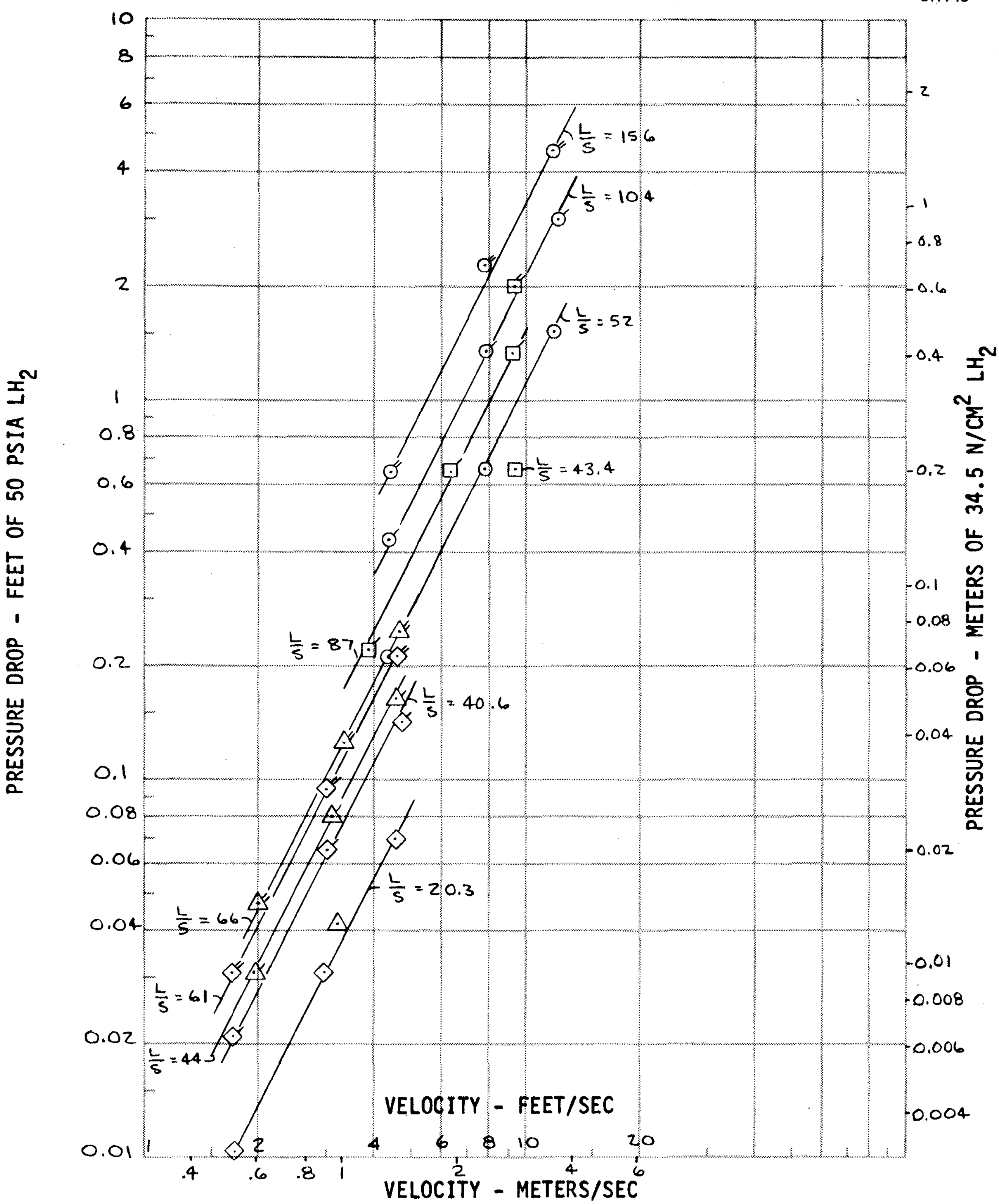

Figure 19. Channel Flow Pressure Drop Correlation – 200 X 1400

not well defined and this region is shown on the Moody graph as a rather wide band. Following the critical region, the flow enters the transition region, where f is a complex function of R and e/D_h. At high values of R, the flow enters the region of complete turbulence for rough pipes and R has no effect, so that

$$f = f(e/D_h) \tag{14}$$

To determine the effects of e/D_h on our channel flow loss and the appropriate roughness parameter, our data were plotted on the Moody graph, as shown in Appendix B for all 10 screens, with typical examples shown in Figures 20 and 21. In these figures, the collection of data points at $R \doteq 10^5$ or higher were the 34.5 N/cm^2 (50 psia) LH_2 data, while the single points at $R \doteq 5,000$ were data taken with ambient GN_2. In our experiments, the direction of fluid flow was always in the direction of the shute wires, which should minimize the pressure drop due to the construction of the Dutch-weave screens. It was noted from the data that the f for the Dutch-weave screens was about half that for square-weave screens of about the same wire diameter and essentially identical geometry and flow conditions.

To determine the value of e more precisely, it was computed, based on the experimental data, from the Colebrook equation (ref. 20) which describes the relation between f, R and e/D_h in the turbulent-transition regime:

$$\frac{1}{\sqrt{f}} = -2 \log \left(\frac{e/D_h}{3.7} + \frac{2.51}{R\sqrt{f}} \right) \tag{15}$$

The value of e based on the experimental data and actual channel spacing, and equation (15) is shown in Table IX, compared to e based on physical wire dimensions—i.e., the wire diameter for the square-weave screens, and half the shute-wire diameter for the Dutch-weave screens. The values in Table IX substantiate the use of wire diameter (or half the shute-wire diameter) as the appropriate roughness dimension. It is, of course, desirable that this roughness parameter be based on a general physical characteristic of the screen, rather than on specific experimental data for each screen.

The physical rationale behind this is shown in Figure 22, which schematically shows a cross-section through the screens in the direction of flow. The construction of the Dutch-weave screens is such that the shute wires are pressed tightly together so that essentially only half the shute wire contributes "roughness." On the other hand, the square-weave screens are woven with definite "pitch", or spaces between wires, so that the flow sees the full wire diameter as "roughness." A similar effect was found by Edwards and Sheriff (ref. 21), who determined that at low pitches (1 to 4 diameters) the friction factor increases nearly linearly with pitch. For our case, the pitch of the square-weave screens is 2 to 2.5 wire diameters, while for the Dutch-weave screens the pitch is effectively 1 diameter.

It can be seen from the roughness values of Table IX, and from Figures 20 and 21, that there is considerable data scatter. There are a number

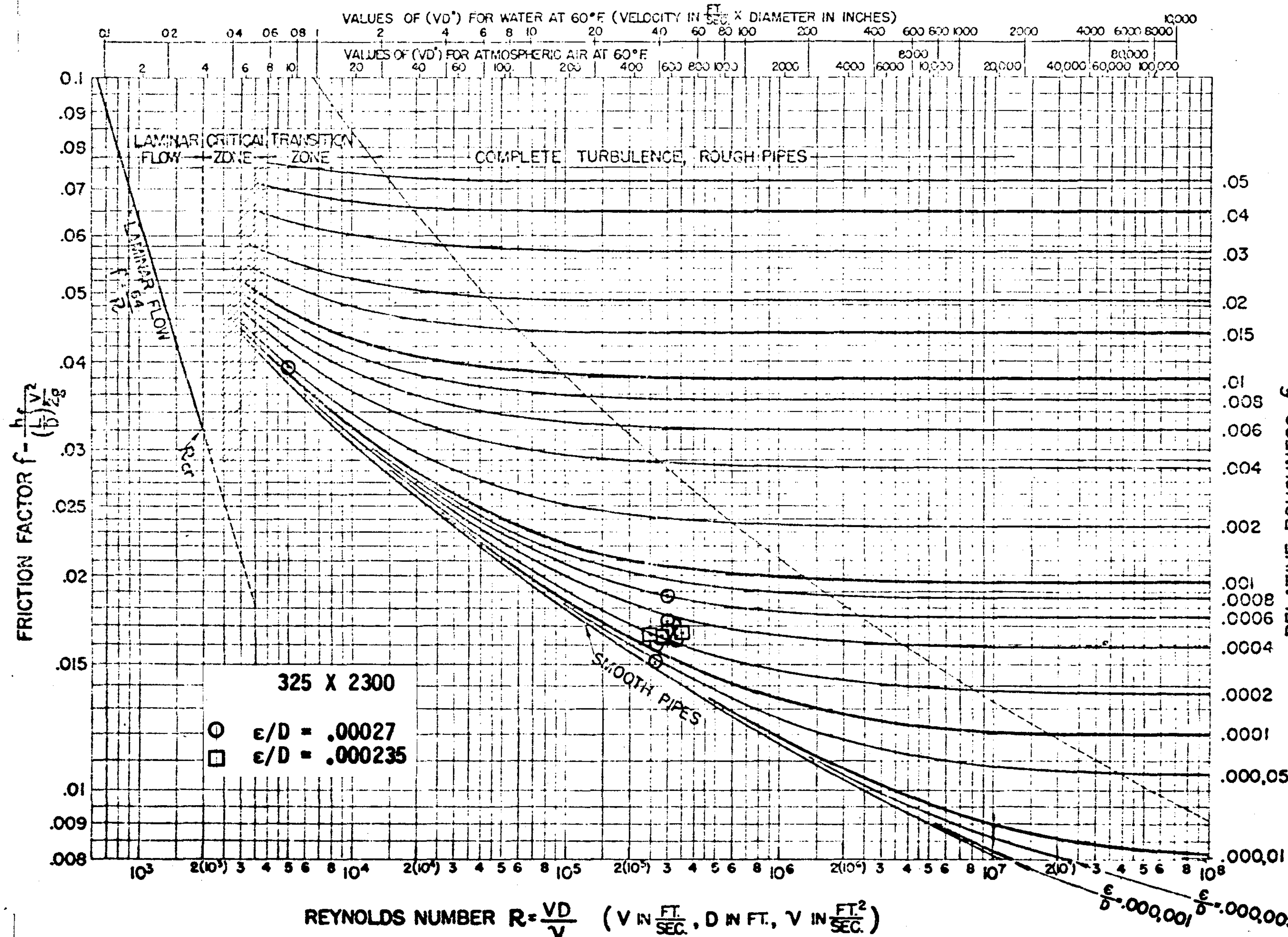

Figure 20. Dimensionless Channel Flow Loss Correlation – 325 x 2300

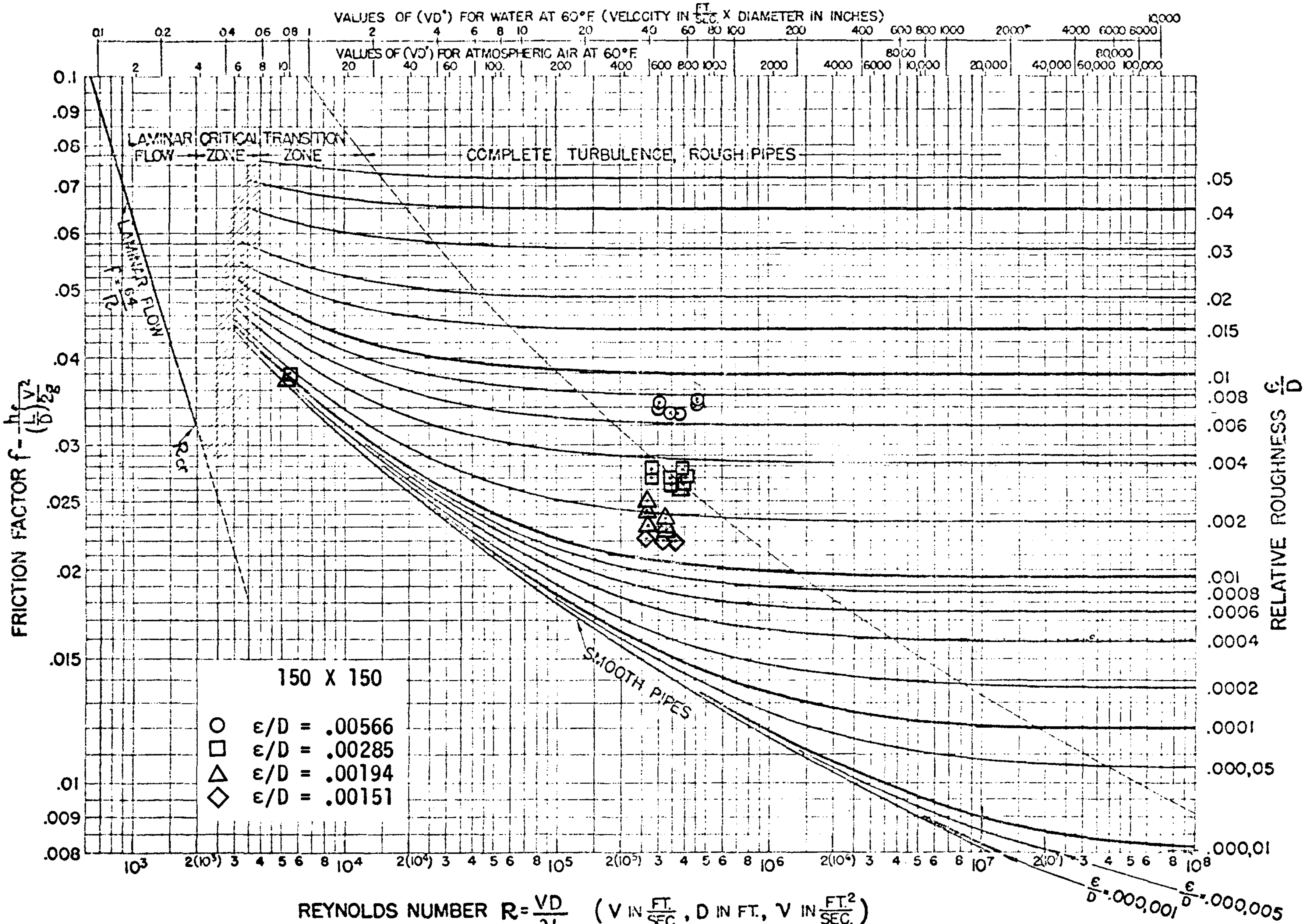

Figure 21. Dimensionless Channel Flow Loss Correlation — 150 x 150

TABLE IX. - SCREEN WIRE SIZE AND ROUGHNESS PARAMETERS

Screen	Wire diameter - in. warp/shute	Roughness parameter - e - cm Based on experimental data and Colebrook equation[a]				Roughness parameter - e - in. Based on experimental data and Colebrook equation[a]				Roughness parameter e - cm - (in.) based on physical wire dimensions
325 x 2, 300	0.0015/0.001	0.00127 (2.89)[b]	0.001295 (3.444)			0.00050 (1.138)[c]	0.00051 (1.356)			0.00127 (0.0005)
200 x 1, 400	0.0028/0.0016	0.00353 (0.635)	0.00183 (0.762)	0.00239 (1.499)	0.00173 (1.626)	0.00139 (0.250)	0.00072 (0.300)	0.00094 (0.590)	0.00068 (0.640)	0.00203 (0.0008)
720 x 140	0.0014/0.0043	0.00719 (0.622)	0.00462 (0.747)	0.00617 (1.514)	0.00538 (1.638)	0.00283 (0.245)	0.00182 (0.294)	0.00243 (0.596)	0.00212 (0.645)	0.00546 (0.00215)
165 x 800	0.0029/0.002	0.00244 (0.610)	0.00312 (1.255)	0.00310 (1.984)	0.00241 (2.629)	0.00096 (0.240)	0.00123 (0.494)	0.00122 (0.781)	0.00095 (1.035)	0.00254 (0.001)
50 x 250	0.0055/0.0045	0.00686 (0.589)	0.00584 (1.234)	0.00630 (1.963)	0.00460 (2.609)	0.0027 (0.232)	0.0023 (0.486)	0.00248 (0.773)	0.00181 (1.027)	0.00572 (0.00225)
24 x 110	0.015/0.0105	0.02159 (0.457)	0.01854 (0.531)	0.01397 (1.011)	0.01257 (1.085)	0.0085 (0.180)	0.0073 (0.209)	0.0055 (0.398)	0.00495 (0.427)	0.01334 (0.00525)
500 x 500	0.001	0.00277 (1.090)	0.00254 (1.643)			0.00109 (0.429)	0.001 (0.647)			0.00254 (0.001)
150 x 150	0.0026	0.00838 (0.612)	0.00749 (1.278)	0.00772 (1.974)	0.00610 (2.639)	0.0033 (0.241)	0.00295 (0.503)	0.00304 (0.777)	0.0024 (1.039)	0.0066 (0.0026)
60 x 60	0.0075	0.02743 (0.587)	0.02045 (1.252)	0.02997 (1.948)	0.02045 (2.614)	0.01080 (0.231)	0.00805 (0.493)	0.0118 (0.767)	0.00806 (1.029)	0.01905 (0.0075)
40 x 40	0.01	0.0396 (0.455)	0.0368 (0.554)	0.0290 (1.034)	0.0247 (1.133)	0.0156 (0.179)	0.0145 (0.218)	0.0114 (0.407)	0.00974 (0.446)	0.0254 (0.01)

a Reference 20.

b Values in parenthesis are channel spacing in cm.

c Values in parenthesis are channel spacing in inches.

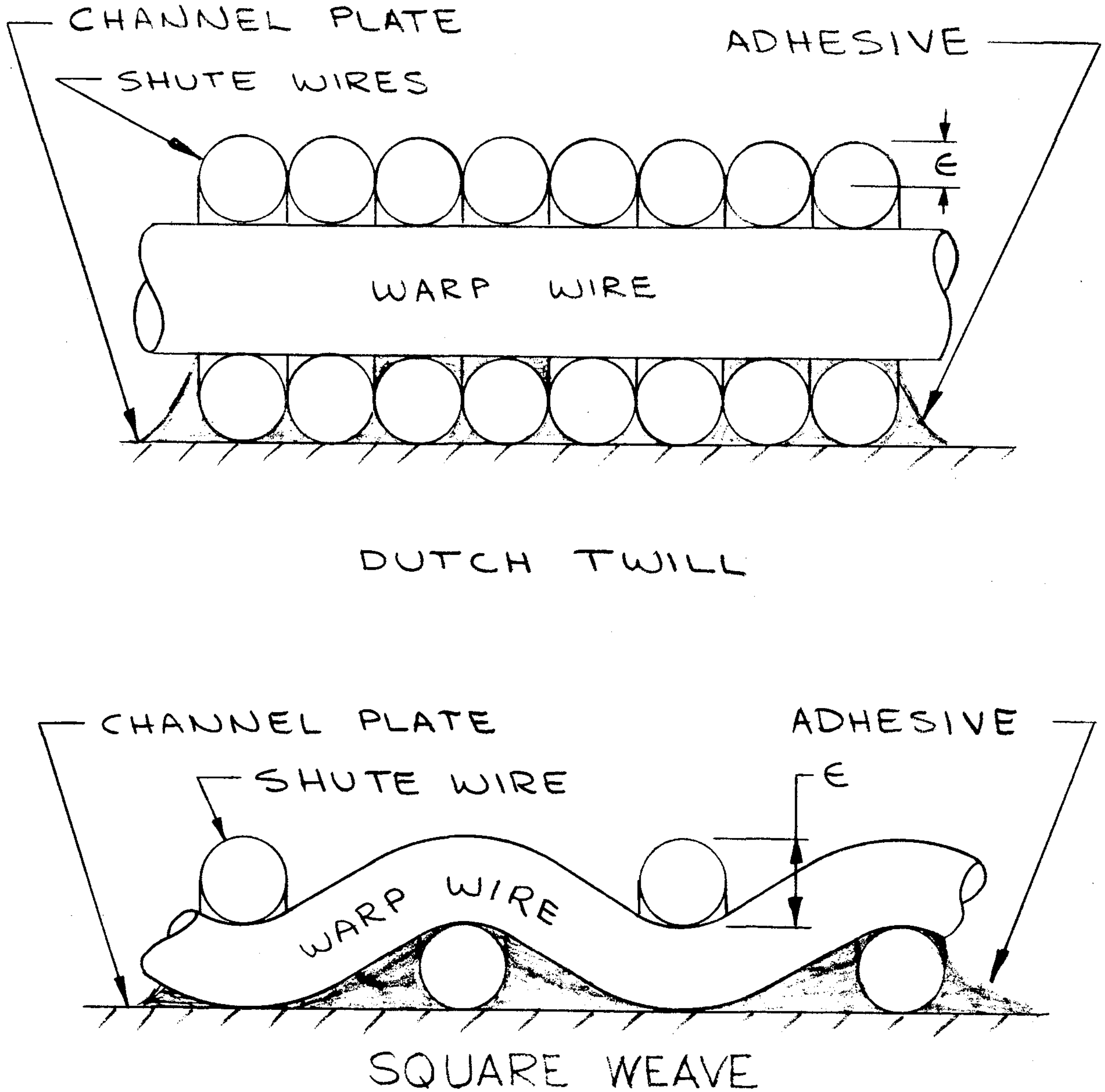

Figure 22. Schematic Cross-Section of Screens in Direction of Flow

of cogent reasons for the data scatter. First, it was extremely difficult to obtain accurate data using as the flow medium a near-saturated liquid, which must undergo a phase change prior to use in the measurement system, i. e., the LH_2 in the apparatus must be converted to warm GH_2 outside the apparatus before pressurizing the manometers. In many cases, pulsing of the pressure was noticed, especially at the lower flowrates. In general, most frictional pressure drop experimentation is done with ambient-temperature low-pressure gases, to obviate this problem. Note that the low-pressure GN_2 data, at about $R \doteq 5,000$, show very little scatter relative to the LH_2 data. Another severe problem was the use of a high-pressure flow medium. Using LH_2 at 34.5 N/cm^2 (50 psia) greatly magnifies the effects of very minor leakage when determining pressure drops of perhaps 0.0007 N/cm^2 (0.001 psi). Extensive effort was expended during the test program to find and eliminate leakage from all sources, including the instrumentation.

Substitution of equation (12) into equation (10) and examination of the Moody graph reveals another potential source of error. The friction factor is a very weak function of the relative roughness, where e may be rather accurately specified (for screens), but varies essentially as the cube of the channel spacing, s, which may be neither well-defined nor constant along the channel, due to normal manufacturing tolerances. Further, in the turbulent regime, the friction factor varies as the square of the flowrate, which showed variations of a few percent during our tests. All of these considerations may contribute to the observed data scatter.

Another interesting feature observed from Figure 21 (and Appendix B) is that the data for the small channel spacing ($s < 0.64$ cm (0.25 in.) - see Table IX) appears high compared to the computed ϵ/D. It is thought that this may be due to the large w/s ratio for these cases. In laminar flow, solution of the equations of motion leads to equation (13) where the value of the constant, C, depends on the boundary conditions and the geometry of the duct. Eckert and Irvine (ref. 22) show curves giving the value of C for rectangles, triangles, ellipses, and annuli. While for circular ducts, $C = 64$, for very elongated rectangles or for thin annuli, C approaches 96, assuming f and R based on hydraulic diameter. For rectangles increasing from $w/s \doteq 5$ to $w/s \doteq 20$ (the range of our conditions), the value of C increases from 76 to 90. Schlicting (ref. 23), in describing the work of L. Schiller and J. Nikuradse on turbulent flow in noncircular ducts, indicates that use of hydraulic diameter for all of these ducts leads to accurate correlation in the turbulent regime. The Moody graph is for circular pipes and implies applicability to noncircular ducts when correlated with hydraulic diameter only. However, all normal noncircular ducts have values of C close to that for circular pipes, i. e., a $w/s = 3$ rectangle has $C = 68$, equilateral and isosceles triangles have $C \simeq 53$, etc. No data are known at this time for very flat rectangles or thin annuli in turbulent flow, however, it is conjectured that the variation in f due to thin annuli or very flat rectangles which occurs in laminar flow may also persist into the turbulent regime and may account for the small upward deviation of our data from the Moody graph.

Analytical Models for the Experimental Data

The correlation of f and R, with e based on screen characteristics, described previously was based on flow data from rectangular channels. To use the data correlations in the analysis of the wall screen liner, which is a very thin annulus with no sidewalls (only a screen side and a tank wall side), either the data must be corrected for the effects of the sidewalls, or the effects of the sidewalls must be shown to be insignificant. An analysis to verify that the sidewall contribution to the total channel pressure drop can be ignored is shown in Appendix C. The results of this analysis indicate that at worst, the sidewall effect is much less than the data scatter, and at best, is insignificant.

In addition, while our data correlate well with the Moody graph in the transition/turbulent regimes, the range of R for the system analysis task is from about 3 to over 100,000. Thus, our correlation(s) must cover the complete range of flows in the laminar, critical, transition, and turbulent regimes.

In the laminar regime, the correlation should clearly be, or approximate, equation (13) with C = 96 for thin annuli (the case for our tankage systems). In the critical regime, no correlation is available, and in the transition/turbulent regimes, our data are correlated by the Colebrook function of equation (15).

It can be seen that at large R, the f values approach the Von Karman rough pipe formula:

$$\frac{1}{\sqrt{f}} = 2 \log \frac{3.7}{\epsilon / D_h} \qquad (16)$$

Determination of the friction factor from equation (15) is awkward, since the equation is only implicit in f. Further, in our tankage system analysis, for steady flow around a spherical annulus of constant width, the velocity in the annulus will be varying with angular position in the annulus. Therefore, both f and R will be varying with velocity, and equation (15) should be integrated around the spherical annular flow field. While this integration could be performed numerically, it would be very time consuming for the many cases of our extensive analysis matrix. In addition, since channel flow loss is only part of the total pressure loss, which includes head, velocity, and screen flow-through losses, such analytical tedium is unwarranted. Also, solution of equation (15) would still not solve the problem of the determination of f in the critical regime.

Therefore, a similar correlation to the screen flow-through loss correlation was assumed for the channel flow loss. This correlation was asymptotic to the laminar function, equation (13) at low R and to the rough pipe formula equation (16), at high R, and is:

$$f = \frac{96}{R} + \frac{1}{4\left(\log \frac{3.7}{e/D_h}\right)^2} \qquad (17)$$

This expression is shown in Figure 23 compared to the laminar function, equation (13), and to the Colebrook function, equation (15). At low values of e/D_h, typical of most of our higher R cases, equation (17) is an excellent

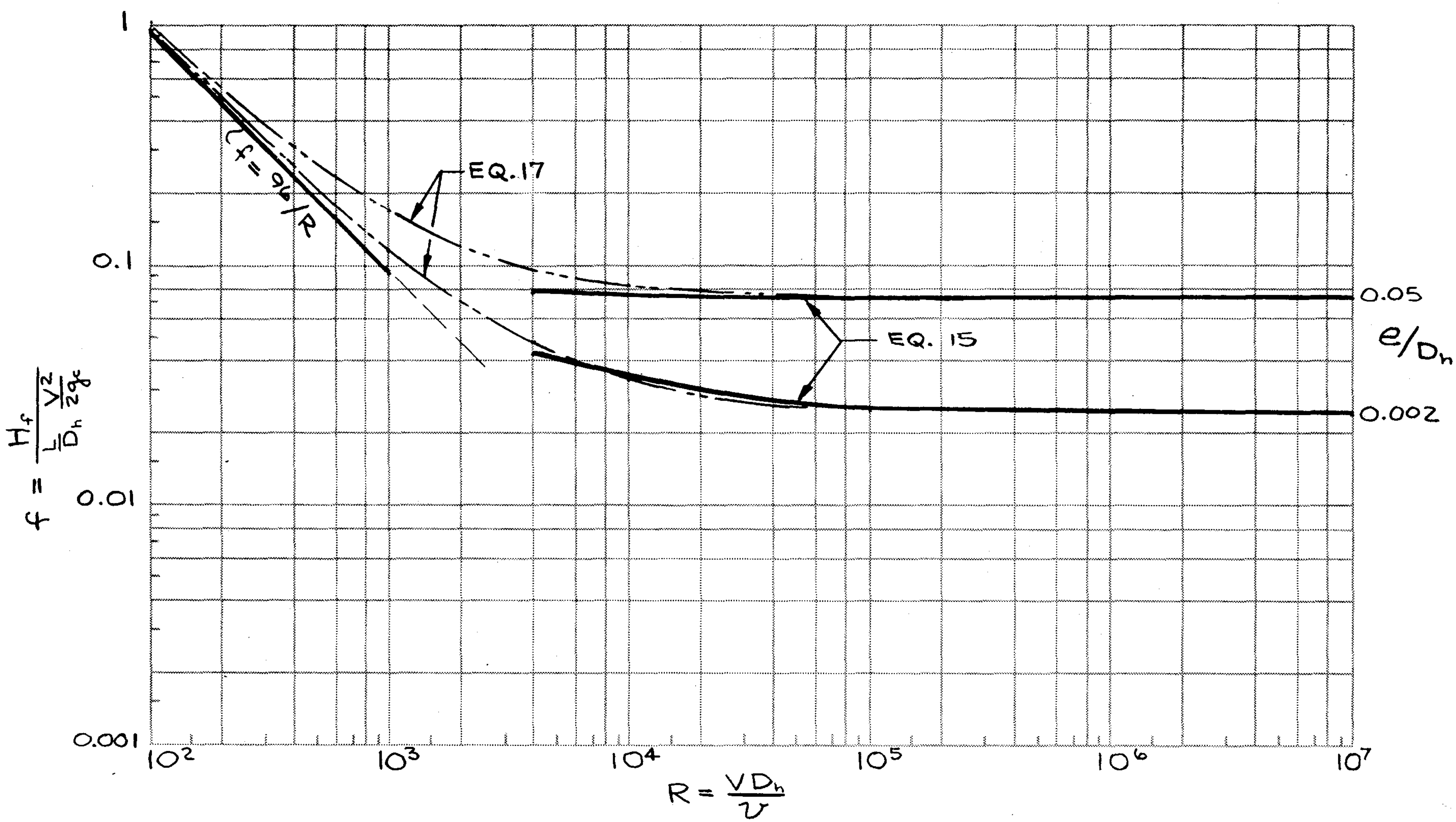

Figure 23. Comparison of Approximate Correlation (Eq 17) with Colebrook Function (Eq 15)

approximation of equation (15), gives conservative f values in the critical regime, and closely approximates equation (13) at $R < 10^3$. At very coarse roughness values ($e/D_h = 0.05$), the f values are more conservative, but in our analysis matrix, the coarse screens are usually appropriate to systems with very low R, where the deviation from the laminar expression is small.

Another consideration merits discussion. In ordinary pipe flow, where C = 64, the critical jump from laminar to turbulent flow occurs usually at an R of 2,000 to 4,000, and since f is small (0.032-0.016) the jump in f is upward to the turbulent value. However, the critical regime can start at R as low as 1,000, depending on geometry, initial flow disturbances, entrance length, flow bends, etc. (References 20 and 22). It is conjectured here that the flow through the screen at the beginning of the channel flow annulus, though small, could act as a turbulence generator, thus triggering transition to turbulent flow at fairly low R ($< 10^3$). At this low R, f would have a value of 0.096 or above, which is above the f values for turbulent flow. It is not reasonable that at transition the f values would drop abruptly to the values predicted by the Colebrook function, equation (15), but rather that the f values would make a smooth transition to the turbulent regime.

The correlation of equation (17) provided this kind of smooth transition from laminar to turbulent flow, and could also be expressed with pressure drop as an explicit function of velocity in the form:

$$\Delta P = \frac{96\mu}{2g_c D_h^2} LV + \frac{\rho}{8\left(\log \frac{3.7}{e/D_h}\right)^2 g_c D_h} LV^2 \tag{18}$$

which is a convenient form for the Task 3 Analysis.

ANALYTICAL EVALUATION OF TANKAGE SYSTEMS

Tankage System Operation and Weight Parameterization

Prior to the analytical study of the tankage system, the operational aspects of the system were assumed as follows: during LH_2 inflow to the empty tank, an auxiliary fill vent valve operates while filling the annulus and standpipe in low-gravity (10^{-5} g's with the g-vector toward the inflow line), also cooling all tankage and internal structure (Figure 1). The fill vent will be closed after the annulus and standpipe are full, and inflow will continue, nonvented, with pressure rise to 34.5 N/cm^2 (50 psia). During storage for periods of 30 and 300 days, the TVS is assumed to operate continuously, at a g-level of 10^{-5} g's with the g-vector toward the inflow line, and it is assumed that the tank is an adiabatic system at a temperature of 25.2 °K (45.4 °R) with suitable control to maintain a constant tank pressure of 34.5 N/cm^2 (50 psia) with hydrogen liquid and vapor as the only contained fluids. During outflow at constant pressure, the g-level vector of 10^{-5} g's is away from the outflow line.

All six tanks shown in Table I were studied at the following specified flowrates:

- Inflow Rate - 1% (of tank volume)/min
- Outflow Rate - 1 and 0.01% (of tank volume)/min
- TVS Flowrate - 1 and 0.1% (of tank volume)/min

The entire tankage system shown in Figure 1 was examined to determine the weight sensitivity of various system components for a given tank. The components and their functional weight relationship are shown in Table X. There are a number of discrete categories of related weight components. For example, items 5, 7, and 13 are only minor functions of things other than tank size, and thus can be considered fixed for a given tankage system and will not affect the weight optimization. The annulus residual and puddle residual are functions of the standoff distance (annulus gap) and screen type, as is the weight of the wall screen liner; these are parameterized and optimized in the next section. Items 10 and 11, the vent loss (boiloff) from external heat leak and the tank insulation weight, are interrelated and independent from the optimization analysis except as the total vent (boiloff) rate, together with the specified TVS flowrate (1%/minute or 0.1%/minute), affects the TVS heat exchanger weight. The weight analysis for these items will be described in a later section.

The items remaining (2, 6, 8, and 9) are all functions of pump size and will influence the overall system weight optimization. These items will be optimized in the section on determination of pump power requirements.

The final section in the analysis will use the results of the above optimization analyses to determine the optimum system configuration in terms of minimum weight.

TABLE X. - SYSTEM WEIGHT FUNCTIONAL RELATIONSHIPS FOR A GIVEN TANK

Weight component	Weight a major function of	Weight a minor function of
1. Annulus residual	Standoff distance	
2. Standpipe residual	Pump size	
3. Puddle residual	Standoff distance, screen	
4. Wall screen liner	Screen	
5. Wall screen liner supports		Screen
6. Standpipe	Pump size, material	
7. Standpipe supports		Standpipe size
8. TVS pump/motor	Pump size	
9. Boiloff from TVS pump	Pump size, mission time	
10. Boiloff from external heat leak	Mission time, insulation type	
11. Insulation	Mission time, insulation type	
12. TVS heat exchanger	TVS pump flowrate	Standpipe size, boiloff rate
13. Baffles		Tank diameter

Screen Size and Wall Spacing Analysis

To evalute the performance of the wall screen liner system for LH_2 acquisition during outflow, the annulus flow correlation and model developed from the channel flow loss data in the previous section was adapted to a spherical annulus, such as shown in Figure 24. Equation (18) described pressure loss, ΔP, as a function of velocity V, (see symbols):

$$\Delta P = \frac{96\,\mu}{2 g_c D_h^2} LV + \frac{\rho}{8\,(\log \frac{3.7}{e/D_h})^2 g_c D_h} LV^2$$

Equation (18) was integrated around the spherical annulus, shown in Figure 24 where

$$L = \frac{D_T}{2}\, d\phi \qquad (19)$$

in polar coordinates.

Equation (18) became:

$$\Delta P = A \int_{\phi_1}^{\phi_2} V \frac{D_T}{2}\, d\phi + B \int_{\phi_1}^{\phi_2} V^2 \frac{D_T}{2}\, d\phi \qquad (20)$$

CR 140

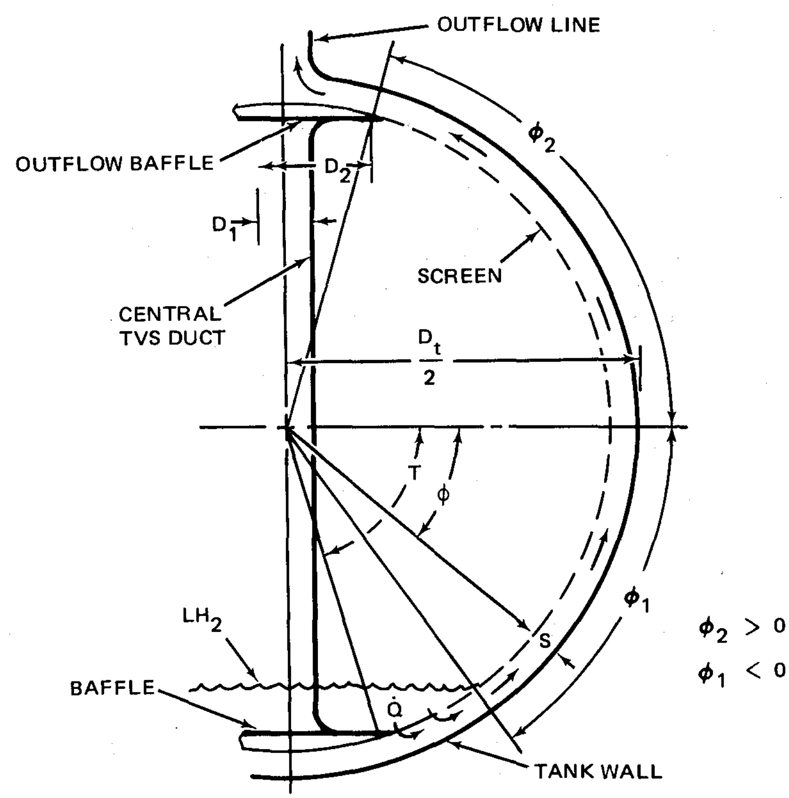

Figure 24. Polar Coordinate System for Spherical Screen Annulus Model During Outflow

where

$$A = \frac{96\,\mu}{2 g_c\, D_h^2}, \qquad B = \frac{\rho}{8\,(\log \frac{3.7}{e/D})^2\, g_c\, D_h}$$

For steady volumetric flow,

$$\dot{Q} \doteq V s \pi D_T \cos\phi = \text{constant} \tag{21}$$

Substituting in equation (20) gave:

$$\Delta P = \frac{A\dot{Q}}{2\pi s} \int_{\phi_1}^{\phi_2} \cos\phi\, d\phi + \frac{B\dot{Q}^2}{2\pi^2 s^2 D_T} \int_{\phi_1}^{\phi_2} \cos^2\phi\, d\phi \tag{22}$$

and integrating gave:

$$\Delta P = \frac{96\,\mu\,\dot{Q}}{2\, g_c\, D_h^2\, 2\pi s} [\sin\phi_2 + \sin\phi_1] + \frac{\rho\,\dot{Q}^2}{2\pi^2 s^2 D_T\, 8\,(\log \frac{3.7}{e/D_h})^2\, g_c D_h}$$

$$\left[\frac{\phi_2}{2} + \frac{\phi_1}{2} + \frac{\sin 2\phi_2}{4} + \frac{\sin 2\phi_1}{4}\right] \tag{23}$$

This equation was, in fact, erroneous, because it was based on rectilinear flow in a cylindrical annulus which was artificially integrated in spherical coordinates in a way which did not properly account for the curvature of the streamlines in the spherical annulus. To obtain the correct expression, the equations of motion must be solved in spherical coordinates with the appropriate boundary conditions. This solution can only be obtained in closed form for very slow laminar flow, i. e., such that the inertial terms in the momentum equation can be neglected. This analysis is shown in Appendix D, and, dimensionally correcting μ in Appendix D to μ/g_c and using the nomenclature of Figure 24, gives the expression:

$$\Delta P = \frac{6\,\mu\,\dot{Q}}{g_c\,\pi s^3} \ln\left[\tan\frac{\phi_2 + \pi/2}{2} \Big/ \tan\frac{\pi/2 - \phi_1}{2}\right] \tag{24}$$

The first term, or laminar portion, of equation (23), with $D_h = 2\,s$ for an annulus, is

$$\Delta P = \frac{6\,\mu\,\dot{Q}}{g_c\,\pi s^3} \left[\sin\phi_2 + \sin\phi_1\right] \tag{25}$$

The difference in the two equations is confined to the final trigonometric terms, which, for comparison, are plotted with $\phi_2 = \phi_1$ in Figure 25. The functions are essentially equal at angles less than $\pi/6$ radians, but diverge widely at angles near $\pi/2$ radians. At angles of $5\pi/12$ radians, which are typical values for our spacing analysis discussed below, the correct value is twice the previously modeled value. While the correct function could be substituted in the laminar component of equation (23), no equivalent expression exists for the turbulent component of equation (23).

As an approximation, it was assumed that the first part of equation (23) accounts for viscous flow (that which ignores inertia terms in the momentum equation) while the second part of equation (23) accounts for the inertial effects. At the same time the ratio

$$\frac{\ln\left[\tan\left(\frac{\phi_2 + \pi/2}{2}\right)\Big/\tan\left(\frac{\pi/2 - \phi_1}{2}\right)\right]}{\sin\phi_2 + \sin\phi_1} \tag{26}$$

corrects for the geometric conditions of curvature of the streamlines in laminar flow. Streamlines would also be present in turbulent flow, even though velocity-dominated turbulence would be superimposed on the streamlines. Curvature of the turbulent streamlines because of geometry should require the same kind of pressure correction. Therefore, it was assumed that the entire pressure loss described in equation (23) be multiplied by the geometry ratio of equation (26). This would give a reasonable approximation of the pressure loss in the spherical annulus. In the straight annulus of tanks with an L/D ratio above 1, the original correlation for a cylindrical annulus (without the above correction) was used. It should also be noted that the spherical annulus flow loss is only part of the total flow loss which includes static and dynamic head loss and loss through the screen. Thus, errors in the annulus flow loss would be less significant relative to the total loss. Further, the screen spacing analysis described below indicated that screen flow-through loss, rather than annulus loss, was strongly dominant for most configurations studied.

Expressions for static head loss, dynamic head loss, and residual were also derived. Referring to Figure 24, the configuration shown is the worst case, since the static head is maximum, the channel length is maximum, and the screen flow-through area is minimum. This situation would occur at the end of outflow, with the tank nearly empty, and screen breakdown about to occur at the outflow baffle. The TVS flow case would be exactly reversed, the g-vector reversed, and the flow going from the outflow baffle to the other baffle. Because screen flow-through loss does not occur, the TVS case is not as severe as the outflow case.

The g-level during outflow was specified as 10^{-5} g's. The static head loss, H_g, was thus the g-level times the length from outflow baffle to liquid surface, or:

$$H_g = 10^{-5}\left[\left(\frac{L}{D_T} - 1\right) D_T + \left(\sin\phi_1 + \sin\phi_2\right)\left(D_T/2 - s\right)\right] \tag{27}$$

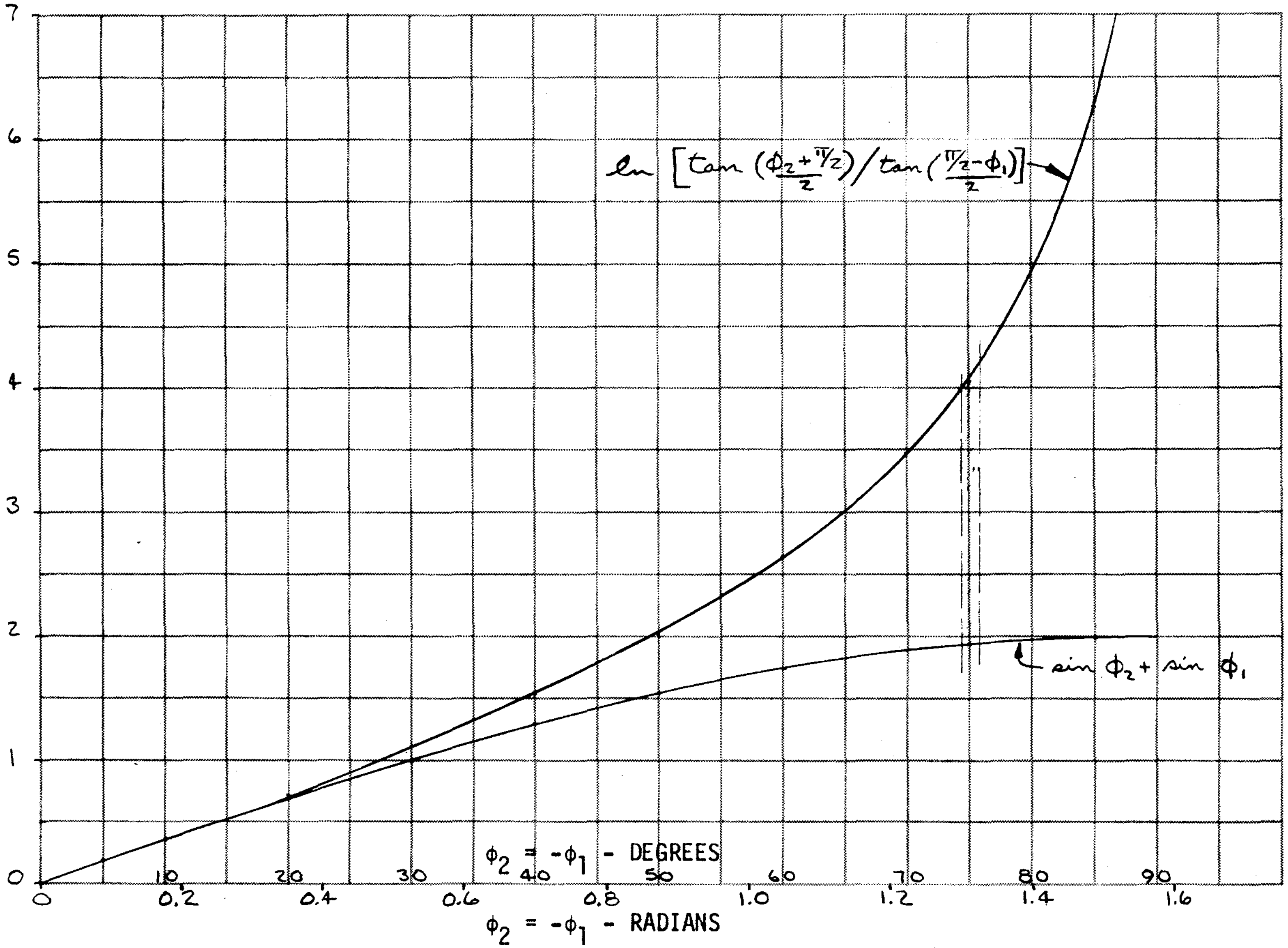

Figure 25. Comparison of Trigonometric Functions

Since breakdown would occur at the screen next to the outlet baffle, the dynamic head loss, H_d, at the outlet baffle was determined by the velocity in the annulus at the outlet baffle location, or:

$$H_d = V^2/2g_c \qquad \text{where} \qquad V = \frac{\dot{Q}}{\pi D_2 s} \tag{28}$$

The pressure loss through the screen, H_s, was determined from the flow loss correlation described in equation (7) and Table VIII.

$$H_s = AV_1 + BV_1^2 \tag{29}$$

where A and B are the experimentally determined coefficients from Table VIII, and V_1 is the velocity through the screen, which depends on the flowrate and the spherical segment screen area, A, where $V_1 = \dot{Q}/A$ and:

$$A = 2\pi (\sin T - \sin \phi_1)(D_T/2 - s)^2 \tag{30}$$

The head loss in the annulus was added to the screen flow-through loss, the dynamic head loss, and the static head loss to give the total loss. The screen bubble point was divided by the total head loss to give the safety factor.

The residual in the tank was made up of the annulus residual, the standpipe residual, and the puddle residual, i. e., the residual in the tank bottom between the standpipe and annulus. The annulus residual, X_1, for a thin annulus, was fixed for a given annulus thickness, s, and is:

$$X_1 = \left(\frac{L}{D_T}\right) s \, \pi \, D_T^2 \tag{31}$$

The standpipe residual, X_2, was fixed for a given standpipe diameter, D_1 and is:

$$X_2 = \left[\left(\frac{L}{D_T}\right) D_T - 2s\right] \frac{\pi D_1^2}{4} \tag{32}$$

The puddle residual varied with the angle ϕ_1 and was the volume in the spherical segment between the standpipe and annulus. A flat interface was assumed for convenience, and gives conservative results, since with a curved interface with wetting LH_2, the residual would probably be less, depending on the interface curvature. (In practice, for our analysis cases, the puddle residual was very small, as will be discussed below, so that this conservatism did not materially affect the study conclusions.) The puddle residual, X_3, is:

$$X_3 = \frac{\pi}{6} Y \left(3 Z^2 + Y^2\right) - \frac{\pi D_1^2}{4} Y \qquad (33)$$

where

$$Y = (D_T/2 - s)(1 - \sin \phi_1)$$

and

$$Z = (D_T/2 - s)(\cos \phi_1)$$

The computations were organized as follows: first, the fluid properties of density and viscosity were input, then the tank parameters-volume, L/D_T, standpipe, and baffle diameters were input. Next, the screen characteristics of bubble point, flow-through coefficients (A and B in equation (29)), and roughness dimension, e, were input. Next, the annulus gap (screen standoff distance) and flowrate were input. The program computed and printed the baffle angle, T, and asked for an input of ϕ_1 which had to be less than T to give a positive flow-through area (Figure 24) plus an input flag to instruct the program as to whether the next case would be with a new angle ϕ_1, a new annulus gap, a new screen, or a new tank, baffle, and standpipe configuration. The program then computed and printed tank diameter, submerged screen length, standpipe residual, annulus residual, puddle residual, total residual, percent residual, static head loss, dynamic head loss, screen flow-through head loss, annulus head loss, total head loss, and safety factor. The program was coded for use on the MDAC Time-sharing Computer System and was straightforward in operation: for a given tankage, screen, annulus gap, and flowrate combination, a variation in ϕ_1 gave a variation in puddle residual and safety factor which could then be crossplotted to determine system sensitivities.

The six tanks selected for the analysis were listed in Table I, and will be identified subsequently by volume over L/D ratio, i.e., 5,000/4. Each tankage system was analyzed to determine the choice of standpipe and baffle diameters. Since the standpipe residual is a fixed value which does not affect the screen wall spacing analysis sensitivities, the standpipe sizing was ignored, since it will be optimized along with the pump in the next section. The baffles at each end of the standpipe (Figure 1) were arbitrarily sized at about 1/4 the tank diameter as shown in Table XI. Since the outflow baffle is also part of the tank manhole for TVS system access, Table XI indicates that the arbitrary sizing results in reasonable baffle/manhole sizes and in very small minimum puddle residuals due to baffle size.

Each tank was analyzed with all 10 screens and with annulus gaps from 1% to 5% of tank volume, as shown in Appendix E. The screen performance parameters are summarized in Table XII. Typical results of this analysis, for the 5,000/4 tank, are shown in Figures 26 and 27. Figure 26 shows the performance of the 10 screens in terms of safety factor and puddle residual for the 1% annulus gap (the specified minimum). Since the avowed purpose of the ultimate tradeoff study was to minimize system weight, it was logical to select screens with adequate performance at the minimum annulus gap.

TABLE XI. - TANKAGE SYSTEM AND BAFFLE PARAMETERS

Tank ID	Tank diameter, m (ft)	Upper and lower baffle diameter, m (ft)	Minimum puddle residual, %
5,000/4	3.66 (12.02)	0.91 (3.0)	0.0104
500/4	1.70 (5.58)	0.46 (1.5)	0.014
500/2	2.21 (7.25)	0.55 (1.8)	0.022
500/1	3.00 (9.85)	0.73 (2.4)	0.052
50/2	1.03 (3.37)	0.27 (0.9)	0.03
50/1	1.39 (4.57)	0.37 (1.2)	0.07

For system/screen comparison, a safety factor of 2 was chosen as representative of adequate performance. Figure 26 shows that at a 1% annulus gap, only the 325 x 2,300 and 200 x 1,400 screens gave a safety factor of 2. Since the 325 x 2,300 screen was substantially lighter than the 200 x 1,400 screen, and had a higher bubble point (Table XII) it was the logical choice. Note that the puddle residuals obtained were very small and in fact insignificant compared to the 1.416 m^3 (50 ft^3) residual in the 1% annulus.

From Table XII, there are only two screens lighter in weight than the 325 x 2,300 screen: the 500 x 500 and 150 x 150 screens. The 500 x 500 screen is extremely flimsy, while the 150 x 150 screen appears to have reasonable structural rigidity, perhaps comparable to the 325 x 2,300 screen. Figure 27 shows that at 2% annulus gap, the 150 x 150 screen had comparable performance to the 325 x 2,300 screen in the 1% annulus. Thus, for the 5,000/4 tank with 168.5 m^2 (1,814 ft^2) of screen surface area, the 150 x 150 screen would save 32 kg (71 lb) of screen weight, but at a cost of 1% or 91 kg (200 lb) in annulus LH_2 residual weight – a net increase of 58.5 kg (129 lb) in total weight – assuming comparable structural qualities. The 500 x 500 screen, in a 1.20% annulus, would have comparable performance to the 325 x 2,300 screen in a 1% annulus, and the 18 kg (40 lb) increase in annulus LH_2 residual weight would be more than offset by the 62 kg (136 lb) saving in screen weight – for a net decrease of 44 kg (96 lb) in system weight. However, the extreme flimsiness of the 500 x 500 screen would certainly require some sort of increased structural backup material for installation in a flight vehicle, and the weight of this increased backup material would certainly exceed the 44 kg (96 lb) of weight gained. Thus, for the 5,000/4 tank, the 325 x 2,300 screen would be the logical choice on the basis of weight and performance

Appendix E indicates similar results for the 500/4 tank, where 5 screens have adequate performance; for the 500/2 tank, where 8 screens have ade-

TABLE XII. - SCREEN PERFORMANCE PARAMETERS

Screen	Bubble point, m (ft) LH_2	Flow-through parameters		Roughness, ϵ cm (in.)	Weight, kg/m^2 ($lb/100\ ft^2$)
		A	B (ft)		
325 x 2,300	0.4815 (1.580)	1.14	0.6919 (2.27)	0.00127 (0.0005)	0.532 (10.9)
200 x 1,400	0.3377 (1.108)	0.885	0.6126 (2.01)	0.00203 (0.0008)	0.908 (18.6)
720 x 140	0.1767 (0.580)	0.162	0.2627 (0.862)	0.00546 (0.00215)	0.693 (14.2)
165 x 800	0.1228 (0.403)	0.108	0.0805 (0.264)	0.00254 (0.001)	0.796 (16.3)
50 x 250	0.0682 (0.224)	0.045	0.0631 (0.207)	0.00572 (0.00225)	1.133 (23.2)
24 x 110	0.0336 (0.1105)	0.0165	0.1554 (0.51)	0.01334 (0.00525)	3.1 (63.5)
500 x 500	0.1646 (0.540)	0.0554	0.04267 (0.140)	0.00254 (0.001)	0.166 (3.4)
150 x 150	0.0460 (0.151)	0.0101	0.01347 (0.0442)	0.0066 (0.0026)	0.342 (7.0)
60 x 60	0.0230 (0.0754)	0.00585	0.02761 (0.0906)	0.01905 (0.0075)	1.167 (23.9)
40 x 40	0.0170 (0.0559)	0.00287	0.01497 (0.0491)	0.0254 (0.01)	1.362 (27.9)

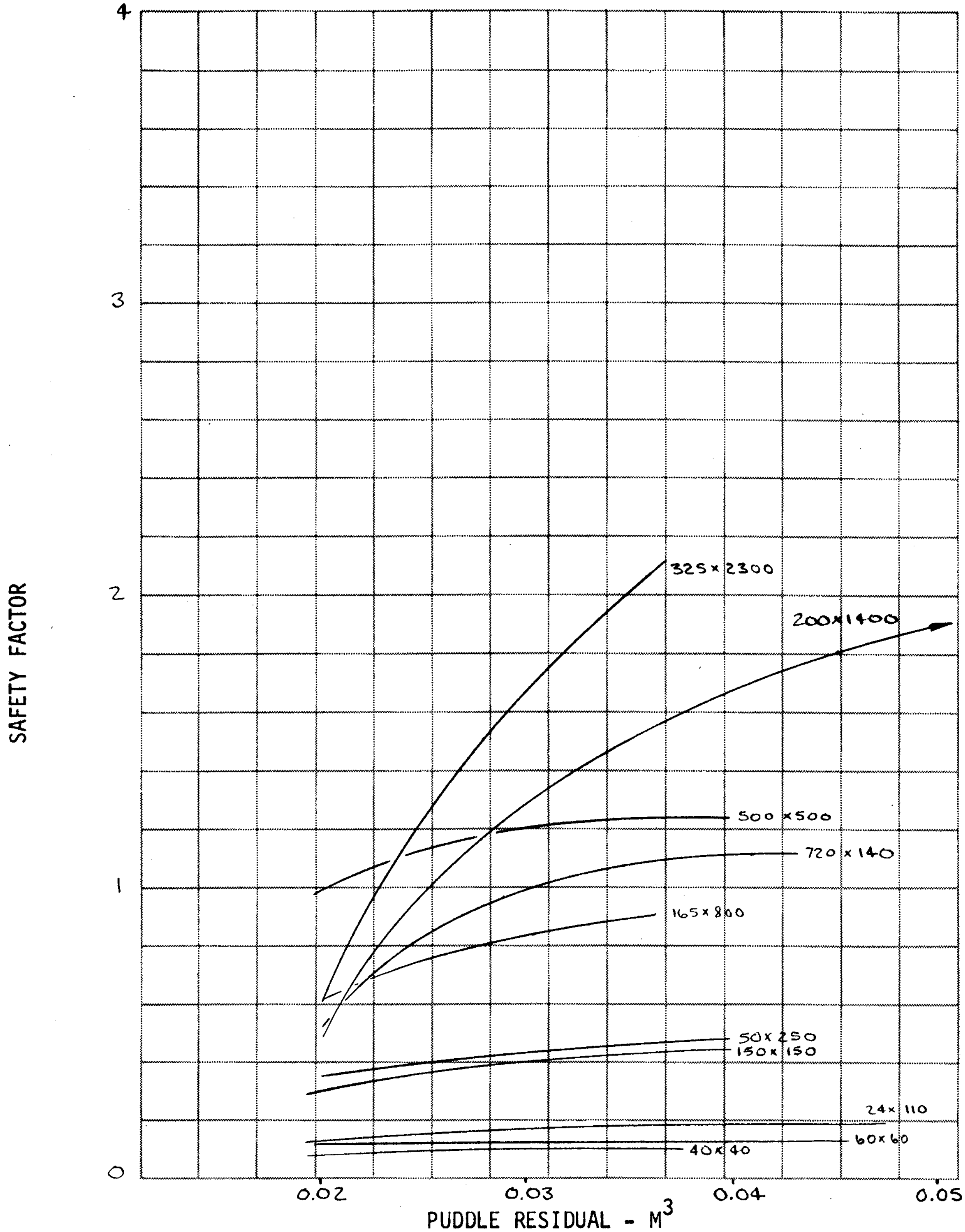

Figure 26. Screen Performance in 1% Annulus for 5,000/4 Tank

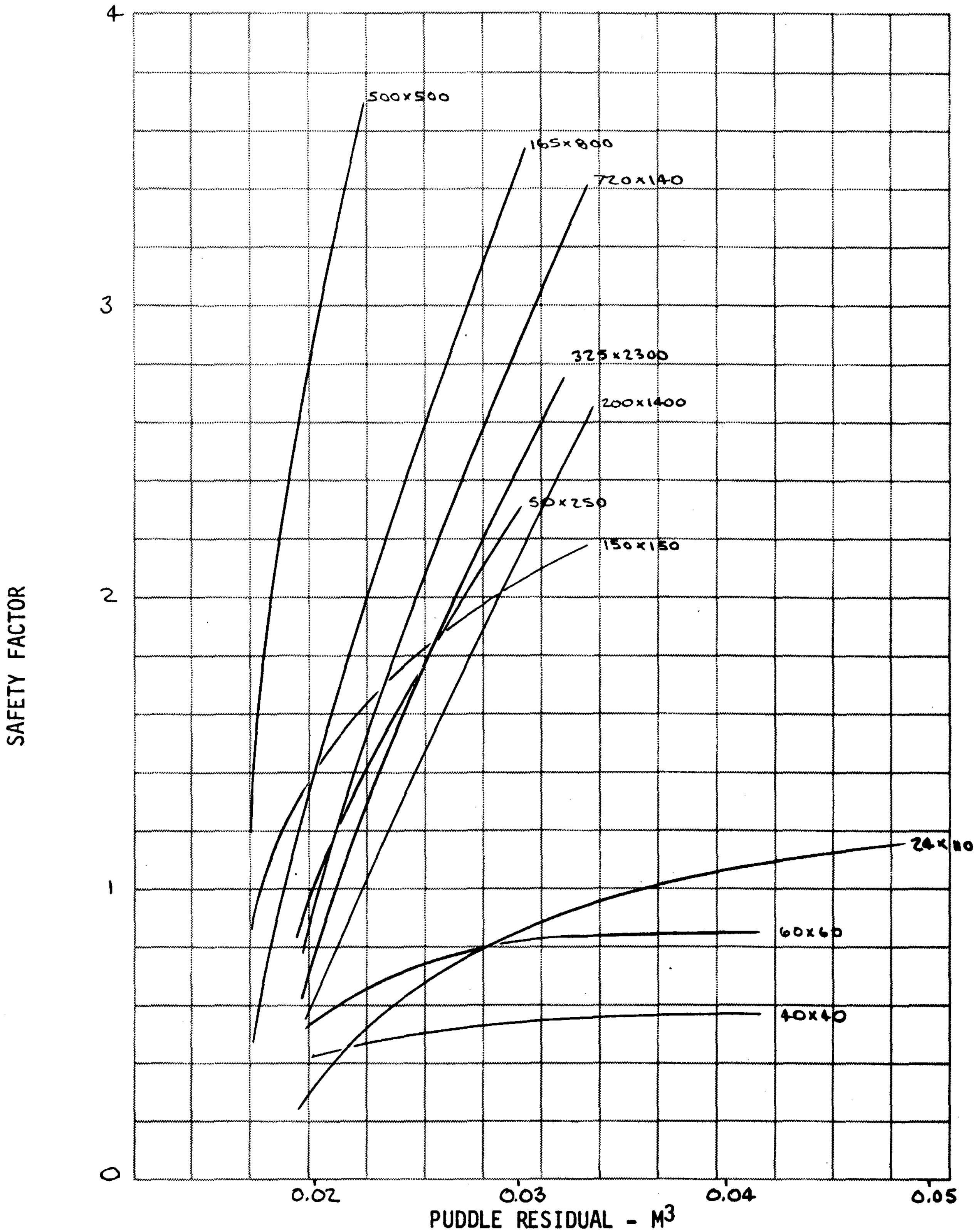

Figure 27. Screen Performance in 2% Annulus for 5,000/4 Tank

quate performance; while all 10 screens would have adequate performance for the remaining tanks. The weight savings using the 150 x 150 screen instead of the 325 x 2,300 screen ranged from 5.9 kg to 1.1 kg (12.9 lb to 2.5 lb) (which were not significant weight savings from a system standpoint) while sacrificing an order of magnitude in bubble point.

The analysis described above was for the maximum outflow rate of 1% of tank volume/minute. At 0.01% outflow rate (or at 0.1% TVS flowrate) there was absolutely no sensitivity to screen type or annulus gap; all 10 screens had adequate performance at the minimum 1% annulus gap. It is probably not possible to significantly reduce the annulus gap below 1%, since the 1% annulus varies from 0.84 cm (0.33-in.) in the 141.6-m^3 (5,000-ft^3) tank to about 0.23 cm (0.09 in.) in the 1.416-m^3 (50-ft^3) tank; these are small values from a system fabrication standpoint. It is clear that at this g-level, flowrate, and annulus gap, the tankage systems flow characteristics were such that a meaningful tradeoff analysis in terms of residual, annulus gap, and performance was not possible.

Therefore the analysis was extended to examine the effects of high outflow rate (3% tank volume/minute) and high g-levels (10^{-2} to 10^{-4} g's) on system performance. Only the high L/D tanks (5,000/4, 500/4, and 50/2) were analyzed because these were generally the more severe cases. Figure 28 shows the effect of increasing the flowrate to 3%/minute on the performance of the 325 x 2,300 screen in the 5,000/4 tank. The annulus gap had to be increased to 2% to achieve adequate performance, and even then, increased residual resulted. The results for the other tanks are also shown in Appendix E.

A similar trend occurred when the g-level was increased from 10^{-5} g's to 10^{-2} g's, as shown also in Appendix E. At 10^{-2} g's, the 325 x 2,300 screen no longer had adequate performance in the 1% gap in the 5,000/4 tank, and the annulus gap had to be increased. In Figure 29, the annulus gap is 2% in the 5,000/4 tank. The 325 x 2,300 screen had adequate performance at all g-levels, but the 150 x 150 screen did not have adequate performance at even 10^{-4} g's. If the annulus gap was increased to 3%, however, the 150 x 150 screen would have adequate performance at even 10^{-3} g's. At 10^{-2} g's, the hydrostatic head in the 5,000/4 tank exceeded the bubble point of the 150 x 150 screen by a factor of 3, so that it could not practically be used.

The conclusion reached from the study of increased flowrate and g-levels is that it is even more important that the lightest high performance (high bubble-point) screen (325 x 2,300) be used. While the lighter 150 x 150 screen may have adequate performance for minor deviations from the original design conditions, it does not have the bubble-point reserve capacity to handle extremes of flowrate or g-level with adequate performance.

Determination of Pump Power Requirements

The standpipe together with the annulus, remains full of LH_2 following outflow. This LH_2 represents a residual weight penalty which it would be desirable to minimize. However, it was noted that arbitrary reduction in

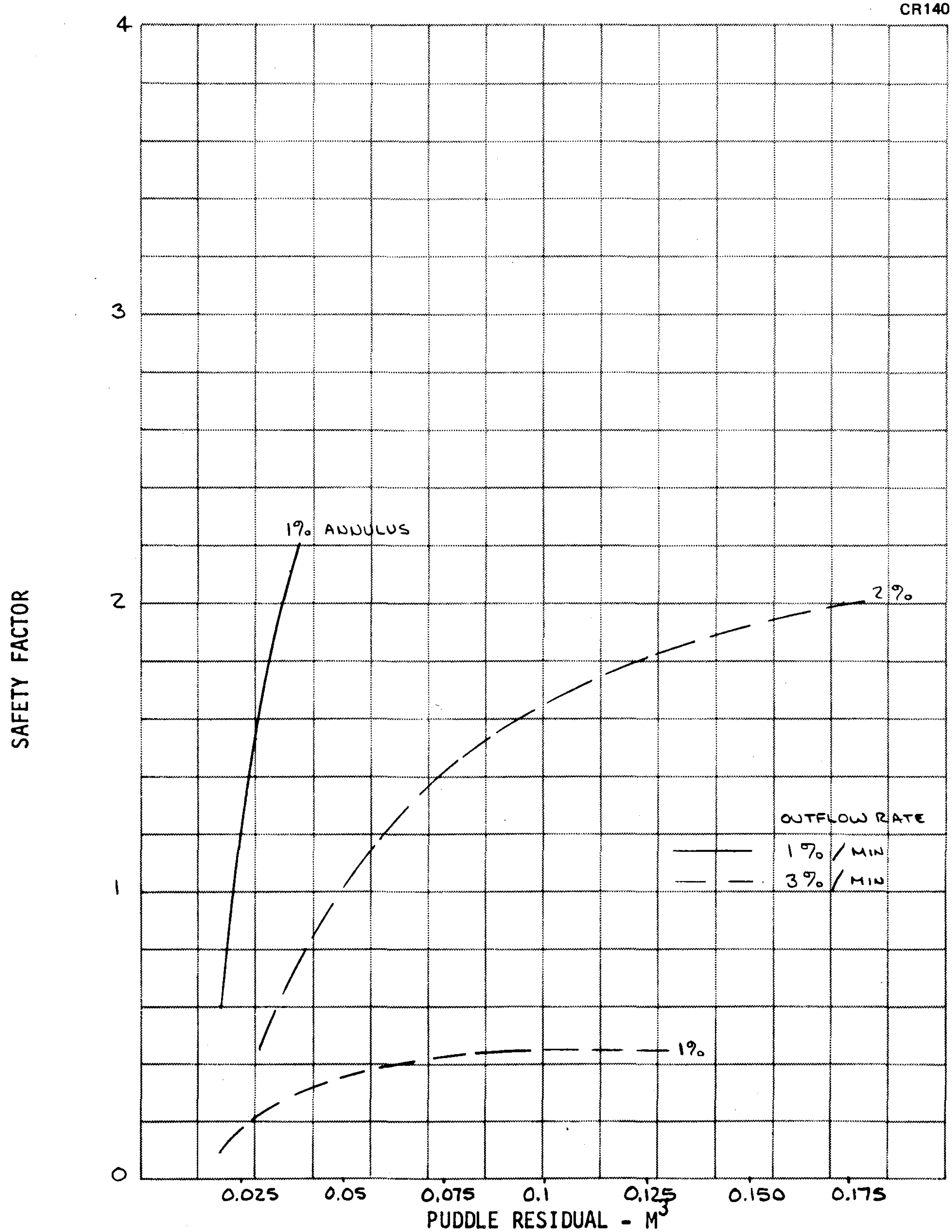

Figure 28. High Outflow Rate Performance of 325 x 2,300 Screen in the 5,000/4 Tank

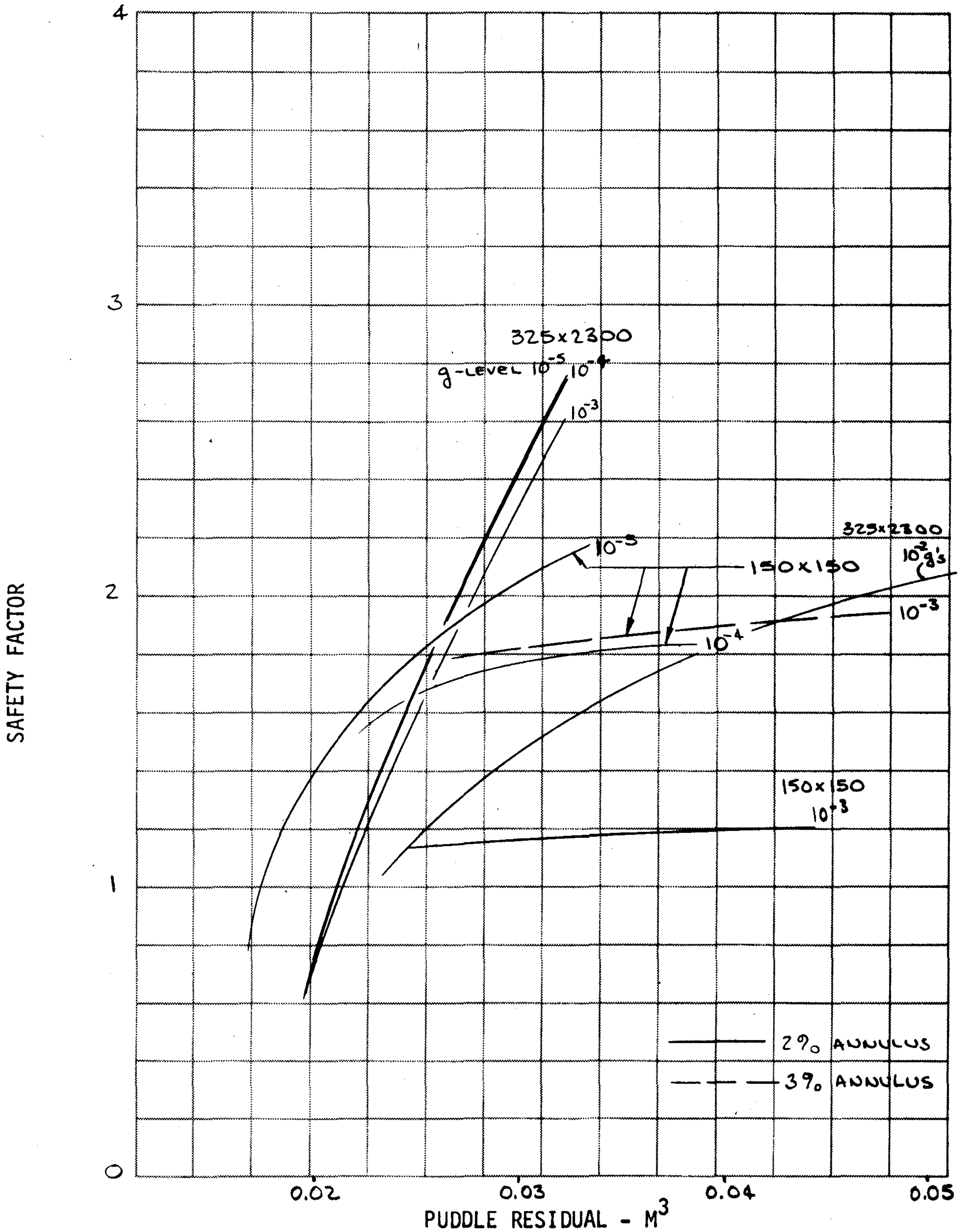

Figure 29. High G-Level Performance of Both Screens in the 5,000/4 Tank

standpipe size, which would decrease the weight of the standpipe and its residual, would also increase the pressure drop down the standpipe, which in turn would increase the power requirements of the TVS pump. This increased power requirement would lead to an increase in TVS pump/motor weight and in increased "boiloff" from the TVS pump/motor inefficiency.

Therefore, it was clear that there was an optimum standpipe diameter which would minimize the combined weight of standpipe, standpipe residual, and pump boiloff due to pressure loss in the standpipe. The pump boiloff due to pressure loss around the annulus was not directly dependent on the standpipe diameter, did not enter this optimization, and will be accounted for later in the analysis. Similarly the pump/motor weight was a very small value, so that it too was ignored in the optimization, and will be accounted for later.

The weight of the standpipe residual, in terms of the standpipe diameter, D_s, and length, L, is (see symbols):

$$W_1 = \frac{\pi D_s^2 L}{4} \rho \qquad (34)$$

The weight of the standpipe depends on the thickness of the standpipe and the material. Since there is essentially no pressure load on the standpipe, the thickness criterion used was that specified by NASA-MSFC as minimum handling gage for ducting in the Space Shuttle. The thickness in meters (inches) is:

$$\begin{aligned} t_{MIN} &= 0.000558 + 0.024\, D_s \\ (t_{MIN} &= 0.022 + 0.024\, D_s) \text{ for Stainless Steel} \\ t_{MIN} &= 0.00076 + 0.036\, D_s \\ (t_{MIN} &= 0.030 + 0.036\, D_s) \text{ for Aluminum} \end{aligned} \qquad (35)$$

Multiplying the thickness by the density of Steel and Aluminum gives, for standpipe weight:

$$W_2 = \pi D_s L (A + BD_s) \qquad (36)$$

where

$A = 4.41, \quad B = 190$ for Stainless Steel

$A = 2.1, \quad B = 99.5$ for Aluminum

The weight of the "boiloff" due to the pump power is equal to the power dissipated in the LH_2 times the mission time and divided by the LH_2 heat of vaporization. It was straightforward to show that essentially all of the input power to the pump/motor is dissipated to the LH_2, causing "boiloff" (see Appendix F). Therefore, the "boiloff" weight is

$$W_3 = \frac{\dot{Q} \rho H}{\eta h_{fg} J} t \tag{37}$$

where t is the mission time, h_{fg} is the heat of vaporization, J is the energy conversion, 0.102 kg-m/joule, and η is the overall efficiency. The fluid power is $\dot{Q} \rho H$, where $\dot{Q}$ is the volumetric flowrate and H is the pressure drop (in m of LH_2) down the standpipe. This head loss is:

$$H = f \frac{L}{D_s} \frac{V^2}{2g_c} \tag{38}$$

In terms of the volume flowrate, $\dot{Q} = VA$, or

$$V = \frac{\dot{Q}}{A} = \frac{\dot{Q} \cdot 4}{\pi D_s^2} \tag{39}$$

The friction factor, f, is a function of Reynolds number, R. For our flow conditions, the flow is turbulent and the standpipe hydraulically smooth so that the correlation of Blasius (ref. 24) is suitable, or:

$$f = \frac{0.316}{R^{0.25}} \tag{40}$$

or since

$$R = \frac{4 \rho \dot{Q}}{\pi \mu D_s}, \qquad f = \frac{0.316 D_s^{0.25}}{(4 \rho \dot{Q}/\pi \mu)^{0.25}} \tag{41}$$

As shown in Figure 30, the Blasius correlation is accurate to within 5% for R from 3,000 to 300,000.

Combining equations (38), (39), and (41) gives:

$$H = \frac{0.316 L (\dot{Q} \cdot 4/\pi)^2}{(4 \rho \dot{Q}/\pi \mu)^{0.25} 2g_c D_s^{4.75}} \tag{42}$$

The total weight, from equations (34), (36), (37), and (42) is:

$$W = \frac{\pi D_s^2 L}{4} \rho + \pi D_s L (A + BD_s)$$
$$+ \frac{\dot{Q} \rho t}{\eta h_{fg} J} \left(\frac{0.316 L (\dot{Q} \cdot 4/\pi)^2}{(4 \rho \dot{Q}/\pi \mu)^{0.25} 2g_c} \right) \frac{1}{D_s^{4.75}} \tag{43}$$

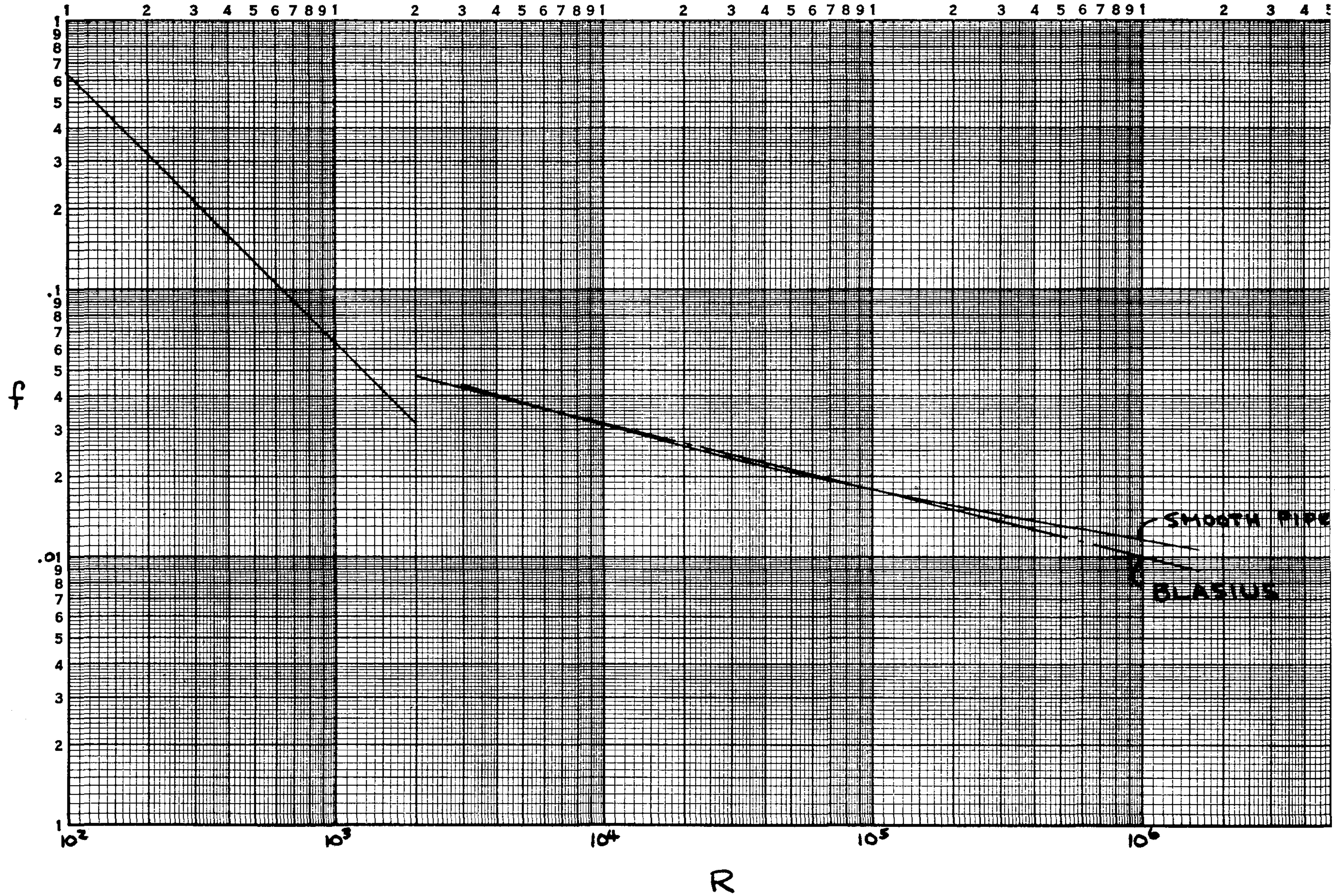

Figure 30. Comparison of Smooth Pipe and Blasius Friction Correlations

Differentiating with respect to D_s and equating to zero gives:

$$2\pi\ L\ \left(\frac{\rho}{4} + B\right)\ D_s^{6.75} + \pi LA\ D_s^{5.75}$$

$$-4.75\left[\frac{\dot{Q}\rho t\ (0.316)\ L\ (\dot{Q}\cdot 4/\pi)^2}{\eta\ h_{fg}\ J\ (4\rho\dot{Q}/\pi\mu)^{0.25}\ 2\ g_c}\right] = 0 \qquad (44)$$

All of the parameters of equation (44) are known except D_s and η. Equation (44) was solved for D_s using the Newton-Raphson iteration technique for various values of η and the results are shown for the six tanks and two values of TVS flowrate (1%/minute and 0.1%/minute) in Appendix E, and typically as the nearly horizontal straight lines in Figure 31.

To determine the value of D_s which minimized system weight, the correct value of η was determined. This value of η was determined from the total pump power, not just that required to overcome the pressure loss in the standpipe. To circulate the TVS flow, the pump must provide dynamic head, hydrostatic head, and enough head to overcome frictional losses in the screen annulus and the standpipe. Actually, the hydrostatic head is recovered and converted to overcoming friction loss in the standpipe, but for conservatism this effect was ignored since the hydrostatic head in these cases was very small. Therefore, the total fluid power (P_f) required is

$$P_f = \dot{Q}\rho\ (H_s + H_g + H_d + H_a) \qquad (45)$$

To determine the overall efficiency, knowing the fluid power, the pump was thoroughly evaluated. The basis of this evaluation was the definitive study of cryogenic mixers by Poth, et al (ref. 25).

One of the basic characteristic parameters associated with pump design and applications is the specific speed. The specific speed, N_s, is defined in this study as

$$N_s = \frac{(n,\ \text{rpm})\ (G,\ \text{gpm})^{1/2}}{(H,\ \text{feet})^{3/4}} \qquad (46)$$

The specific speed as defined is dimensionless but an inconsistent set of units is used.

A constant to account for unit conversion yields a consistent definition of the specific speed, N_s; the specific speed thus defined is

$$N_s' = N_s/2815 \qquad (47)$$

where

$$N_s' = \frac{(\Omega,\ \text{rad/sec})\ (\dot{Q},\ \text{m}^3/\text{sec})^{1/2}}{(g_c H,\ \text{m}^2/\text{sec}^2)^{3/4}}$$

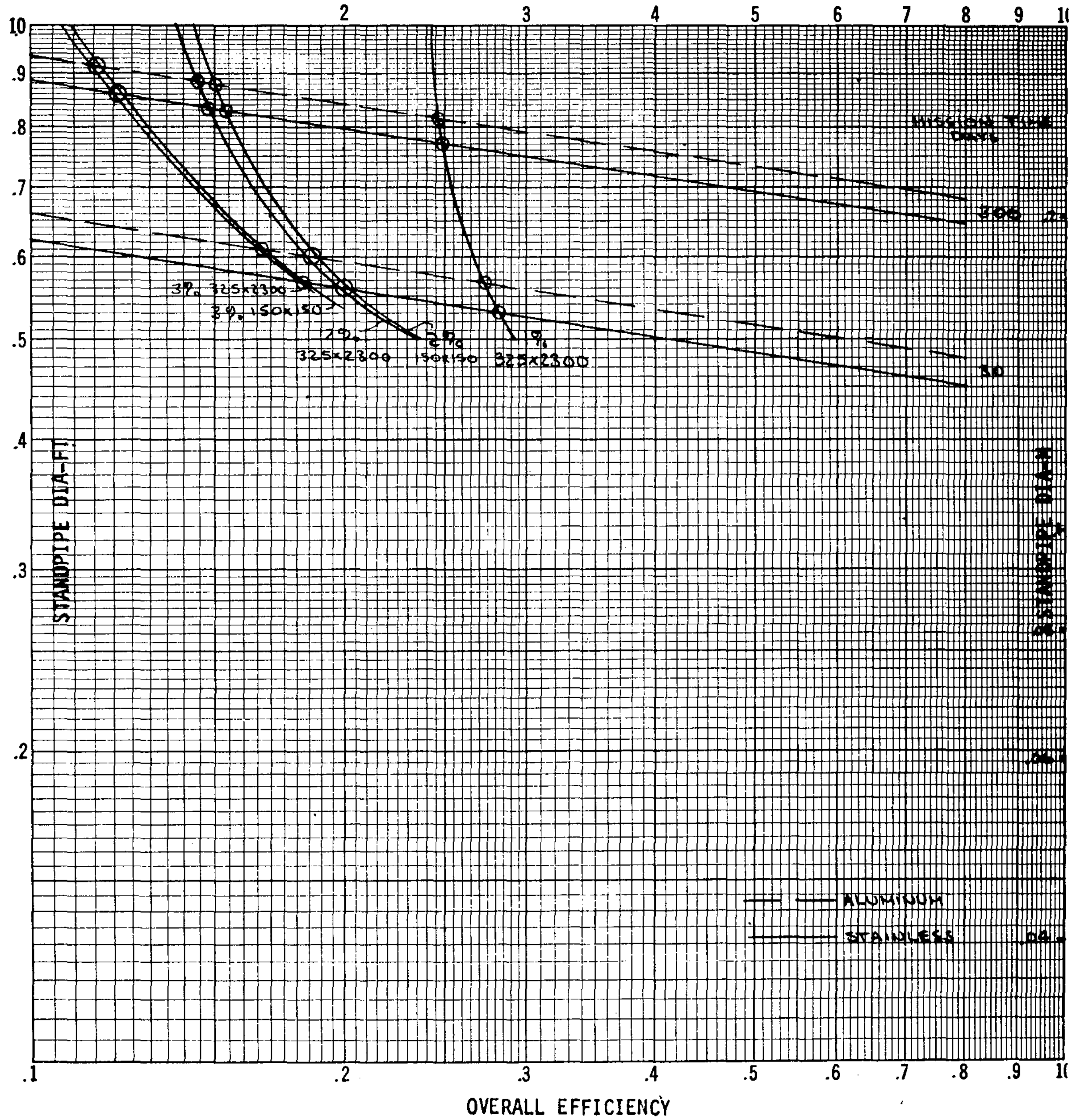

Figure 31. Standpipe Optimization at 1%/Min TVS Flow in the 5,000/4 Tank

N_s' was used when analytical derivations were required. The results are presented in terms of N_s by the use of the appropriate conversion constant, 2,815.

The specific speed characterizes the type of pump required, as shown in Figure 32. For our applications, requiring relatively large flowrate and low pressure rise, the axial flow pump with a high specific speed (>8,000) was the proper choice.

The head coefficient, ψ, is a dimensionless pressure (head) rise of the pump. The head coefficient, ψ, is defined as

$$\psi = \frac{gH}{\Omega^2 \, r_B^2} \tag{48}$$

where r_B is the blade radius.

The pump pressure rise as a function of flowrate is a convenient way to present pump output performance. In nondimensional form, the pressure rise across the pump as a function of flowrate can be represented in terms of the head coefficient ψ and the flow coefficient, ϕ. The flow coefficient, ϕ, can be defined in terms of the specific speed, the head coefficient and the geometry coefficient, ξ, as

$$\phi = (N_s/2815)^2 \; \psi^{3/2}/\pi \, \xi_2 \tag{49}$$

where

$$\xi_2 = A_2/\pi r_B^2$$

and A_2 is the axial flow cross-sectional area of the pump. A vane-axial pump usually has a single rotor stage with a deswirl-stationary stage. The flow into the pump is usually assumed to have no prerotation. As a result, an approximate relation exists between the head coefficient and the flow coefficient.

$$\psi = 1.0 - \phi \cot \beta_2 \tag{50}$$

where β_2 is the rotor stage exit flow angle. Eliminating ϕ from the above equation, a relation between N_s and ψ is obtained so that

$$N_s = 2815 \, (\pi/\cot \beta_2)^{1/2} \left[1 - (r_h/r_B)^2 \right]^{1/2} \left(\frac{1-\psi}{\psi^{3/2}} \right)^{1/2} \tag{51}$$

where r_h is the hub radius.

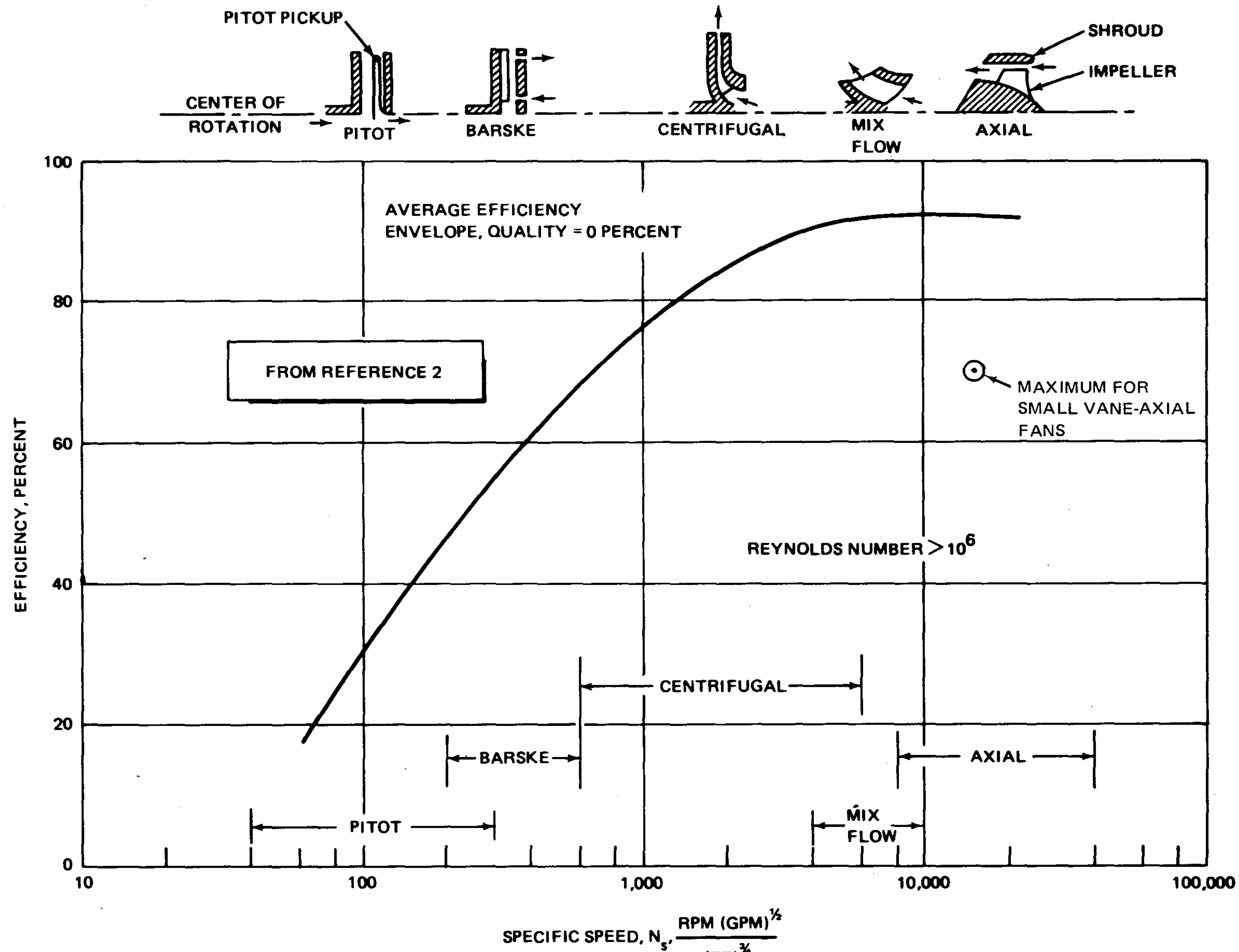

Figure 32. Efficiency of Mixer Designs

Typical values for the rotor stage exit angle, $\beta_2 = 0.366$ radian (21°), and for $r_h/r_B = 0.7$, so that:

$$\psi = \left[\frac{4.88 \times 10^6 \, (1-\psi)}{N_s^2} \right]^{2/3} \tag{52}$$

Also, from equation (48):

$$D_B = 2 \, r_B = 2 \left(\frac{gH}{\Omega^2 \psi} \right)^{1/2} \tag{53}$$

With these equations, the characteristics of the pump were determined. There were two ways chosen to parameterize the performance of the pump for this study. One was to fix the specific speed at the maximum value possible for efficient vane-axial fans, 16,000 (ref. 26), and allow the RPM to vary. With an AC motor, the RPM could be varied by altering AC frequency or poles in the motor or by gearing down the motor speed. The advantage of this method was that the fluid efficiency of the pump could be assumed because the specific speed and Reynolds number of the pump are at normal values. The efficiencies of various pumps are shown in Figure 32. For axial pumps, the efficiency shown is 92% at a Reynolds number of 10^6, however, it is highly probable that the efficiencies shown are for very large machines. As pumps get smaller, fluid efficiency invariably suffers. Therefore it was assumed, for the very small vane-axial pumps required in this study that the maximum fluid efficiency was 70% at a specific speed of 16,000 (ref. 26). The disadvantage of fixing specific speed would be that for low head requirements, the rotational speed was of necessity low, leading to larger pump diameter and heavier pump weight, however, the pump diameters turned out to be very close to the standpipe diameters, which was desirable from a system integration standpoint.

The other pump parameterization method was to fix the pump rotational speed at a value suitable for a normal electric motor, say 100 π radians/sec (3,000 rpm) and allow the specific speed to vary. Unfortunately, for low head rise machines the resulting specific speed was very high, approaching 10^5 to 10^6, and the performance of such high specific speed machines is invariably severely degraded. In fact, the efficiency of axial pumps drops rapidly at specific speeds above 20,000 (ref. 26). Therefore, because use of this pump parameterization method resulted in uncertain (but very low) efficiency definition, it was not used in the final optimization analysis.

Estimates of the overall electric pump motor efficiency as a function of fluid power were required to determine the weight attributable to the pump/motor subsystem. Data were obtained from Stark (ref. 3) and Sterbentz (ref. 2) in previous studies conducted in this area. The results are shown in Figure 33 for both AC and brushless DC motors.

Based on the data available, the DC brushless motors have a higher efficiency, especially at low fluid power. No actual data on the brushless DC motor operating in liquid hydrogen were available, whereas data for AC motor efficiency were obtained from actual LH_2 pumps (ref. 26). As a

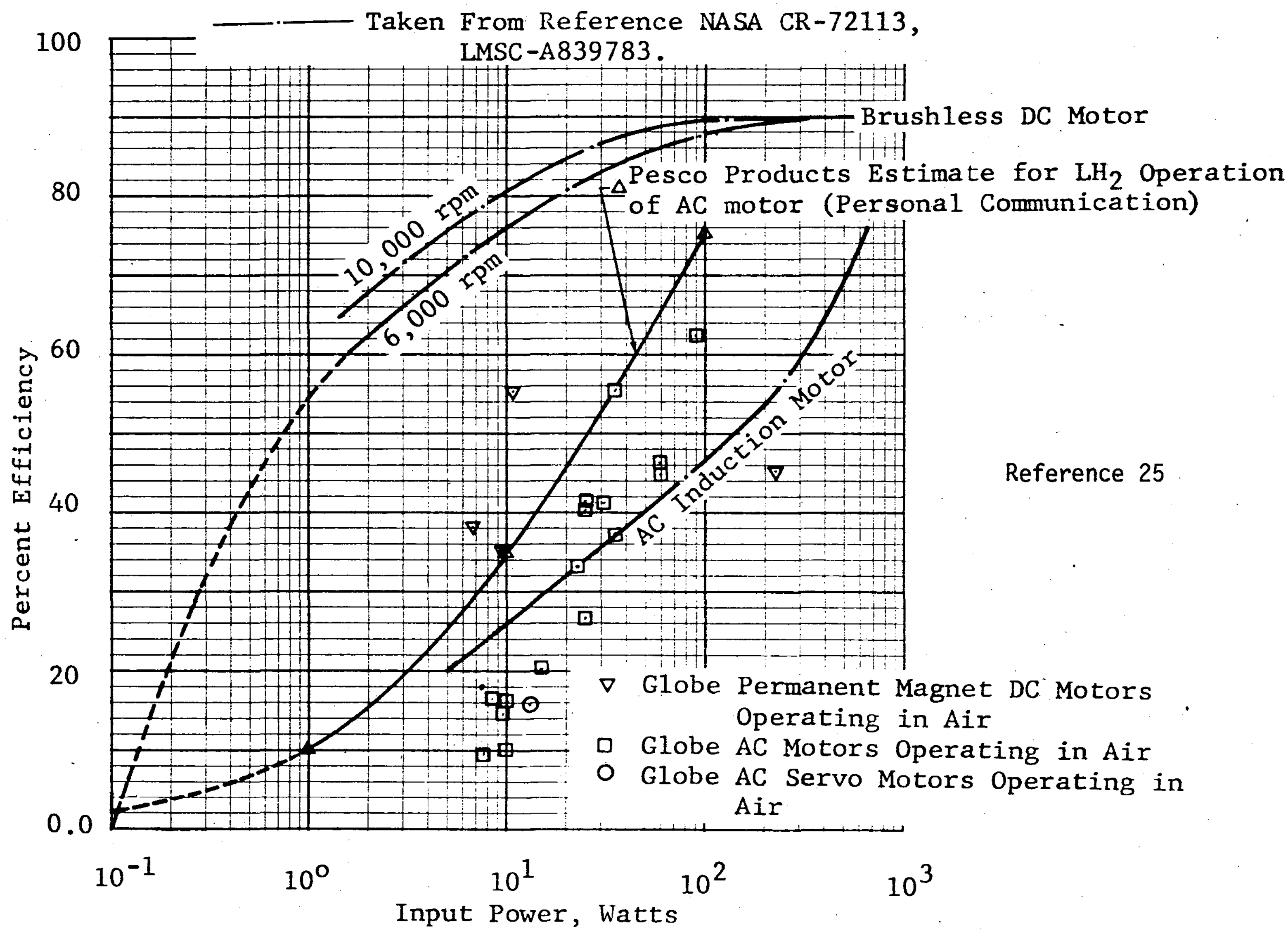

Figure 33. Comparison of Electric Motor Efficiencies

result, the AC motor data were used in the study. A curve fit of the AC motor data at low power resulted in the following equation:

$$\eta_e = 0.121 \, (P_i)^{0.524} \tag{54}$$

where η_e is the electric motor efficiency, and P_i is the input power in watts to the motor. Assuming a fluid efficiency of 70%, the overall efficiency, η_t, in terms of the fluid power in watts, P_f, is:

$$\eta_t = 0.199 \, (P_f)^{0.344} \tag{55}$$

The correlations for pump and motor weight were also taken from curve fits obtained from References 25 and 26. The pump weight correlation in kg includes a 50% factor for additional weight to integrate the pump with the outflow baffle, and is:

$$W_P = 245 \, D_B^{\;2.34} \tag{56}$$

where D_B is the fan blade diameter in meters.

The electric motor weight (kg) is

$$W_M = 7.3 \left(\frac{P_f}{\eta_f \, n}\right)^{0.65} \tag{57}$$

where η_f is the fluid efficiency (set at 70%) and n is the motor rotational speed in rpm.

From equations (42), (45), and (55), the overall efficiency as a function of the total fluid power, including the standpipe loss, was determined and plotted typically in Figure 31 and Appendix E. Where these lines crossed the standpipe optimization lines, the intersection was the value of standpipe diameter which gave the minimum system weight for that annulus gap, screen, and standpipe material. It was assumed that either stainless steel or aluminum could be used for the standpipe because of the presence of the slipjoint in the standpipe (Figure 1) which allowed differential thermal expansion. With the design value of standpipe diameter as an input, and with the other head losses known, the total system weight analysis was completed.

System Weight Optimization Analysis

The overall system weight was divided into four categories: annulus residual, standpipe residual, pump boiloff, and hardware, (which includes standpipe weight, screen weight, pump and motor weight.) The puddle residual, as shown in the annulus gap analysis, was insignificant and was ignored. The tankage insulation system and externally-caused "boiloff" were optimized for both the 30 and 300-day mission as shown in Appendix G. They had no effect on the optimization except as they affected the TVS heat exchanger weight, however, it is of interest to note that after 300 days, the 5, 000/4 tank had lost 11% of the stored LH_2 to external boiloff, while the 500/4, 500/2 and 500/1 tanks had lost about 22%, and the 50/2 and 50/1 tanks, about 43% to external boiloff. As shown in Appendix G, the largest heat exchanger, for the 5, 000/4 tank, consisted of about 6 m (20 ft) of 0. 65-cm (1/4-in. diameter) tubing and weighed less than 0. 7 kg (1. 5 lb); therefore, the effect of the TVS heat exchanger optimization and design on the overall system weight was ignored. The four categories above plus the total weight is shown for the six tanks, for 30 and 300-day missions, for various screens and standpipe materials versus annulus gap in Appendix E, as typically shown in Figures 34 and 35. The results for the 30-day mission are shown typically in Figure 34 and indicated that minimum system weight was achieved with the minimum annulus gap because of the strong influence of annulus residual.

However, for the 300-day mission, the pump boiloff became very important, as shown in Figure 35, so that an optimum annulus gap was found, at which minimum weight occurs. For the 5, 000/4 and 500/4 tanks, this optimum was at about 2. 0 to 2. 2% annulus gap for both the 325 x 2, 300 and the 150 x 150 screens. For the 500/2 and 50/2 tanks, the optimum gap was at about 1. 6%, and for the 500/1 and 50/1 tanks the optimum was at an annulus gap of about 1. 4 to 1. 5%. For the 5, 000/4 tank at 0. 1% tank volume/minute TVS flow, the optimum again occurred at the minimum annulus gap, as was the case for the other five tanks.

The optimum aluminum standpipe resulted in a weight reduction of 8 to 10% of the total compared to the optimum stainless steel standpipe, and use of the 150 x 150 screen resulted in a further weight reduction which was entirely due to use of a lighter screen material.

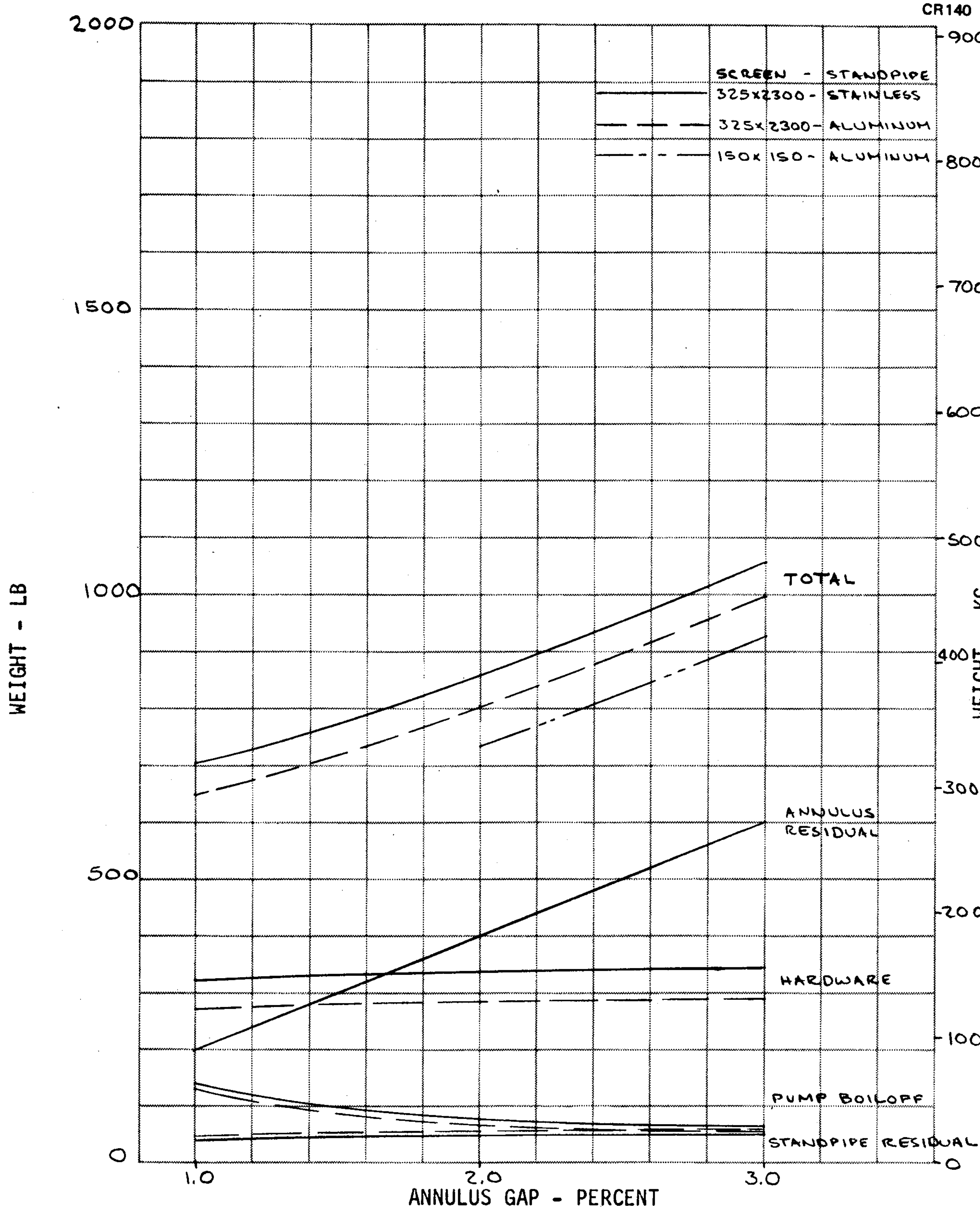

Figure 34. Weight Optimization for 5,000/4 Tank for 30-Day Mission

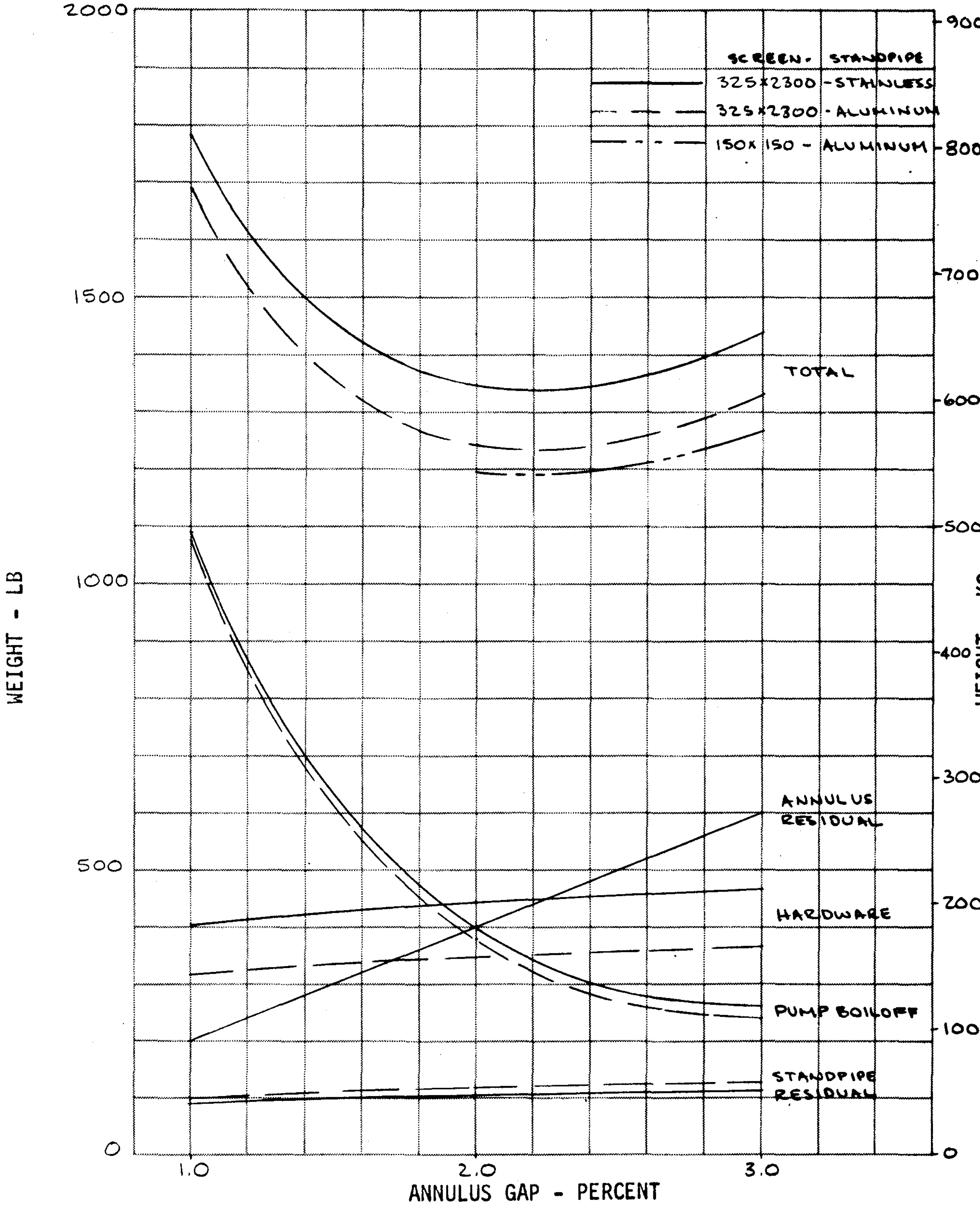

Figure 35. Weight Optimization for 5,000/4 Tank for 300-Day Mission

CONCLUSIONS

The conclusions reached from the wall screen spacing analysis for outflow are that the 325 x 2,300 screen gave maximum performance and reserve safety factor compared to the other nine screens but that the lighter 150 x 150 screen could be used with, at worst, a larger annulus gap. The 150 x 150 screen showed reduced performance compared to the 325 x 2,300 screen at higher flowrates and g-levels. However, the results of the weight optimization based on the TVS pump operation for long storage times may alter the conclusions based on outflow. For example, with the 5,000/4 tank and 30-day storage time, the minimum would be achieved with the 325 x 2,300 screen and 1% annulus gap, because the lighter 150 x 150 screen would not have adequate performance. If, however, the system were designed for a 300-day storage time, the minimum weight design would be with a 2% annulus gap, and the lighter 150 x 150 screen could be used without sacrificing outflow performance.

In our study, both the analytical and experimental work were constrained to Type 304 stainless steel (test apparatus and model tank) so that the screens selected were also of stainless steel for material compatibility. However with aluminum tankage, a further major reduction in screen weight could be obtained by using aluminum screens.

Further conclusions which may be drawn from these results are that for moderate missions (30 days or low TVS flowrate) where the pump boiloff is not really important, inaccuracies in the description of the pump/motor efficiency will not have a marked effect on the results; which, predictably, favor use of the minimum available annulus gap. On the other hand, for the long duration missions (300 days) the determination of pump efficiency is most important because pump boiloff becomes a dominant effect and drives the design of the TVS/WSL system. The curve fit used for the efficiency evaluation was extrapolated over several orders of magnitude from rather scattered data (Figure 33). For the 5,000/4 tank, the input power level was several watts, and there can be some confidence that the efficiencies and power levels are reasonable, and the pump and motor designs achievable. For the other, smaller tanks, the power levels were so low that it is not clear that the pump/motors can be built or that the predicted efficiencies can be achieved. Further definition of practical pump/motor configurations, together with a more confident evaluation of efficiencies should be determined before design of the TVS/WSL system for a 300-day mission be undertaken.

In addition, operational alternatives, such as operating a larger, more efficient pump/motor intermittently to reduce overall heat imput, should be evaluated. This would require definition of in-tank flow fields and thermodynamics in low gravity, and investigation of alternate ways of controlling tank heat input, such as vapor-cooled shields around the tank.

The conclusions reached from the experimental phases are:

A. The bubble points of the 10 representative screens in 34.5 N/cm^2 (50 psia) saturated LH_2 were accurately predicted from bubble-point tests with isopropyl alcohol. The bubble-point data correlation was generally lower (~13%) than the correlation based on other LH_2 data.

B. The screen flow-through pressure loss data taken with both ambient GN_2 and 34.5 N/cm^2 (50 psia) saturated LH_2 agreed well with other flow loss data, and the correlations obtained spanned the full practical range of Reynolds numbers.

C. The channel flow-loss data taken with 34.5 N/cm^2 (50 psia) LH_2 were unique, but the data were well correlated with the friction factor based on a roughness parameter determined from the screen shute wire diameters.

A final conclusion is that for most tanks and mission times, the annulus residual and hardware weight (mostly consisting of the wall screen liner) account for the great majority of the system weight penalty. This is a direct consequence of using a full wall screen liner as the acquisition system.

Now that this study has shown the overall concept to be fluid-dynamically feasible, especially for large tanks, it is recommended that problems of tank thermodynamics and thermal control be investigated, with the hoped-for result of obtaining realistic additional system optimization and weight reduction.

APPENDIX A

SCREEN SURVEY TABULATION

WIRE CLOTH TERMINOLOGY

1.	Bolting Cloth	A precision-woven square-weave cloth woven on special loops of custom drawn wire with a very smooth finish.
2.	Calendered Cloth	Wire cloth which has been passed through a pair of heavy rollers to reduce the thickness, reduce pore size, or flatten the cloth.
3.	Count	Number of openings per lineal inch.
4.	Dutch	Warp and shute wires of different diameter.
5.	Market Grade	An economical straining square-weave cloth.
6.	Plain Dutch	Similar to square weave, except warp wires are heavier and the shute wires are driven closely together.
7.	Reverse Plain Dutch	Warp wires are placed close together and the heavier shute wires are woven tightly over one, under one.
8.	Selvedge	A finish edge on wire cloth to prevent ravelling.
9.	Shute	Wires running crosswise in the cloth as woven. They are passed back and forth through the warp wires by the shuttle of the loom.
10.	Sintered Mesh	Woven wire mesh made more rigid by furnace bonding the wires of the weave at all contact points.
11.	Square Weave	Square mesh has warp and shute wires of equal diameter spaced equally in both direction directions. Wires pass alternately over and under successive wires.
12.	Twilled	Pattern where each wire goes alternately over two wires and then under two successive wires.
13.	Warp	Wires running the long way as the cloth is woven.

14. Weave — The pattern of interlaced warp and shute wires determined by the sequence in which individual warp wires are raised and lowered by the heddle for passage of shuttle carrying and shuttle wire.

15. Weft — See 'shute'.

16. Woof — See 'shute'.

NOMENCLATURE

a = Surface Area to Unit Volume Ratio (1/0.3048 m) (1/ft)

B = Thickness (0.3048 m) (ft)

D_c = Computed Pore Diameter (Inscribed Circle, (0.3048 m) (ft)

d = Wire Diameter (2.54 cm) (in.)

d_s = Shute Wire Diameter (2.54 cm) (in.)

d_w = Warp Wire Diameter (2.54 cm) (in.)

N = Wires Per Inch (1/2.54 cm) (1/in.)

N_s = Shute Wires Per Inch (1/2.54 cm) (1/in.)

N_w = Warp Wires Per Inch (1/2.54 cm) (1/in.)

P = Percent Open Area

W_{100} = Weight, (kg/4.22 m^2) 100 ft^2 Stainless Steel Mesh (lbm)

ϵ = Void Fraction

μ_a = Manufacturer's Absolute Micron Rating ($1\mu = 0.0000394$ in.)

MESH SUPPLIER CODE

1. Cambridge Wire Cloth Company
   Cambridge, Maryland (301) 228-3000

2. Gerard Daniel and Company, Inc.
   New Rochelle, New York (914) 235-2525

3. C.O. Jelliff Corporation
   Southport, Connecticut (203) 259-1615

4. TET/Kressilk
Los Angeles, California (213) 283-3791

5. Wire Cloth Enterprises, Inc.
Pittsburgh, Pennsylvania (412) 731-1390

6. Unique Wire Weaving Company, Inc.
Hillside, New Jersey (201) 688-4600

TWILLED DUTCH[a]

N_w	N_s	μa[b]	Thickness (in.)	$\$/ft^2$
400	2,500	5	0.0025	300
200	1,500	13	0.0051	50
200	1,400	14	0.0054	41.40
200	1,200	22	0.0052	35.90
200	1,150	12	0.0059	34.00
200	900	20	0.0056	28.75
200	600	28	0.0060	22.50
150	800	21	0.0070	26.25
120	600	34	0.0085	18.40
120	400	45	0.0086	10.50
120	330	50	0.0100	10.20
120	290	59	0.0098	8.90
120	250	60	0.0097	8.50
120	200	70	0.0093	6.00
120	180	70	0.0095	5.50
120	160	80	0.0098	5.50

[a] Products of Unique Wire Cloth Co., Inc.

[b] Based on bubble point test in alcohol

SQUARE WEAVE

N, d		P	W_{100}	b	a	ϵ	D_c	$\frac{b a^2}{\epsilon^2}$	$\frac{b}{\epsilon^2}$	$\frac{\$}{FT.^2}$
20,.032	1,2,3*	13.0	157.3	5.33E-03	895	.403	1.50E-03	2.63E+04	3.28E-02	
?20,.028	1,2,3	19.3	116.3	4.67E-03	864	.496	1.83E-03	1.42E+04	1.90E-02	
?20,.025	1,2,3	25.0	90.4	4.17E-03	843	.561	2.08E-03	9.41E+03	1.32E-02	
?20,.023	1,2,3	29.2	75.3	3.83E-03	830	.602	2.25E-03	7.28E+03	1.06E-02	
?20,.020	1,2,3	36.0	55.7	3.33E-03	812	.662	2.50E-03	5.02E+03	7.61E-03	
?20,.018	1,2,3	41.0	44.6	3.00E-03	801	.699	2.67E-03	3.94E+03	6.13E-03	
?20,.017	1,2,3	43.6	39.5	2.83E-03	796	.718	2.75E-03	3.49E+03	5.50E-03	
?20,.016	1,2,3,4,6	46.2	34.8	2.67E-03	792	.736	2.83E-03	3.08E+03	4.92E-03	$2.20
?20,.015	1,2,3,6	49.0	30.4	2.50E-03	787	.754	2.92E-03	2.72E+03	4.40E-03	
?20,.014	1,2,3,4,6	51.8	26.3	2.33E-03	783	.772	3.00E-03	2.40E+03	3.92E-03	
?20,.0135	1,2,3,6	53.3	24.4	2.25E-03	781	.780	3.04E-03	2.25E+03	3.69E-03	
?20,.013	1,2,3,6	54.8	22.6	2.17E-03	779	.789	3.08E-03	2.11E+03	3.48E-03	
?20,.012	1,2,3	57.8	19.2	2.00E-03	775	.806	3.17E-03	1.85E+03	3.08E-03	
?20,.011	1,2,3	60.8	16.0	1.83E-03	772	.823	3.25E-03	1.61E+03	2.71E-03	
?20,.010	1,2,3	64.0	13.2	1.67E-03	769	.840	3.33E-03	1.40E+03	2.36E-03	
?.←20,.0095	1,2,3	65.6	11.9	1.58E-03	767	.848	3.37E-03	1.30E+03	2.20E-03	
?20,.009	1,2,3,4,6	67.2	10.6	1.50E-03	766	.856	3.42E-03	1.20E+03	2.05E-03	$1.00

?

N, d		P	W_{100}	b	a	ϵ	D_c	$\frac{b a^2}{\epsilon^2}$	$\frac{b}{\epsilon^2}$
22,.028	1,2,3	14.7	131.1	4.67E-03	974	.432	1.45E-03	2.38E+04	2.50E-02
?22,.025	1,2,3	20.3	101.5	4.17E-03	947	.507	1.70E-03	1.45E+04	1.62E-02
?22,.023	1,2,3	24.4	84.4	3.83E-03	930	.555	1.87E-03	1.08E+04	1.25E-02
?22,.020	1,2,3	31.4	62.2	3.33E-03	906	.622	2.12E-03	7.06E+03	8.60E-03
?22,.018	1,2,3	36.5	49.6	3.00E-03	892	.665	2.29E-03	5.39E+03	6.77E-03
?22,.017	1,2,3	39.2	43.9	2.83E-03	885	.686	2.37E-03	4.72E+03	6.01E-03
?22,.016	1,2,3,6	42.0	38.6	2.67E-03	879	.707	2.45E-03	4.13E+03	5.34E-03
?22,.015	1,2,3,6	44.9	33.7	2.50E-03	873	.727	2.54E-03	3.61E+03	4.73E-03
?22,.014	1,2,3,6	47.9	29.2	2.33E-03	868	.747	2.62E-03	3.15E+03	4.18E-03

? * SUPPLIER CODE

N, d		P	W_{100}	b	a	ε	D_c	$\frac{b a^2}{\epsilon^2}$	$\frac{b}{\epsilon^2}$
22,.0135	1,2,3,6	49.4	27.1	2.25E-03	865	.757	2.66E-03	2.94E+03	3.93E-03
?22,.013	1,2,3,6	51.0	25.0	2.17E-03	863	.766	2.70E-03	2.75E+03	3.69E-03
?22,.012	1,2,3,6	54.2	21.2	2.00E-03	858	.786	2.79E-03	2.38E+03	3.24E-03
?22,.011	1,2,3	57.5	17.7	1.83E-03	853	.804	2.87E-03	2.06E+03	2.83E-03
?22,.010	1,2,3	60.8	14.6	1.67E-03	849	.823	2.95E-03	1.77E+03	2.46E-03
?22,.0095	1,2,3	62.6	13.1	1.58E-03	847	.832	3.00E-03	1.64E+03	2.29E-03
?22,.009	1,2,3	64.3	11.8	1.50E-03	845	.841	3.04E-03	1.5%E+03	2.12E-03

?

N, d		P	W_{100}	b	a	ε	D_c	$\frac{b a^2}{\epsilon^2}$	$\frac{b}{\epsilon^2}$
24,.025	1,2,3	16.0	113.2	4.17E-03	1055	.450	1.39E-03	2.29E+04	2.05E-02
?24,.023	1,2,3	20.1	93.8	3.83E-03	1033	.505	1.56E-03	1.61E+04	1.50E-02
?24,.020	1,2,3	27.0	68.9	3.33E-03	1004	.582	1.81E-03	9.92E+03	9.85E-03
?24,.018	1,2,3	32.3	54.8	3.00E-03	986	.630	1.97E-03	7.33E+03	7.55E-03
?24,.017	1,2,3	35.0	48.5	2.83E-03	977	.654	2.06E-03	6.33E+03	6.63E-03
?24,.016	1,2,3	37.9	42.6	2.67E-03	969	.677	2.14E-03	5.47E+03	5.82E-03
?24,.015	1,2,3	41.0	37.1	2.50E-03	962	.699	2.22E-03	4.72E+03	5.11E-03
?24,.014	1,2,3,4,6	44.1	32.1	2.33E-03	954	.722	2.31E-03	4.08E+03	4.48E-03
?24,.0135	1,2,3,6	45.7	29.7	2.25E-03	951	.733	2.35E-03	3.79E+03	4.19E-03
?24,.013	1,2,3,6	47.3	27.5	2.17E-03	948	.743	2.39E-03	3.52E+03	3.92E-03
?24,.012	1,2,3,6	50.7	23.3	2.00E-03	942	.765	2.47E-03	3.03E+03	3.42E-03
?24,.011	1,2,3,6	54.2	19.4	1.83E-03	936	.786	2.56E-03	2.60E+03	2.97E-03
?24,.010	1,2,3,4,6	57.8	16.0	1.67E-03	930	.806	2.64E-03	2.22E+03	2.56E-03
?24,.0095	1,2,3	59.6	14.4	1.58E-03	928	.816	2.68E-03	2.05E+03	2.38E-03
?24,.009	1,2,3	61.5	12.9	1.50E-03	926	.826	2.72E-03	1.88E+03	2.20E-03
?24,.0085	1,2,3	63.4	11.4	1.42E-03	923	.836	2.76E-03	1.73E+03	2.02E-03
?24,.008	1,2,3	65.3	10.1	1.33E-03	921	.846	2.81E-03	1.58E+03	1.86E-03
?24,.0075	1,2,3,4,6	67.2	8.9	1.25E-03	919	.856	2.85E-03	1.44E+03	1.70E-03

?

SQUARE WEAVE

N, d		P	W_{100}	b	a	ϵ	D_c	$\frac{b a^2}{\epsilon^2}$	$\frac{b}{\epsilon^2}$
26, .020	1,2,3	23.0	75.8	3.33E-03	1105	.540	1.54E-03	1.40E+04	1.14E-02
?26, .018	1,2,3	28.3	60.2	3.00E-03	1082	.594	1.70E-03	9.95E+03	8.50E-03
?26, .017	1,2,3	31.1	53.1	2.83E-03	1072	.620	1.79E-03	8.45E+03	7.36E-03
?26, .016	1,2,3	34.1	46.6	2.67E-03	1062	.646	1.87E-03	7.20E+03	6.39E-03
?26, .015	1,2,3	37.2	40.6	2.50E-03	1052	.671	1.96E-03	6.14E+03	5.55E-03
?26, .014	1,2,3,6	40.4	35.1	2.33E-03	1043	.696	2.04E-03	5.24E+03	4.82E-03
?26, .0135	1,2,3,6	42.1	32.5	2.25E-03	1039	.708	2.08E-03	4.85E+03	4.49E-03
?26, .013	1,2,3,6	43.8	30.0	2.17E-03	1035	.720	2.12E-03	4.48E+03	4.18E-03
?26, .012	1,2,3,6	47.3	25.4	2.00E-03	1027	.743	2.21E-03	3.82E+03	3.62E-03
?26, .011	1,2,3,6	51.0	21.2	1.83E-03	1019	.766	2.29E-03	3.24E+03	3.12E-03
?26, .010	1,2,3,6	54.8	17.4	1.67E-03	1013	.789	2.37E-03	2.75E+03	2.68E-03
?26, .0095	1,2,3,6	56.7	15.6	1.58E-03	1010	.800	2.41E-03	2.52E+03	2.47E-03
?26, .009	1,2,3	58.7	14.0	1.50E-03	1007	.811	2.46E-03	2.31E+03	2.28E-03
?26, .0085	1,2,3	60.7	12.4	1.42E-03	1004	.822	2.50E-03	2.11E+03	2.10E-03
?26, .008	1,2,3	62.7	11.0	1.33E-03	1001	.833	2.54E-03	1.93E+03	1.92E-03
?26, .0075	1,2,3,4,6	64.8	9.6	1.25E-03	999	.844	2.58E-03	1.75E+03	1.75E-03

?

N, d		P	W_{100}	b	a	ϵ	D_c	$\frac{b a^2}{\epsilon^2}$	$\frac{b}{\epsilon^2}$
28, .018	1,2,3	24.6	65.7	3.00E-03	1182	.557	1.48E-03	1.35E+04	9.68E-03
?28, .017	1,2,3	27.5	58.0	2.83E-03	1168	.586	1.56E-03	1.13E+04	8.25E-03
?28, .016	1,2,3	30.5	50.8	2.67E-03	1157	.614	1.64E-03	9.45E+03	7.06E-03
?28, .015	1,2,3	33.6	44.2	2.50E-03	1145	.642	1.73E-03	7.95E+03	6.06E-03
?28, .014	1,2,3	37.0	38.1	2.33E-03	1134	.669	1.81E-03	6.70E+03	5.21E-03
?28, .0135	1,2,3	38.7	35.3	2.25E-03	1128	.683	1.85E-03	6.15E+03	4.83E-03
?28, .013	1,2,3,6	40.4	32.6	2.17E-03	1123	.696	1.89E-03	5.65E+03	4.48E-03
?28, .012	1,2,3,6	44.1	27.5	2.00E-03	1114	.722	1.98E-03	4.76E+03	3.84E-03
?28, .011	1,2,3,6	47.9	22.9	1.83E-03	1105	.747	2.06E-03	4.01E+03	3.29E-03
?28, .010	1,2,3,6	51.8	18.8	1.67E-03	1096	.772	2.14E-03	3.36E+03	2.80E-03

?

SQUARE WEAVE

N	d		P	W_{100}	b	a	ε	D_c	$\frac{ba^2}{\epsilon^2}$	$\frac{b}{\epsilon^2}$	$\frac{\$}{FT.^2}$
28	.0095	1,2,3,6	53.9	16.9	1.58E-03	1092	.784	2.18E-03	3.07E+03	2.58E-03	
?28	.009	1,2,3,6	56.0	15.1	1.50E-03	1089	.796	2.23E-03	2.81E+03	.37E-03	
?28	.0085	1,2,3	58.1	13.5	1.42E-03	1085	.808	2.27E-03	2.56E+03	2.17E-03	
?28	.008	1,2,3	60.2	11.9	1.33E-03	1082	.820	2.31E-03	2.32E+03	1.98E-03	
?28	.0075	1,2,3,4,6	62.4	10.4	1.25E-03	1079	.831	2.35E-03	2.10E+03	1.81E-03	

?

N	d		P	W_{100}	b	a	ε	D_c	$\frac{ba^2}{\epsilon^2}$	$\frac{b}{\epsilon^2}$	$\frac{\$}{FT.^2}$
30	.017	1,2,3	24.0	63.0	2.83E-03	1270	.550	1.36E-03	1.51E+04	9.35E-03	
?30	.016	1,2,3	27.0	55.1	2.67E-03	1255	.582	1.44E-03	1.24E+04	7.88E-03	
?30	.015	1,2,3	30.3	47.9	2.50E-03	1240	.612	1.53E-03	1.03E+04	6.67E-03	
?30	.014	1,2,3	33.6	41.3	2.33E-03	1227	.642	1.61E-03	8.51E+03	5.66E-03	
?30	.0135	1,2,3	35.4	38.2	2.25E-03	1220	.657	1.65E-03	7.77E+03	5.22E-03	
?30	.013	1,2,3,6	37.2	35.2	2.17E-03	1214	.671	1.69E-03	7.09E+03	4.81E-03	
?30	.012	1,2,3,4,6	41.0	29.7	2.00E-03	1202	.699	1.78E-03	5.91E+03	4.09E-03	$2.50
?30	.011	1,2,3,6	44.9	24.7	1.83E-03	1191	.727	1.86E-03	4.92E+03	3.47E-03	
?30	.010	1,2,3,6	49.0	20.3	1.67E-03	1181	.754	1.94E-03	4.09E+03	2.93E-03	
30	.0095	1,2,3,6	51.1	18.2	1.58E-03	1176	.767	1.99E-03	3.72E+03	2.69E-03	
?30	.009	1,2,3,6	53.3	16.3	1.50E-03	1171	.780	2.03E-03	3.38E+03	2.46E-03	
?30	.0085	1,2,3,6	55.5	14.5	1.42E-03	1167	.793	2.07E-03	3.07E+03	2.25E-03	
?30	.008	1,2,3	57.8	12.8	1.33E-03	1163	.806	2.11E-03	2.78E+03	2.05E-03	
?30	.0075	1,2,3	60.1	11.2	1.25E-03	1159	.819	2.15E-03	2.51E+03	1.86E-03	
?30	.0065	4,6	64.8	8.4	1.08E-03	1152	.844	2.24E-03	2.02E+03	1.52E-03	$1.20

?

N	d		P	W_{100}	b	a	ε	D_c	$\frac{ba^2}{\epsilon^2}$	$\frac{b}{\epsilon^2}$	$\frac{\$}{FT.^2}$
32	.016	1,2,3	23.8	59.5	2.67E-03	1355	.548	1.27E-03	1.63E+04	8.87E-03	
?32	.015	1,2,3	27.0	51.7	2.50E-03	1338	.582	1.35E-03	1.32E+04	7.38E-03	
?32	.014	1,2,3	30.5	44.5	2.33E-03	1322	.614	1.44E-03	1.08E+04	6.18E-03	
?32	.0135	1,2,3	32.3	41.1	2.25E-03	1314	.630	1.48E-03	9.78E+03	5.66E-03	
?32	.013	1,2,3	34.1	37.9	2.17E-03	1307	.646	1.52E-03	8.86E+03	5.19E-03	
?32	.012	1,2,3,6	37.9	31.9	2.00E-03	1292	.677	1.60E-03	7.29E+03	4.36E-03	
?32	.011	1,2,3,6	42.0	26.6	1.83E-03	1279	.707	1.69E-03	6.00E+03	3.67E-03	

?

SQUARE WEAVE

N	d	P	W_{100}	b	a	ϵ	D_c	$\frac{b a^2}{\epsilon^2}$	$\frac{b}{\epsilon^2}$
32,	.010	1,2,3,6							
		46.2	21.7	1.67E-03	1267	.736	1.77E-03	4.93E+03	3.08E-03
?32,	.0095	1,2,3,6							
		48.4	19.5	1.58E-03	1261	.750	1.81E-03	4.47E+03	2.81E-03
?32,	.009	1,2,3,6							
		50.7	17.4	1.50E-03	1255	.765	1.85E-03	4.04E+03	2.57E-03
?32,	.0085	1,2,3,6							
		53.0	15.5	1.42E-03	1250	.779	1.90E-03	3.65E+03	2.34E-03
?32,	.008	1,2,3,6							
		55.4	13.7	1.33E-03	1245	.792	1.94E-03	3.29E+03	2.12E-03
?32,	.007	1,2,3							
		60.2	10.4	1.17E-03	1236	.820	2.02E-03	2.65E+03	1.74E-03
?32,	.0075	1,2,3							
		57.8	12.0	1.25E-03	1241	.806	1.98E-03	2.96E+03	1.92E-03
?32,	.0065	4,6							
		62.7	8.9	1.08E-03	1232	.833	2.06E-03	2.37E+03	1.56E-03
?									
34,	.0065	4,6							
		60.7	9.5	1.08E-03	1313	.822	1.91E-03	2.76E+03	1.60E-03
?									
35,	.016	1,2,3							
		19.4	66.4	2.67E-03	1512	.496	1.05E-03	2.48E+04	1.08E-02
?35,	.015	1,2,3							
		22.6	57.5	2.50E-03	1490	.534	1.13E-03	1.94E+04	8.76E-03
?35,	.014	1,2,3							
		26.0	49.4	2.33E-03	1469	.571	1.21E-03	1.54E+04	7.15E-03
?35,	.0135	1,2,3							
		27.8	45.6	2.25E-03	1459	.590	1.26E-03	1.38E+04	6.47E-03
?35,	.013	1,2,3							
		29.7	42.0	2.17E-03	1450	.607	1.30E-03	1.23E+04	5.87E-03
?35,	.012	1,2,3							
		33.6	35.4	2.00E-03	1431	.642	1.38E-03	9.93E+03	4.85E-03
?35,	.011	1,2,3,4,6							
		37.8	29.4	1.83E-03	1414	.676	1.46E-03	8.02E+03	4.01E-03
?35,	.010	1,2,3,6							
		42.3	24.0	1.67E-03	1398	.709	1.55E-03	6.48E+03	3.32E-03
?35.,	.0095	1,2,3,6							
		44.6	21.5	1.58E-03	1390	.725	1.59E-03	5.83E+03	3.01E-03
?35,	.009	1,2,3,6							
		46.9	19.2	1.50E-03	1383	.741	1.63E-03	5.23E+03	2.73E-03
?35,	.0085	1,2,3,6							
		49.4	17.1	1.42E-03	1377	.756	1.67E-03	4.69E+03	2.48E-03
?35,	.008	1,2,3,6							
		51.8	15.0	1.33E-03	1370	.772	1.71E-03	4.20E+03	2.24E-03
?35,	.0075	1,2,3							
		54.4	13.2	1.25E-03	1364	.787	1.76E-03	3.76E+03	2.02E-03
?35,	.007	1,2,3							
		57.0	11.4	1.17E-03	1358	.802	1.80E-03	3.35E+03	1.81E-03
?									
36,	.0065	4,6							
		58.7	10.1	1.08E-03	1394	.811	1.77E-03	3.20E+03	1.65E-03
?									

SQUARE WEAVE

N, d		P	W_{100}	b	α	ϵ	D_c	$b\alpha^2/\epsilon^2$	b/ϵ^2	$/Ft.²
38,.014	1,2,3	21.9	54.6	2.33E-03	1623	.527	1.03E-03	2.21E+04	8.41E-03	
?38,.0135	1,2,3	23.7	50.4	2.25E-03	1610	.547	1.07E-03	1.95E+04	7.52E-03	
?38,.013	1,2,3	25.6	46.3	2.17E-03	1598	.567	1.11E-03	1.72E+04	6.73E-03	
?38,.012	1,2,3	29.6	38.9	2.00E-03	1574	.606	1.19E-03	1.35E+04	5.44E-03	
?38,.011	1,2,3	33.9	32.2	1.83E-03	1553	.644	1.28E-03	1.07E+04	4.42E-03	
?38,.010	1,2,3,6	38.4	26.3	1.67E-03	1533	.681	1.36E-03	8.45E+03	3.60E-03	
?38,.0095	1,2,3,6	40.8	23.6	1.58E-03	1523	.699	1.40E-03	7.53E+03	3.24E-03	
?38,.009	1,2,3,6	43.3	21.0	1.50E-03	1514	.716	1.44E-03	6.70E+03	2.92E-03	
?38,.0085	1,2,3,6	45.8	18.7	1.42E-03	1505	.733	1.48E-03	5.97E+03	2.63E-03	
?38,.008	1,2,3,6	48.4	16.4	1.33E-03	1497	.750	1.53E-03	5.31E+03	2.37E-03	
?38,.0075	1,2,3	51.1	14.4	1.25E-03	1490	.767	1.57E-03	4.71E+03	2.12E-03	
?38,.007	1,2,3	53.9	12.5	1.17E-03	1482	.784	1.61E-03	4.17E+03	1.90E-03	
?38,.0065	4,6	56.7	10.7	[illegible].08E-03	1476	.800	1.65E-03	3.68E+03	1.69E-03	

?

N, d		P	W_{100}	b	α	ϵ	D_c	$b\alpha^2/\epsilon^2$	b/ϵ^2	$/Ft.²
40,.0135	1,2,3	21.2	53.6	2.25E-03	1714	.518	9.58E-04	2.46E+04	8.39E-03	
?40,.013	1,2,3	23.0	49.3	2.[illegible]-03	1700	.540	1.00E-03	2.15E+04	7.44E-03	
?40,.012	1,2,3,6	21.0	41.3	2.00E-03	1673	.582	1.08E-03	1.65E+04	5.91E-03	
?40,.011	1,2,3,6	31.4	34.2	1.83E-03	1647	.622	1.17E-03	1.28E+04	4.73E-03	
?40,.010	1,2,3,4,6	36.0	27.9	1.67E-03	1624	.662	1.25E-03	1.00E+04	3.81E-03	$ 2.60
?40,.0095	1,2,3,6	38.4	25.0	1.58E-03	1613	.681	1.29E-03	8.89E+03	3.42E-03	
?40,.009	1,2,3,6	41.0	22.3	1.50E-03	1603	.699	1.33E-03	7.87E+03	3.07E-03	
?40,.0085	1,2,3,6	43.6	19.7	1.42E-03	1593	.718	1.37E-03	6.97E+03	2.75E-03	
?40,.008	1,2,3,6	46.2	17.4	1.33E-03	1583	.736	1.42E-03	6.17E+03	2.46E-03	
?40,.0075	1,2,3	49.0	15.2	1.25E-03	1574	.754	1.46E-03	5.45E+03	2.20E-03	
?40,.007	1,2,3	51.8	13.2	1.17E-03	1566	.772	1.50E-03	4.80E+03	1.96E-03	
?40,.0065	4,6	54.8	11.3	1.08E-03	1558	.789	1.54E-03	4.22E+03	1.74E-03	$ 1.40

?

N, d		P	W_{100}	b	α	ϵ	D_c	$b\alpha^2/\epsilon^2$	b/ϵ^2	$/Ft.²
42,.0135	1,2,3	18.7	56.9	2.25E-03	1820	.488	8.59E-04	3.13E+04	9.45E-03	
?42,.013	1,2,3	20.6	52.3	2.17E-03	1804	.511	9.01E-04	2.70E+04	8.28E-03	
?42,.012	1,2,3	24.6	43.8	2.00E-03	1773	.557	9.84E-04	2.03E+04	6.45E-03	

?

SQUARE WEAVE

N d		P	W_{100}	b	a	ε	D_c	$\frac{ba^2}{\epsilon^2}$	$\frac{b}{\epsilon^2}$
42, .011	1,2,3	28.9	36.2	1.83E-03	1744	.600	1.07E-03	1.54E+04	5.09E-03
?42, .010	1,2,3,6	33.6	29.5	1.67E-03	1717	.642	1.15E-03	1.19E+04	4.04E-03
?42, .0095	1,2,3,6	36.1	26.4	1.58E-03	1705	.663	1.19E-03	1.05E+04	3.61E-03
?42, .009	1,2,3,6	38.7	23.5	1.50E-03	1693	.683	1.23E-03	9.22E+03	3.22E-03
?42, .0055	4,6	59.1	8.4	9.17E-04	1625	.814	1.53E-03	3.66E+03	1.38E-03
?									
43, .0050	4	61.6	7.1	8.33E-04	1657	.827	1.52E-03	3.34E+03	1.22E-03
?									
44, .0055	4,6	57.5	8.9	9.17E-04	1707	.804	1.44E-03	4.13E+03	1.42E-03
?									
45, .013	1,2,3	17.2	57.0	2.17E-03	1965	.468	7.69E-04	3.83E+04	9.91E-03
?45, .012	1,2,3	21.2	47.6	2.00E-03	1928	.518	8.52E-04	2.77E+04	7.45E-03
?45, .011	1,2,3	25.5	39.3	1.83E-03	1893	.566	9.35E-04	2.05E+04	5.72E-03
?45, .010	1,2,3	30.3	31.9	1.67E-03	1860	.612	1.02E-03	1.54E+04	4.44E-03
?45, .0095	1,2,3,6	32.8	28.6	1.58E-03	1845	.635	1.06E-03	1.34E+04	3.93E-03
?45, .009	1,2,3,6	35.4	25.4	1.50E-03	1830	.657	1.10E-03	1.16E+04	3.48E-03
?45, .0085	1,2,3,6	38.1	22.5	1.42E-03	1816	.678	1.14E-03	1.02E+04	3.08E-03
?45, .008	1,2,3,6	41.0	19.8	1.33E-03	1803	.699	1.19E-03	8.86E+03	2.73E-03
?45, .0075	1,2,3,6	43.9	17.3	1.25E-03	1790	.720	1.23E-03	7.72E+03	2.41E-03
?									
46, .0045	4	62.9	6.2	7.50E-04	1771	.834	1.44E-03	3.38E+03	1.08E-03
?46, .0055	4,6	55.8	9.3	9.17E-04	1789	.795	1.35E-03	4.64E+03	1.45E-03
?									
48, .0055	4,6	54.2	9.7	9.17-04	1872	.786	1.28E-03	5.20E+03	1.49E-03
?; 48, .0045	4	61.5	6.4	7.50E-04	1851	.826	1.36E-03	3.76E+03	1.10E-03
?									

SQUARE WEAVE

N	d		P	W_{100}	b	a	ϵ	D_c	$\frac{b a^2}{\epsilon^2}$	$\frac{b}{\epsilon^2}$
50,	.012	1,2,3,6	16.0	54.3	2.00E-03	2198	.450	6.67E-04	4.76E+04	9.86E-03
?50,	.011	1,2,3,6	20.3	44.7	1.83E-03	2151	.507	7.50E-04	3.30E+04	7.13E-03
?50,	.010	1,2,3,6	25.0	36.2	1.67E-03	2107	.561	8.33E-04	2.35E+04	5.30E-03
?50,	.0095	1,2,3,6	27.6	32.3	1.58E-03	2087	.587	8.75E-04	2.00E+04	4.60E-03
?50,	.009	1,2,3,4,6	30.3	28.7	1.50E-03	2067	.612	9.17E=04	1.71E+04	4.00E-03
?50,	.0085	1,2,3,6	33.1	25.4	1.42E-03	2048	.637	9.58E-04	1.46E+04	3.49E-03
?50,	.008	1,2,3,6	35.9	22.3	1.33E-03	2030	.662	1.00E-03	1.26E+04	3.05E-03
?50,	.0075	1,2,3,6	39.0	19.4	1.25E-03	2013	.685	1.04E-03	1.08E+04	2.66E-03
?50,	.0055	4,6	52.6	10.1	9.17E-04	1955	.776	1.21E-03	5.82E+03	1.52E-03
?50,	.0045	4	60.1	6.7	7.50E-04	1932	.819	1.29E-03	4.18E+03	1.12E-03-
52,	.0055	4,6	51.0	10.6	9.17E-04	2039	.766	1.14E-03	6.49E+03	1.56E-03
?										
54,	.0055	4,6	49.4	11.0	9.17E-04	2124	.757	1.08E-03	7.22E+03	1.60E-03
?54,	.0040	4	61.5	5.7	6.67E-04	2083	.826	1.21E-03	4.23E+03	9.76E-04
?										
55,	.011	1,2,3,6	15.6	50.3	1.83E-03	2423	.445	5.98E-04	5.45E+04	9.27E-03
?55,	.010	1,2,3,6	20.3	40.6	1.67E-03	2366	.507	6.82E-04	3.63E+04	6.48E-03
?55,	.0095	1,2,3,6	22.8	36.2	1.58E-03	2334	.537	7.23E-04	3.01E+04	5.49E-03
?55,	.009	1,2,3,6	25.5	32.2	1.50E-03	2314	.566	7.65E-04	2.50E+04	4.68E-03
?55,	.0085	1,2,3,6	28.4	28.4	1.42E-03	2289	.595	8.07E-04	2.10+04	4.01E-03
?55,	.008	1,2,3,6	31.4	24.9	1.33E-03	2265	.622	8.48E-04	1.77E+04	3.44E-03
?55,	.0075	1,2,3,6	34.5	21.6	1.25E-03	2243	.650	8.90E-04	1.49E+04	2.96E-03
?55,	.007	1,2,3,6	37.8	18.7	1.17E-03	2222	.676	9.32E-04	1.26E+04	2.55E-03
?										
56,	.0040	4	60.2	5.9	6.67E-04	2163	.820	1.15E-03	4.64E+03	9.92E-04
?										

SQUARE WEAVE

N d	P	W_{100}	b	a	ε	D_c	ba^2/ϵ^2	b/ϵ^2	\$/FT.^{2}
58,.0045	4,6								
	54.6	7.9	7.50E-04	2260	.788	1.06E-03	6.17E+03	1.21E-03	
?58,.0040	4								
	59.0	6.2	6.67E-04	2245	.813	1.10E-03	5.08E+03	1.01E-03	
?									
60,.011	1,2,3,6								
	11.6	56.3	1.83E-03	2710	.379	4.72E-04	9.38E+04	1.28E-02	
?60,.010	1,2,3,6								
	16.0	45.2	1.67E-03	2638	.450	5.56E-04	5.72E+04	8.21E-03	
?60,.009	1,2,3,6								
	21.2	35.7	1.50E-03	2571	.518	6.39E-04	3.69E+04	5.59E-03	
?60,.008	1,2,3,6								
	27.0	27.6	1.33E-03	2509	.582	7.22E-04	2.48E+04	3.94E-03	
?60,.0075	1,2,3,4,6								
	30.3	23.9	1.25E-03	2480	.612	7.64E-04	2.05E+04	3C.3E-03	\$2.80
?60,.007	1,2,3,6								
	33.6	20.6	1.17E-03	2453	.642	8.06E-04	1.70E+04	2.83E-03	
?60,.0065	1,2,3,4								
	37.2	17.6	1.08E-03	2428	.671	8.47E-04	1.42E+04	2.40E-03	
?60,.006	1,2,3,6								
	41.0	14.9	1.00E-03	2404	.699	8.89E-04	1.18E+04	2.04E-03	
?60,.0045	4,6								
	53.3	8.1	7.50E-04	2343	.780	1.01E-03	6.76E+03	1.23E-03	
?60,.004	4								
	57.8	6.4	6.67E-04	2326	.806	1.06E-03	5.55E+03	1.03E-03	
?									
62,.0045	4,6								
	52.0	8.4	7.50E-04	2427	.773	9.69E-04	7.40E+03	1.26E-03	
?									
64,.0045	4,6								
	50.7	8.7	7.50E-04	2511	.765	9.27E-04	8.09E+03	1.28E-03	
?									
65,.0075	1,2,3								
	26.3	26.3	1.25E-03	2726	.574	6.57E-04	2.82E+04	3.79E-03	
?65,.0065	1,2,3								
	33.4	19.3	1.08E-03	2660	.640	7.40E-04	1.87E+04	2.65E-03	
?									
66,.0045	4								
	49.4	9.0	7.50E-04	2596	.757	8.88E-04	8.82E+03	1.31E-03	
?66,.0040	4								
	54.1	7.1	6.67E-04	2573	.786	9.29E-04	7.15E+03	1.08E-03	
?									
70,.009	1,2,3,6								
	13.7	43.4	1.50E-03	3119	.415	4.40E-04	8.46E+04	8.70E-03	
?70,.008	1,2,3,6								
	19.4	33.2	1.33E-03	3025	.496	5.24E-04	4.96E+04	5.42E-03	
?70,.007	1,2,3,6								
	26.0	24.7	1.17E-03	2939	.571	6.07E-04	3.09E+04	3.57E-03	
?70,.006	1,2,3,6								
	33.6	17.7	1.00E-03	2862	.642	6.90E-04	1.99E+04	2.42E-03	
?70,.0037	1,2,3,6								
	54.9	6.4	6.17E-04	2726	.790	8.82E-04	7.35E+03	9.88E-04	
?									

SQUARE WEAVE

N · d	P	W_{100}	b	a	e	D_c	$\frac{b a^2}{e^2}$	$\frac{b}{e^2}$	$\frac{\$}{FT.^2}$
72, .0040	4								
	50.7	7.8	6.67E-04	2825	.765	8.24E-04	9.10E+03	1.14E-03	
?72, .0037	4,6								
	53.8	6.6	6.17E-04	2809	.783	8.49E-04	7.93E+03	1.00E-03	
?									
74, .0040	4								
	49.6	8.0	6.67E-04	2909	.758	7.93E-04	9.83E+03	1.16E-03	
?74, .0037	4,6								
	52.7	6.8	6.17E-04	2892	.777	8.18E-04	8.54E+03	1.02E-03	
?									
75, .007	1,2,3								
	22.6	26.9	1.17E-03	3193	.534	5.28E-04	4.17E+04	4.09E-03	
?75, .0065	1,2,3								
	26.3	22.8	1.08E-03	3146	.574	5.69E-04	3.25E+04	3.29E-03	
?75, .006	1,2,3								
	30.3	19.2	1.00E-03	3101	.612	6.11E-04	2.56E+04	2.67E-03	
?									
76, .0040	4								
	48.4	8.2	6.67E-04	2995	.750	7.63E-04	1.06E+04	1.18E-03	
?76, .0037	4,6								
	51.7	7.0	6.17E-04	2976	.771	7.88E-04	9.20E+03	1.04E-03	
?									
78, .0040	4								
	47.3	8.5	6.67E-04	3080	.743	7.35E-04	1.14E+04	1.21E-03	
?78, .004	4								
	47.3	8.5	6.67E-04	3080	.743	7.35E-04	1.14E+04	1.21E-03	
?78, .0037	4,6								
	50.6	7.2	6.17E-04	3061	.764	7.60E-04	9.89E+03	1.06E-03	
?									
80, .0075	1,2,3,6								
	16.0	33.9	1.25E-03	3517	.450	4.17E-04	7.62E+04	6.16E-03	
?80, .007	1,2,3,6								
	19.3	29.1	1.17E-03	3457	.496	4.57E-04	5.67E+04	4.74E-03	
?80, .0065	1,2,3,6								
	23.0	24.6	1.08E-03	3399	.540	5.00E-04	4.30E+04	3.72E-03	
?80, .006	1,2,3,6								
	27.0	20.7	1.00E-03	3345	.582	5.42E-04	3.31E+04	2.95E-03	
?80, .0055	1,2,3,6								
	31.4	17.1	9.17E-04	3295	.622	5.83E-04	2.57E+04	2.37E-03	$ 3.00
?80, .005	1,2,3,6								
	36.0	13.9	8.33E-04	3248	.662	6.25E-04	2.01E+04	1.90E-03	
?80, .0040	4								
	46.2	8.7	6.67E-04	3167	.736	7.08E-04	1.23E+04	1.23E-03	
?80, .0037	4,6								
	49.6	7.4	6.17E-04	3145	.758	7.33E-04	1.06E+04	1.07E-03	$ 2.40
?									
84, .0040	4								
	44.1	9.2	6.67E-04	3341	.722	6.59E-04	1.43E+04	1.28E-03	
?84, .0035	4,6								
	49.8	6.9	5.83E-04	3301	.759	7.00E-04	1.10E+04	1.01E-03	
?									

SQUARE WEAVE

N d		P	W_{100}	b	a	ϵ	D_c	$\frac{b\alpha^2}{\epsilon^2}$	$\frac{b}{\epsilon^2}$	$\frac{\$}{FT^2}$
88, .0040	4									
		42.0	9.7	6.67E-04	3517	.707	6.14E-04	1.65E+04	1.33E-03	
?88, .0035	4,6									
		47.9	7.3	5.83E-04	3471	.747	6.55E-04	1.26E+04	1.05E-03	
?										
90, .006	1,2,3,6									
		21.2	23.8	1.00E-03	3856	.518	4.26E-04	5.54E+04	3.73E-03	
?90, .0055	1,2,3,6									
		25.5	19.7	9.17E-04	3786	.566	4.68E-04	4.10E+04	2.86E-03	
?90, .005	1,2,3,6									
		30.3	16.0	8.33E-04	3721	.612	5.09E-04	3.08E+04	2.22E-03	
?90, .0035	4,6									
		46.9	7.5	5.83E-04	3557	.741	6.34E-04	1.35E+04	1.06E-03	
?										
94, .0040	4									
		38.9	10.4	6.67E-04	3786	.685	5.53E-04	2.04E+04	1.42E-03	
?94, .0035	4,6									
		45.0	7.8	5.83E-04	3731	.728	5.95E-04	1.53E+04	1.10E-03	
?										
100, .005	1,2,3,6									
		25.0	18.1	8.33E-04	4215	.561	4.17E-04	4.70E+04	2.65E-03	
?100, .0045	1,2,3,4,6									
		30.3	14.4	7.50E-04	4134	.612	4.58E-04	3.42E+04	2.00E-03	
?100, .004	1,2,3,6									
		36.0	11.1	6.67E-04	4060	.662	5.00E-04	2.51E+04	1.52E-03	
?100, .0035	1,2,3,6									
		42.3	8.4	5.83E-04	3994	.709	5.42E-04	1.85E+04	1.16E-03	
?100, .003	1,2,3,6									
		49.0	6.1	5.00E-04	3936	.754	5.83E-04	1.36E+04	8.79E-04	
?										
105, .003	4,5,6									
		46.9	6.4	5.00E-04	4150	.741	5.44E-04	1.57E+04	9.12E-04	
?										
120, .004	1,2									
		27.0	13.8	6.67E-04	5018	.582	3.61E-04	4.96E+04	1.97E-03	
?120, .0037	1,2,3,4,5,6									
		30.9	11.6	6.17E-04	4950	.618	3.86E-04	3.95E+04	1.61E-03	\$3.70
?120, .0026	4,5,6									
		47.3	5.5	4.33E-04	4739	.743	4.78E-04	1.76E+04	7.84E-04	
?120, .0035	3									
		33.6	10.3	5.83E-04	4907	.642	4.03E-04	3.41E+04	1.41E-03	
?										
130, .0038	1,2									
		25.6	13.5	6.33E-04	5466	.567	3.24E-04	5.88E+04	1.97E-03	
?130, .0034	1,2,6									
		31.1	10.6	5.67E-04	5358	.620	3.58E-04	4.23E+04	1.47E-03	
?										

SQUARE WEAVE

N	d	P	W_{100}	b	a	ε	D_c	$\frac{ba^2}{\epsilon^2}$	$\frac{b}{\epsilon^2}$	$\frac{\$}{FT.^2}$
135,	.0023	4,5								
		47.5	4.8	3.83E-04	5329	.745	4.26E-04	1.96E+04	6.91E-:4	
?										
140,	.0033	1,2								
		28.9	10.9	5.50E-04	5814	.600	3.20E-04	5.16E+04	1.53E-03	
?140,	.0029	1,2,3,6								
		35.3	8.2	4.83E-04	5696	.656	3.54E-04	3.65E+04	1.12E-03	
?										
145,	.0022	4,5,6								
		46.4	4.8	3.67E-04	5738	.737	3.91E-04	2.22E+04	6.75E-04	
?										
150,	.0030	1,2								
		30.3	9.6	5.00E-04	6201	.612	3.06E-04	5.13E+04	1.33E-03	
?150,	.0026	1,2,3,4,5,6								
		37.2	7.0	4.33E-04	6070	.671	3.39E-04	3.54E+04	9.62E-04	
?										
160,	.0028	1,2								
		30.5	8.9	4.67E!04	6610	.614	2.87E-04	5.40E+04	1.24E-03	
?160,	.0025	1,2,3,6								
		36.0	7.0	4.17E-04	6497	.662	3.13E-04	4.02E+04	9.52E-04	$4.60
?										
165,	.0019	4,6								
		47.1	4.0	3.17E-04	6519	.742	3.47E-04	2.44E+04	5.75E-04	
?										
170,	.0026	1,2								
		31.1	8.1	4.33E-04	7007	.620	2.74E-04	5.53E+04	1.13E-03	
?170,	.0024	1,2,3,6								
		35.0	6.8	4.00E-04	6922	.654	2.90E-04	4.48E+04	9.35E-04	
?										
180,	.0025	1,2								
		30.3	8.0	4.17E-04	7441	.612	2.55E-04	6.15E+04	1.11E-03	
?180,	.0024	2								
		32.3	7.3	4.00E-04	7392	.630	2.63E-04	5.50E+04	1.01E-03	
?180,	.0023	1,2,3,6								
		34.3	6.7	3.83E-04	7344	.648	2.71E-04	4.92E+04	9.13E-04	
?										
190,	.0022	3								
		33.9	6.4	3.67E-04	7763	.644	2.55E-04	5.33E+04	8.84E-04	
?										
200,	.0023	1,2								
		29.2	7.5	3.83E-04	8299	.602	2.25E-04	7.28E+04	1.06E-03	$ 4.20
?200,	.0021	1,2,3,5,6								
		33.6	6.2	3.50E-04	8178	.642	2.42E-04	5.68E+04	8.49E-04	
?200,	.0016	4,5,6								
		46.2	3.5	2.67E-04	7916	.736	2.83E-04	3.08E+04	4.92E-04	
?										
230,	.0014	4,5,6								
		46.0	3.1	2.33E-04	9109	.734	2.46E-04	3.59E+04	4.33E-04	
?										

SQUARE WEAVE

N, d	P	W_{100}	b	a	ϵ	D_c	$\frac{ba^2}{\epsilon^2}$	$\frac{b}{\epsilon^2}$	$\frac{\$}{FT.^2}$
250, .0016	5,6								
	36.0	4.5	2.67E-04	10151	.662	2.00E-04	6.28E+04	6.09E-04	
?									
280, .0014	5								
	37.0	3.8	2.33E-04	11338	.669	1.81E-04	6.70E+04	5.21E-04	$4.20
?280, .0012	5								
	44.1	2.8	2.00E-04	11136	.722	1.98E-04	4.76E+04	3.84E-04	
?									
325, .0012	5								
	37.2	3.2	2.00E-04	13151	.671	1.56E-04	7.68E+04	4.44E-04	$4.10
?325, .0011									
	41.3	2.7	1.83E-04	13012	.702	1.65E-04	6.30E+04	3.72E-04	
?									
400, .0010	5								
	36.0	2.8	1.67E-04	16241	.662	1.25E-04	1.00E+05	3.81E-04	$16.40
?400, .0009	5								
	41.0	2.2	1.50E-04	16027	.699	1.33E-04	7.87E+04	3.07E-04	
?									

TWILLED SQUARE

N	d		P	W_{100}	b	a	ϵ	D_c	$\frac{b a^2}{\epsilon^2}$	$\frac{b}{\epsilon^2}$	$\frac{\$}{FT^2}$
100,	.0045	3 *	30.3	13.7	7.50E-04	3952	.630	4.58E-04	2.96E+04	1.89E-03	$ 2.25
?110,	.0045	3,6	25.5	15.2	7.50E-04	4387	.589	3.83E-04	4.16E+04	2.16E-03	
?120,	.0037	3	30.9	11.1	6.17E-04	4737	.635	3.86E-04	3.43E+04	1.53E-03	
?130,	.0038	3,6	25.6	12.8	6.33E-04	5184	.590	3.24E-04	4.89E+04	1.82E-03	
?140,	.0033	3,6	28.9	10.4	5.50E-04	5546	.619	3.20E-04	4.42E+04	1.44E-03	
?150,	.0028	3	33.6	7.9	4.67E-04	5894	.656	3.22E-04	3.77E+04	1.08E-03	
?160,	.0028	3,6	30.5	8.5	4.67E-04	6321	.631	2.87E-04	4.68E+04	1.17E-03	
165,	.0026	3	32.6	7.5	4.33E-04	6494	.648	2.88E-04	4.35E+04	1.03E-03	
?170,	.0026	3,6	31.1	7.8	4.33E-04	6708	.637	2.74E-04	4.81E+04	1.07E-03	
?180,	.0025	3,6	30.3	7.6	4.17E-04	7114	.630	2.55E-04	5.32E+04	1.05E-03	
?190,	.0024	3	29.6	7.4	4.00E-04	7518	.624	2.39E-04	5.80E+04	1.03E-03	
?200,	.0023	3,4,6	29.2	7.2	3.83E-04	7920	.621	2.25E-04	6.24E+04	9.96E-04	$ 2.25
?200,	.0020	5	36.0	5.4	3.33E-04	7830	.674	2.50E-04	4.50E+04	7.34E-04	
?230,	.0018	3	34.3	5.0	3.00E-04	9028	.661	2.12E-04	5.59E+04	6.86E-04	
?250,	.0016	3,4,6	36.0	4.3	2.67E-04	9788	.674	2.00E-04	5.63E+04	5.87E-04	
?270,	.0016	3,4,6	32.3	4.7	2.67E-04	10633	.646	1.75E-04	7.24E+04	6.40E-04	
?300,	.0015	3,6	30.3	4.6	2.50E-04	11856	.630	1.53E-04	8.87E+04	6.31E-04	$7.80
?325,	.0014	3,4,5,6	29.7	4.3	2.33E-04	12857	.625	1.40E-04	9.87E+04	5.97E-04	
?400,	.0010	3,4,5,6	36.0	2.7	1.67E-04	15660	.674	1.25E-04	9.00E+04	3.67E-04	
?450,	.00106	5	27.4	3.4	1.77E-04	17880	.605	9.69E-05	1.54E+05	4.82E-04	
?500,	.0010	4	25.0	3.4	1.67E-04	19962	.584	8.33E-05	1.95E+05	4.88E-04	$43.00
?508,	.00108	5	20.4	4.1	1.80E-04	20498	.539	7.40E-05	2.61E+05	6.20E-04	
?508,	.000866	5	31.4	2.6	1.44E-04	20037	.639	9.19E-05	1.42E+05	3.54E-04	
?635,	.0008	4	24.2	2.8	1.33E-04	25395	.577	6.46E-05	2.58E+05	4.01E-04	$137.00
?850,	.00063	4	21.6	2.3	1.05E-04	34197	.551	4.55E-05	4.04E+05	3.46E-04	$139.00

? * SUPPLIER CODE

PLAIN DUTCH

N_W	N_S	d_W	d_S	Supplier code*	W_{100}	b	a	ε	$\frac{1.3ba^2}{\epsilon^2}$	$\frac{1.3b}{\epsilon^2}$	$\frac{\$}{FT.^2}$	μ_a
10	52	.028	.023	3*	125.2	6.17E-03	827	.589	1.58E+04	2.31E-02	$ 3.60	375
?12	64	.023	.0165	3	82.9	4.67E-03	973	.641	1.40E+04	1.48E-02		335
?12	88	.014	.013	3,2	58.2	3.33E-03	1292	.647	1.73E+04	1.04E-02		330
?14	64	.020	.0165	3	81.4	4.42E-03	1043	.627	1.59E+04	1.46E-02		320
?14	88	.020	.013	3	71.1	3.83E-03	1262	.625	2.03E+04	1.28E-02	$5.75	305
?14	95	.015	.012	3	57.5	3.25E-03	1381	.642	1.95E+04	1.02E-02		253
?14	100	.015	.012	3	60.0	3.25E-03	1443	.627	2.24E+04	1.08E-02		250
?20	120	.014	.010	3	55.7	2.83E-03	1786	.602	3.24E+04	1.02E-02		200
?24	110	.015	.0105	2,3,4,6	63.5	3.00E-03	1795	.572	3.84E+04	1.19E-02	$ 2.75	155
?24	175	.011	.0065	3	35.3	2.00E-03	2353	.643	3.49E+04	6.30E-03		140
?30	150	.009	.007	2,4	34.2	1.92E-03	2352	.639	3.38E+04	6.11E-03		
?30	160	.009	.007	2,3,6	36.0	1.92E-03	2479	.620	3.98E+04	6.48E-03		120
?40	200	.007	.0055	2,3,6	28.2	1.50E-03	3162	.619	5.08E+04	5.08E-03		73
?50	250	.0055	.0045	2,3,5,6	23.2	1.21E-03	3985	.611	6.67E+04	4.20E-03	$2.42	65
?												

* SUPPLIER CODE

REVERSE PLAIN DUTCH

N_s	N_w	d_s	d_w		W_{100}	b	a	ε	$\frac{1.3ba^2}{\epsilon^2}$	$\frac{1.3b}{\epsilon^2}$	$\frac{\$}{FT.^2}$	μ_a
15	64	.0276	.0159	Z*	99.5	4.95E-03	1034	.593	1.95E+04	1.83E-02		
?18	64	.0276	.0159	Z	110.8	4.95E-03	1136	.547	2.77E+04	2.15E-02		
?18	107	.0238	.00943	Z	68.8	3.56E-03	1418	.608	2.51E+04	1.25E-02		
?20	107	.0238	.00943	Z	73.6	3.56E-03	1491	.581	3.04E+04	1.37E-02		
?36	173	.0138	.00593	1,Z	46.3	2.14E-03	2579	.562	5.86E+04	8.81E-03		
?38	132	.0159	.00793	1,Z	67.3	2.65E-03	2393	.486	8.36E+04	1.46E-02		
?41	173	.0119	.00593	1,Z	43.2	1.98E-03	2790	.559	6.41E+04	8.24E-03		
?48	173	.0119	.00593	1,Z	47.9	1.98E-03	3049	.511	9.18E+04	9.87E-03		
?50	175	.012	.006	4	50.7	2.00E-03	3161	.487	1.10E+05	1.10E-02	$6.20	
?50	180	.012	.0057	4	48.5	1.95E-03	3174	.496	1.04E+05	1.03E-02		100
?69	292	.0087	.00343	1,Z	31.4	1.30E-03	4619	.510	1.38E+05	6.47E-03		
?70	280	.0083	.0035	4	30.0	1.27E-03	4564	.524	1.26E+05	6.03E-03	$8.30	54
?76	292	.0079	.00343	1,Z	30.0	1.23E-03	4909	.506	1.50E+05	6.24E-03		
?102	635	.0064	.00158	1,Z	20.1	7.97E-04	7676	.489	2.55E+05	4.33E-03		
?114	635	.0051	.00158	1,Z	16.0	6.88E-04	8409	.529	2.26E+05	3.20E-03		
?120	180	.004	.0035	Z	15.8	9.17E-04	4550	.651	5.82E+04	2.81E-03		
?120	200	.004	.0031	Z	14.4	8.50E-04	4785	.658	5.85E+04	2.55E-03		
?120	400	.0036	.0022	Z	12.7	6.67E-04	7088	.616	1.15E+05	2.29E-03	$4.20	
?120	670	.0047	.0015	4	14.7	6.42E-04	8894	.538	2.28E+05	2.88E-03	$11.40	27
?125	600	.0049	.0016	4	16.1	6.75E-04	8608	.517	2.43E+05	3.28E-03	$11.60	27
?125	400	.0036	.0022	Z	13.0	6.67E-04	7243	.606	1.24E+05	2.36E-03		
?125	600	.0048	.0016	Z	15.7	6.67E-04	8621	.524	2.34E+05	3.15E-03		
?130	635	.0051	.00158	1,Z	17.7	6.88E-04	9091	.479	3.22E+05	3.90E-03		
?140	720	.0043	.0014	4	14.2	5.92E-04	10044	.514	2.94E+05	2.91E-03	$12.00	21
?135	635	.0051	.00158	1,Z	18.3	6.88E-04	9308	.463	3.61E+05	4.17E-03		
?152	747	.0044	.00134	1,Z	15.3	5.90E-04	10635	.476	3.83E+05	3.38E-03		
?155	850	.004	.0012	4	13.1	5.33E-04	11369	.503	3.55E+05	2.74E-03	$14.40	20

?

* SUPPLIER CODE

TWILLED DUTCH

N_W N_S d_W d_S		W_{100}	b	a	ϵ	$\frac{1.3ba^2}{\epsilon^2}$	$\frac{1.3b}{\epsilon^2}$	$\frac{\$}{FT.^2}$	μ_a
16,200,.011,.010	3*	72.7	2.58E-03	2713	.430	1.33E+05	1.81E-02		130
?20,250,.010,.0085	3,4,6	66.8	2.25E-03	3345	.399	2.06E+05	1.84E-02		80
?20,250,.0036,.008	2	53.3	1.63E-03	4036	.340	2.99E+05	1.84E-02		
?20,280,.011,.0075	3	60.5	2.17E-03	3465	.435	1.78E+05	1.49E-02		132
?20,200,.011,.010	3	75.3	2.58E-03	2803	.411	1.57E+05	1.99E-02		110
?20,350,.007,.006	3	44.6	1.58E-03	4514	.430	2.27E+05	1.11E-02		68
?28,500,.007,.0045	3,6	38.0	1.33E-03	5897	.423	3.37E+05	9.68E-03		60
?30,250,.010,.008	2	65.0	2.17E-03	3533	.393	2.28E+05	1.82E-02		
?30,260,.010,.008	3,6	67.2	2.17E-03	3657	.372	2.72E+05	2.03E-02		75
?30,370,.010,.006	4	55.1	1.83E-03	4526	.391	3.19E+05	1.56E-02		100
?30,500,.008,.006	3	66.9	1.67E-03	6347	.188	2.47E+06	6.14E-02		57
?40,570,.0071,.0040	4	37.4	1.26E-03	6669	.398	4.58E+05	1.03E-02		70
?50,700,.006,.003	3	27.2	1.00E-03	7858	.450	3.97E+05	6.42E-03		50
?80,700,.004,.003	1,2,3,4,6	26.0	8.33E-04	9702	.369	7.51E+05	7.98E-03	$7.50	43
?150,800,.0027,.0021	3	16.3	5.75E-04	12458	.427	6.35E+05	4.09E-03		35
?164,800,.0028,.002	1	15.9	5.67E-04	12626	.432	6.31E+05	3.96E-03		26
?165,800,.0028,.0020	4	16.0	5.67E-04	12654	.430	6.38E+05	3.98E-03		26
?165,800,.0029,.0020	2	16.3	5.75E-04	12606	.426	6.55E+05	4.12E-03		
?165,1200,.0028,.0016	2	15.3	5.00E-04	16389	.381	1.20E+06	4.47E-03		
?165,1400,.0028,.0016	1,2,4	17.1	5.00E-04	18636	.306	2.41E+06	6.93E-03		18
?165,1400,.0026,.0016	3	16.5	4.83E-04	18925	.311	2.33E+06	6.49E-03		21
200,600,.0023,.0018		10.6	4.92E-04	10852	.562	2.38E+05	2.02E-03		
?200,600,.0026,.0018	2	11.7	5.17E-04	10819	.542	2.68E+05	2.29E-03	$9.00	
?200,600,.0021,.0016	3	8.4	4.42E-04	10649	.614	1.73E+05	1.52E-03		30
?200,900,.0020,.0014	2	8.9	4.00E-04	14073	.550	3.40E+05	1.72E-03		

?

* SUPPLIER CODE

TWILLED DUTCH

N_w	N_s	d_w	d_s		W_{100}	b	a	ϵ	$\frac{1.3ba^2}{\epsilon^2}$	$\frac{1.3b}{\epsilon^2}$	$\frac{\$}{FT.^2}$	μ_a
200	1400	.0028	.0016	1,2,4	18.6	5.00E-04	19930	.248	4.21E+06	1.06E-02	$12.00	14
?200	1400	.0021	.0016	3	15.9	4.42E-04	20865	.273	3.34E+06	7.68E-03		16
?250	1370	.0022	.0016	3	17.4	4.50E-04	22045	.217	6.03E+06	1.24E-02	$15.10	
?250	1400	.0022	.0016	1,2,4	17.7	4.50E-04	22444	.204	7.09E+06	1.41E-02		12
?250	1620	.0022	.0016	2	19.9	4.50E-04	25367	.106	3.32E+07	5.16E-02		
?325	1480	.0014	.0012	2	10.0	3.17E-04	24857	.360	1.97E+06	3.18E-03		
?325	1700	.0014	.0012	2	11.2	3.17E-04	27881	.284	3.96E+06	5.10E-03		
?325	1900	.0014	.0011	2	10.6	3.00E-04	29808	.287	4.20E+06	4.73E-03		
?325	1900	.0014	.0012		12.3	3.17E-04	30630	.215	8.32E+06	8.87E-03		
?325	1900	.0015	.0012	4	12.7	3.25E-04	30393	.211	8.79E+06	9.51E-03		9
?325	2300	.0014	.0011	2	12.4	3.00E-04	35080	.166	1.74E+07	1.41E-02	$41.50	
?325	2300	.0015	.0010	4	10.9	2.92E-04	33598	.245	7.11E+06	6.30E-03		10
?325	2300	.0018	.001	1	12.2	3.17E-04	32638	.223	8.79E+06	8.26E-03		10
?325	2800	.0014	.0010	2	12.3	2.83E-04	40255	.119	4.19E+07	2.59E-02		
?375	2300	.0014	.0010	1,4	11.1	2.83E-04	35727	.207	1.10E+07	8.58E-03		8
?375	2400	.0012	.0009	2	8.9	2.50E-04	36501	.280	5.51E+06	4.14E-03		
?400	2800	.0011	.00078	2	7.8	2.22E-04	41077	.291	5.74E+06	3.40E-03		
?450	2750	.001	.0008	1,4	8.0	2.17E-04	43000	.256	7.94E+06	4.29E-03	$165.00	7
?508	3600	.0010	.0006	4	6.4	1.83E-04	51061	.289	7.43E+06	2.85E-03		6

?

APPENDIX B

FLOW TEST DATA CORRELATION

Screen Flow-Through Loss Data

The screen flow-through loss data, plotted in Armour and Cannon form, are shown for all 10 screens in Figures 36 through 42. Also shown in these figures are data from all other known sources. These data have been normalized to agree with the geometric characteristics of our screens (especially specified pore diameter) as shown in Table VIII.

Figure 36 shows the available data for the 325 x 2,300 screen, including gas data from the MDAC-MSFC contract NAS8-27685 (ref. 12) which agree with our data rather well. Water test data from Kressilk (ref. 13) and Wintec Corp. (ref 14) are also shown, together with the generalized Armour and Cannon correlation for all screens, which overpredicts the friction factor and thus the pressure loss for this screen by 170%.

Many data have been accumulated for the 200 x 1,400 screen, and our data are generally centered on the normalized available data, as shown in Figure 37. Some of the data scatter evident in Figure 37 may be caused by unaccounted differences in the screens tested (wire diameter, void fraction, etc.) or to the rather large variations in the properties of the test fluids. Again, the generalized Armour and Cannon correlation is substantially above the correlation for our data.

Figure 38 shows the correlation for the 720 x 140 reverse Dutch screen, which lies above, but close to the generalized Armour and Cannon correlation. Previous MDAC data also agree well with our data. Figure 39 shows the correlation for the 165 x 800 screen. The GDA data were definitely obtained with a different type of 165 x 800 screen (different wire diameter), but when normalized to our 165 x 800 screen characteristics, agree very well with our data. Figure 40 shows the correlation for our 50 x 250 plain Dutch screen, which again agrees very well with the normalized GDA data (ref. 15) using GH_2 and GN_2. Figure 41 shows the correlation for the 24 x 110 plain Dutch screen, which coincidentally falls right on the generalized Armour and Cannon correlation, as does the Kressilk data. Therefore, the α and β values from the Armour and Cannon correlation were retained for the 24 x 110 screen.

The correlations for the square weave screens are all shown in Figure 42, and were discussed previously.

Channel Flow Loss Data

The data, plotted as head loss in meters of 34.5 N/cm^2 LH_2 versus channel flow velocity in meters/sec with length (L) over channel height (s) as a parameter, are shown for the 10 screens in Figures 43 through 52. As anticipated in test planning, the pressure drop was linear with length: in

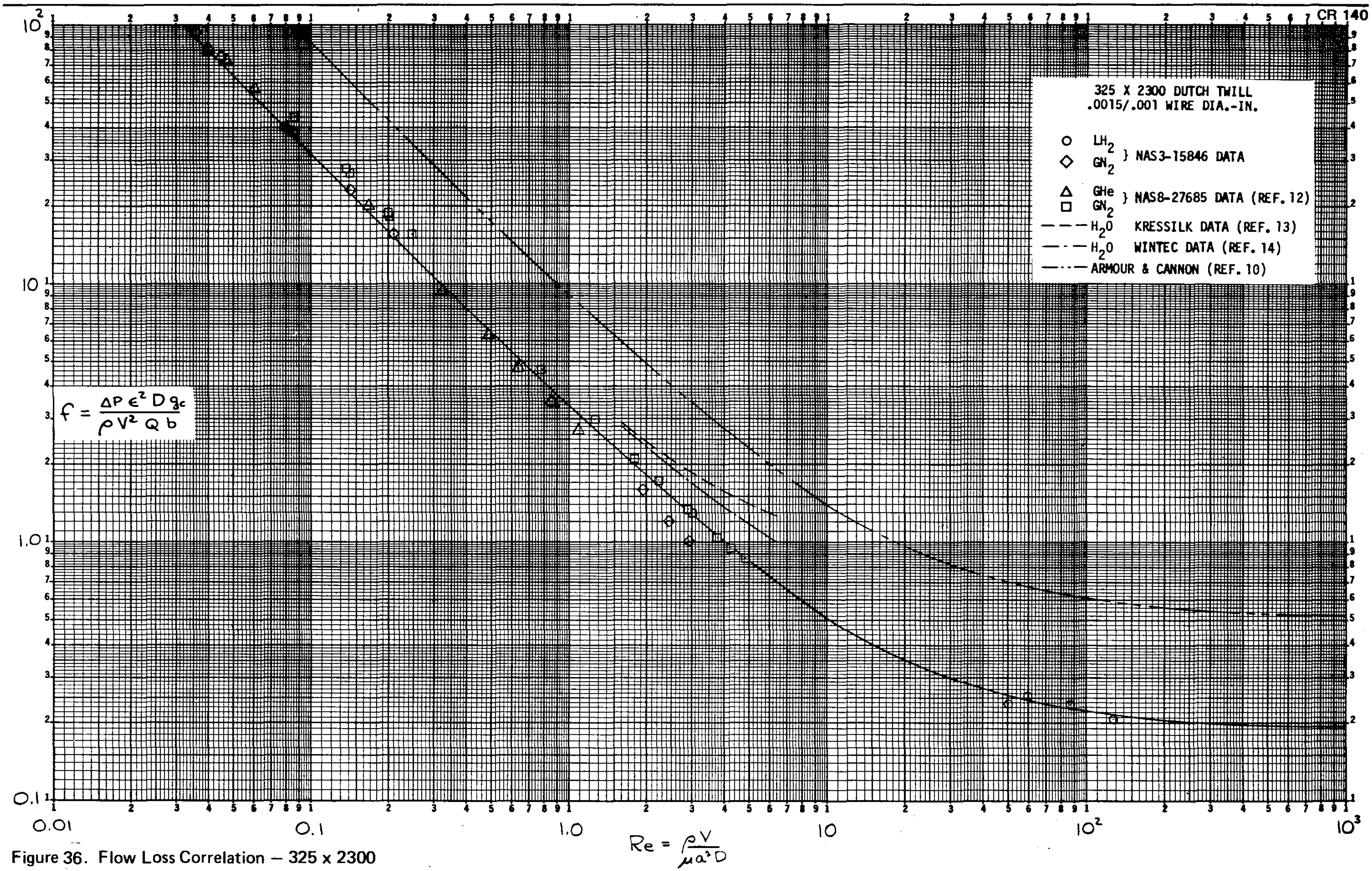

Figure 36. Flow Loss Correlation – 325 x 2300

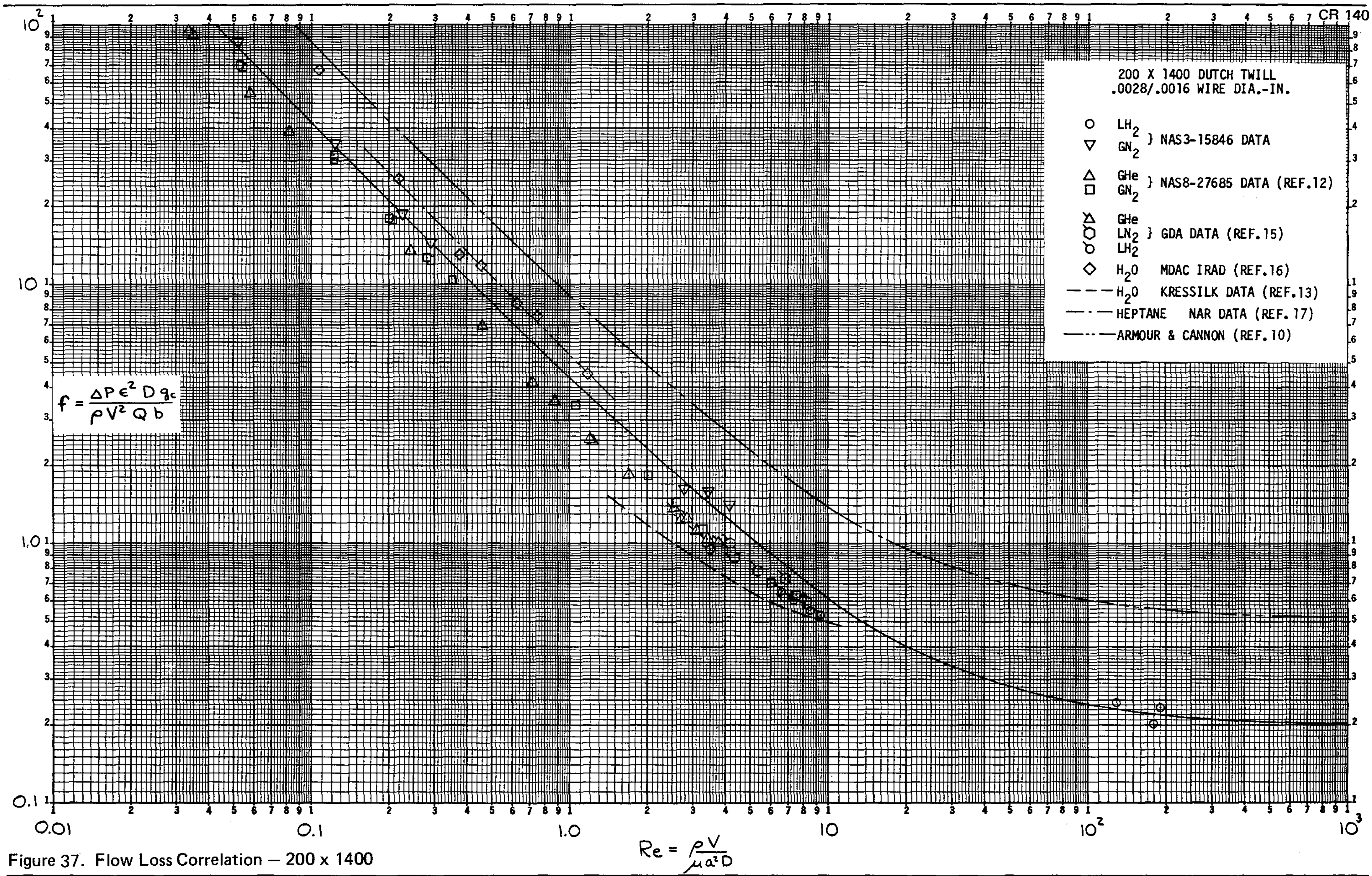

Figure 37. Flow Loss Correlation — 200 x 1400

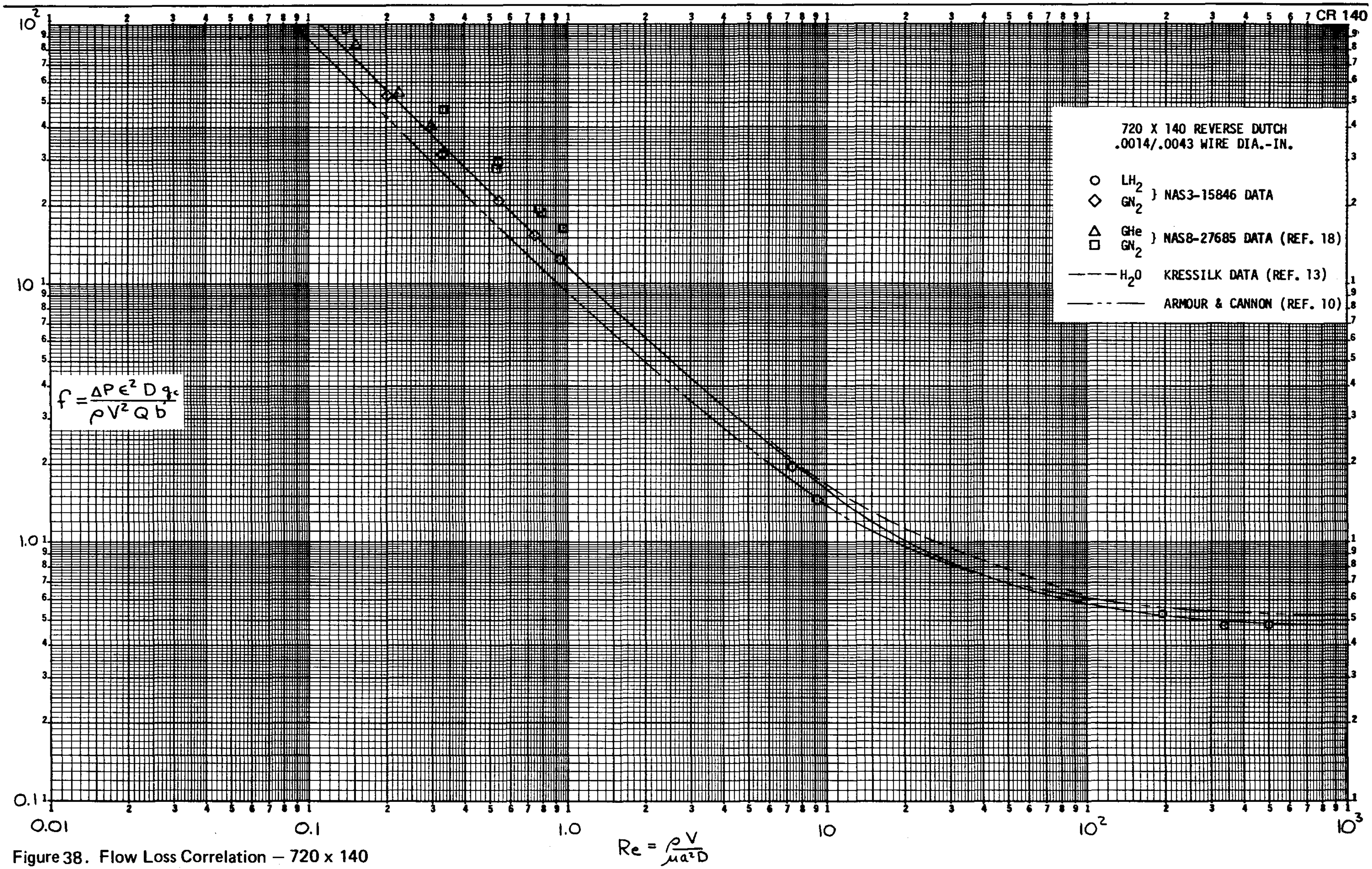

Figure 38. Flow Loss Correlation – 720 x 140

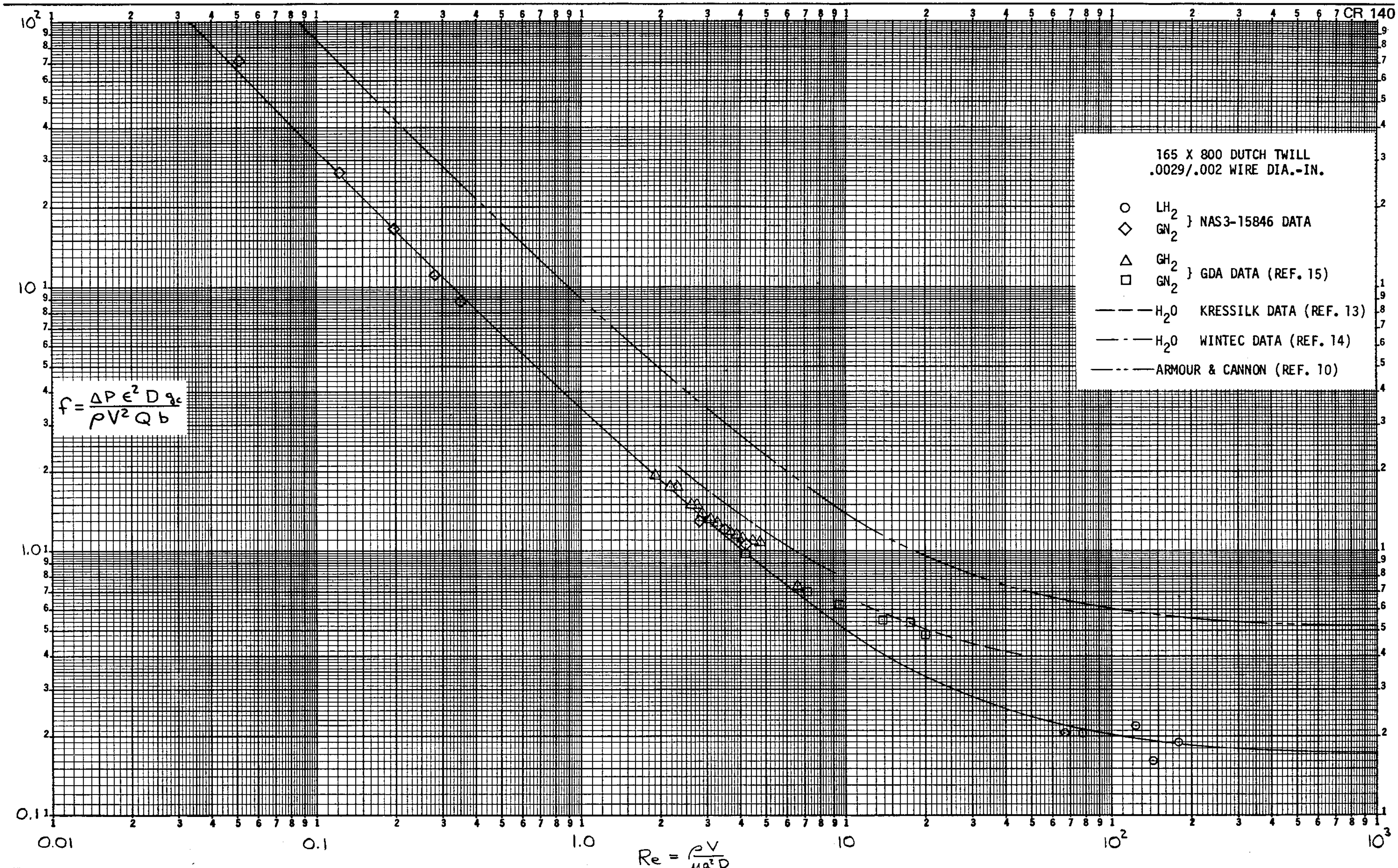

Figure 39. Flow Loss Correlation — 165 x 800

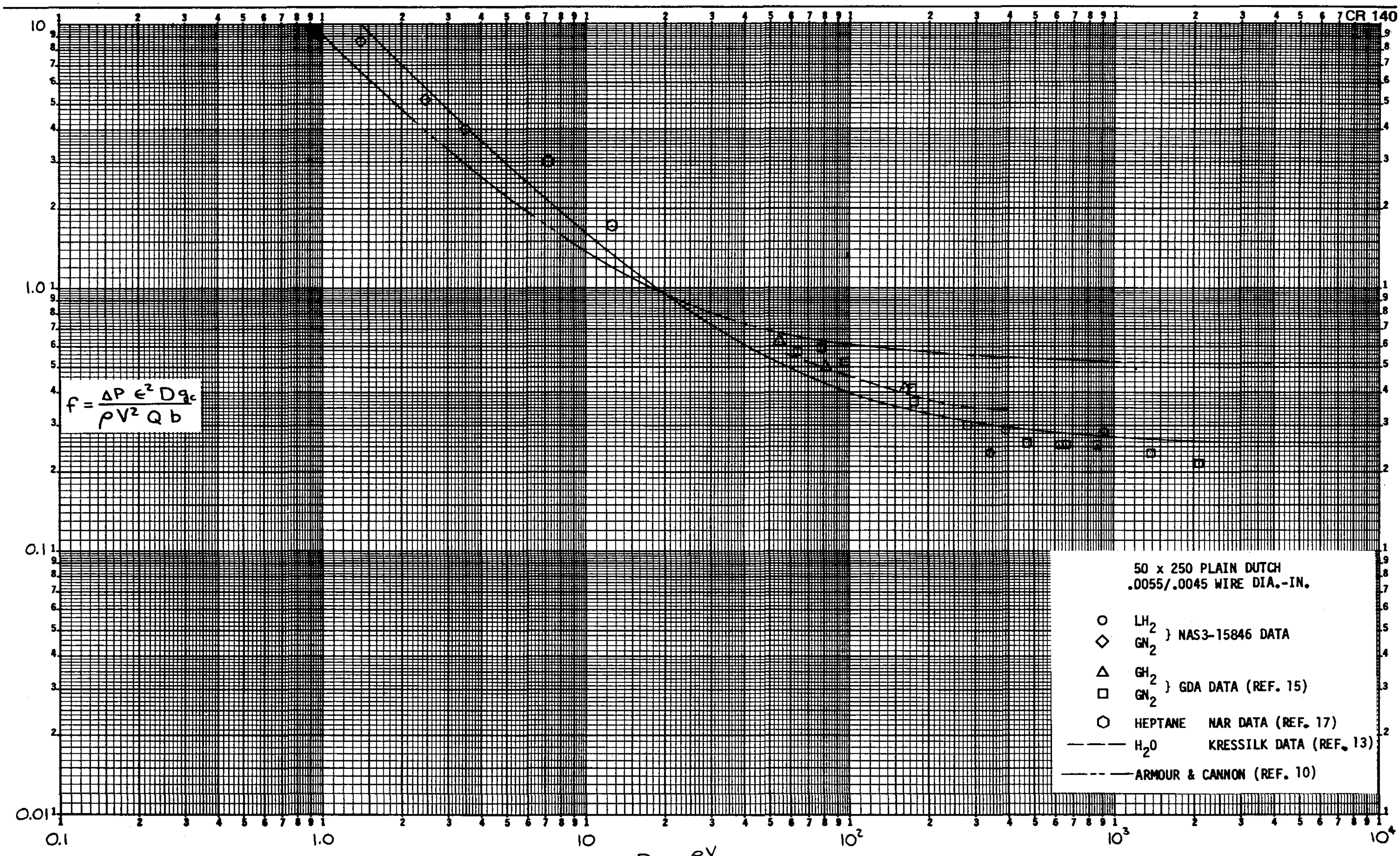

Figure 40. Flow Loss Correlation — 50 x 250

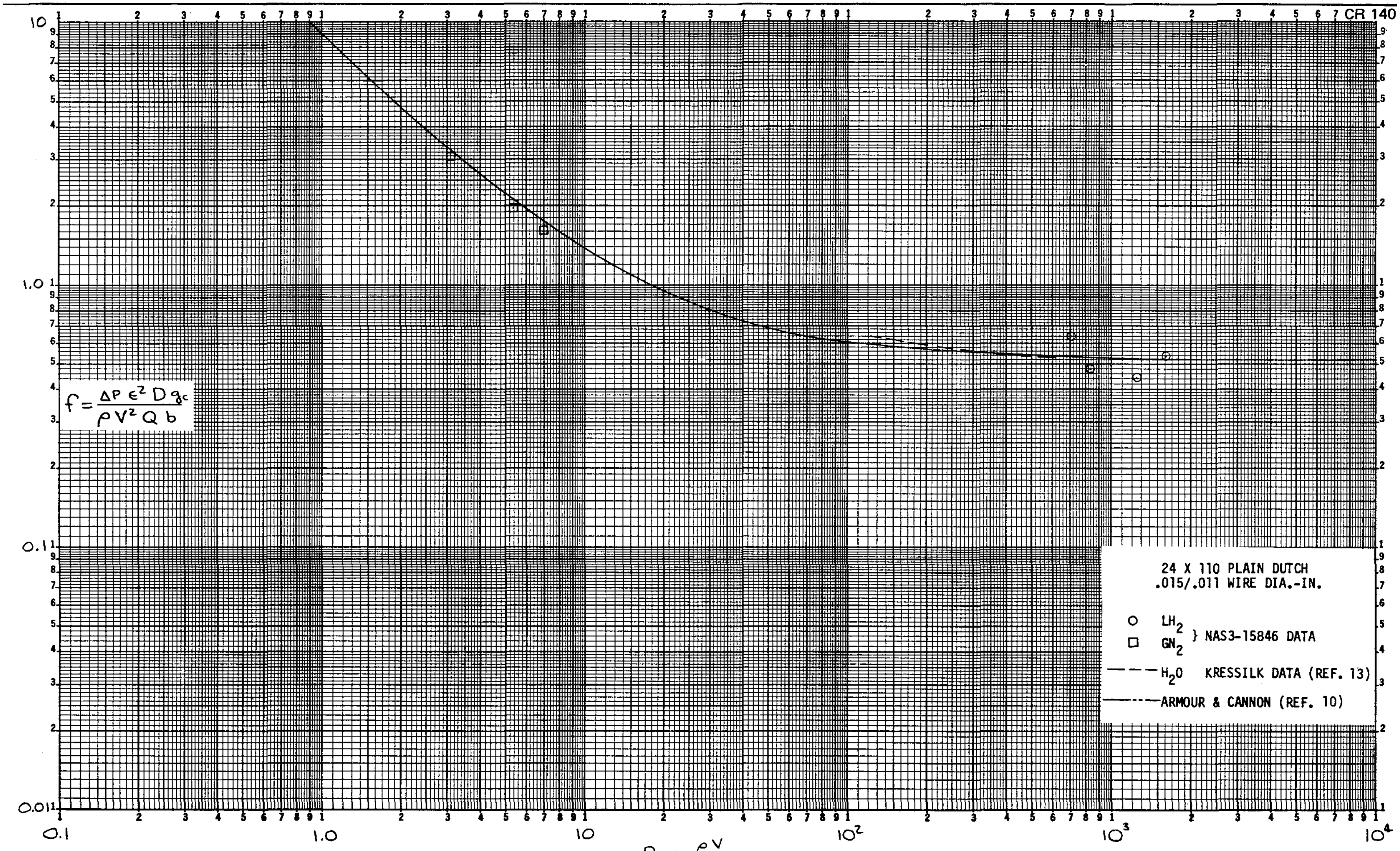

Figure 41. Flow Loss Correlation — 24 x 110

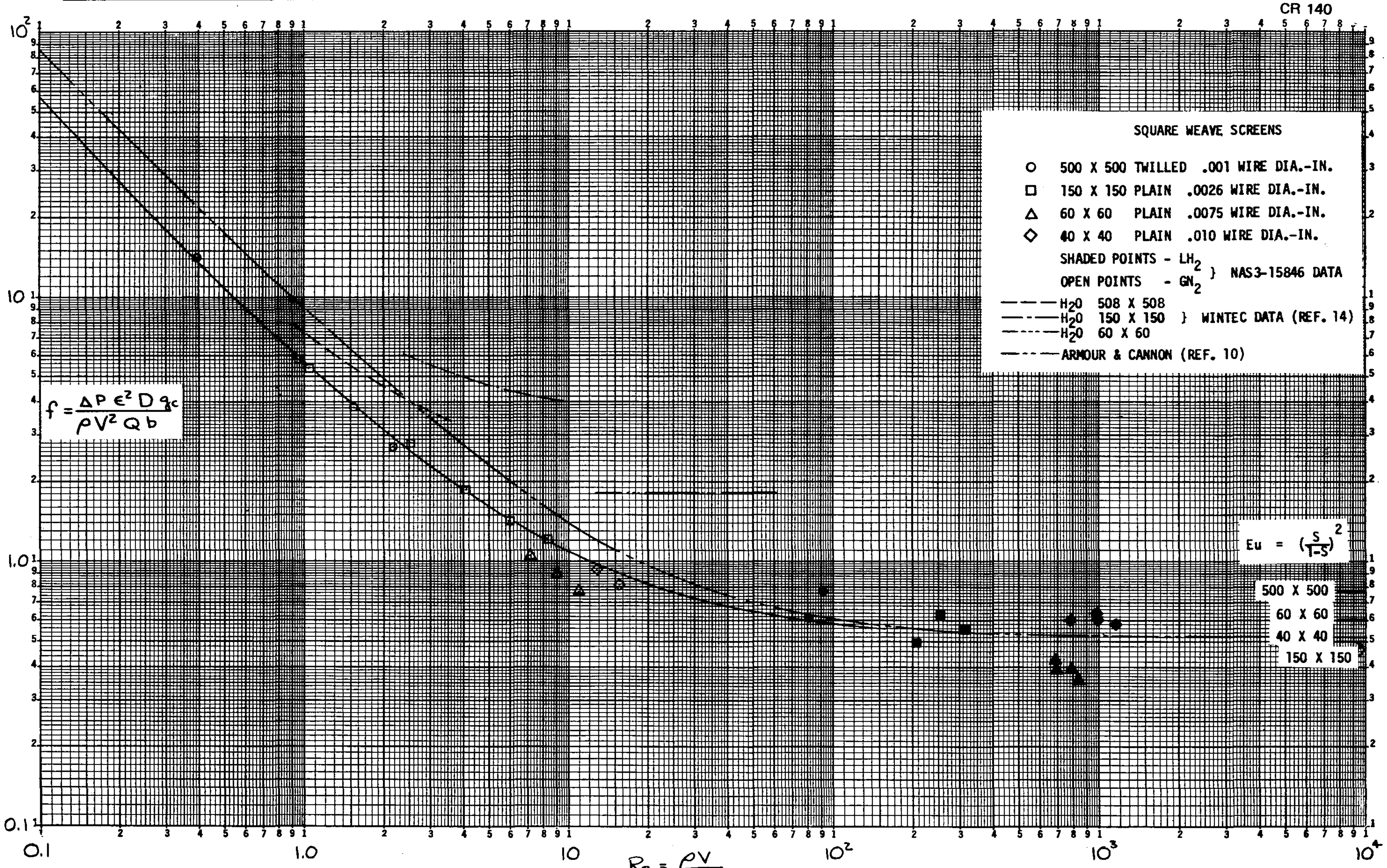

Figure 42. Flow Loss Correlation – Square Weave Screens

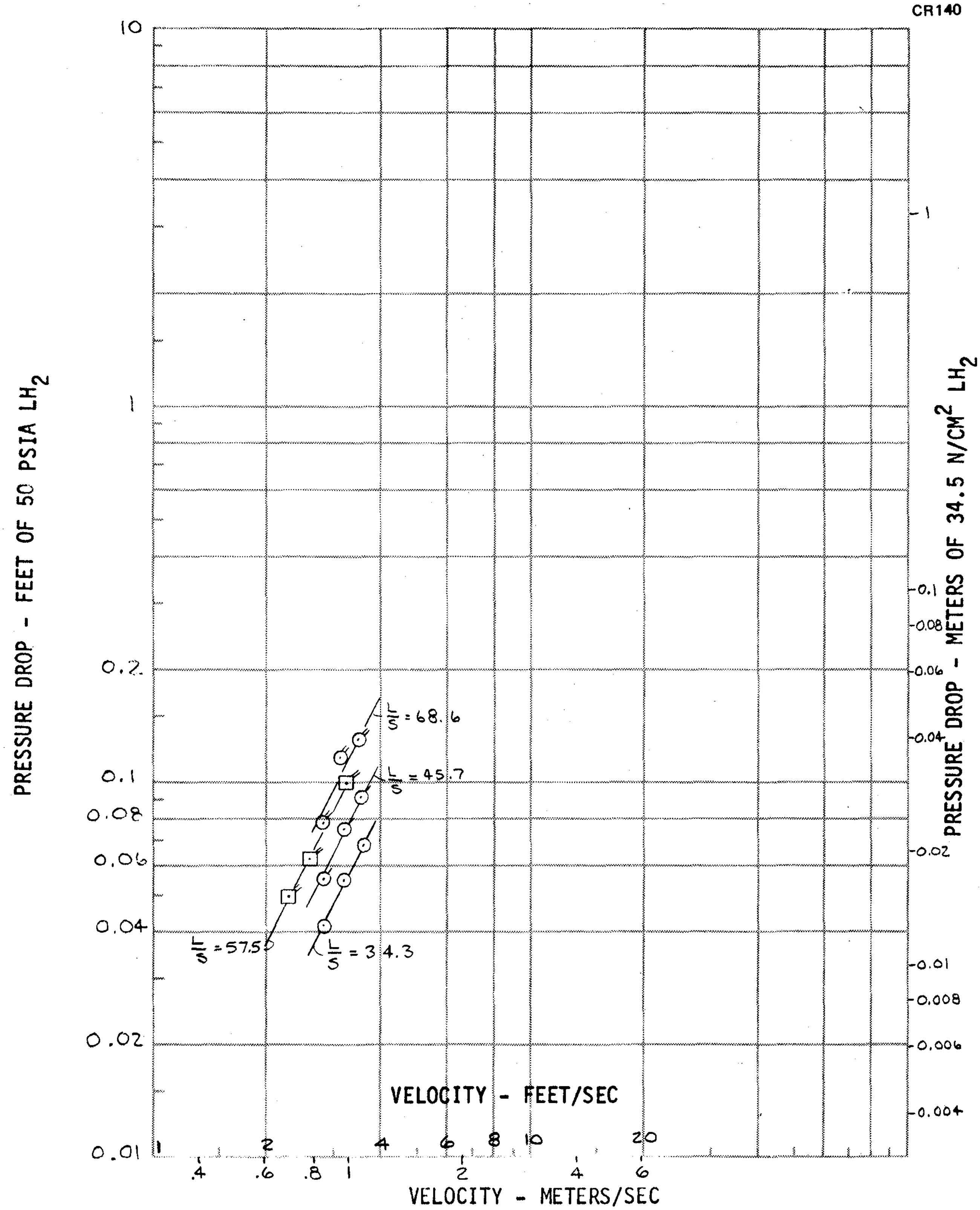

Figure 43. Channel Flow Pressure Drop Correlation — 325 X 2300

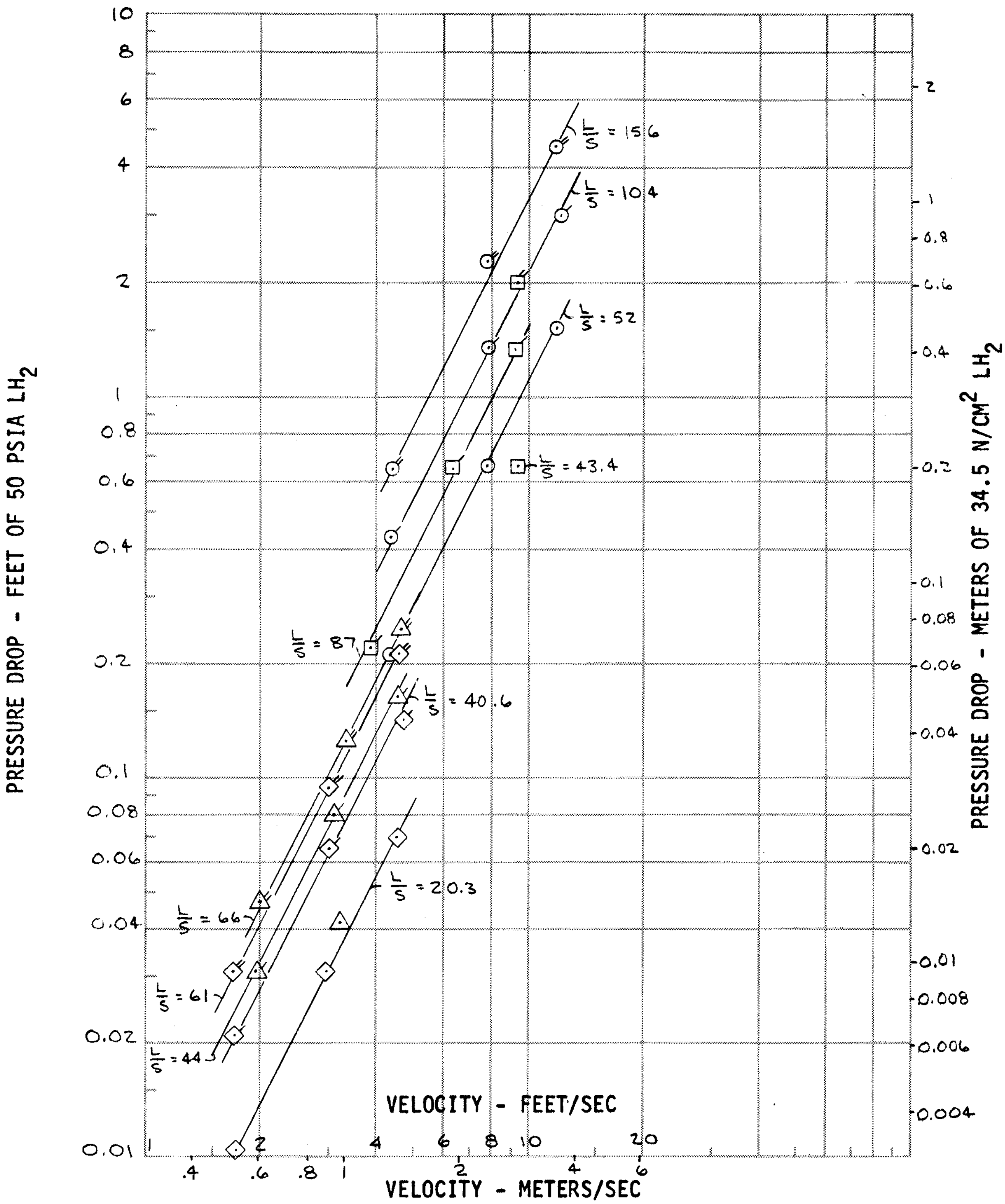

Figure 44. Channel Flow Pressure Drop Correlation — 200 X 1400

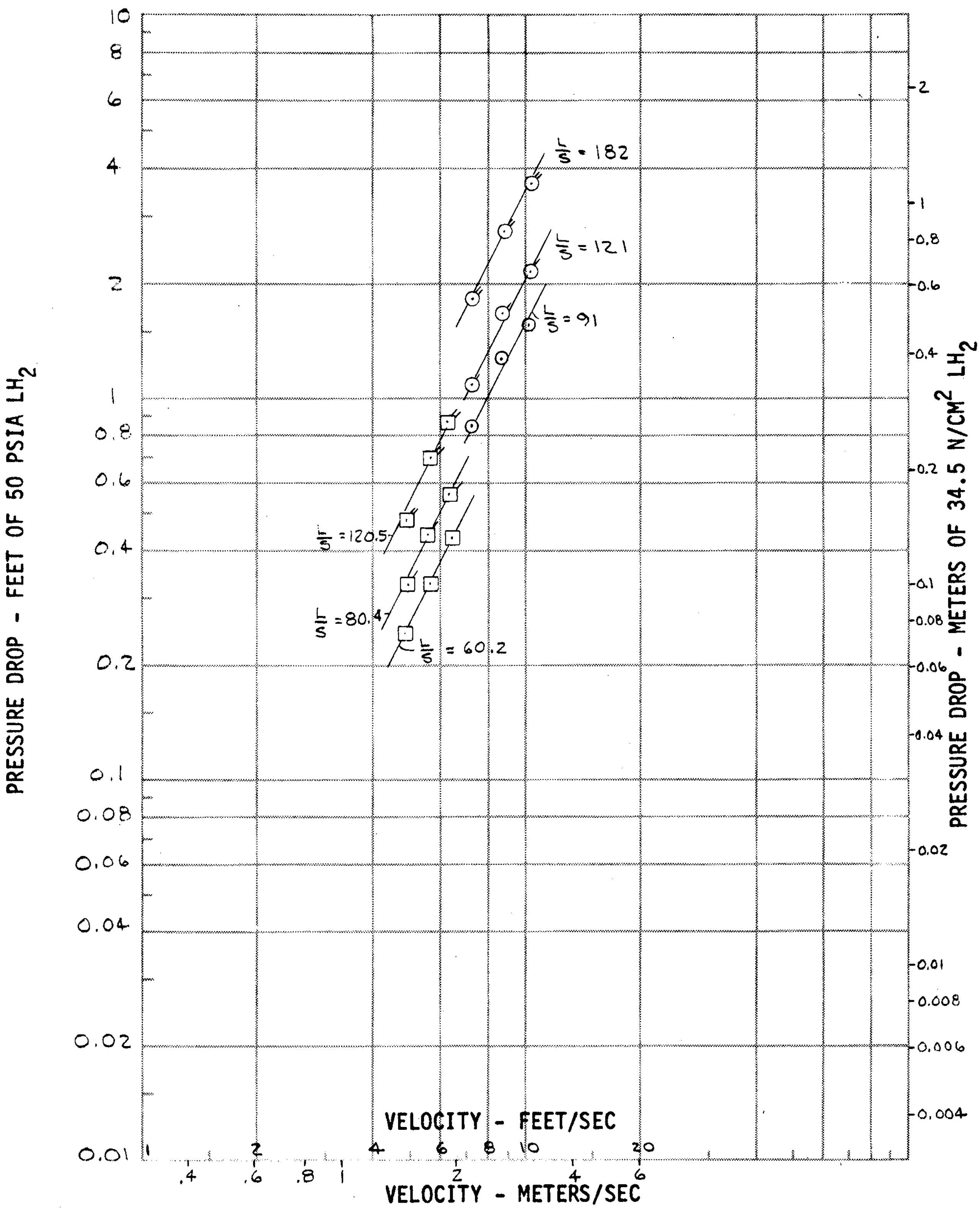

Figure 45. Channel Flow Pressure Drop Correlation — 500 X 500

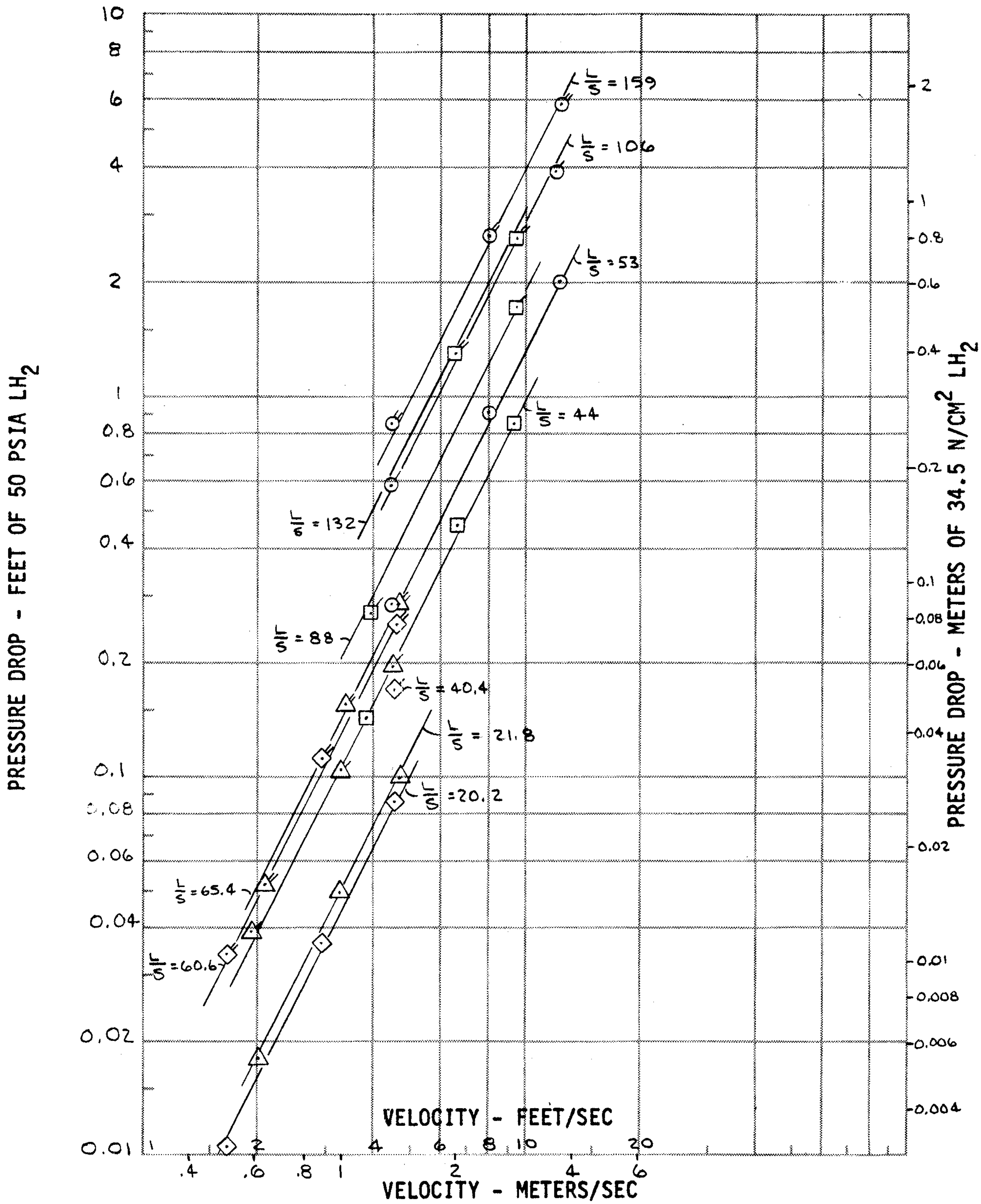

Figure 46. Channel Flow Pressure Drop Correlation — 720 X 140

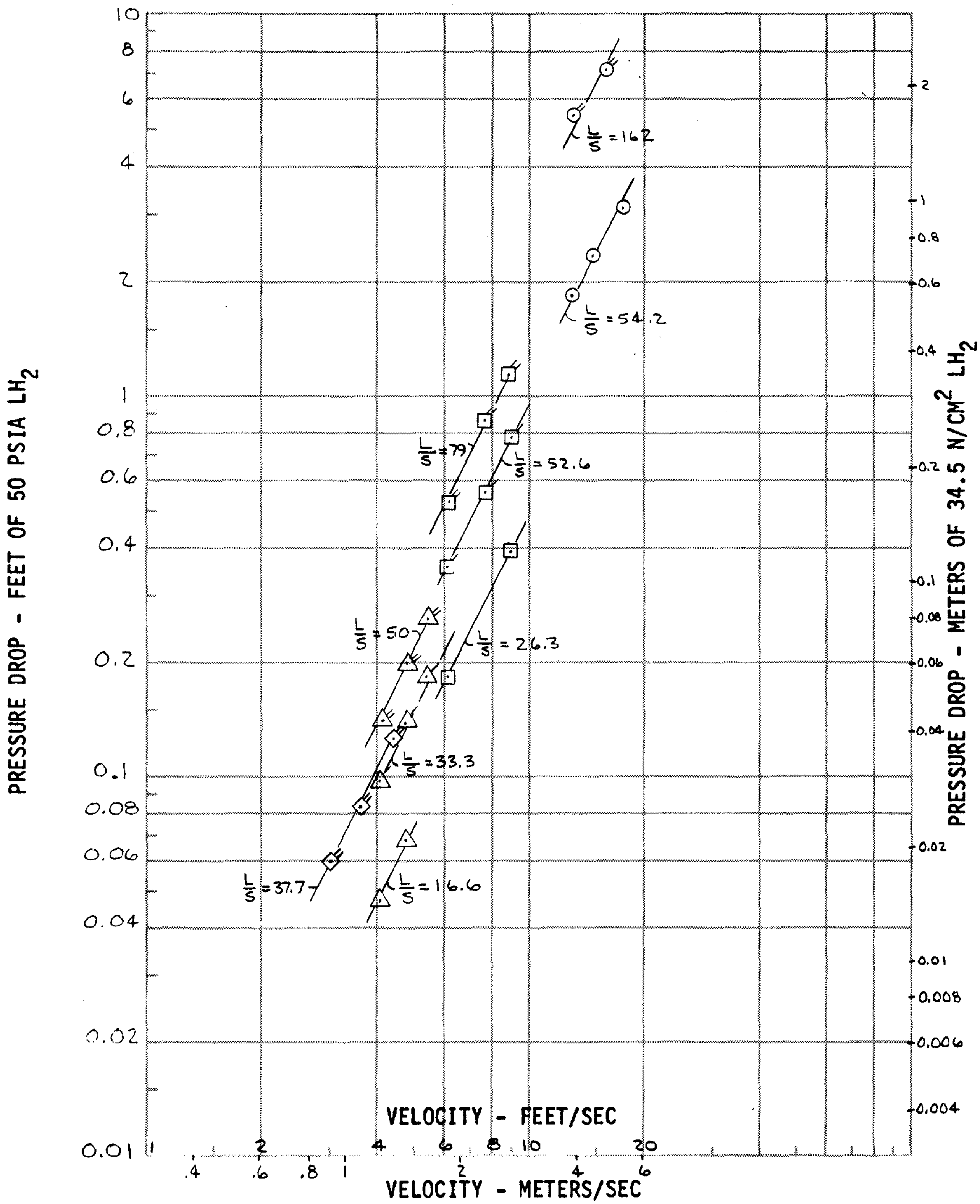

Figure 47. Channel Flow Pressure Drop Correlation — 165 X 800

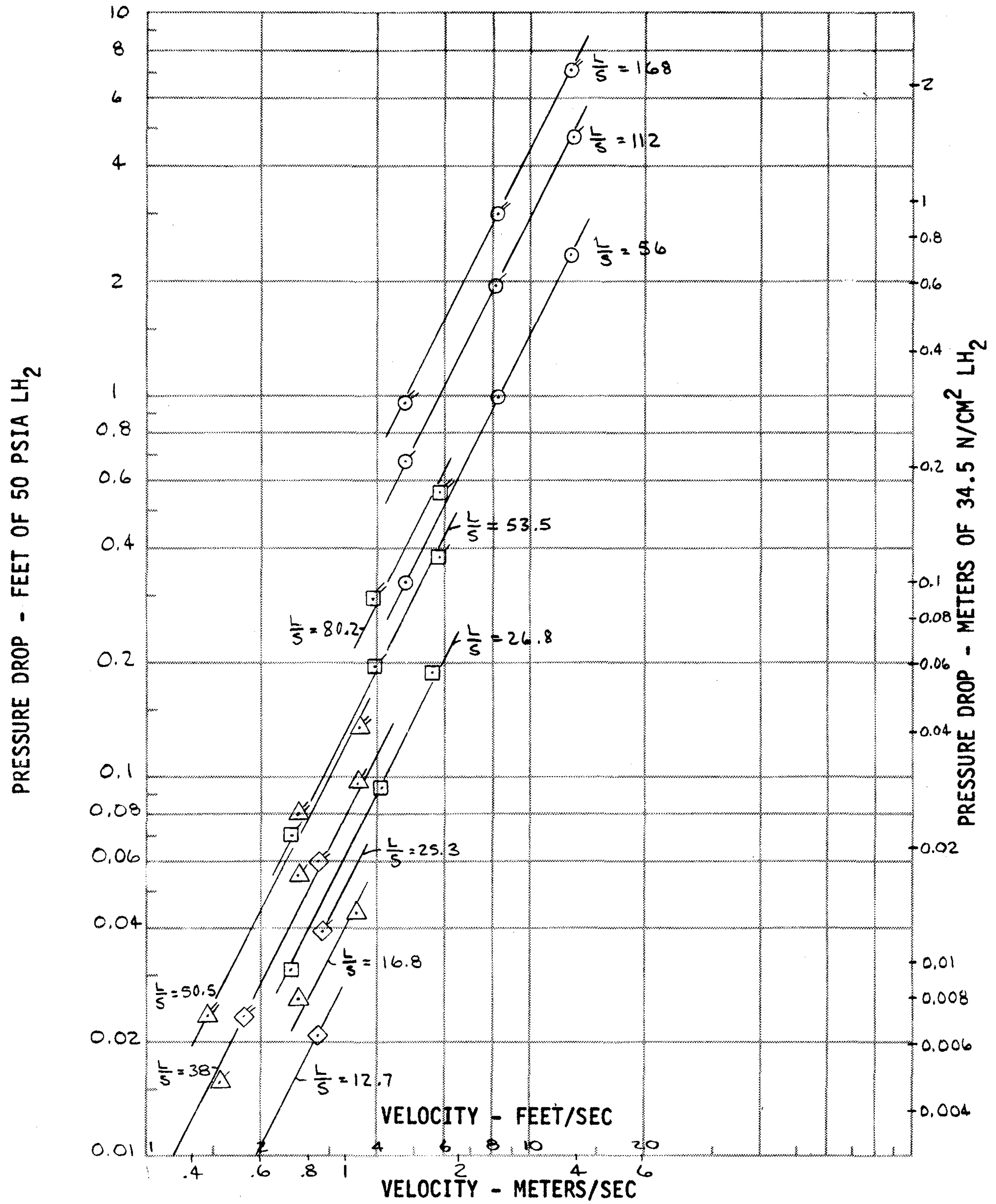

Figure 48. Channel Flow Pressure Drop Correlation — 50 X 250

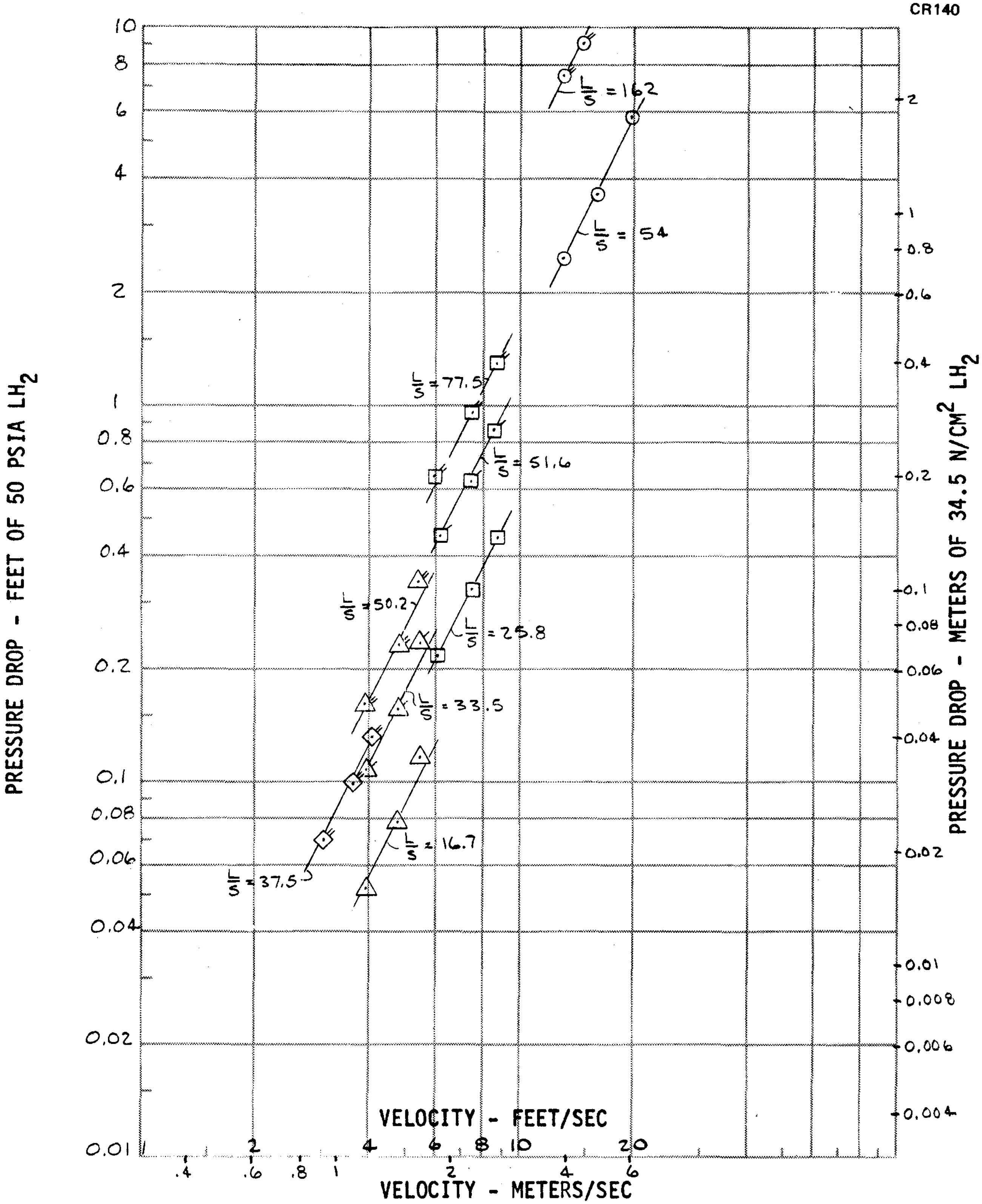

Figure 49. Channel Flow Pressure Drop Correlation — 150 X 150

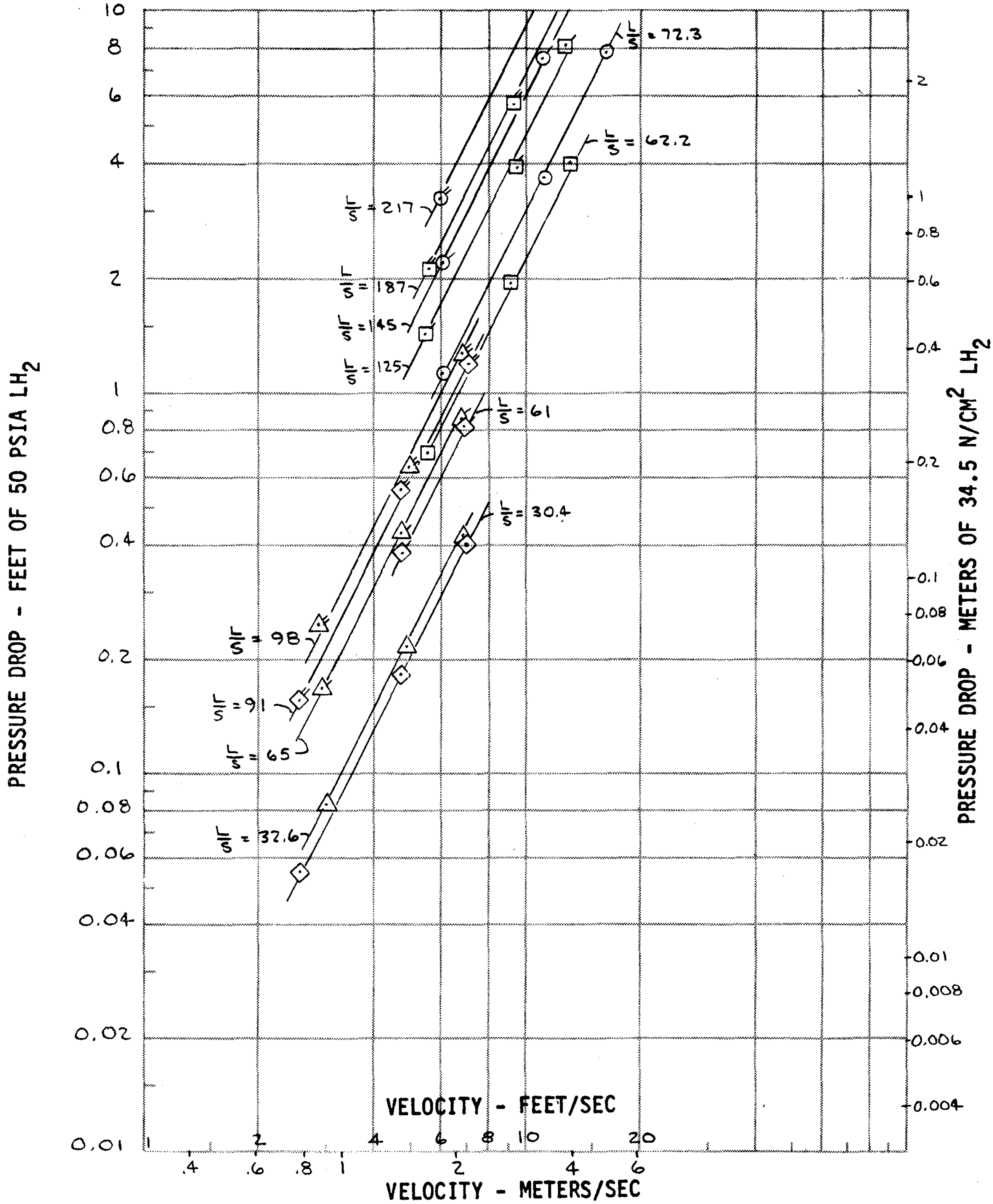

Figure 50. Channel Flow Pressure Drop Correlation — 24 X 110

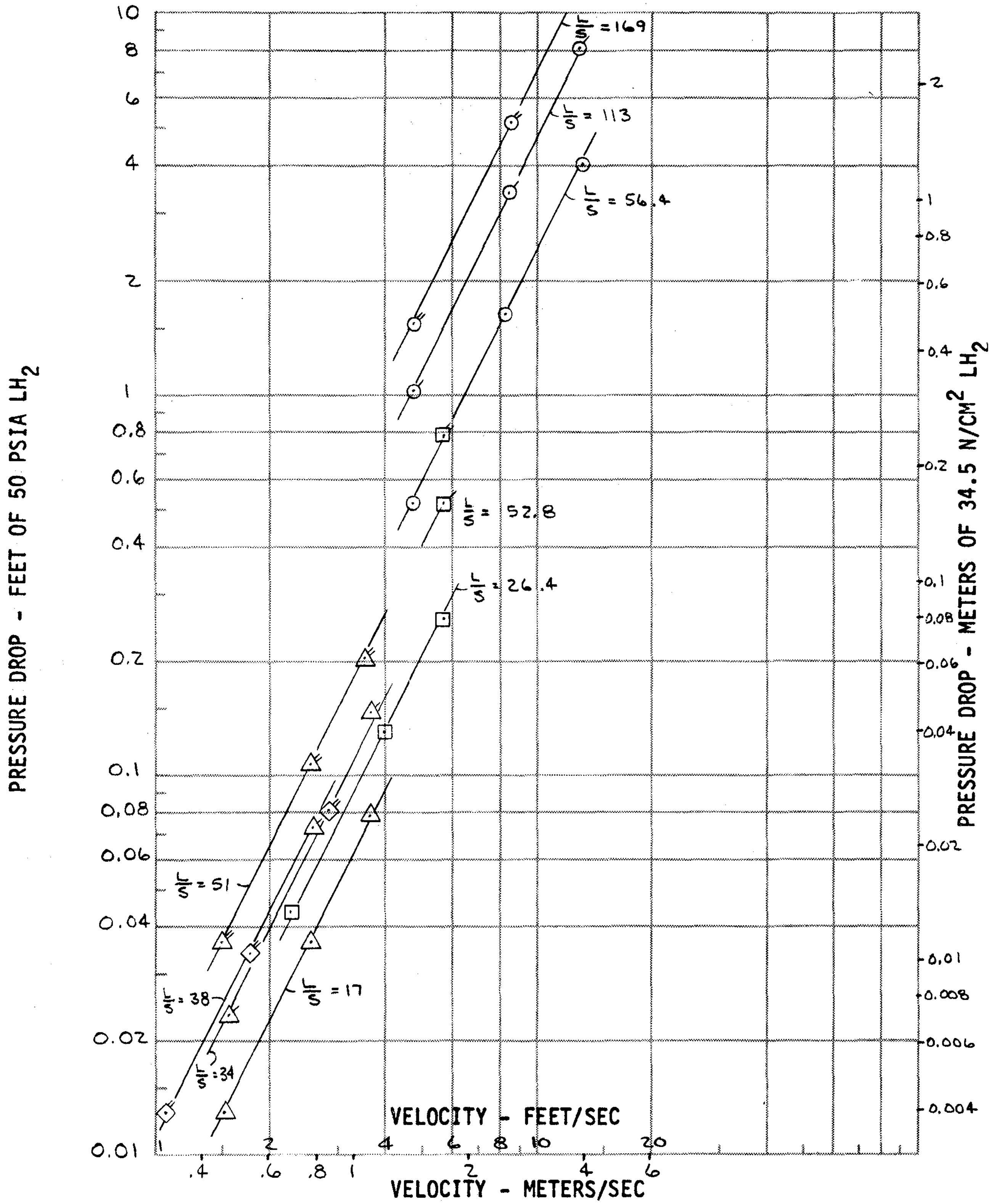

Figure 51. Channel Flow Pressure Drop Correlation – 60 X 60

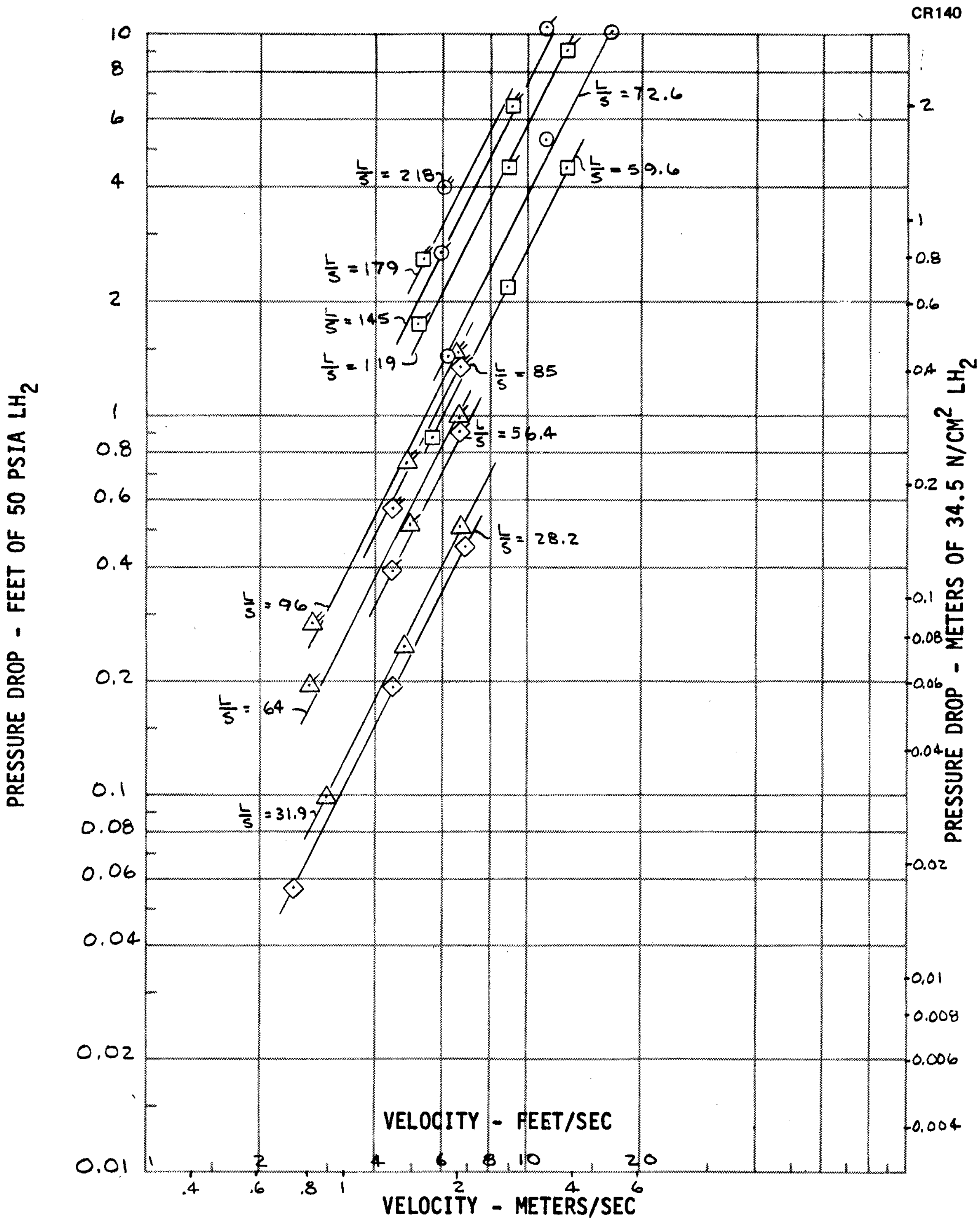

Figure 52. Channel Flow Pressure Drop Correlation — 40 X 40

Figures 43 through 52, the plain symbols are for the 33 cm (13-inch) length, the primed symbols are for 66 cm (26-inch), and the double-primed symbols for the 99 cm(39-inch) length (except for the 325 x 2,300 and 500 x 500 screens where they correspond to 99, 132, and 198 cm (39, 52, and 78-inches) respectively. Because the channel flow lies in the turbulent regime, the pressure drop varies essentially as the channel flow velocity squared, as shown by the slope of the lines on Figures 43 through 52. In general, the pressure drop increases with increasing L/s, but in some cases, extreme channel height values cause jumps in the L/s correlation because of the effect of channel height on friction factor; see, for example Figures 44, 46, 50, and 52.

To determine the effects of channel height (or effectively, e/D_h) on our channel flow loss and the appropriate roughness parameter, our data were plotted on the Moody graph, as shown in Figures 53 through 62. In these figures, the collection of data points at $R \doteq 10^5$ or higher were the 34.5 N/cm^2 (50 psia) LH_2 data, while the single points at $R \doteq 5,000$ were taken with ambient GN_2. In our experiments, the direction of fluid flow was always in the direction of the shute wires, which should minimize the pressure drop due to the construction of the Dutch-weave screens. It was noted from the data that the f for the Dutch-weave screens was about half that for square-weave screens of about the same wire diameter and essentially identical geometry and flow conditions. This is shown, for example, by comparing the 24 x 110 screen (Figure 60) with the 40 x 40 screen (Figure 62), or the 165 x 800 screen (Figure 57) with the 150 x 150 screen (Figure 59).

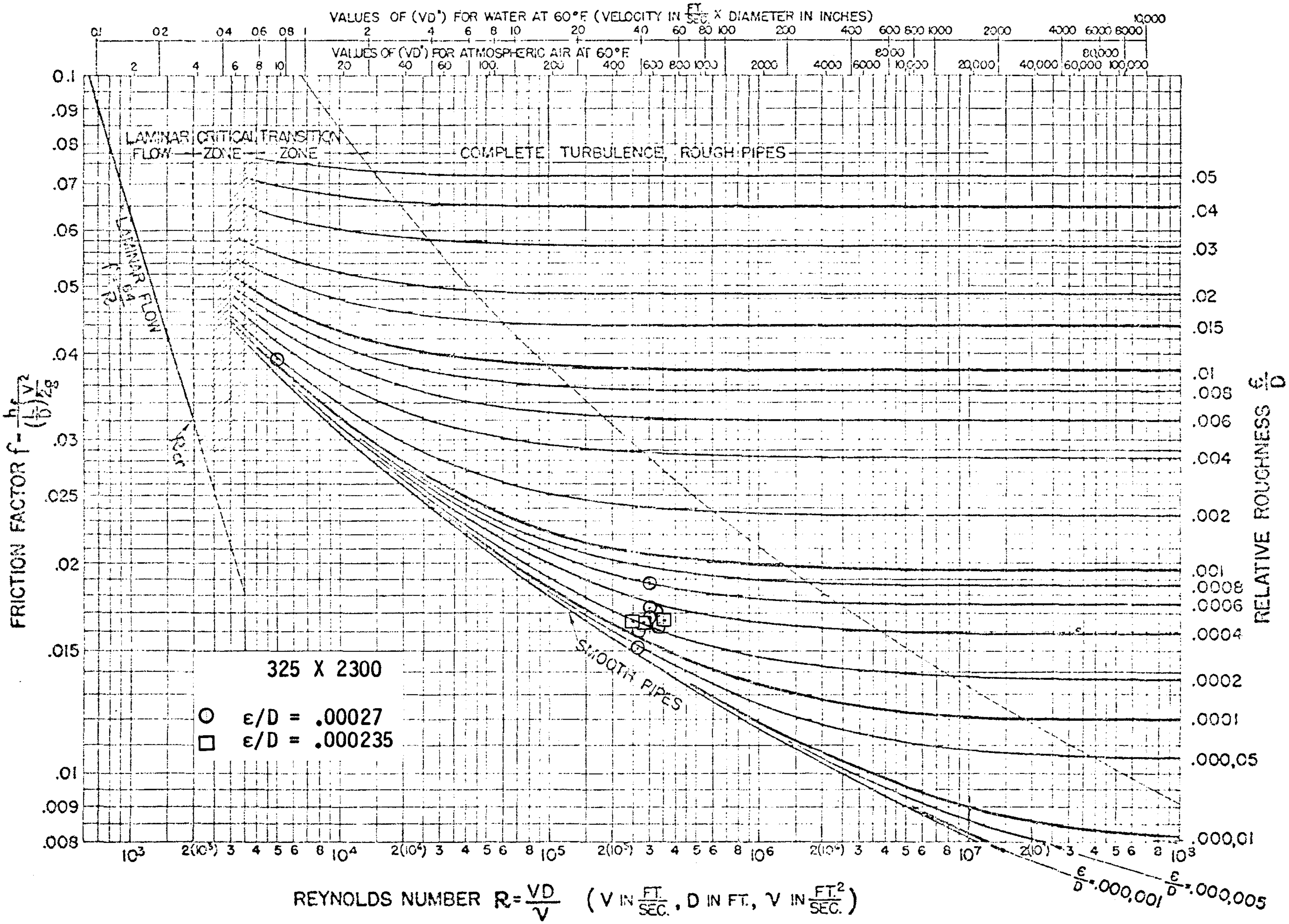

Figure 53. Dimensionless Channel Flow Loss Correlation – 325 x 2300

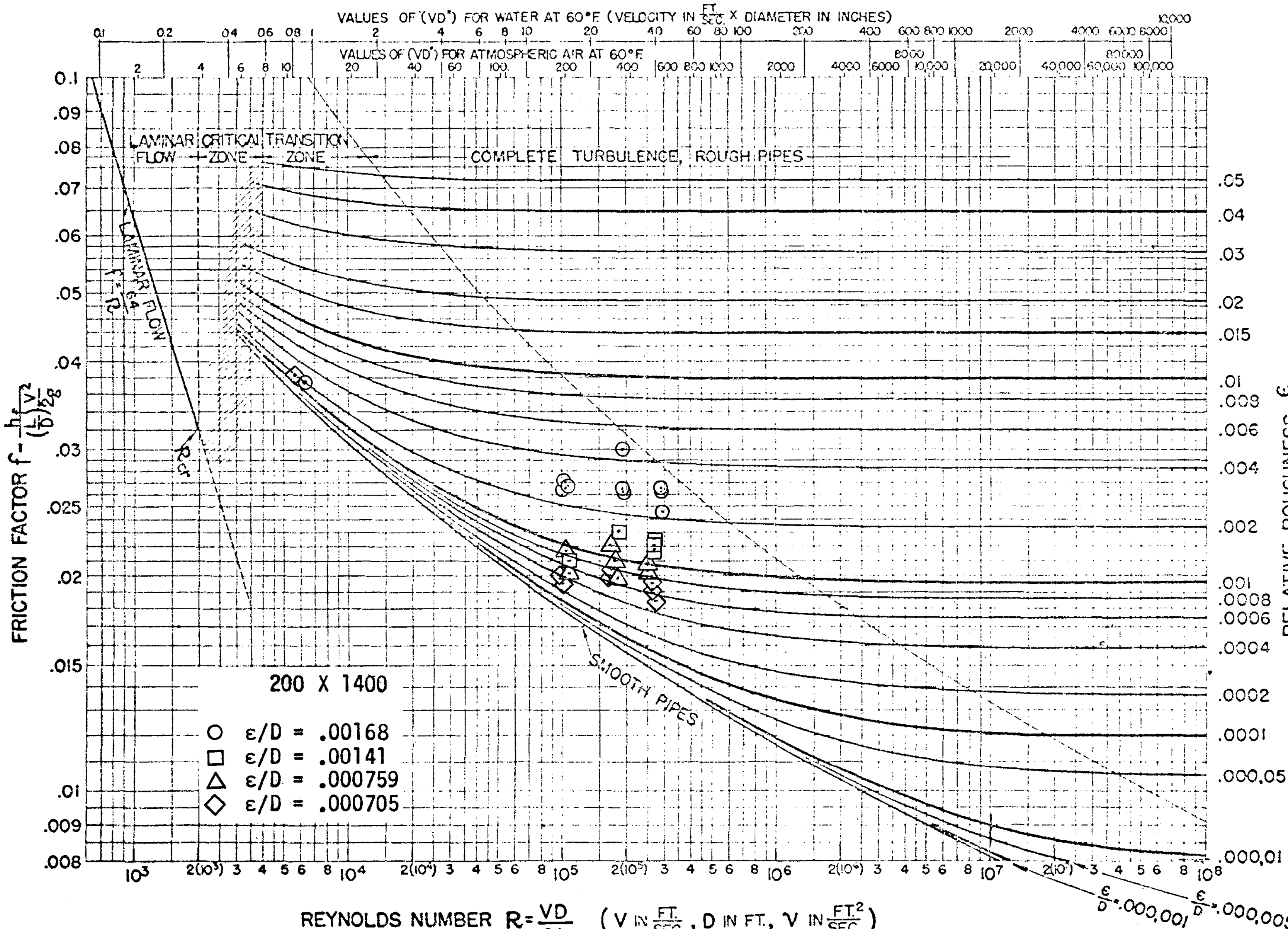

Figure 54. Dimensionless Channel Flow Loss Correlation – 200 x 1400

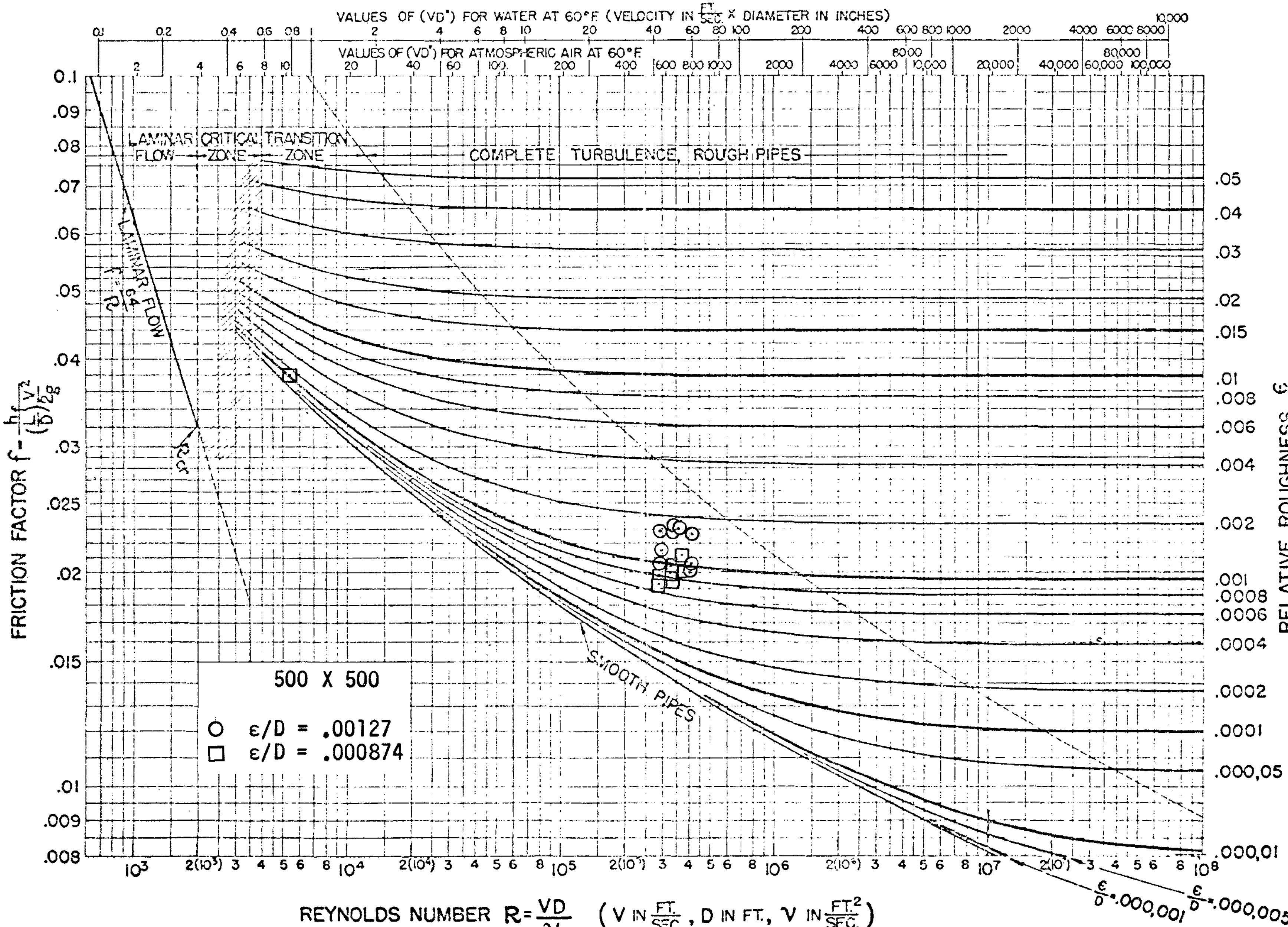

Figure 55. Dimensionless Channel Flow Loss Correlation — 500 x 500

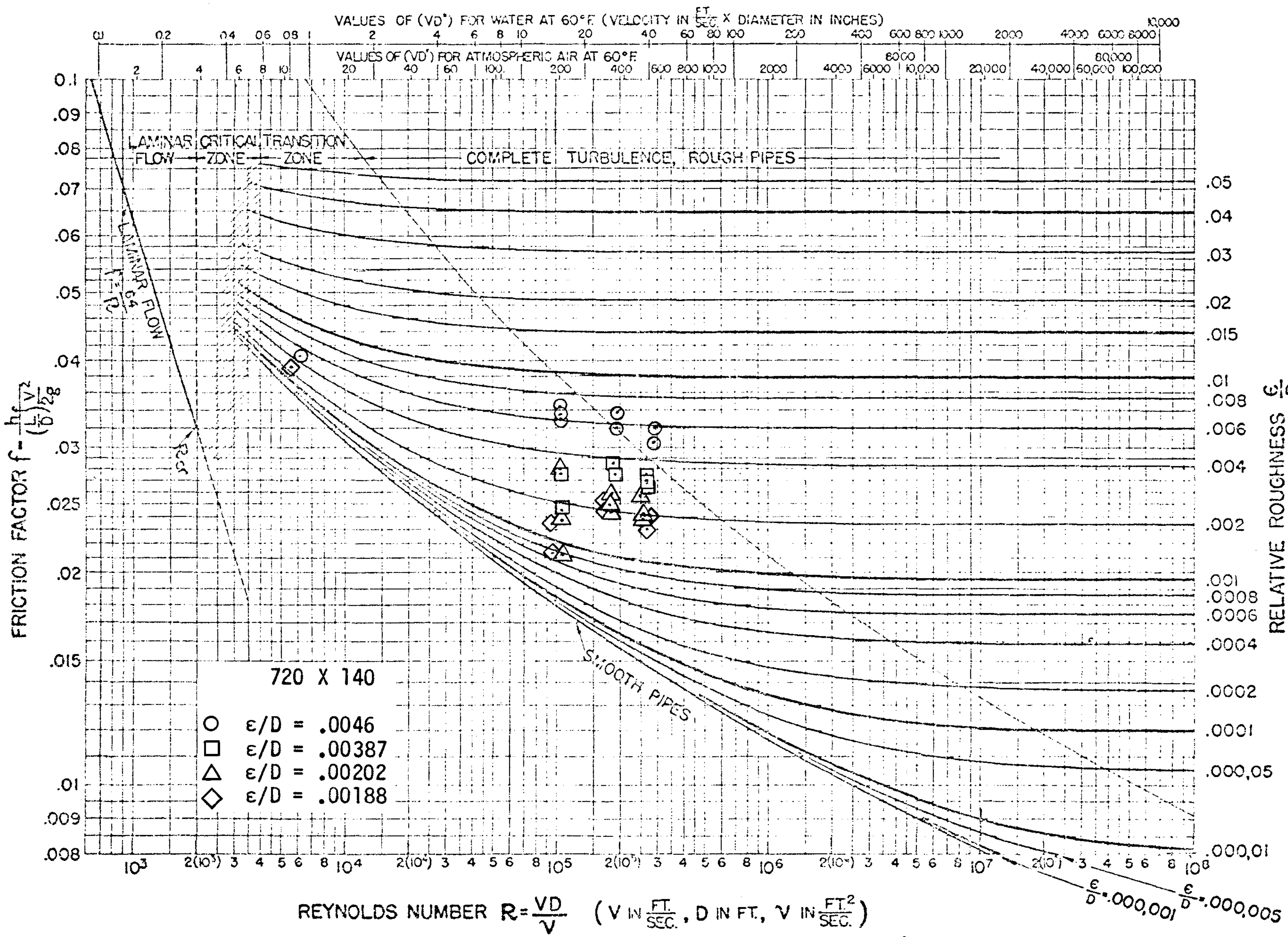

Figure 56. Dimensionless Channel Flow Loss Correlation – 720 x 140

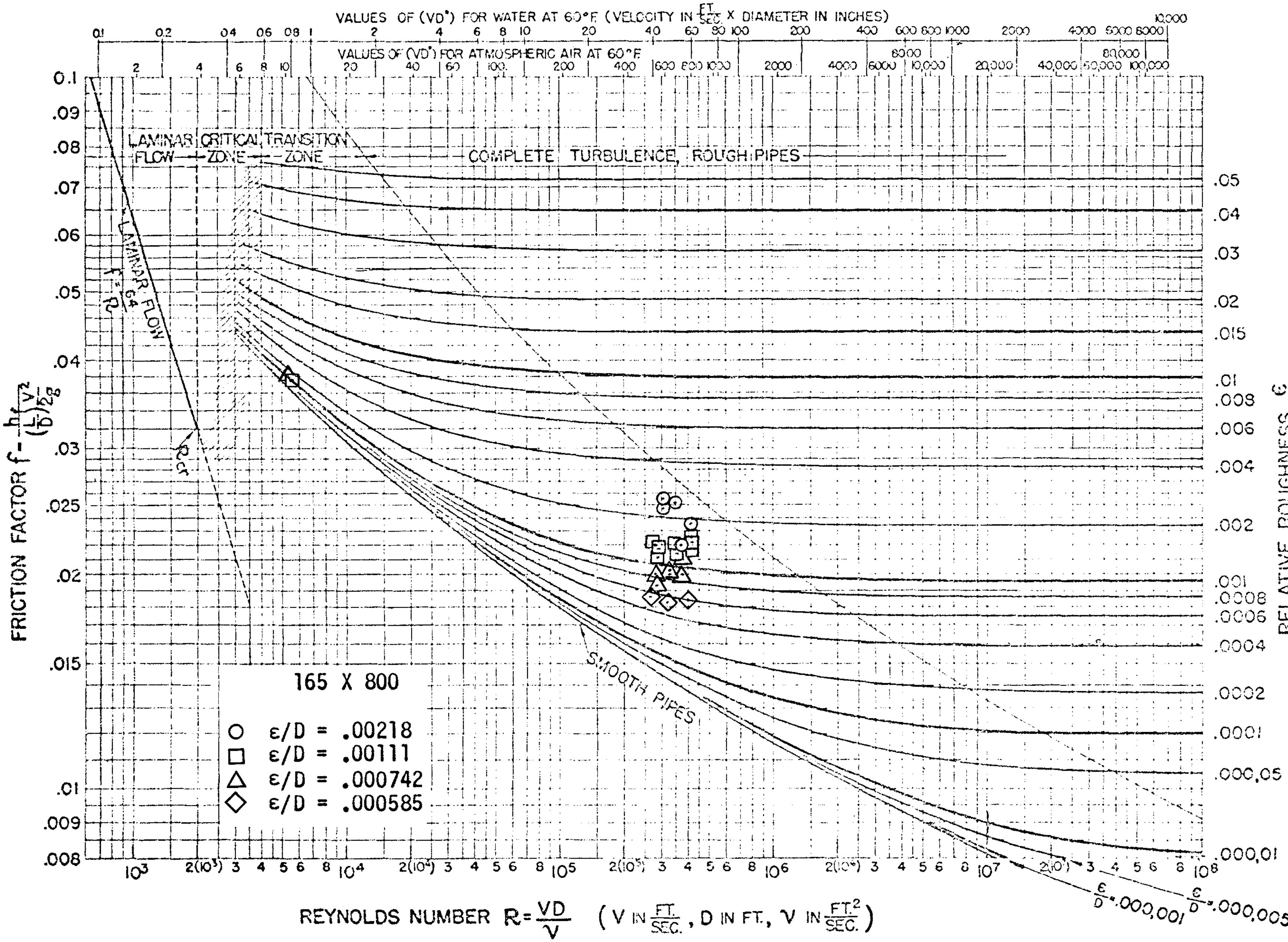

Figure 57. Dimensionless Channel Flow Loss Correlation – 165 x 800

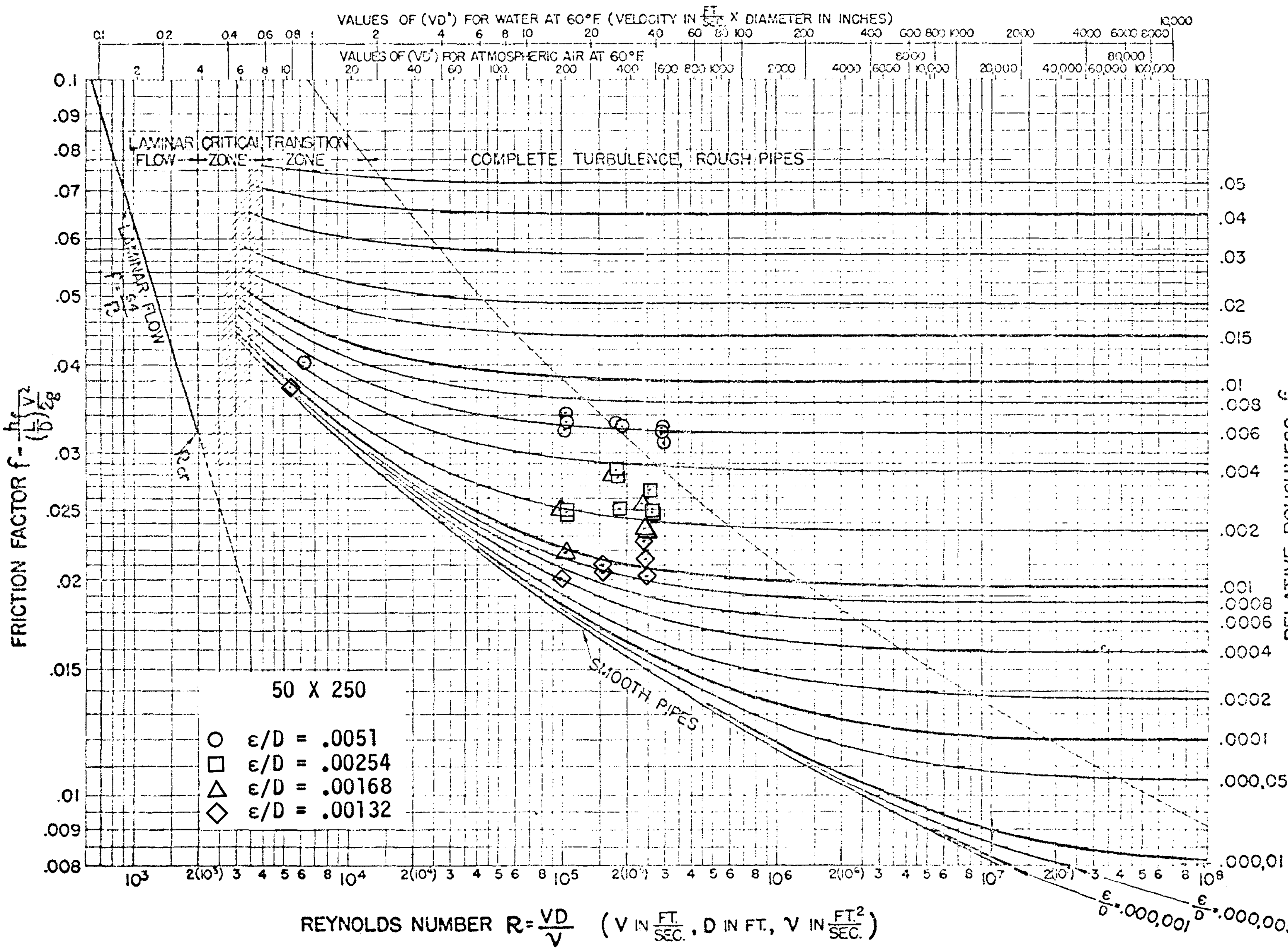

Figure 58. Dimensionless Channel Flow Loss Correlation — 50 x 250

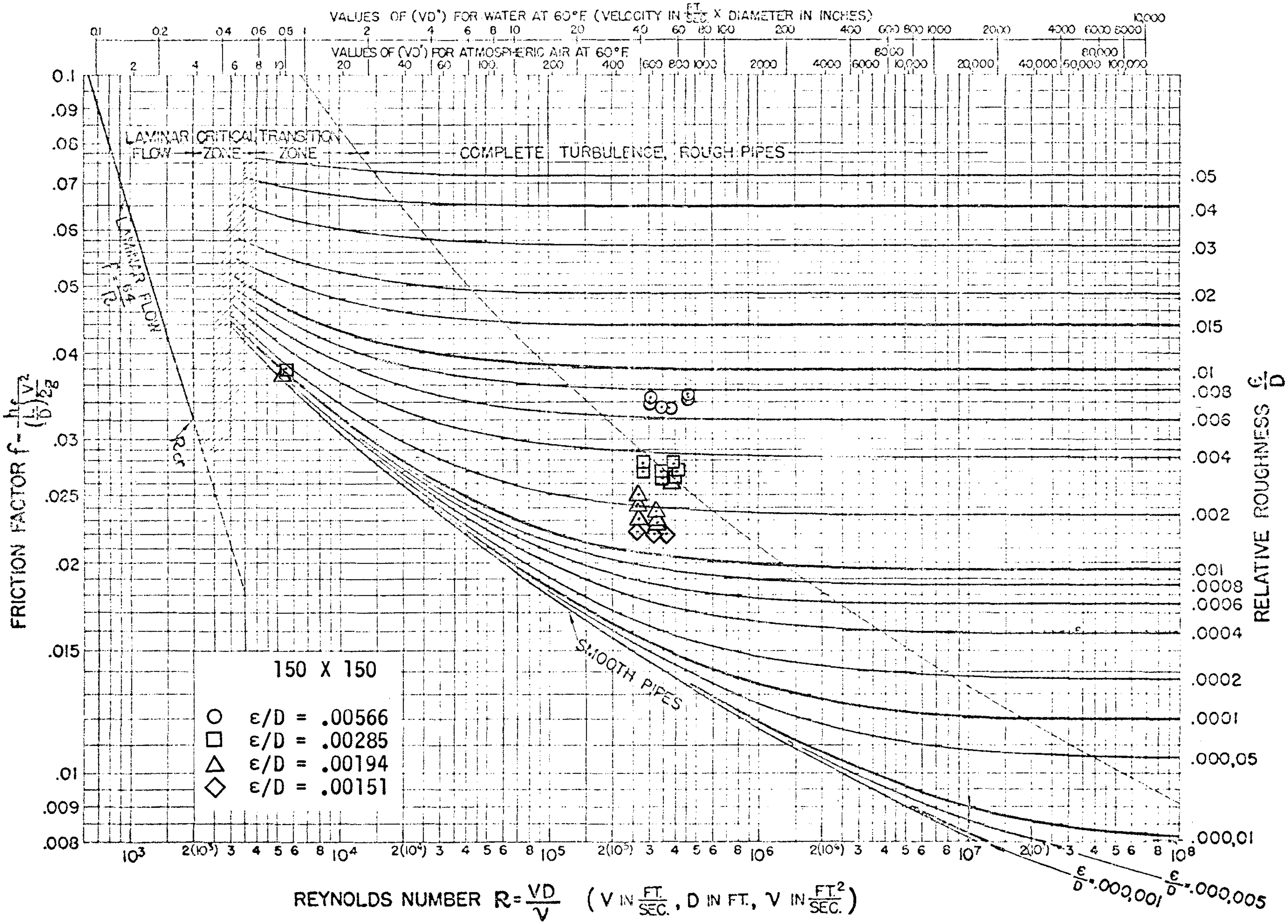

Figure 59. Dimensionless Channel Flow Loss Correlation — 150 x 150

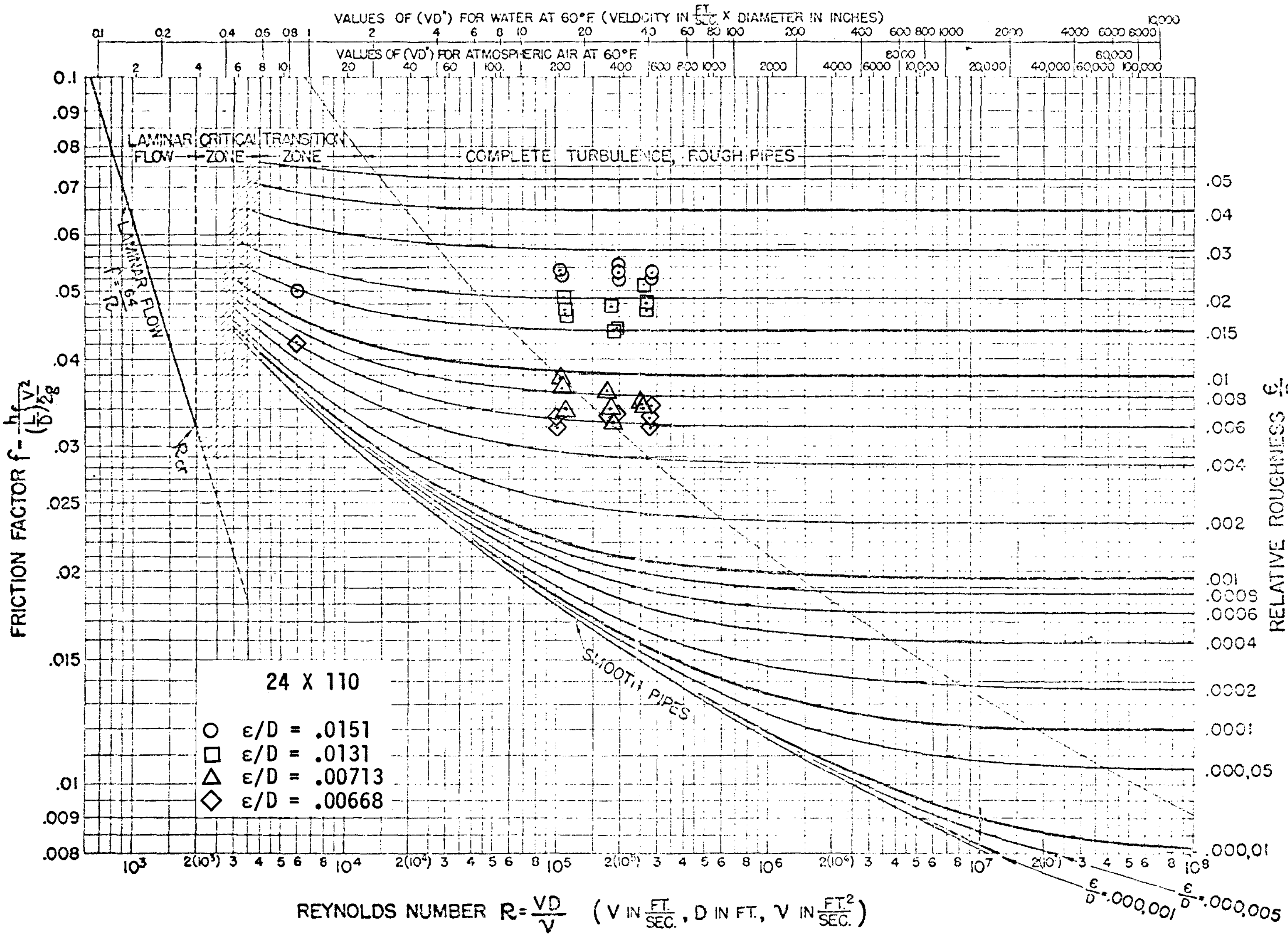

FIG. 1

Figure 60. Dimensionless Channel Flow Loss Correlation — 24 x 110

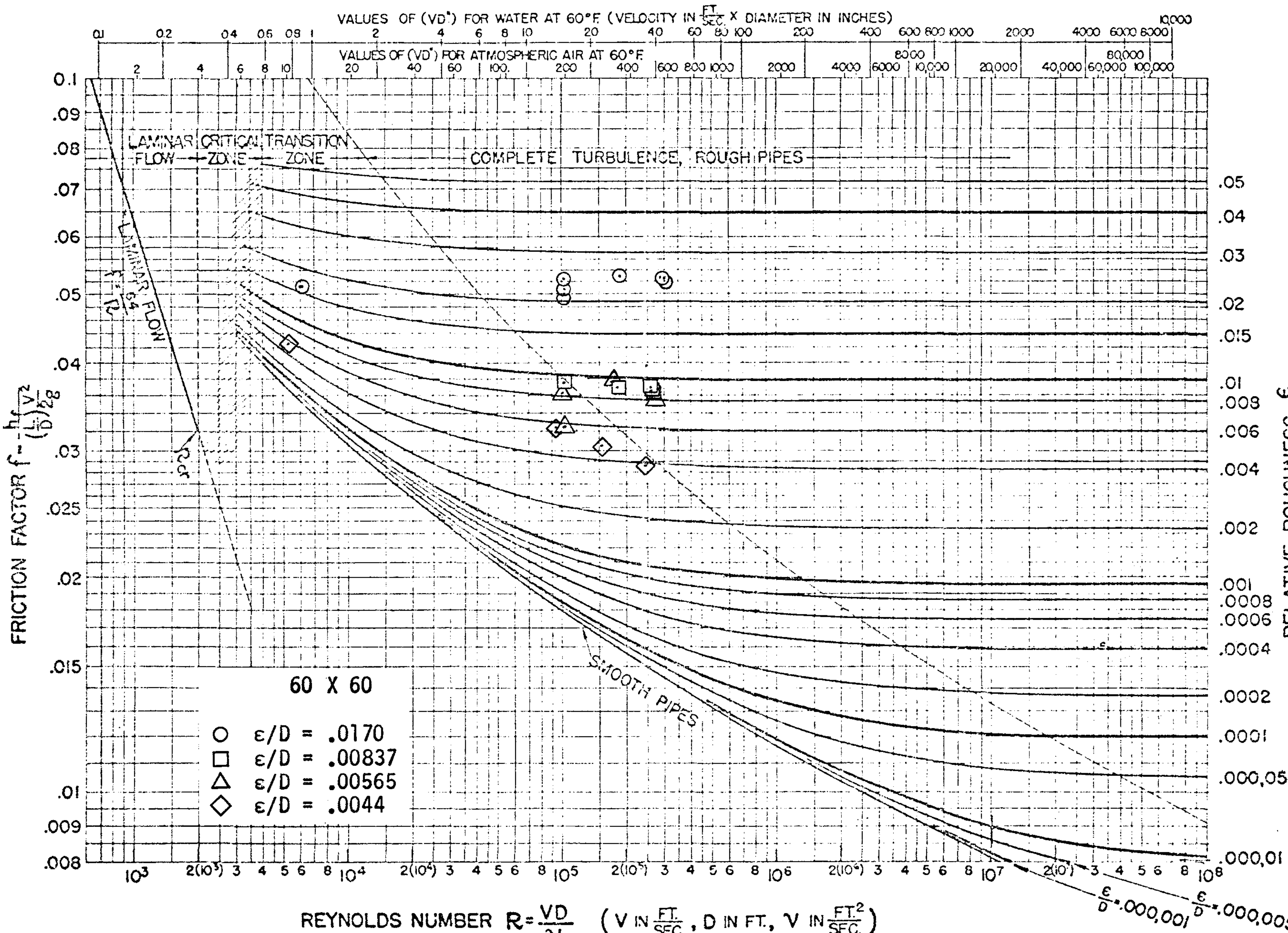

Figure 61. Dimensionless Channel Flow Loss Correlation – 60 x 60

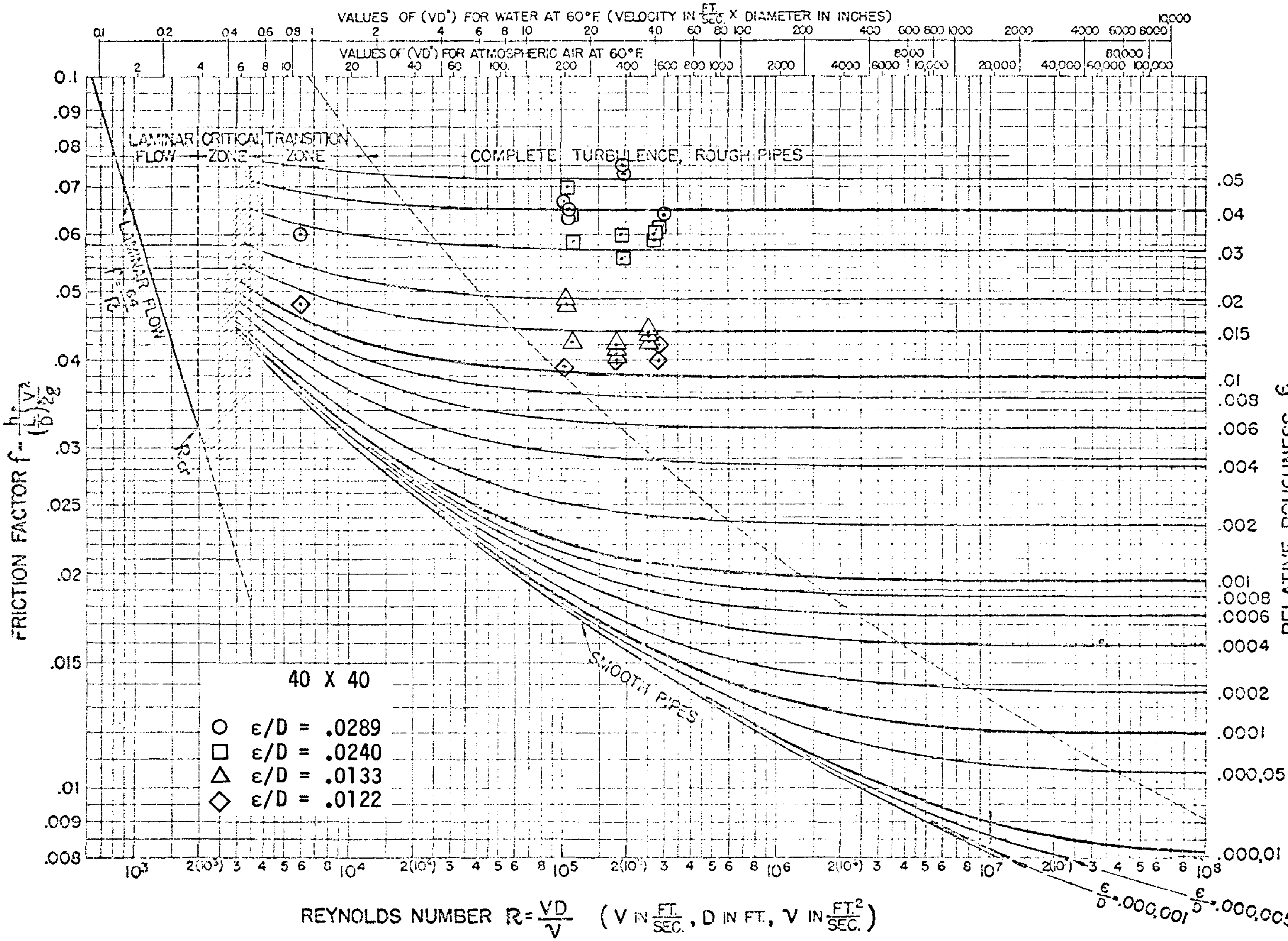

Figure 62. Dimensionless Channel Flow Loss Correlation – 40 x 40

APPENDIX C

EVALUATION OF SIDE-WALL CONTRIBUTION TO CHANNEL FLOW PRESSURE LOSS

In the channel flow apparatus, the direction of flow is in the direction of the shute wires in the screen. It is assumed that the equivalent roughness of the screen is the ratio of the shute wire diameter to the hydraulic diameter for square weave screens, and the ratio of half the shute wire diameter to the hydraulic diameter for Dutch-weave screens. Because the other channel walls are made from rolled stainless-steel sheet, it is further assumed that the equivalent roughness of the other channel walls is approximated by the roughness of drawn tubing or e = 0.000152 cm (0.00006 in.). Finally, it is assumed that the total roughness of the channel is the sum of the roughness contribution of each of the channel walls, or:

$$\left.\frac{e}{D_h}\right|_{TOTAL} = \left.\frac{e}{D_h}\right|_{SCREEN}\left(\frac{w}{2w + 2s}\right) + \left.\frac{e}{D_h}\right|_{SIDEWALLS}\left(\frac{2s}{2w + 2s}\right) + \left.\frac{e}{D_h}\right|_{WALL}\left(\frac{w}{2w + 2s}\right) \tag{C-1}$$

The sidewall contribution to the total is

$$\frac{\left.\frac{e}{D_h}\right|_{SIDEWALLS}\left(\frac{2s}{2w + 2s}\right)}{\left.\frac{e}{D_h}\right|_{SCREEN}\left(\frac{w}{2w + 2s}\right) + \left.\frac{e}{D_h}\right|_{SIDEWALLS}\left(\frac{2s}{2w + 2s}\right) + \left.\frac{e}{D_h}\right|_{WALL}\left(\frac{w}{2w + 2s}\right)} \tag{C-2}$$

or

$$\frac{0.000152\ (2s)}{e_{SCREEN}\ w + 0.000152\ (2s) + 0.000152\ w} \tag{C-3}$$

The sidewall contribution from equation (C-3), based on the screens tested in the as-built channel height (s) and width (w) is shown in Table XIII.

TABLE XIII. - SIDEWALL CONTRIBUTION TO CHANNEL FLOW LOSS

Screen	Roughness e(cm)	Actual channel spacing depth		Sidewall contribution (%)
		(cm)	(in.)	
40 x 40	0.0254	0.455	0.179	0.043
		0.554	0.218	0.053
		1.034	0.407	0.098
		1.133	0.446	0.108
24 x 110	0.01334	0.457	0.180	0.082
		0.531	0.209	0.096
		1.011	0.398	0.182
		1.085	0.427	0.195
720 x 140	0.00546	0.622	0.245	0.269
		0.747	0.294	0.323
		1.514	0.596	0.652
		1.638	0.645	0.705
200 x 1,400	0.00203	0.635	0.250	0.703
		0.762	0.300	0.842
		1.499	0.590	1.643
		1.626	0.640	1.780
60 x 60	0.01905	0.587	0.231	0.074
		1.252	0.493	0.158
		1.948	0.767	0.246
		2.614	1.029	0.330
50 x 250	0.00572	0.589	0.232	0.243
		1.234	0.486	0.508
		1.963	0.773	0.799
		2.609	1.027	1.069
150 x 150	0.0066	0.612	0.241	0.220
		1.278	0.503	0.458
		1.974	0.777	0.706
		2.639	1.039	0.942
165 x 800	0.00254	0.610	0.240	0.548
		1.255	0.494	1.121
		1.984	0.781	1.761
		2.629	1.035	2.320
500 x 500	0.00254	1.090	0.429	0.975
		1.643	0.647	1.463
325 x 2,300	0.00127	2.890	1.138	4.71
		3.444	1.356	5.563

APPENDIX D

VISCOUS PRESSURE DROP IN A SPHERICAL ANNULUS

The viscous pressure drop for steady incompressible flow between a spherical screen annulus was determined based on the approach given, for example, by Bird, Stewart, and Lightfoot, (ref. 27). Creeping flow was assumed so that inertial terms could be neglected in the momentum equation. It was also assumed that $v_r = v_\phi = 0$ and $v_\theta = v_\theta (r, \theta)$. The coordinates and geometry are shown in Figure 63.

The governing equations are:

Continuity

$$\frac{\delta \rho}{\delta t} + \frac{1}{r^2} \frac{\delta}{\delta r} (\rho r^2 v_r) + \frac{1}{r \sin \theta} \frac{\delta}{\delta \theta} (\rho v_\theta \sin \theta) + \frac{1}{r \sin \theta} \frac{\delta}{\delta \phi} (\rho v_\phi) = 0 \quad \text{(D-1)}$$

CR 140

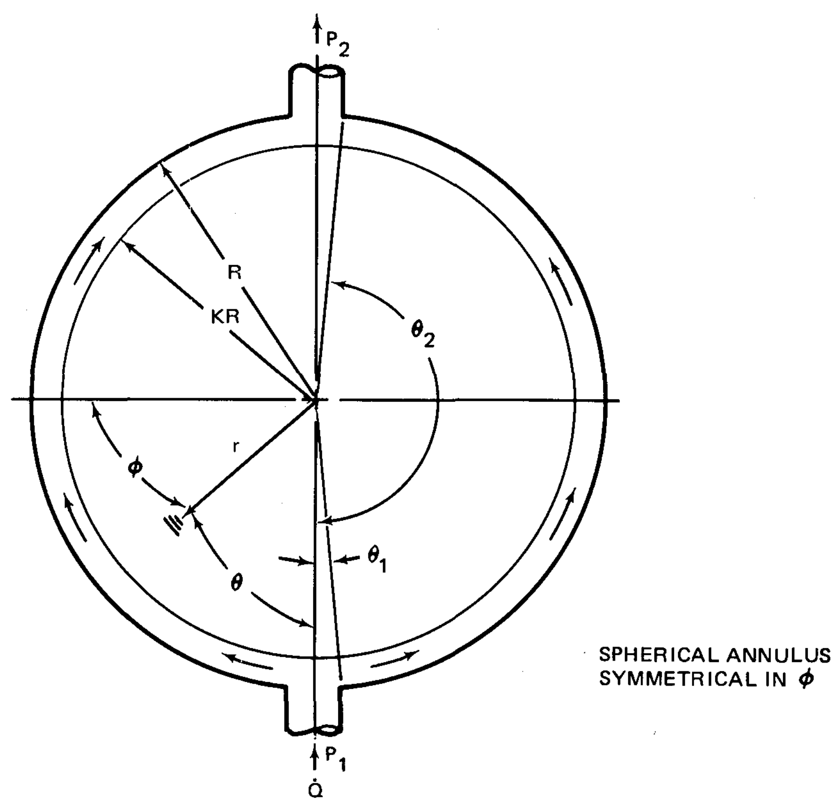

Figure 63. Laminar Flow in a Spherical Annulus – Coordinates and Geometry

Momentum (θ - component)

$$\rho\left(\frac{\delta v_\theta}{\delta t}+v_r\frac{\delta v_\theta}{\delta r}+\frac{v_\theta}{r}\frac{\delta v_\theta}{\delta\theta}+\frac{v_\phi}{r\sin\theta}\frac{\delta v_\theta}{\delta\phi}+\frac{v_r v_\theta}{r}-v_\phi^2\frac{\cot\theta}{r}\right)$$

$$=-\frac{1}{r}\frac{\delta P}{\delta\theta}+\mu\left(\bar{\nabla}^2 v_\theta+\frac{2}{r^2}\frac{\delta v_r}{\delta\theta}-\frac{v_\theta}{r^2\sin^2\theta}-\frac{2\cos\theta}{r^2\sin^2\theta}\frac{\delta v_\phi}{\delta\phi}\right)+\rho g_\theta \qquad (D\text{-}2)$$

Where

$$\bar{\nabla}^2=\frac{1}{r^2}\frac{\delta}{\delta r}\left(r^2\frac{\delta}{\delta r}\right)+\frac{1}{r^2\sin\theta}\frac{\delta}{\delta\theta}\left(\sin\theta\frac{\delta}{\delta\theta}\right)+\frac{1}{r^2\sin^2\theta}\left(\frac{\delta^2}{\delta\phi^2}\right) \qquad (D\text{-}3)$$

The continuity equation simplifies to

$$\frac{\delta}{\delta\theta}(v_\theta\sin\theta)=0 \qquad (D\text{-}4)$$

Thus,

$$v_\theta\sin\theta=u(r) \qquad (D\text{-}5)$$

The momentum equation simplifies to:

$$0=-\frac{1}{r}\frac{\delta P}{\delta\theta}+\mu\left(\frac{1}{r^2}\frac{\delta}{\delta r}\left(r^2\frac{\delta v_\theta}{\delta r}\right)+\frac{1}{r^2\sin\theta}\frac{\delta}{\delta\theta}\left(\sin\theta\frac{\delta v_\theta}{\delta\theta}\right)\right.$$

$$\left.-\frac{v_\theta}{r^2\sin^2\theta}\right)+\rho g_\theta \qquad (D\text{-}6)$$

Since

$$\sin\theta\frac{\delta v_\theta}{\delta\theta}=\frac{\delta}{\delta\theta}\cancelto{0}{(v_\theta\sin\theta)}-v_\theta\cos\theta=-v_\theta\cos\theta, \qquad (D\text{-}7)$$

the terms given below can be shown to be zero; i. e.,

$$\sin\theta \frac{\delta}{\delta\theta}\left(\sin\theta \frac{\delta v_\theta}{\delta\theta}\right) - v_\theta = \sin\theta \frac{\delta}{\delta\theta}(- v_\theta \cos\theta) - v_\theta$$

$$= v_\theta \sin^2\theta - \sin\theta\cos\theta \frac{\delta v_\theta}{\delta\theta} - v_\theta$$

$$= v_\theta (1 - \cos^2\theta) - \sin\theta\cos\theta\frac{\delta v_\theta}{\delta\theta} - v_\theta \qquad \text{(D-8)}$$

$$= - \cos\theta \left(\cos\theta\, v_\theta - \sin\theta \frac{\delta v_\theta}{\delta\theta}\right)$$

$$= \cos\theta \frac{\delta}{\delta\theta}(v_\theta \sin\theta) = 0$$

With $\sin\theta\, v_\theta = u(r)$,

$$0 = - \frac{1}{r}\frac{\delta P}{\delta\theta} + \mu\left(\frac{1}{\sin\theta} \cdot \frac{1}{r^2}\frac{d}{dr}\left(r^2 \frac{du}{dr}\right)\right) \qquad \text{(D-9)}$$

Using separation of variables gives

$$\sin\theta \frac{dp}{d\theta} = B \qquad \text{(D-10)}$$

$$\frac{\mu}{r}\frac{d}{dr}\left(r^2 \frac{du}{dr}\right) = B \qquad \text{(D-11)}$$

Integrating equation (D-10) over the limits P_1, P_2, and θ_1, θ_2, gives

$$\int_{P_1}^{P_2} dp = \int_{\theta_1}^{\theta_2} \frac{B d\theta}{\sin\theta} \qquad \text{(D-12)}$$

$$\Delta P = P_1 - P_2 = - B \ln\left[\frac{\tan\theta_2/2}{\tan\theta_1/2}\right] \qquad \text{(D-13)}$$

Integrating equation (D-11) twice gives

$$\int d\left(r^2 \frac{du}{dr}\right) = \frac{Br}{\mu} dr + C \qquad \text{(D-14)}$$

$$r^2 \frac{du}{dr} = \frac{Br^2}{2\mu} + C \qquad \text{(D-15)}$$

and

$$u = \frac{Br}{2\mu} - \frac{C}{r} + D \qquad \text{(D-16)}$$

The boundary conditions are

$$\begin{aligned} u &= 0 \text{ at } r = R \\ u &= 0 \text{ at } r = KR \end{aligned} \qquad \text{(D-17)}$$

Thus, the integration constants in (D-16) are obtained from

$$0 = \frac{BR}{2\mu} - \frac{C}{R} + D \qquad \text{(D-18)}$$

and

$$0 = \frac{BKR}{2\mu} - \frac{C}{KR} + D \qquad \text{(D-19)}$$

Solving the above gives

$$C = \frac{B(R - KR)}{2\mu\left(\frac{1}{R} - \frac{1}{KR}\right)} \qquad \text{(D-20)}$$

$$D = -\frac{BR}{2\mu}(K + 1) \qquad \text{(D-21)}$$

Thus, u (r) is

$$u = -\frac{BR}{2\mu}\left[1 - \frac{r}{R} + K\left(1 - \frac{R}{r}\right)\right] \qquad \text{(D-22)}$$

or,

$$u = \frac{\Delta P R \left[1 - \frac{r}{R} + K\left(1 - \frac{R}{r}\right)\right]}{2\,\mu\,\ln\left[\dfrac{\tan\theta_2/2}{\tan\theta_1/2}\right]} = v_\theta \sin\theta \tag{D-23}$$

The total flowrate is, at any point,

$$\dot{m} = \int \rho v_\theta \, dA_{cs} \quad \text{or} \quad \dot{Q} = \int v_\theta \, dA_{cs} \tag{D-24}$$

Thus, at $\theta = \pi/2$, $dA = 2\pi r dr$ and

$$u = v_\theta \sin\theta = v_\theta$$

therefore,

$$\dot{Q} = \int_{KR}^{R} v_\theta \, 2\pi r \, dr \tag{D-25}$$

$$= \frac{2\pi \Delta P R}{2\,\mu\,\ln\left[\dfrac{\tan\theta_2/2}{\tan\theta_1/2}\right]} \int_{KR}^{R} r\left[1 - \frac{r}{R} + K\left(1 - \frac{R}{r}\right)\right] dr$$

$$= \frac{\pi \Delta P R^3}{\mu\,\ln\left[\dfrac{\tan\theta_2/2}{\tan\theta_1/2}\right]} \left[\frac{1}{2} - \frac{K^2}{2} - \frac{1}{3} + \frac{K^3}{3} + \frac{K}{2} - \frac{K^3}{2} - K + K^2\right]$$

or,

$$\dot{Q} = \frac{\pi \Delta P R^3}{6\,\mu\,\ln\left[\dfrac{\tan\theta_2/2}{\tan\theta_1/2}\right]} \left[1 + 3K^2 - 3K - K^3\right] \tag{D-26}$$

The flowrate is

$$\dot{Q} = \frac{\pi \Delta P R^3 (1 - K)^3}{6\,\mu\,\ln\left[\dfrac{\tan\theta_2/2}{\tan\theta_1/2}\right]} \tag{D-27}$$

where

$\Delta P = P_1 - P_2$

The pressure drop is

$$\Delta P \simeq \frac{6 \mu \dot{Q}}{\pi R^3 (1 - K)^3} \ln \left[\frac{\tan \theta_2/2}{\tan \theta_1/2}\right] \tag{D-28}$$

or, since

$$s = (R - KR) \tag{D-29}$$

$$\Delta P = \frac{6 \mu \dot{Q}}{\pi s^3} \ln \left[\frac{\tan \theta_2/2}{\tan \theta_1/2}\right] \tag{D-30}$$

APPENDIX E

WALL-SCREEN SPACING AND TANK OPTIMIZATION ANALYSIS

Wall-Screen Spacing Analysis

Each tank was analyzed with all 10 screens and with annulus gaps from 1% to 5% of tank volume. The results of this analysis for the 5,000/4 tank are shown in Figures 64 and 65. Figure 64 shows the performance of the 10 screens in terms of safety factor and puddle residual for the 1% annulus gap (the specified minimum). Since the avowed purpose of the ultimate tradeoff study was to minimize system weight, it was logical to select screens with adequate performance at the minimum annulus gap. For system/screen comparison, a safety factor of 2 was chosen as representative of adequate performance. Figure 64 shows that at a 1% annulus gap, only the 325 x 2,300 and 200 x 1,400 screens gave a safety factor of 2. Since the 325 x 2,300 screen was substantially lighter than the 200 x 1,400 screen and had a higher bubble point, it was the logical choice.

Figure 65 shows that at 2% annulus gap, the 150 x 150 screen had comparable performance to the 325 x 2,300 screen in the 1% annulus.

Figure 66 shows the results for the 500/4 tank. At a 1% annulus gap, five screens had adequate performance, of which the 325 x 2,300 screen was the lightest in weight (except for the 500 x 500 screen). To use the 150 x 150 screen, with a safety factor of 2, the annulus gap would have had to be increased to 1.27%, which would have incurred an increased residual of 2.7 kg (6 lb), while saving screen weight of 6.8 kg (15 lb), for a net weight reduction of 4.1 kg (9 lb). Similarly, Figure 67 indicates that eight screens, including both the 325 x 2,300 and 150 x 150, would have adequate performance in the 500/2 tank, while Figures 68, 69, and 70 indicate that all 10 screens would have adequate performance for the remaining tanks. The weight savings using the 150 x 150 screen instead of the 325 x 2,300 screen ranged from 5.9 kg to 1.1 kg (12.9 lb to 2.5 lb) (which were not significant weight savings from a system standpoint) while sacrificing an order of magnitude in bubble point.

The analysis described above was for the maximum outflow rate of 1% of tank volume/minute. At 0.01% outflow rate (or at 0.1% TVS flow rate) there was absolutely no sensitivity to screen type or annulus gap; all 10 screens had adequate performance at the minimum 1% annulus gap. It is clear that at this g-level, flowrate, and annulus gap, the tankage systems flow characteristics were such that a meaningful tradeoff analysis in terms of residual, annulus gap, and performance was not possible.

Therefore the analysis was extended to examine the effects of high outflow rate (3% tank volume/minute) and high g-levels (10^{-2} to 10^{-4} g's) on system performance. Only the high L/D tanks (5,000/4, 500/4, and 50/2) were analyzed because these were generally the more severe cases. Figure 71 shows the effect of increasing the flowrate to 3%/minute on the performance of the 325 x 2,300 screen in the 5,000/4 tank. The annulus gap had to be increased to 2% to achieve adequate performance, and even then, increased residual resulted. In Figure 72, the performance effects for the

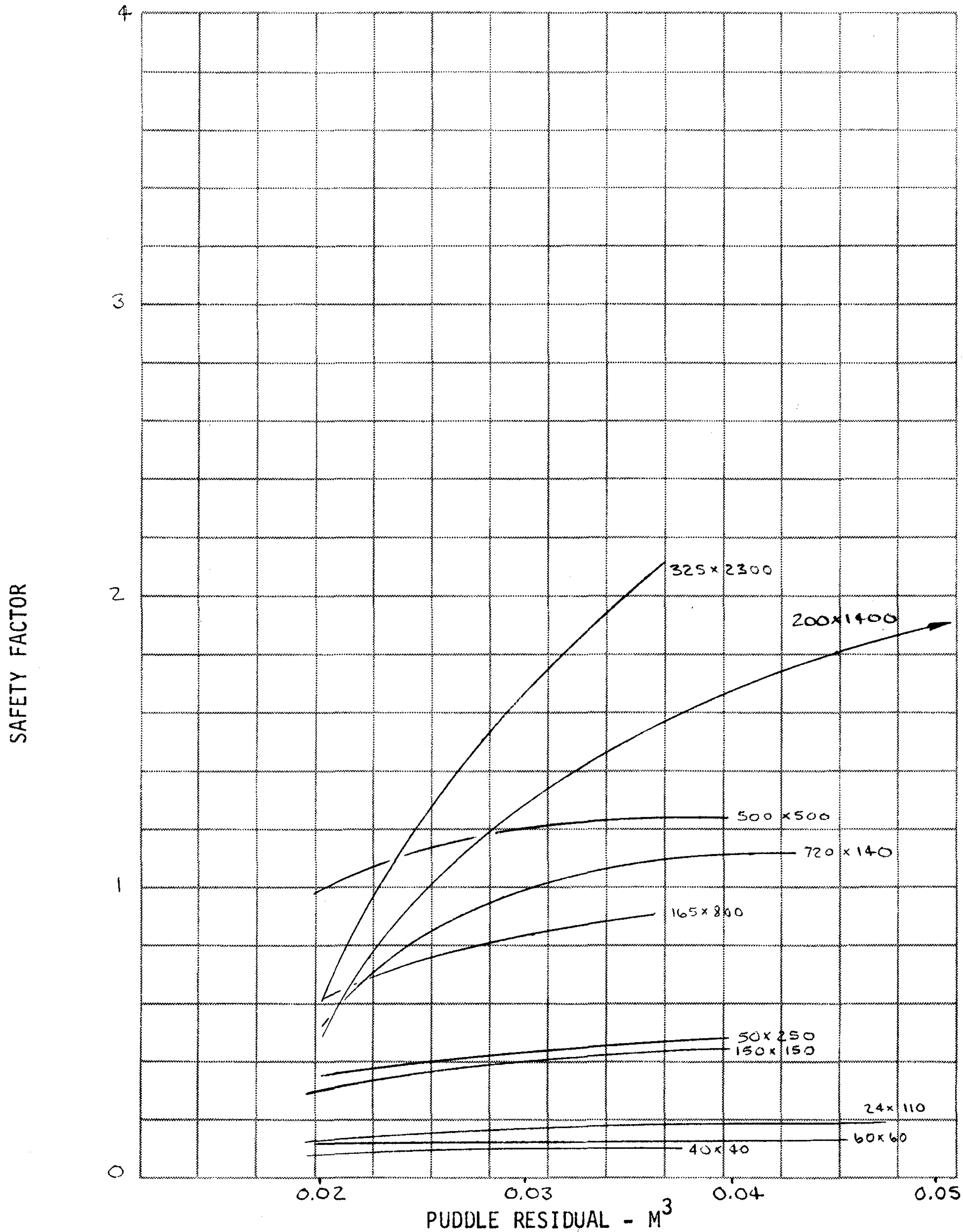

Figure 64. Screen Performance in 1% Annulus for 5,000/4 Tank

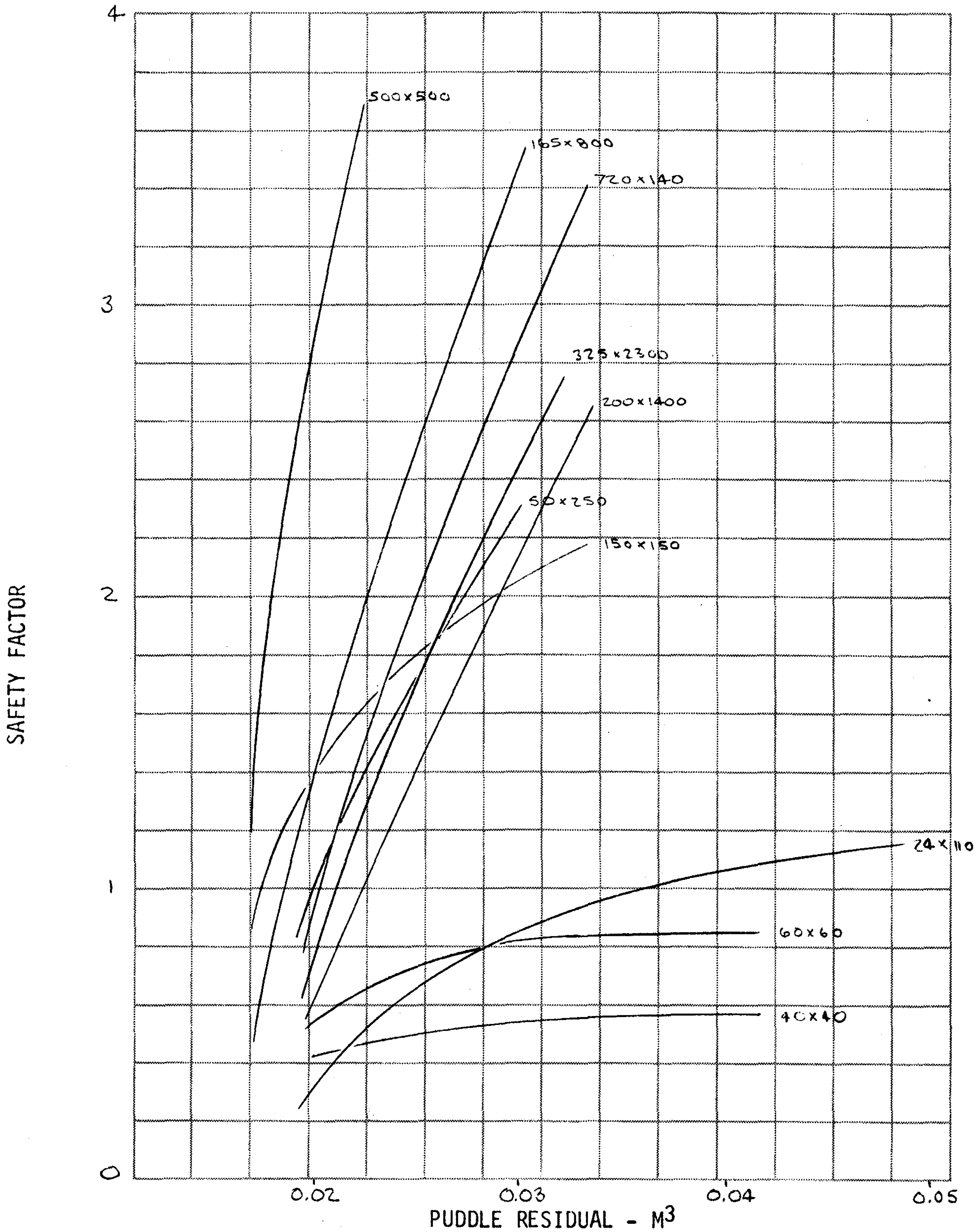

Figure 65. Screen Performance in 2% Annulus for 5,000/4 Tank

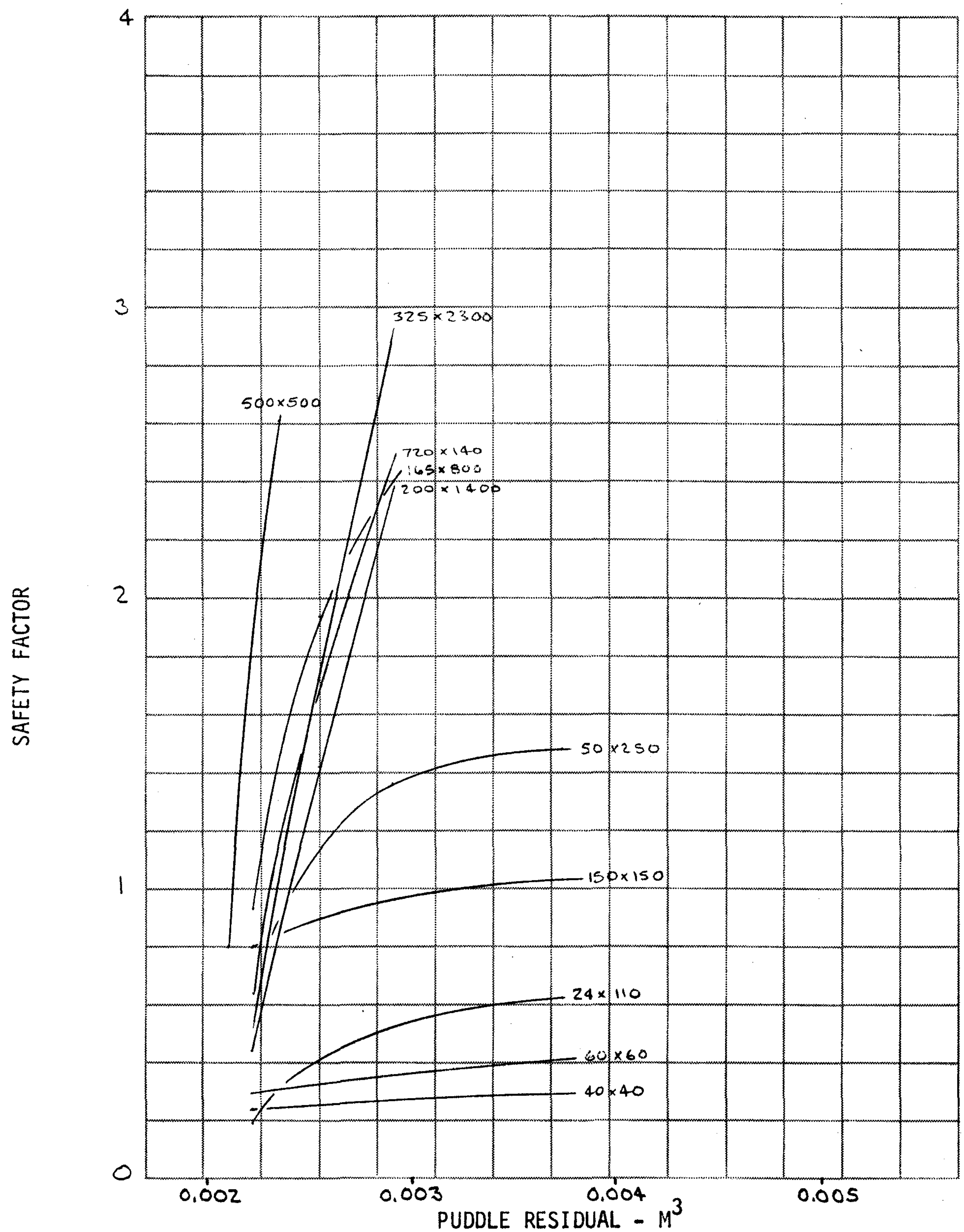

Figure 66. Screen Performance in 1% Annulus for 500/4 Tank

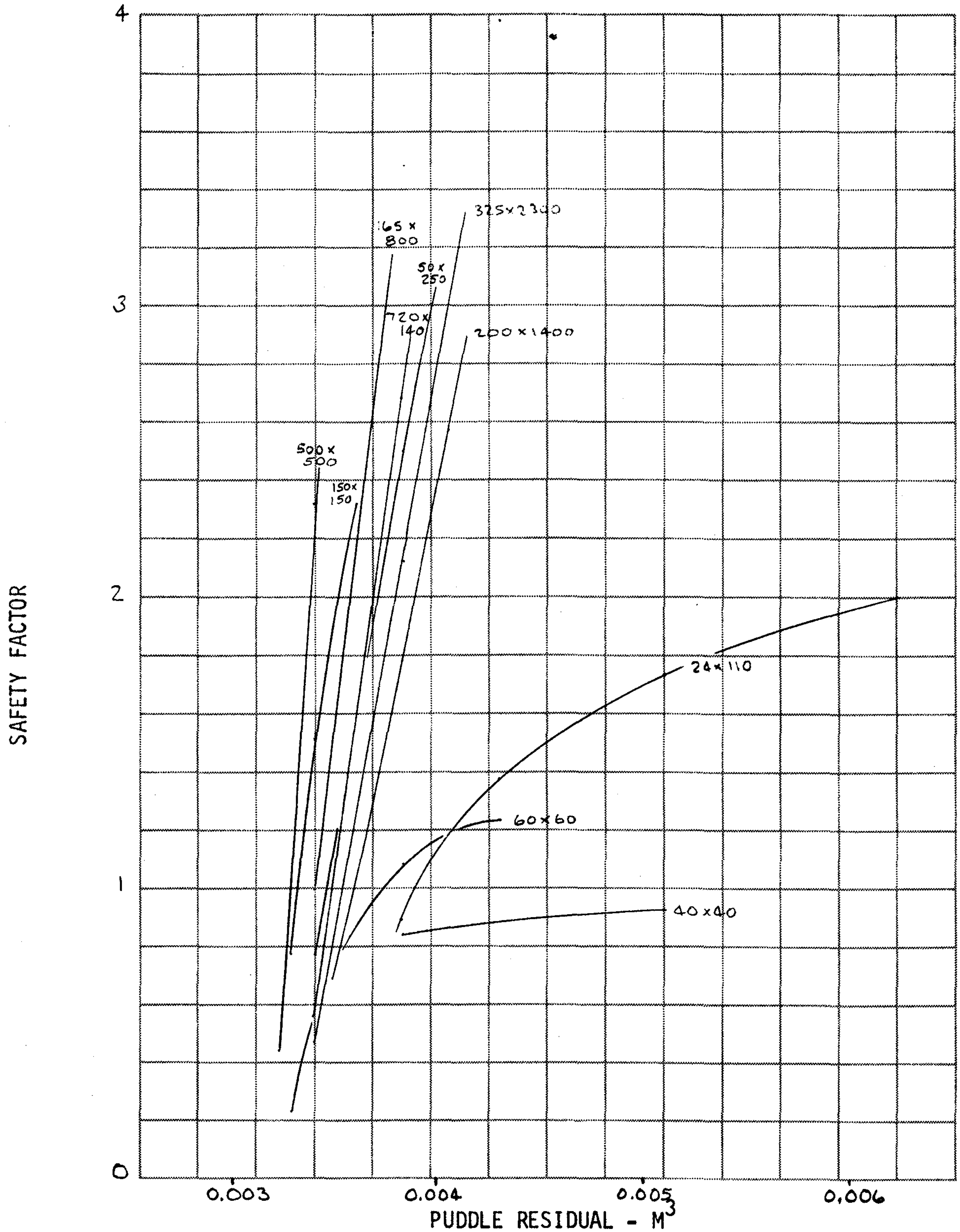

Figure 67. Screen Performance in 1% Annulus for 500/2 Tank

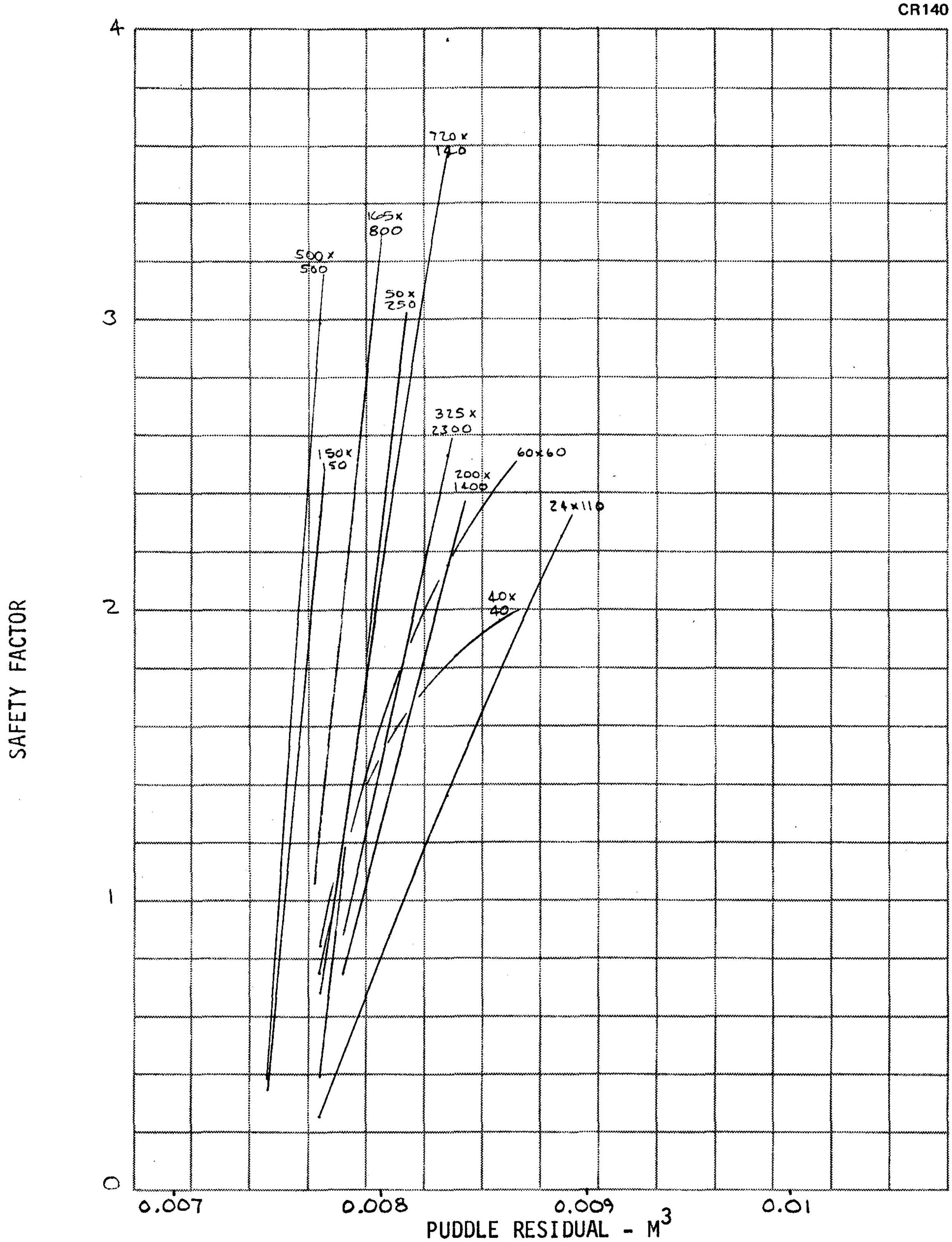

Figure 68. Screen Performance in 1% Annulus for 500/1 Tank

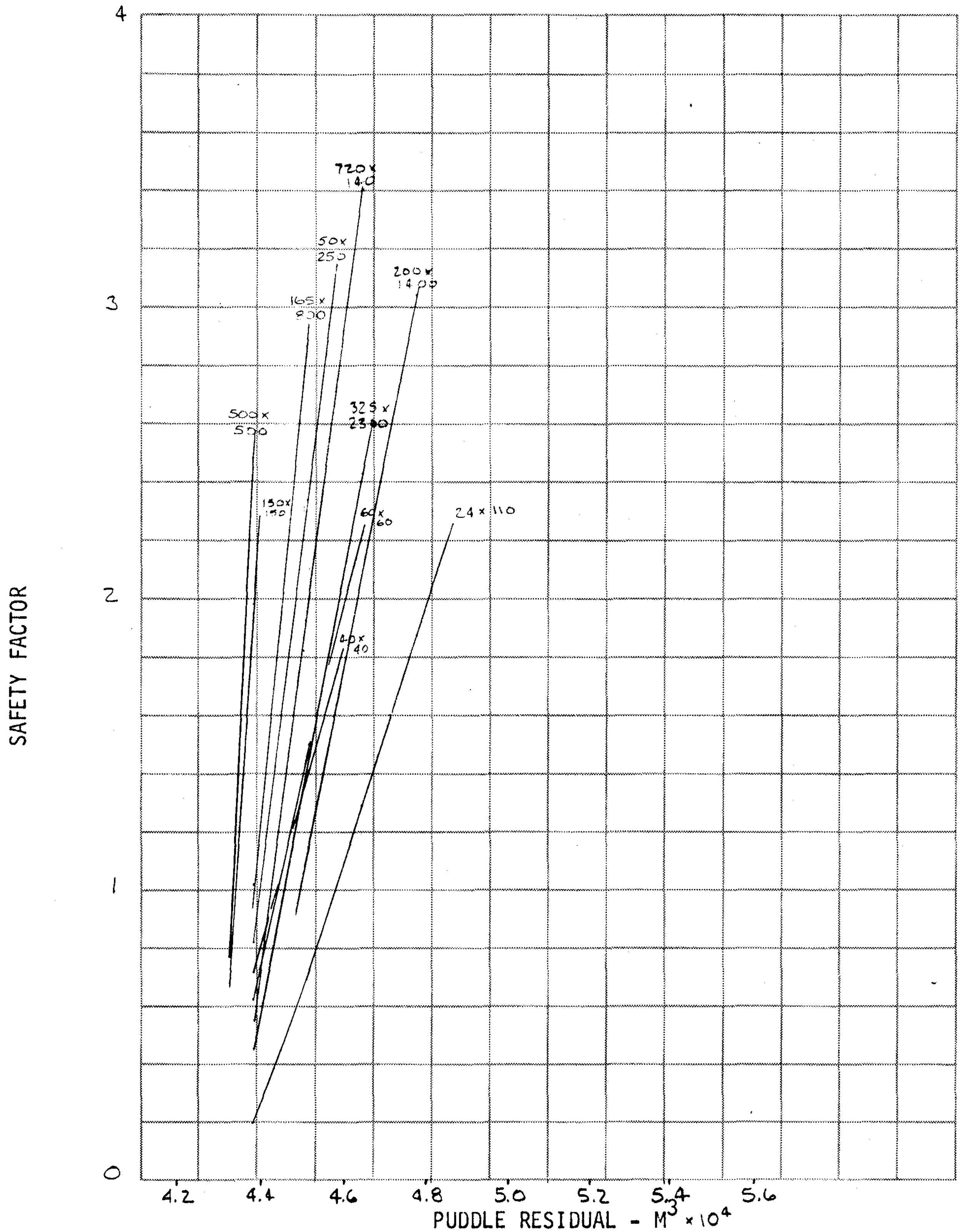

Figure 69. Screen Performance in 1% Annulus for 50/2 Tank

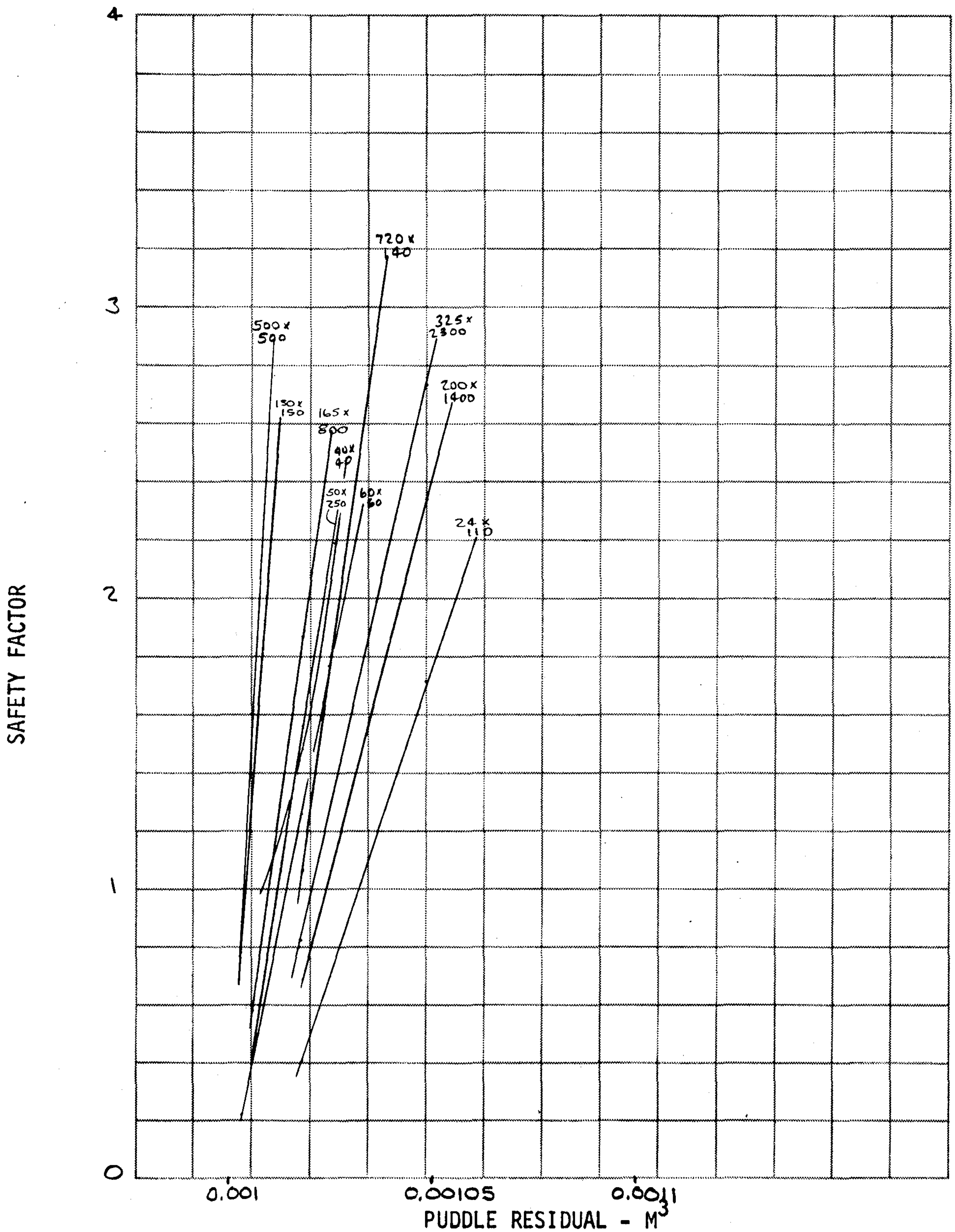

Figure 70. Screen Performance in 1% Annulus for 50/1 Tank

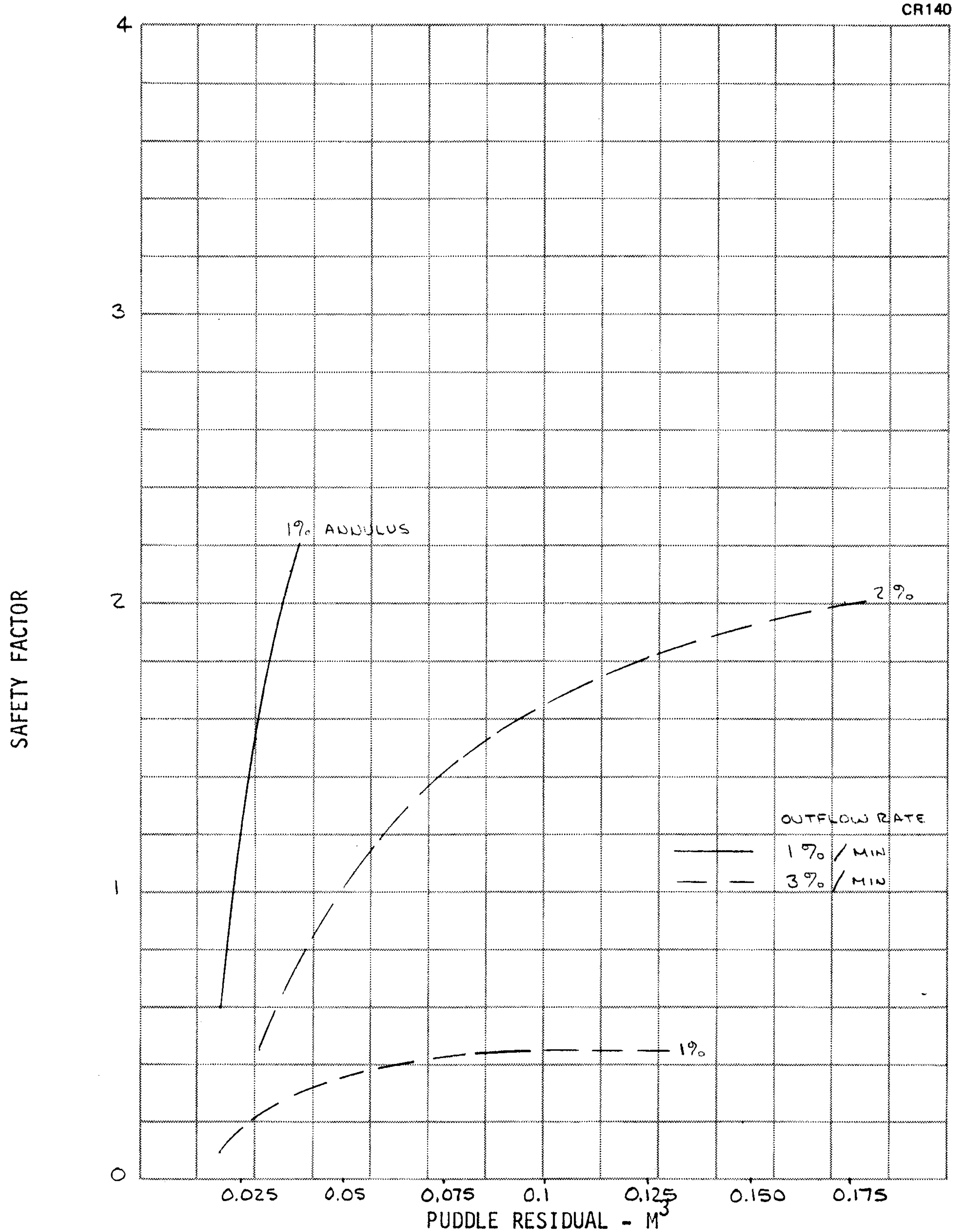

Figure 71. High Outflow Rate Performance of 325 x 2,300 Screen in the 5,000/4 Tank

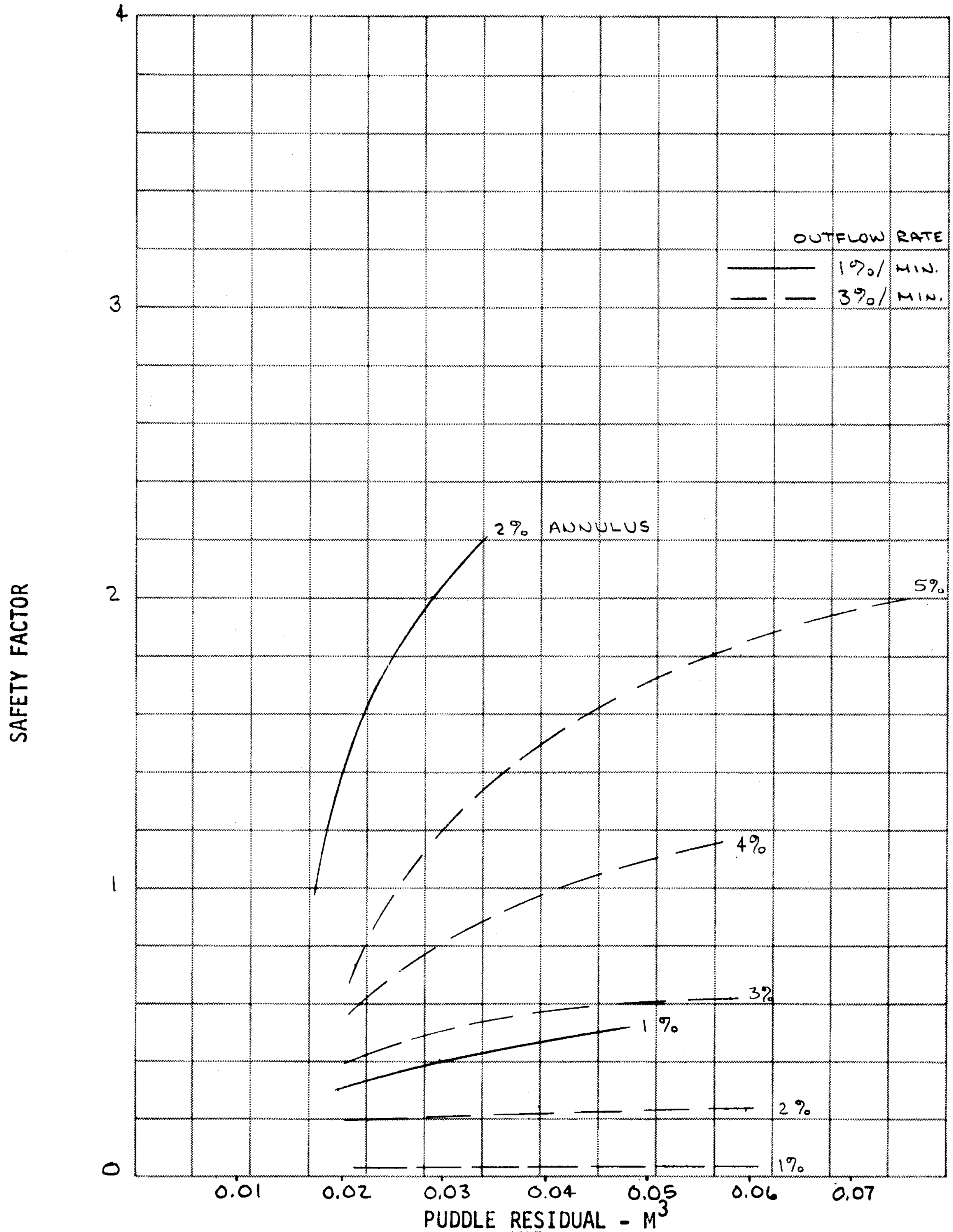

Figure 72. High Outflow Rate Performance of 150 x 150 Screen in the 5,000/4 Tank

150 x 150 screen in the 5,000/4 tank are shown. The annulus gap had to be increased from 2% to 5% to obtain adequate performance. Figure 73 shows that for the 500/4 tank with increased flowrate, the annulus gap had to be increased from 1% to 2% for the 325 x 2,300 screen, and from 2% to 3% for the 150 x 150 screen. (These were the only screens analyzed further since they represented the minimum weight and maximum bubble-point screens.) Figure 74 shows that for the 50/2 tank, the 325 x 2,300 screen had adequate performance with a 1% annulus gap at increased flowrate but that the annulus gap for the 150 x 150 screen had to be increased from 1% to 2%.

A similar trend occurred when the g-level was increased from 10^{-5} g's to 10^{-2} g's. Figure 75 shows the performance of the 325 x 2,300 screen in a 1% annulus in the 5,000/4 tank at various g-levels. At 10^{-2} g's, the 325 x 2,300 screen no longer had adequate performance, and the annulus gap had to be increased. In Figure 76, the annulus gap is 2% in the 5,000/4 tank. The 325 x 2,300 screen had adequate performance at all g-levels, but the 150 x 150 screen did not have adequate performance at even 10^{-4} g's. If the annulus gap was increased to 3%, however, the 150 x 150 screen would have adequate performance at even 10^{-3} g's. At 10^{-2} g's, the hydrostatic head in the 5,000/4 tank exceeded the bubble point of the 150 x 150 screen by a factor of 3, so that it could not practically be used. Similarly, in Figure 77 the performance of the 325 x 2,300 screen in a 1% annulus and the 150 x 150 screen in a 2% annulus is shown for the 500/4 tank, and in Figure 78, the performance for these screens in the 50/2 tank is shown.

Pump/Standpipe Optimization

The standpipe optimization equation (equation 44) is plotted as the nearly horizontal lines in Figures 79 through 90 for the six tanks and two values of TVS flowrate.

From equations (42), (45), and (55), the overall efficiency as a function of the total fluid power, including the standpipe loss, was determined and plotted in Figures 79 through 90. Where these lines crossed the standpipe optimization lines, the intersection was the value of standpipe diameter which gave the minimum system weight for that annulus gap, screen, and standpipe material. It was assumed that either stainless steel or aluminum could be used for the standpipe because of the presence of the slipjoint in the standpipe (Figure 1) which allowed differential thermal expansion. With the design value of standpipe diameter as an input, and with the other head losses known, the total system weight analysis was completed.

System Weight Optimization Analysis

The overall system weight was divided into four categories: annulus residual, standpipe residual, pump boiloff, and hardware, (which includes standpipe weight, screen weight, pump and motor weight.) The four categories above plus the total weight is shown for the six tanks, for 30 and 300-day missions, for various screens and standpipe materials versus annulus gap in Figures 91 through 103. The results for the 30-day mission are shown in Figures 91 through 96 and indicated that minimum system weight was achieved with the minimum annulus gap because of the strong influence of annulus residual.

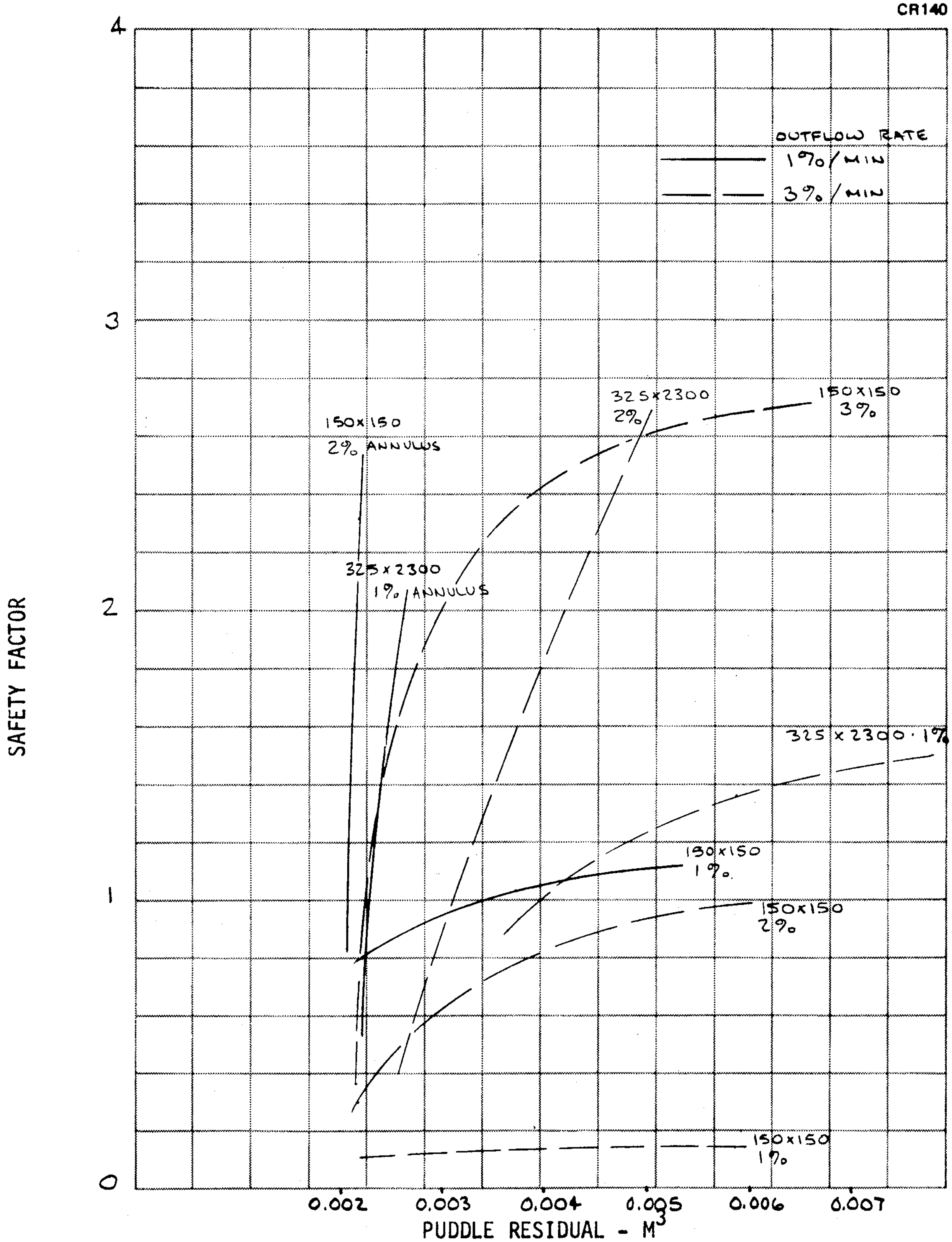

Figure 73. High Outflow Rate Performance in the 500/4 Tank

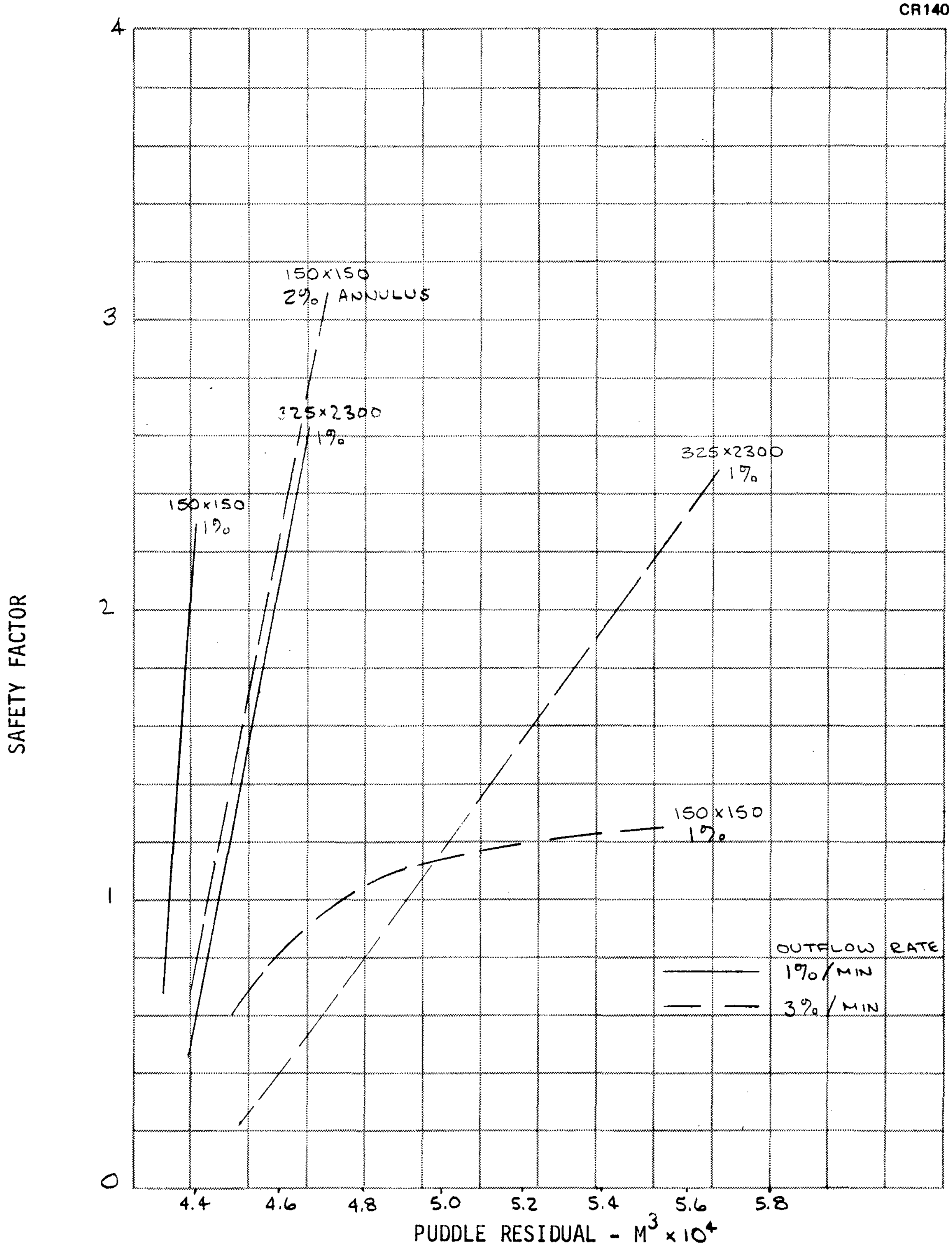

Figure 74. High Outflow Rate Performance in the 50/2 Tank

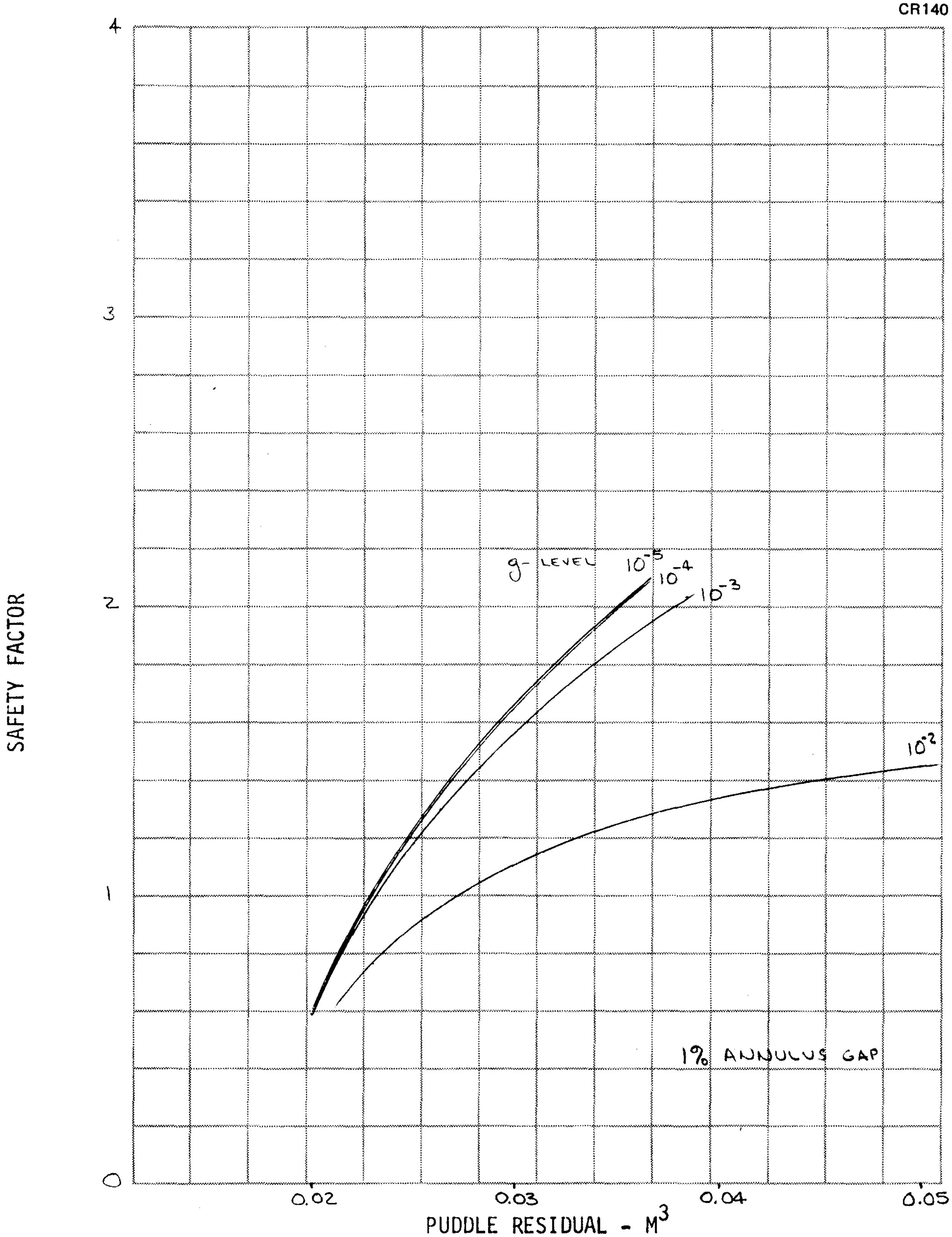

Figure 75. High G-Level Performance of 325 x 2,300 Screen in the 5,000/4 Tank

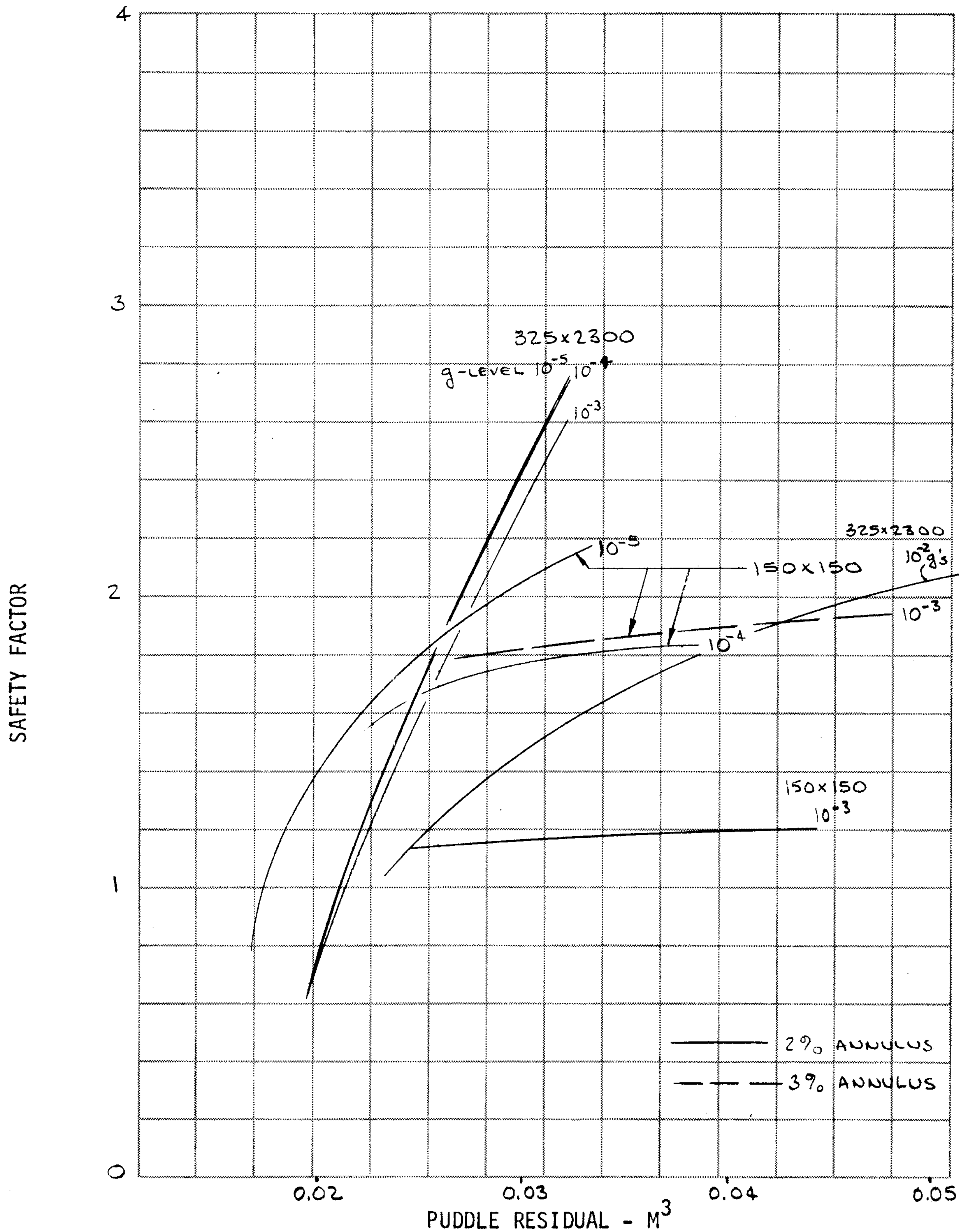

Figure 76. High G-Level Performance of Both Screens in the 5,000/4 Tank

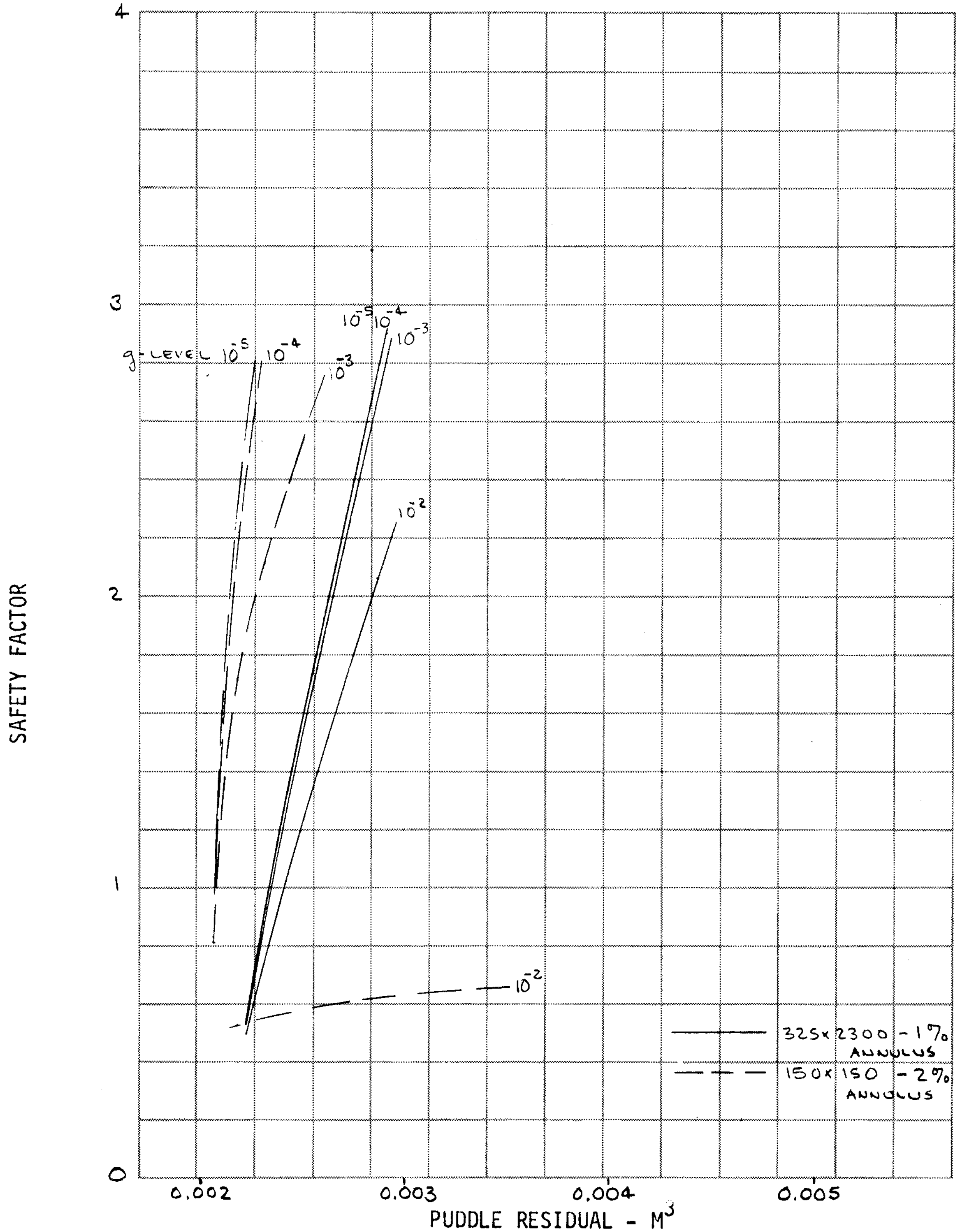

Figure 77. High G-Level Performance of Both Screens in the 500/4 Tank

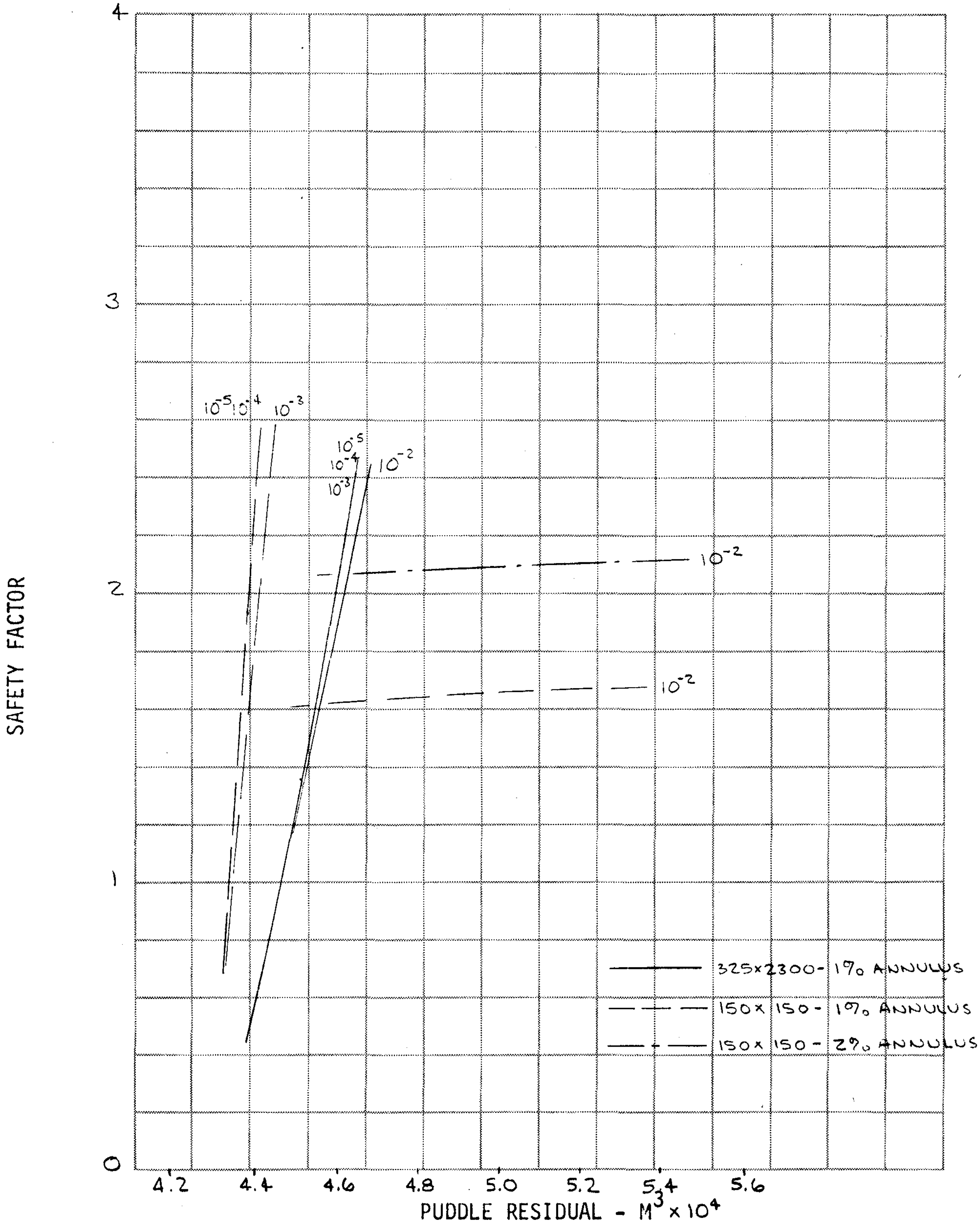

Figure 78. High G-Level Performance of Both Screens in the 50/2 Tank

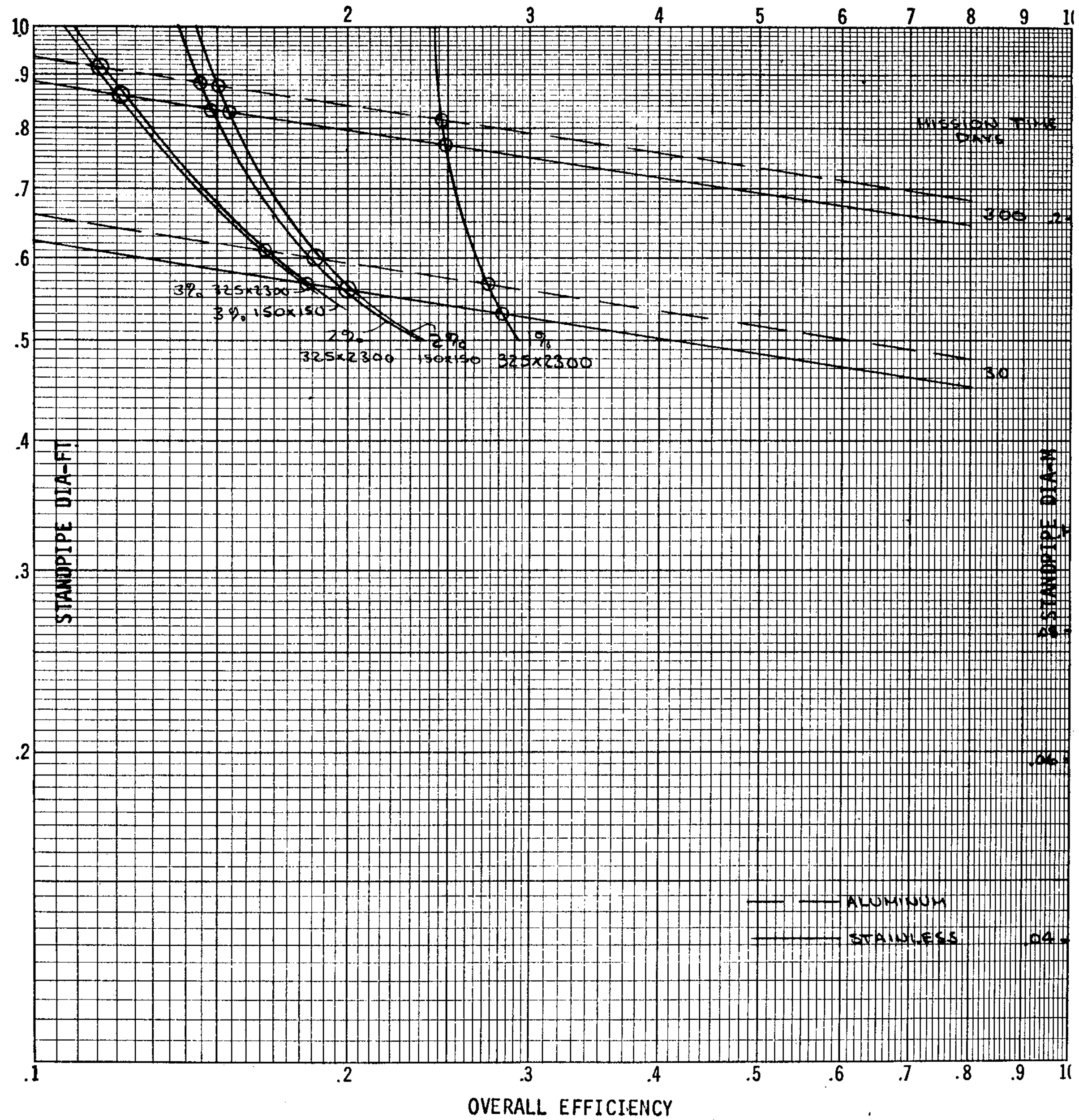

Figure 79. Standpipe Optimization at 1%/Min TVS Flow in the 5,000/4 Tank

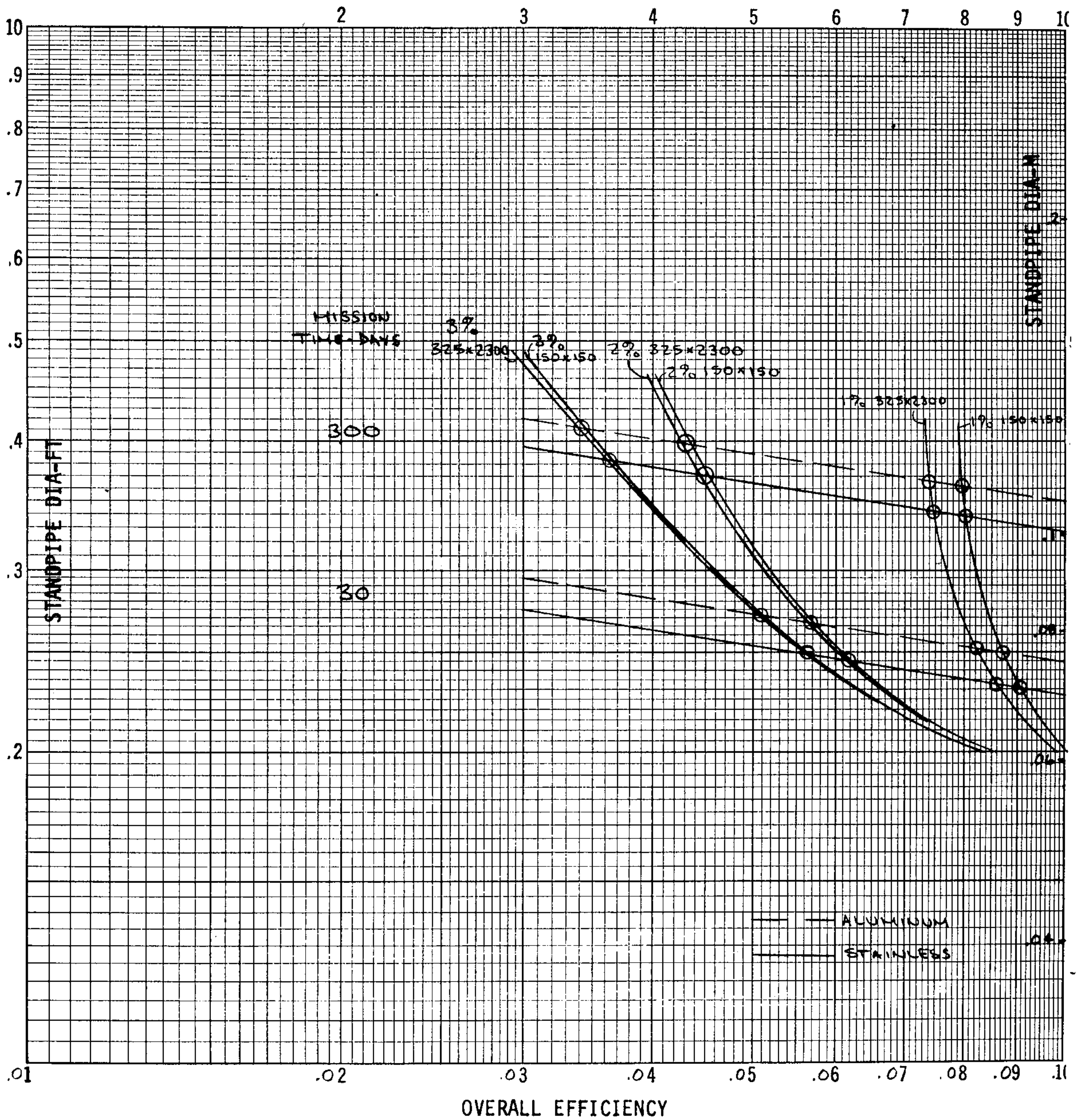

Figure 80. Standpipe Optimization at 1%/Min TVS Flow in the 500/4 Tank

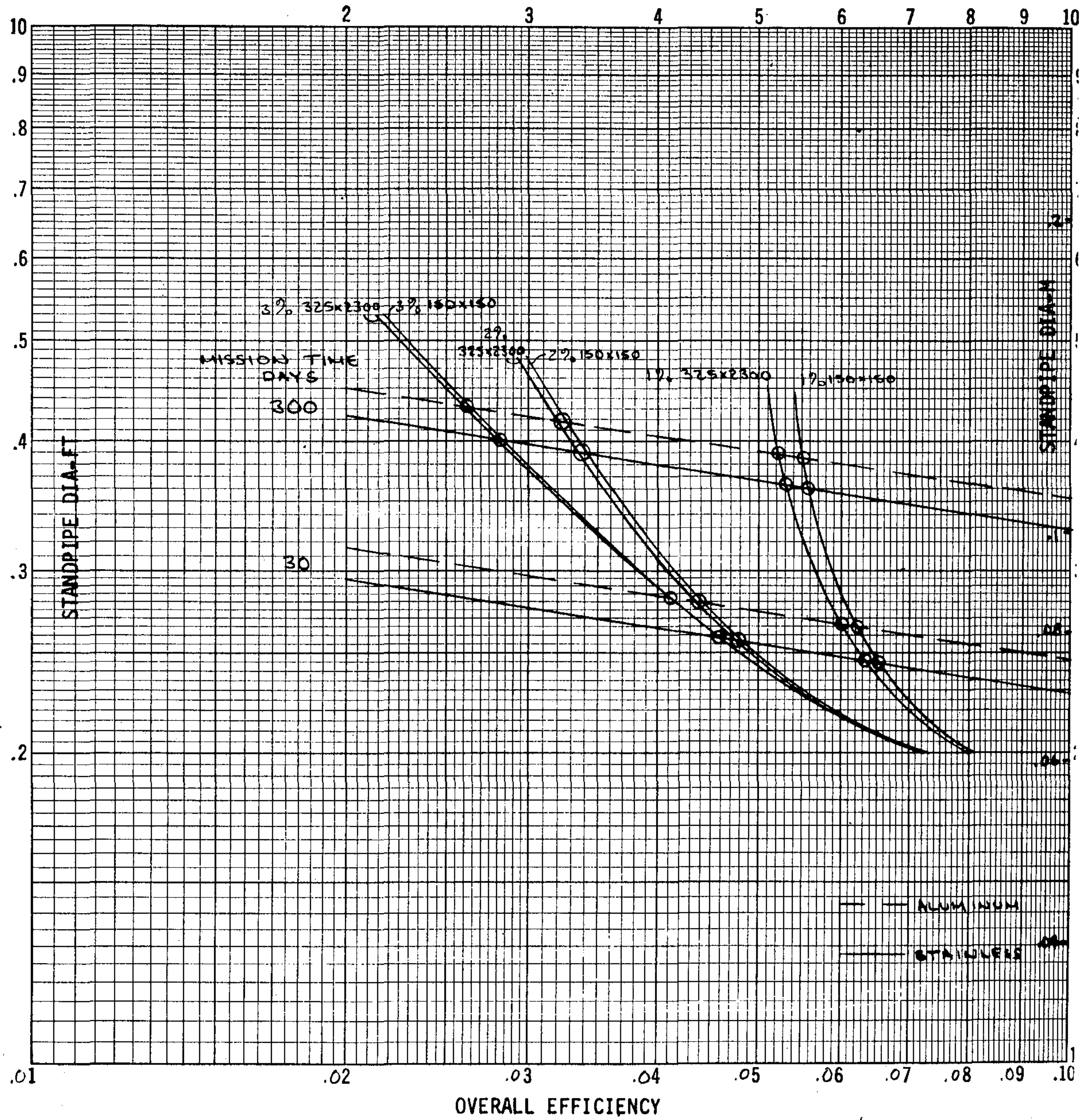

Figure 81. Standpipe Optimization at 1%/Min TVS Flow in the 500/2 Tank

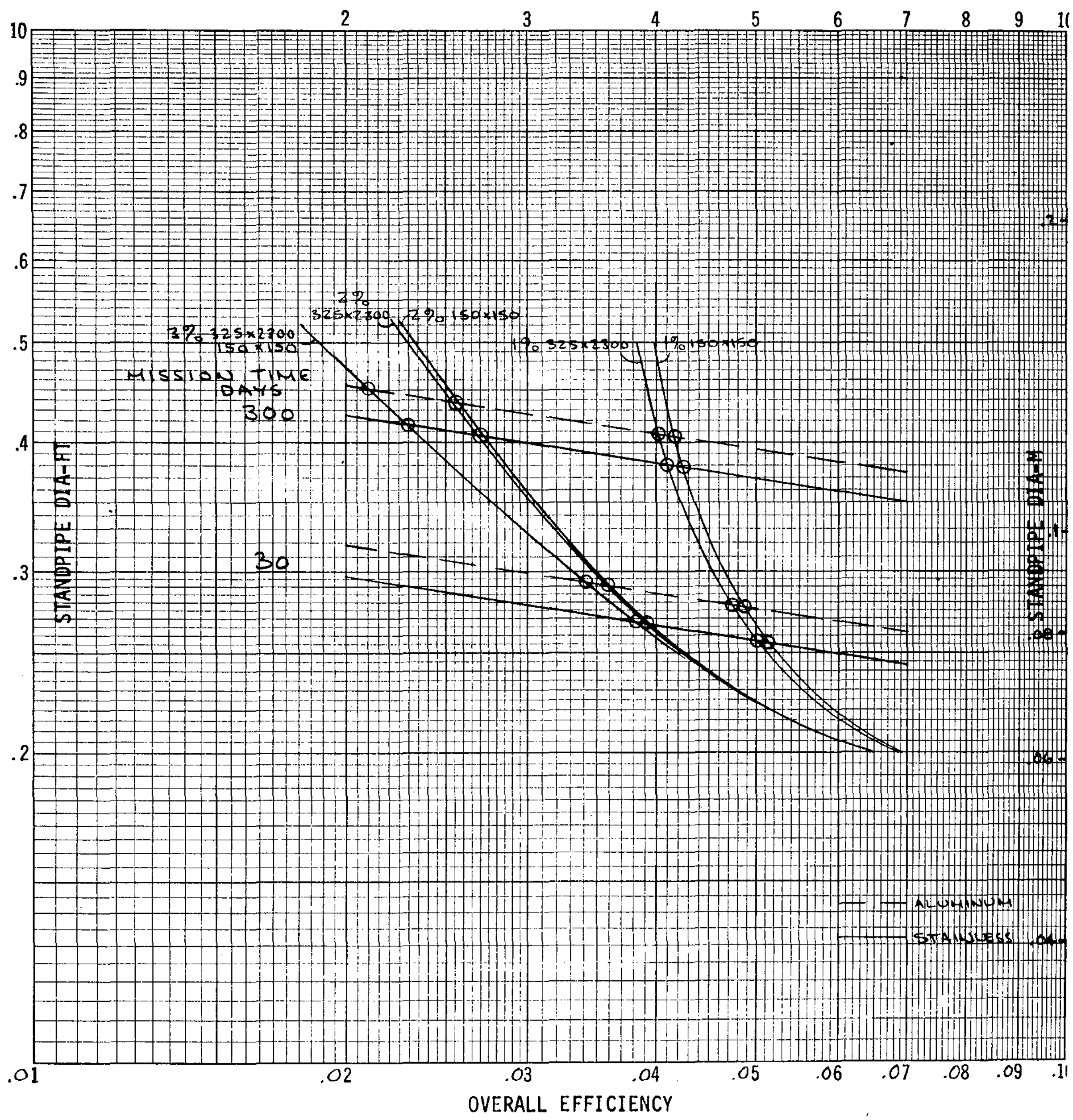

Figure 82. Standpipe Optimization at 1%/Min TVS Flow in the 500/1 Tank

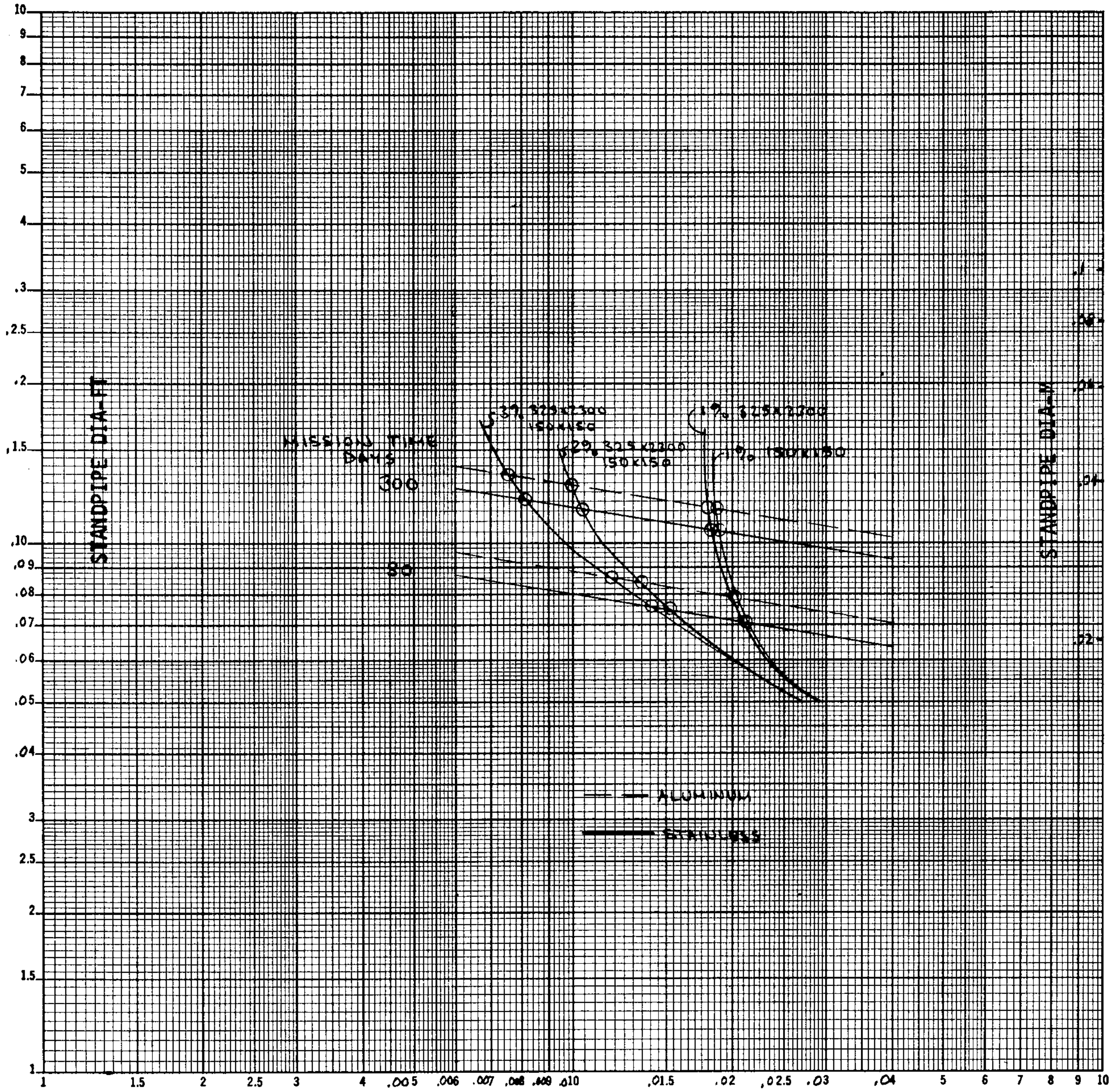

Figure 83. Standpipe Optimization at 1%/Min TVS Flow in the 50/2 Tank

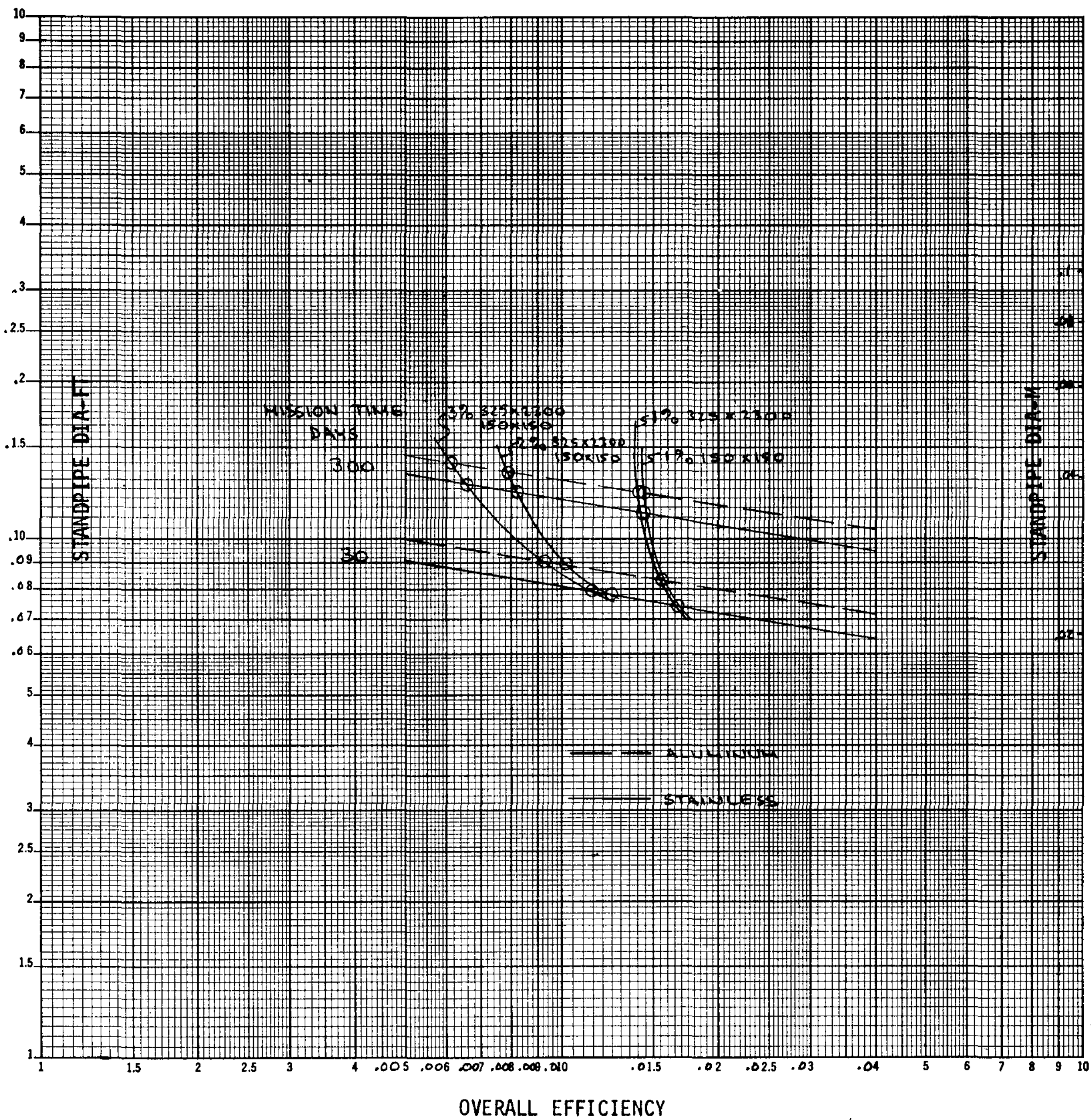

Figure 84. Standpipe Optimization at 1%/Min TVS Flow in the 50/1 Tank

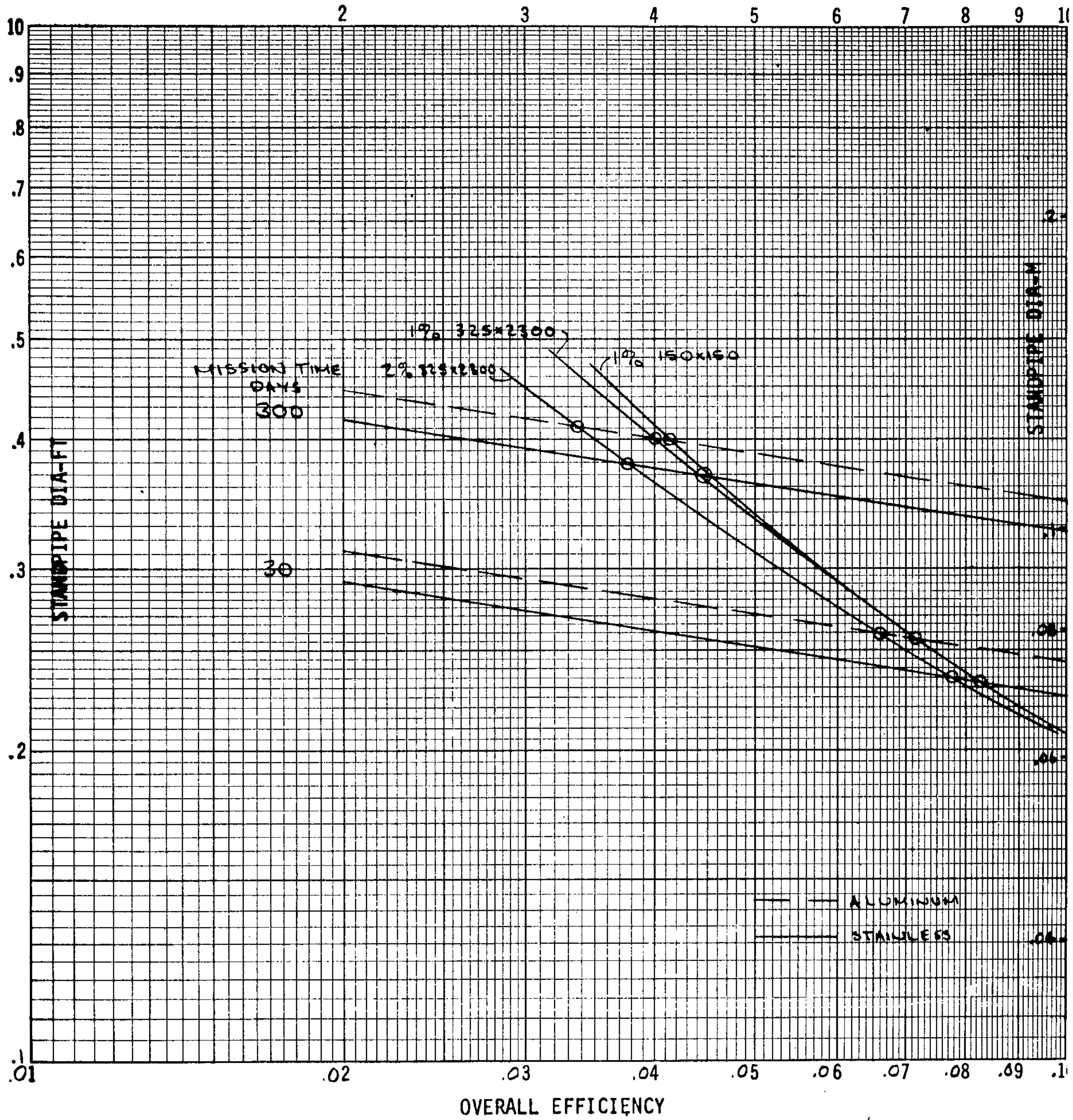

Figure 85. Standpipe Optimization at 0.1%/Min TVS Flow in the 5,000/4 Tank

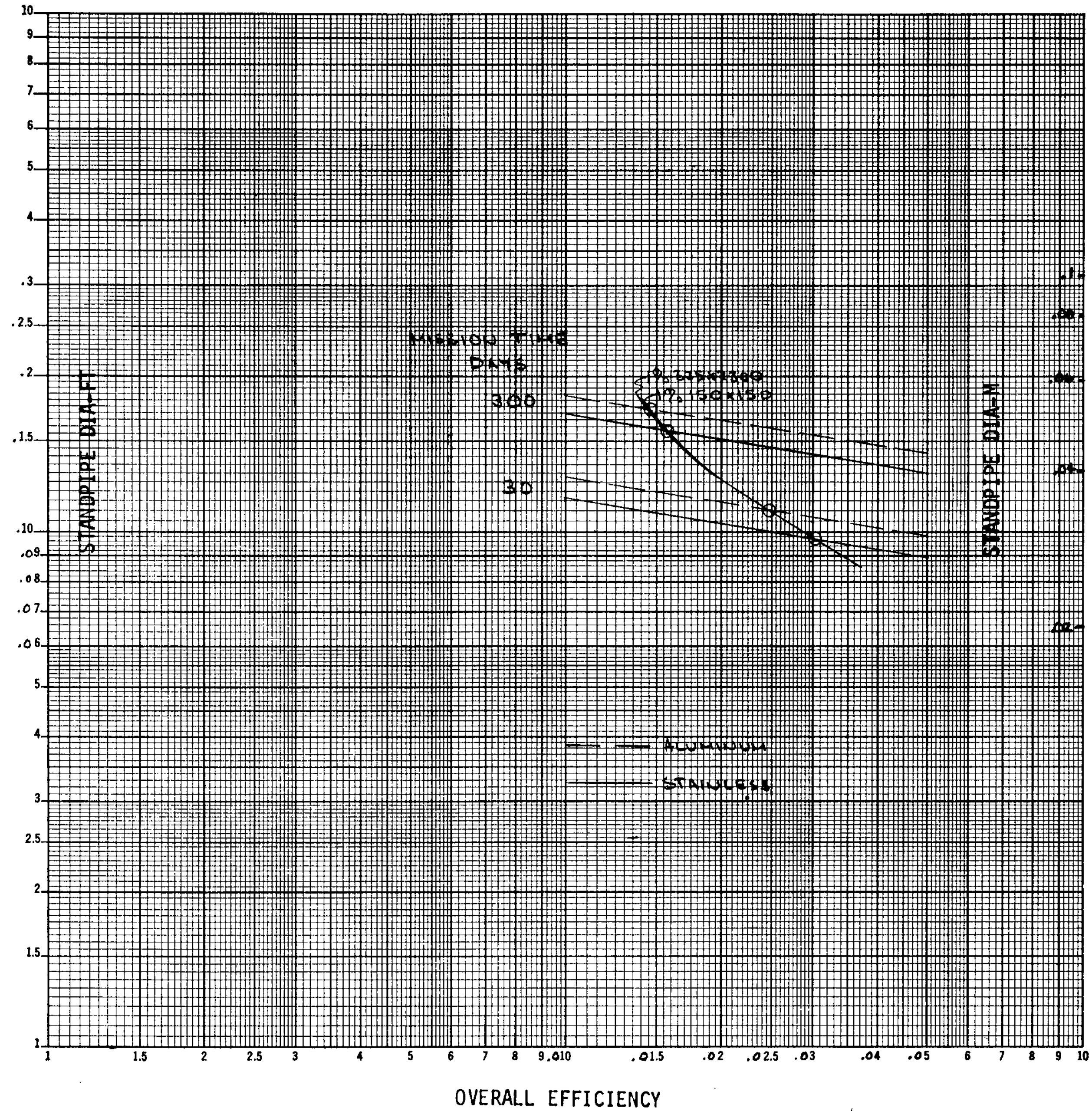

Figure 86. Standpipe Optimization at 0.1%/Min TVS Flow in the 500/4 Tank

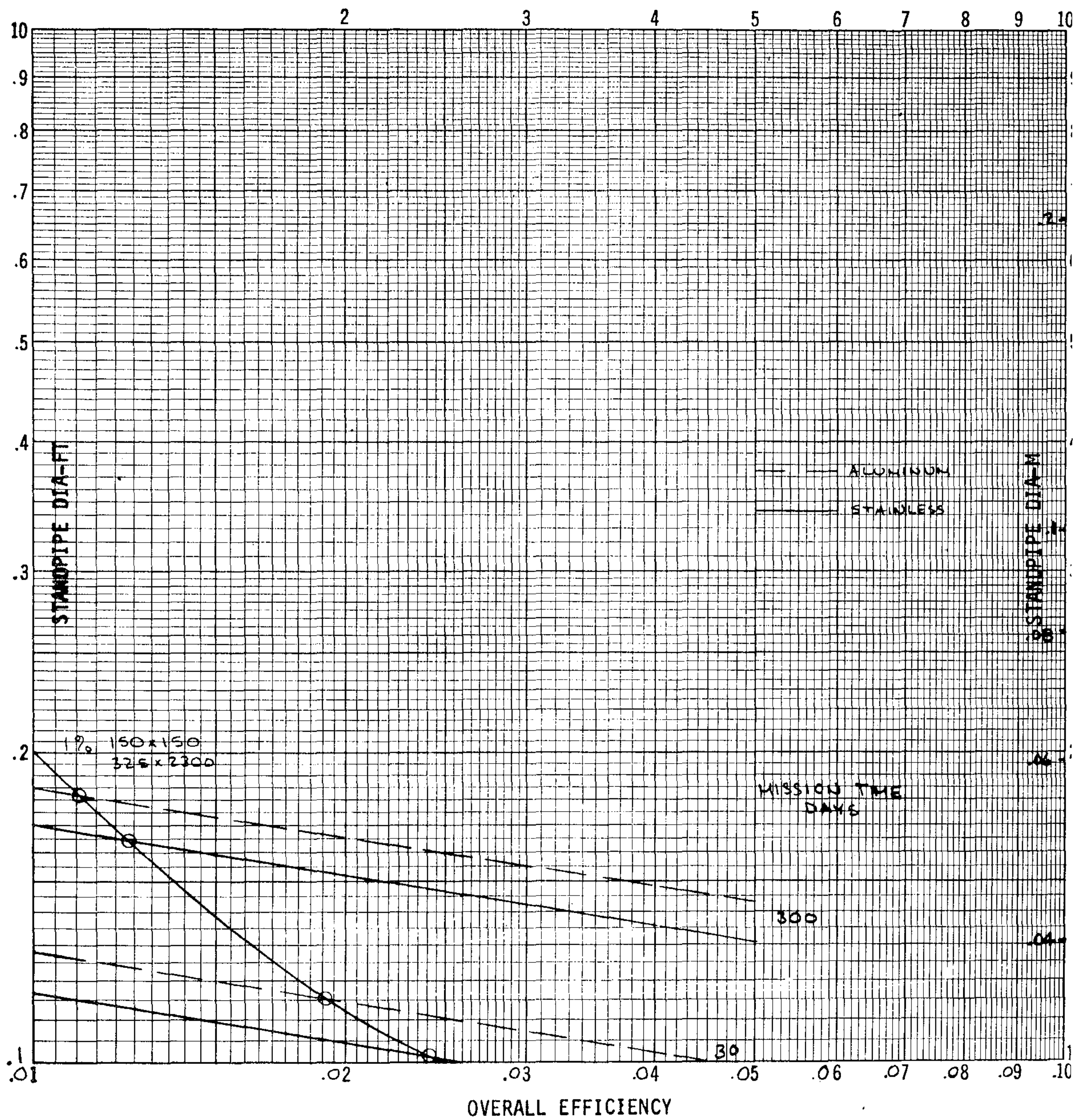

Figure 87. Standpipe Optimization at 0.1%/Min TVS Flow in the 500/2 Tank

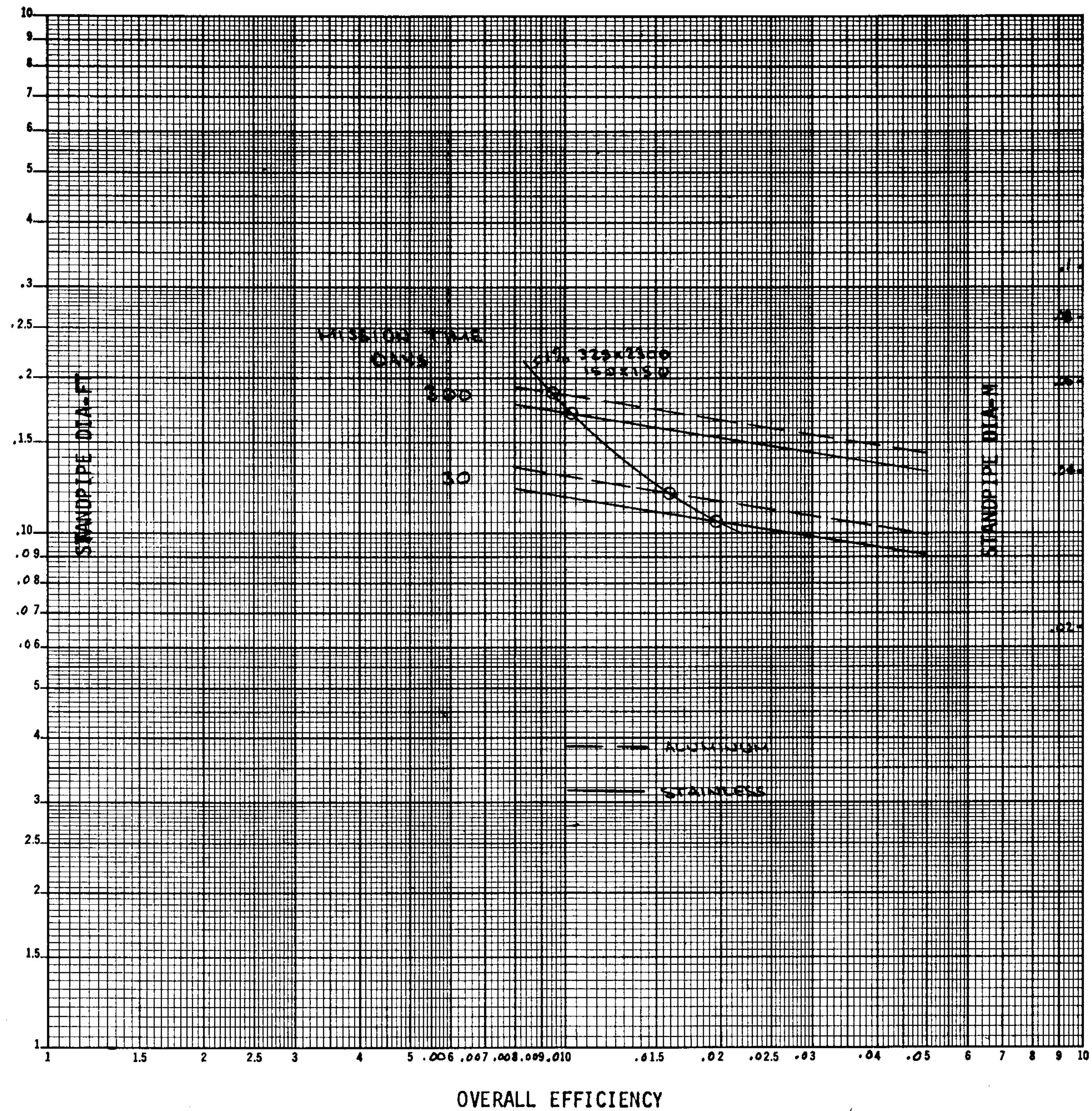

Figure 88. Standpipe Optimization at 0.1%/Min TVS Flow in the 500/1 Tank

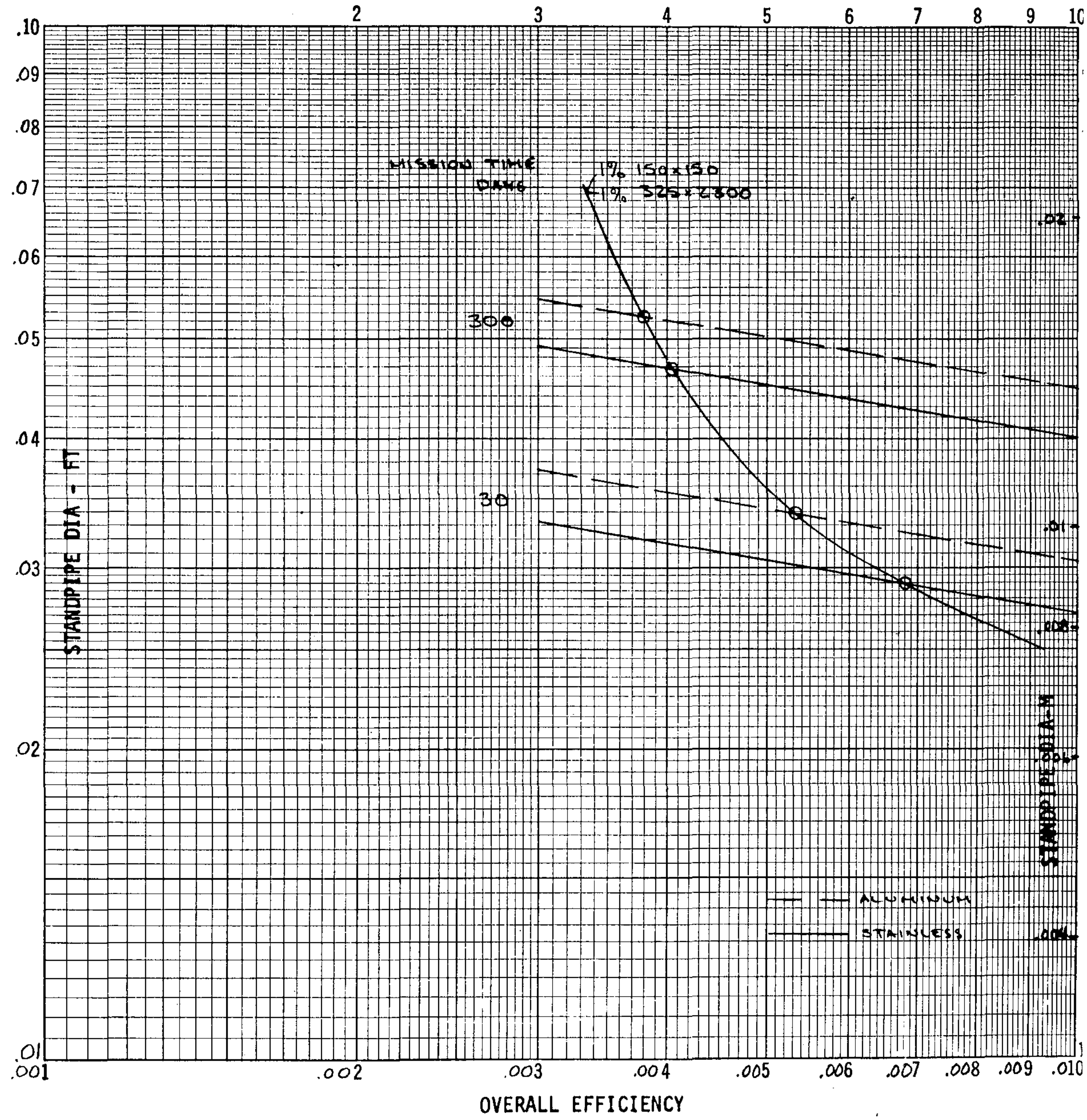

Figure 89. Standpipe Optimization at 0.1%/Min TVS Flow in the 50/2 Tank

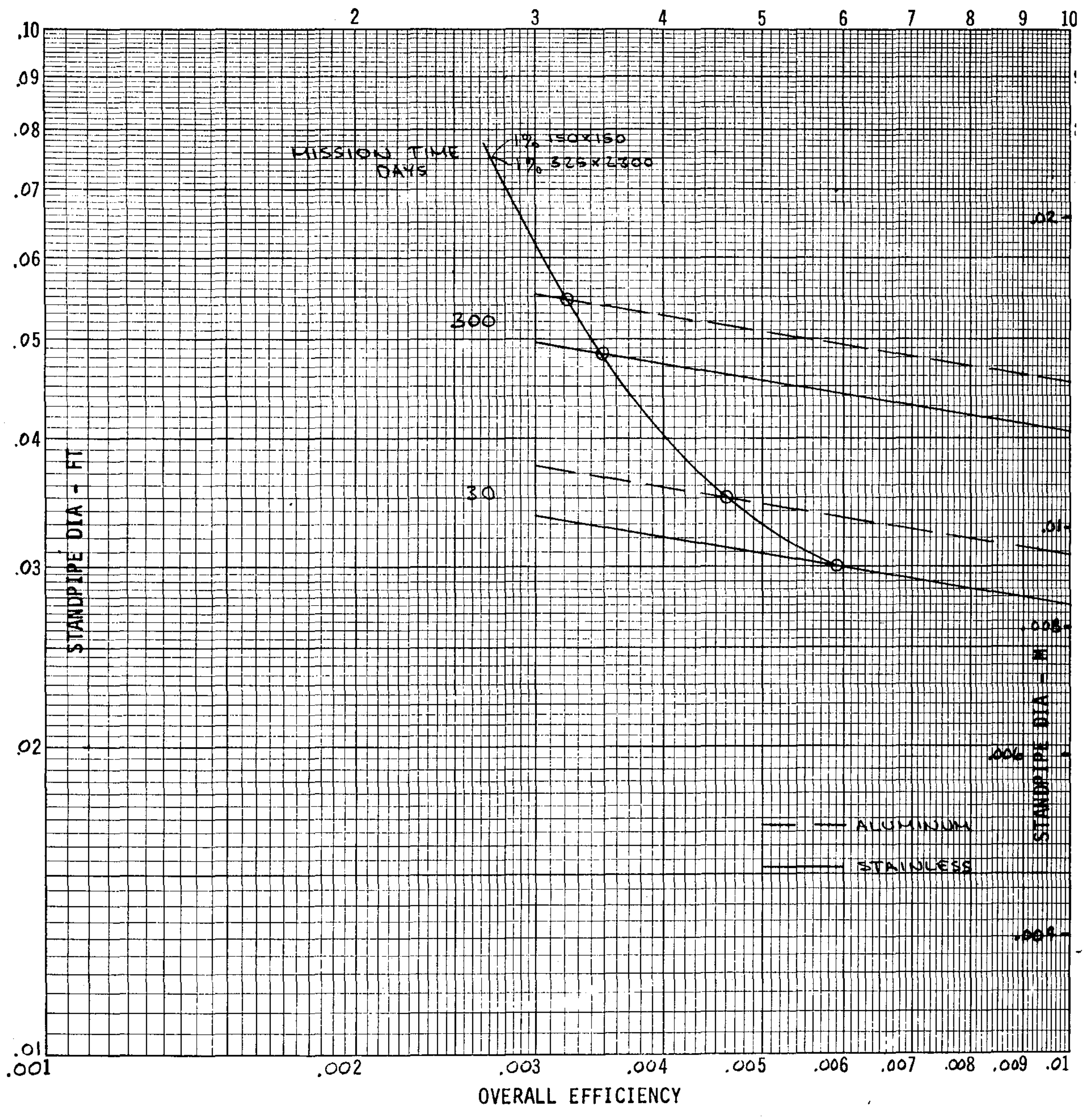

Figure 90. Standpipe Optimization at 0.1%/Min TVS Flow in the 50/1 Tank

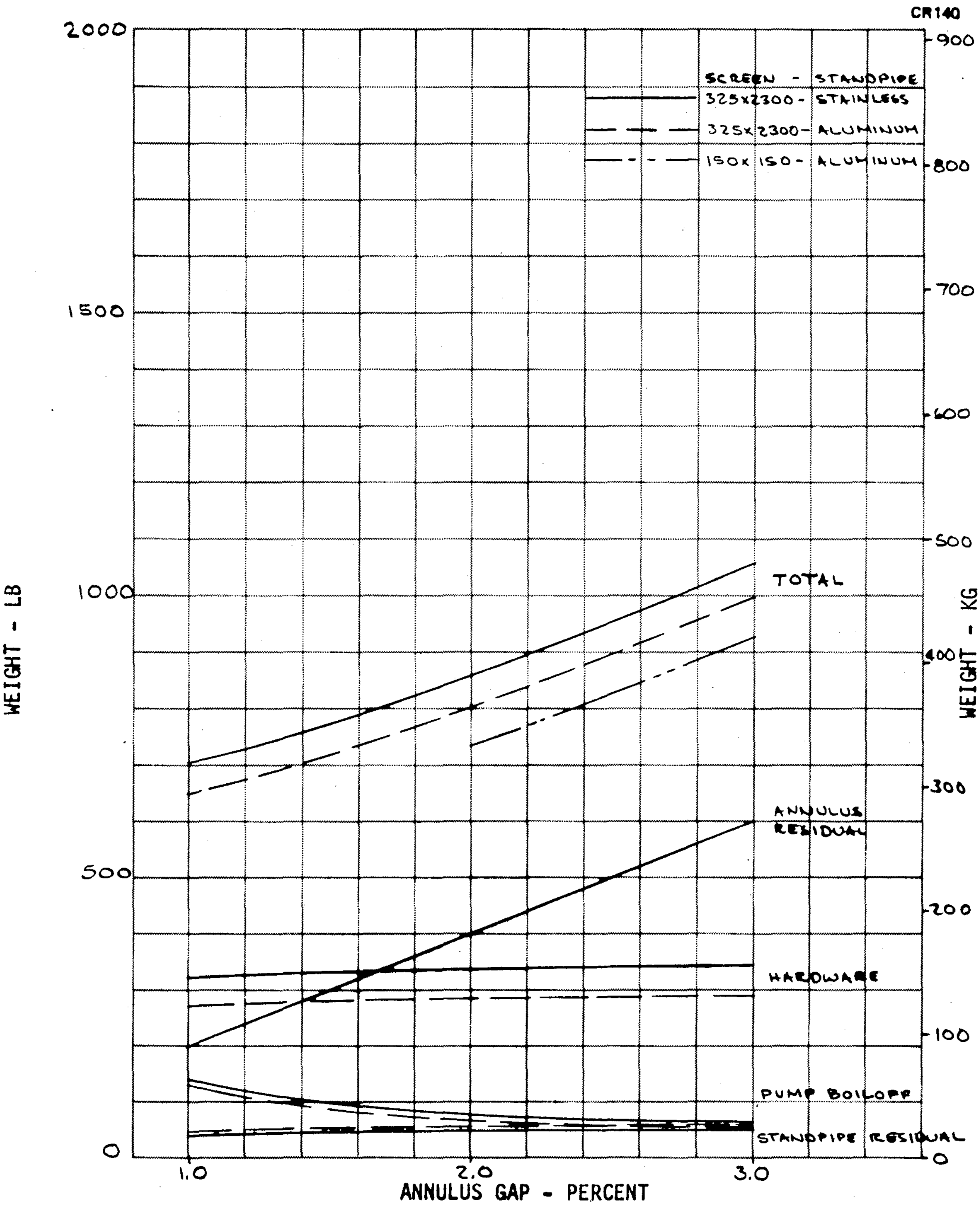

Figure 91. Weight Optimization for 5,000/4 Tank for 30-Day Mission

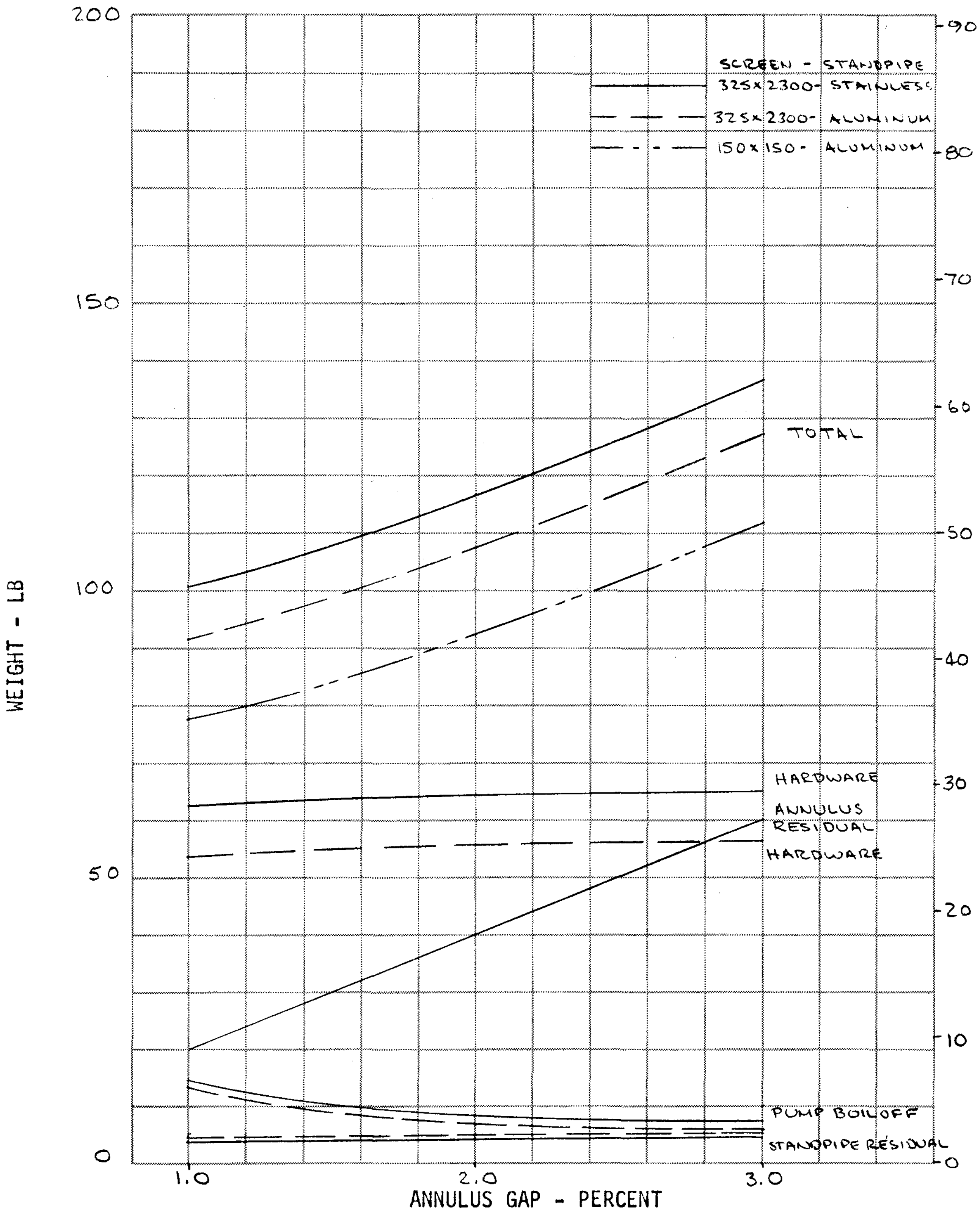

Figure 92. Weight Optimization for 500/4 Tank for 30-Day Mission

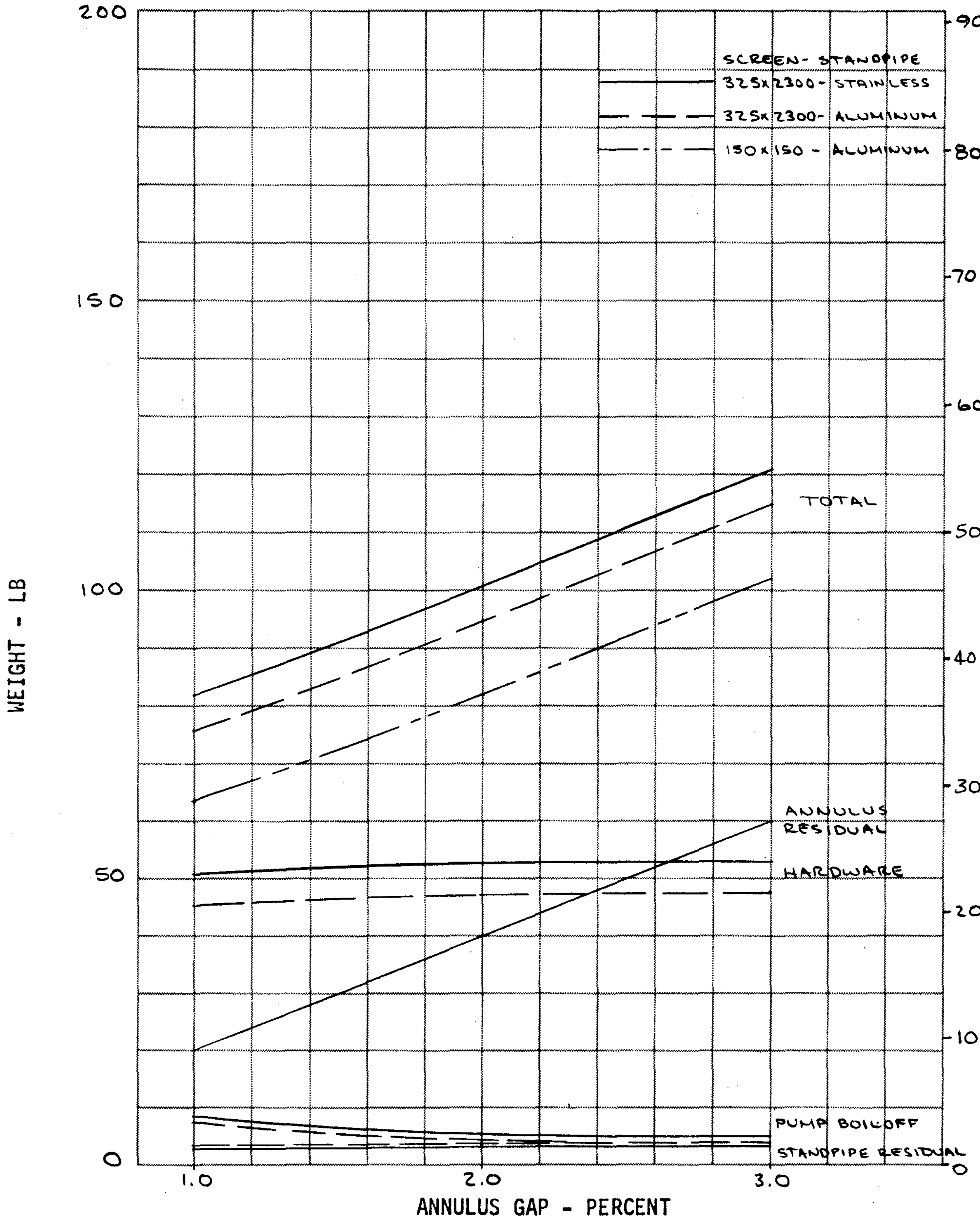

Figure 93. Weight Optimization for 500/2 Tank for 30-Day Mission

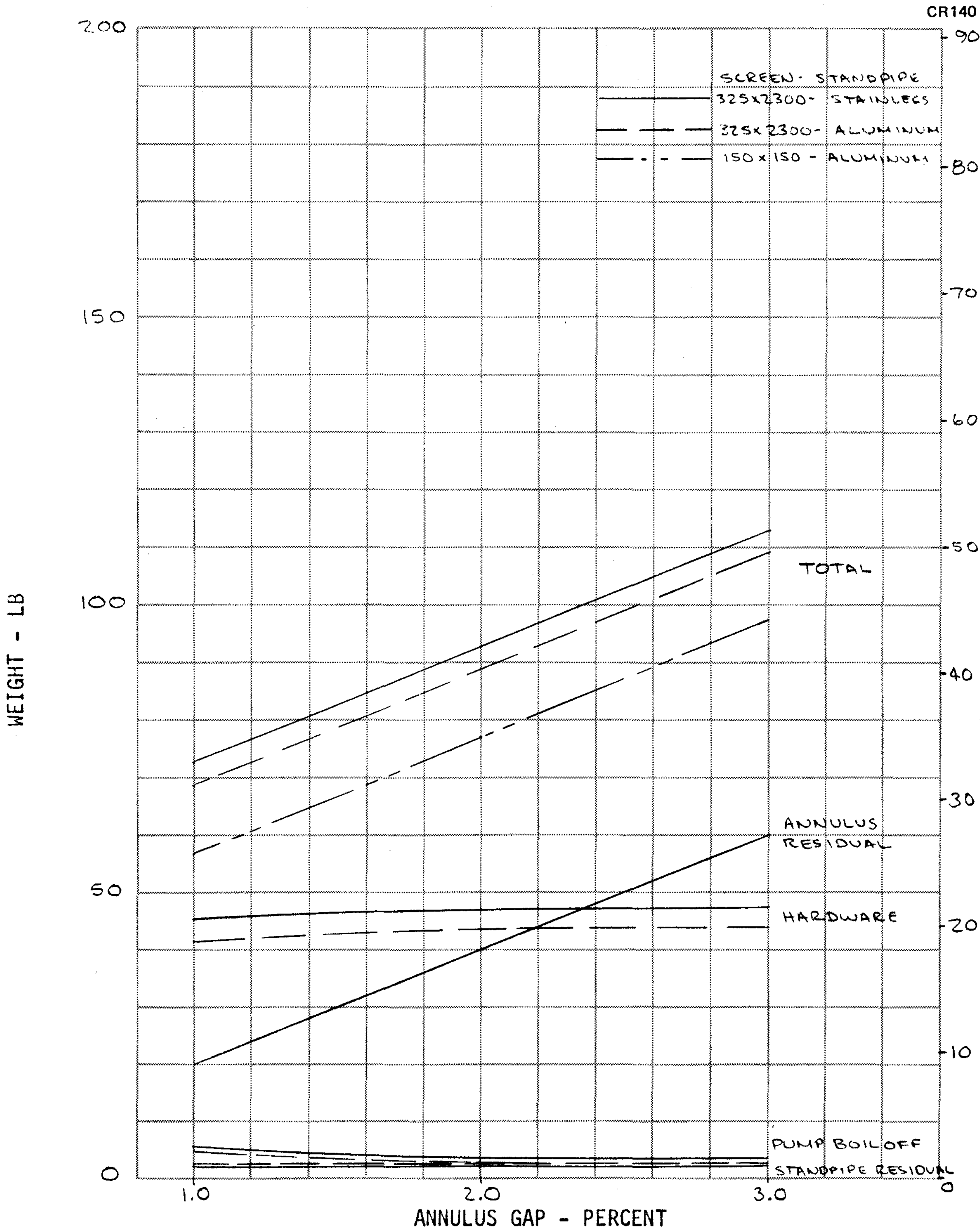

Figure 94. Weight Optimization for 500/1 Tank for 30-Day Mission

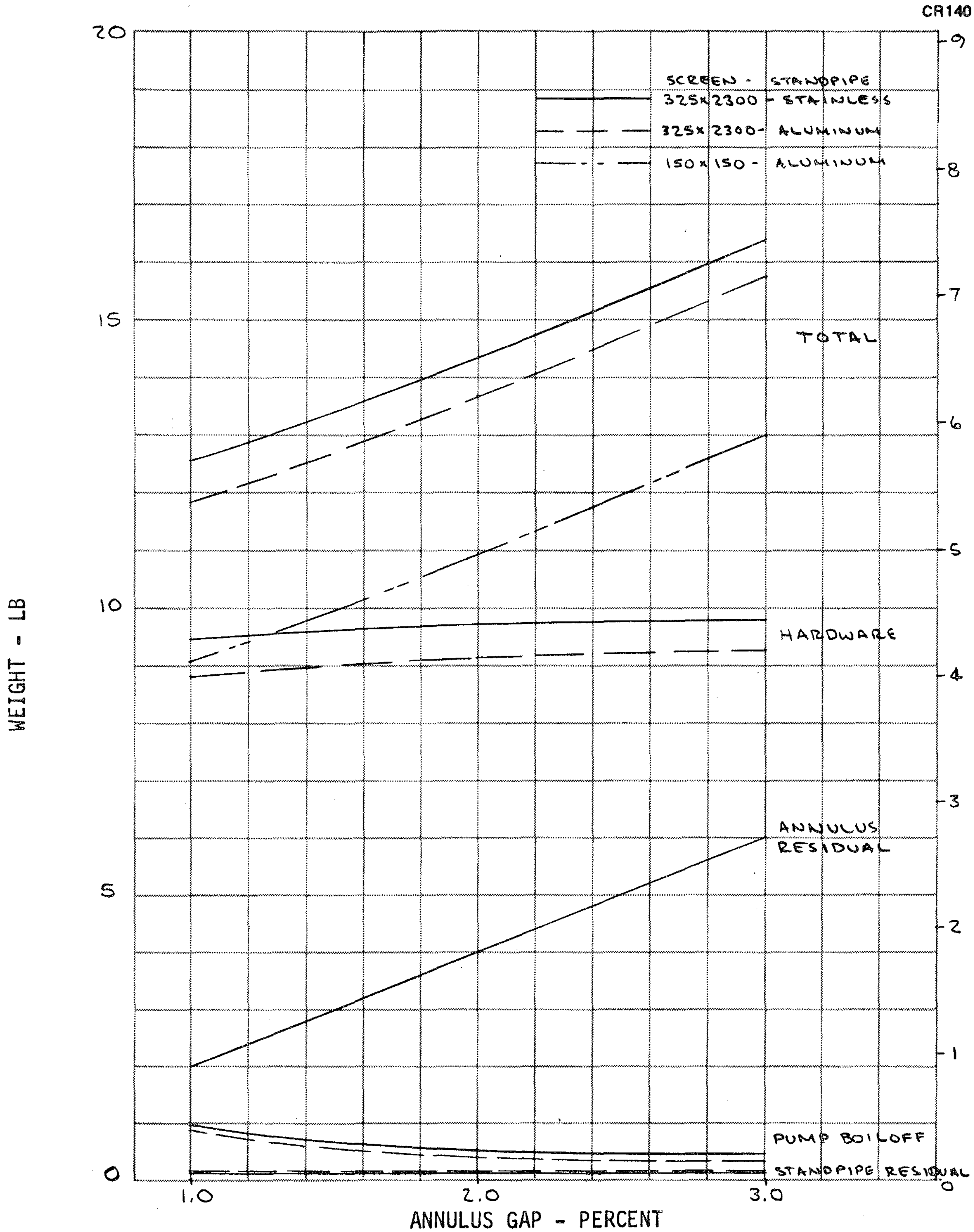

Figure 95. Weight Optimization for 50/2 Tank for 30-Day Mission

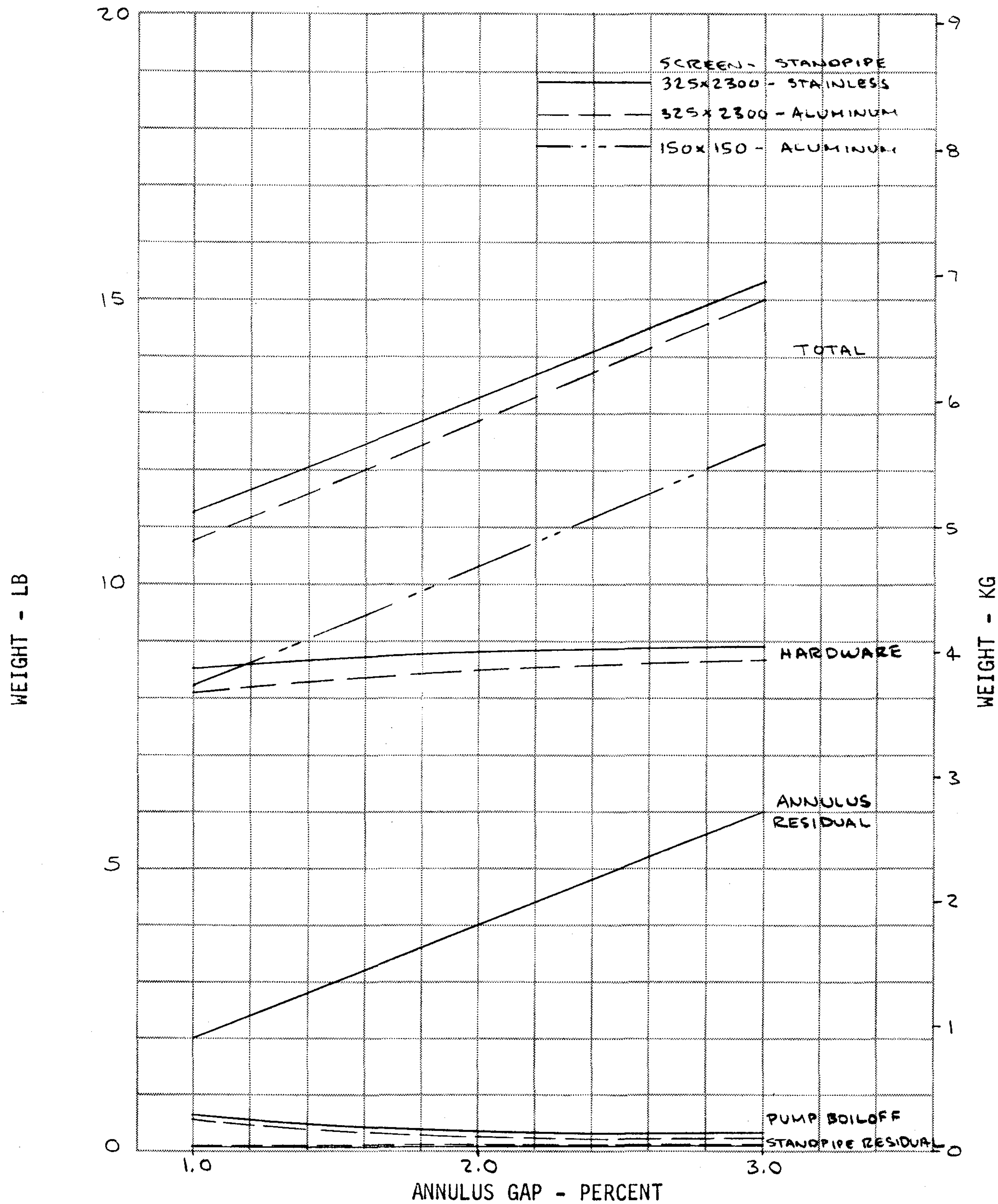

Figure 96. Weight Optimization for 50/1 Tank for 30-Day Mission

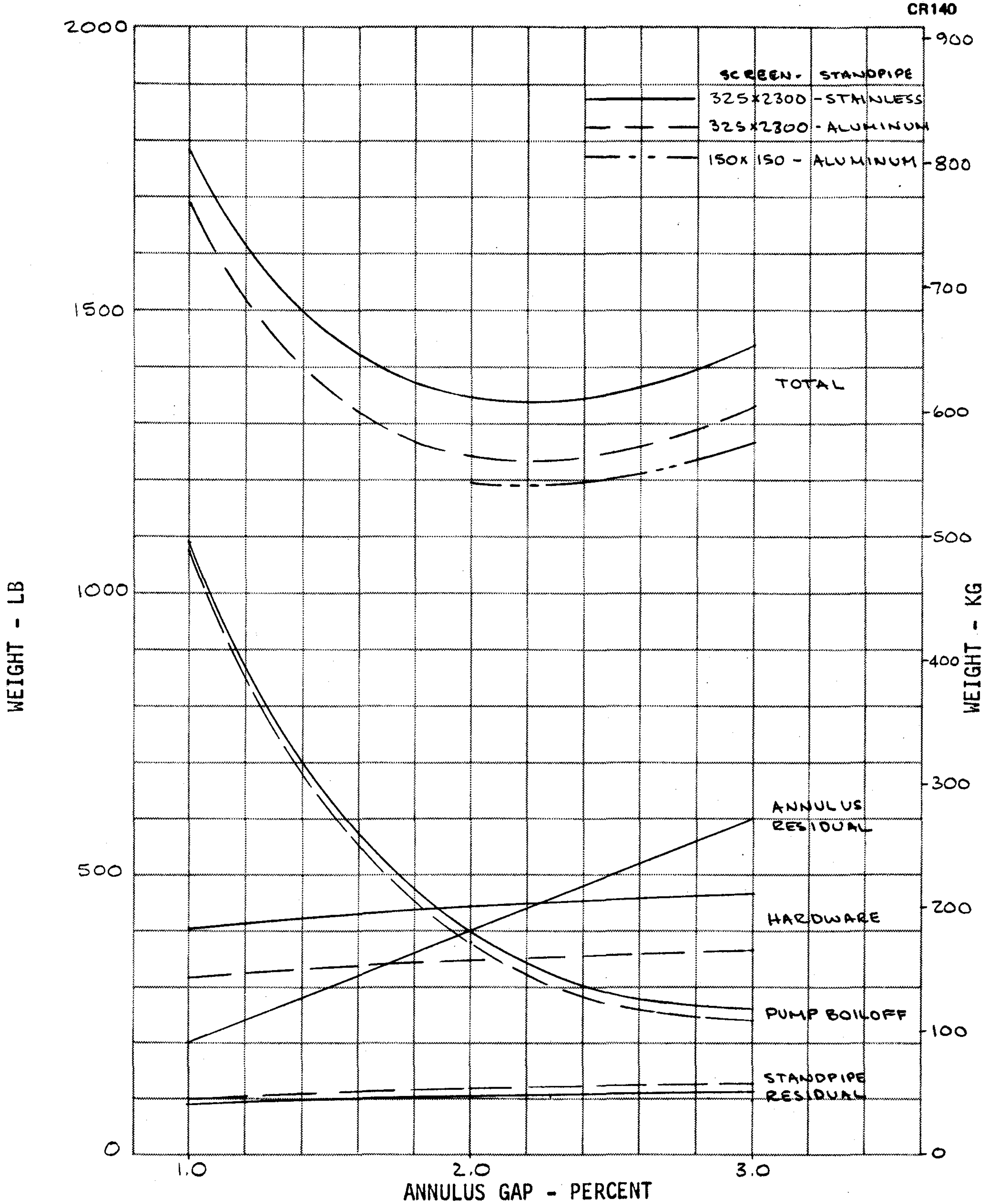

Figure 97. Weight Optimization for 5,000/4 Tank for 300-Day Mission

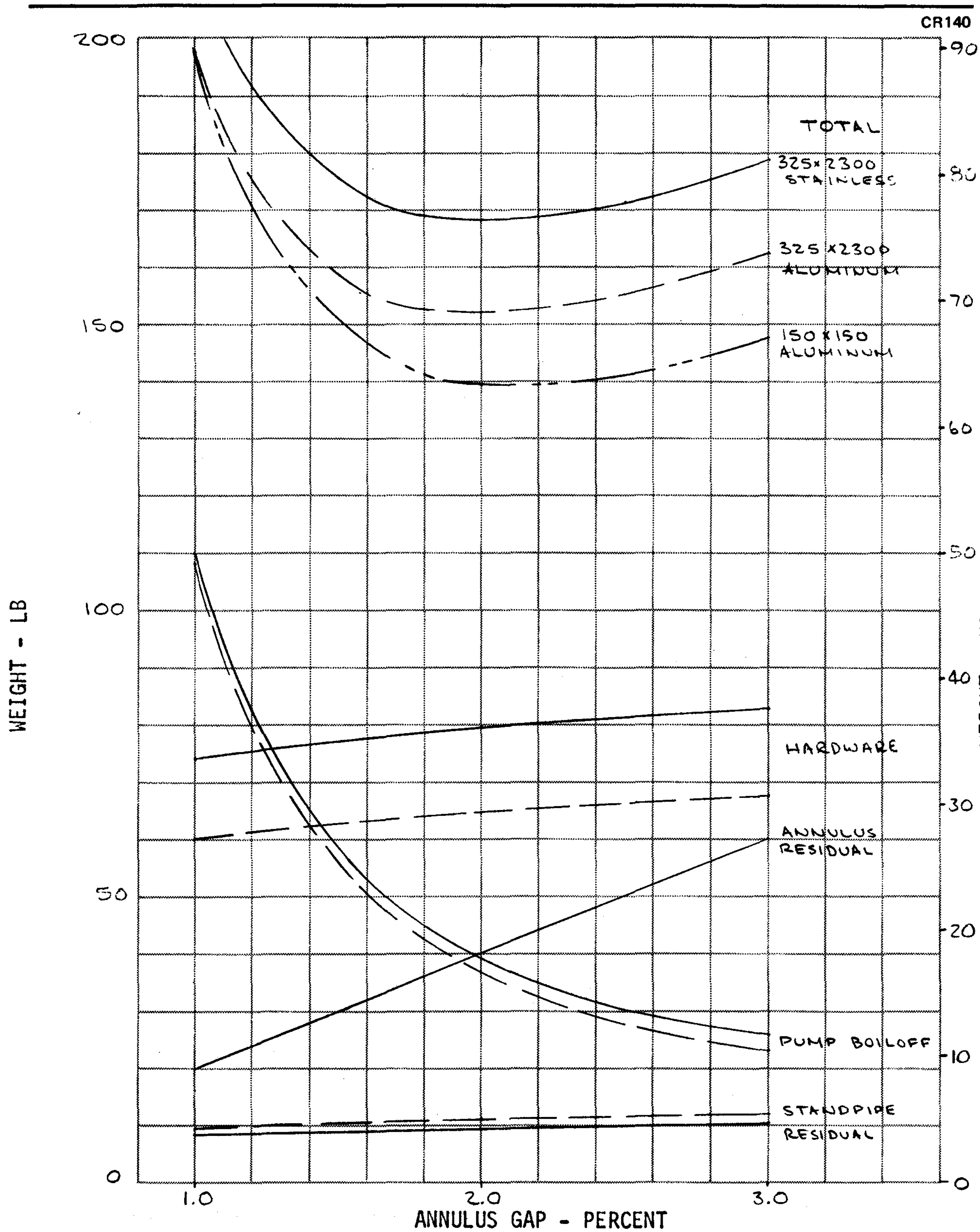

Figure 98. Weight Optimization for 500/4 Tank for 300-Day Mission

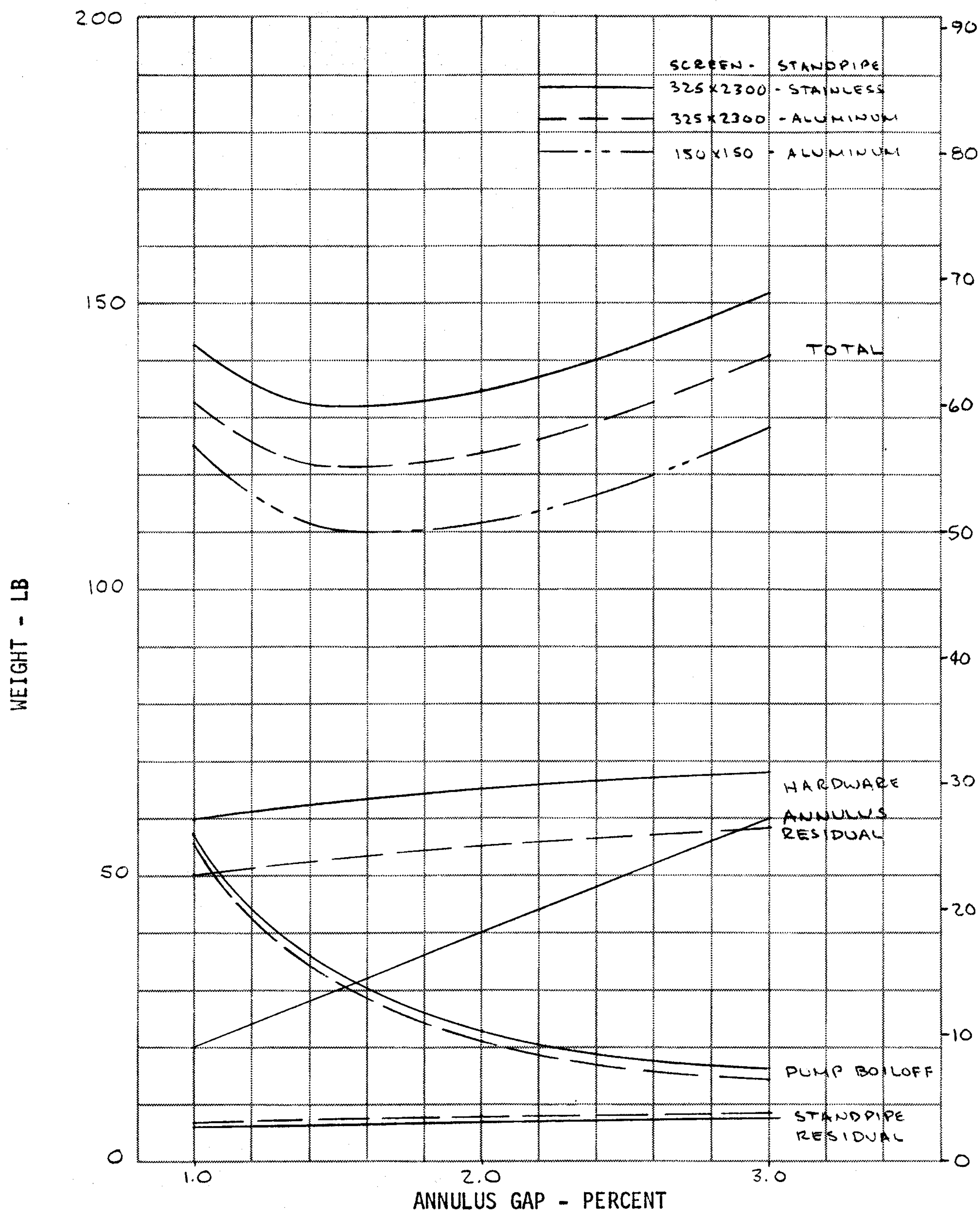

Figure 99. Weight Optimization for 500/2 Tank for 300-Day Mission

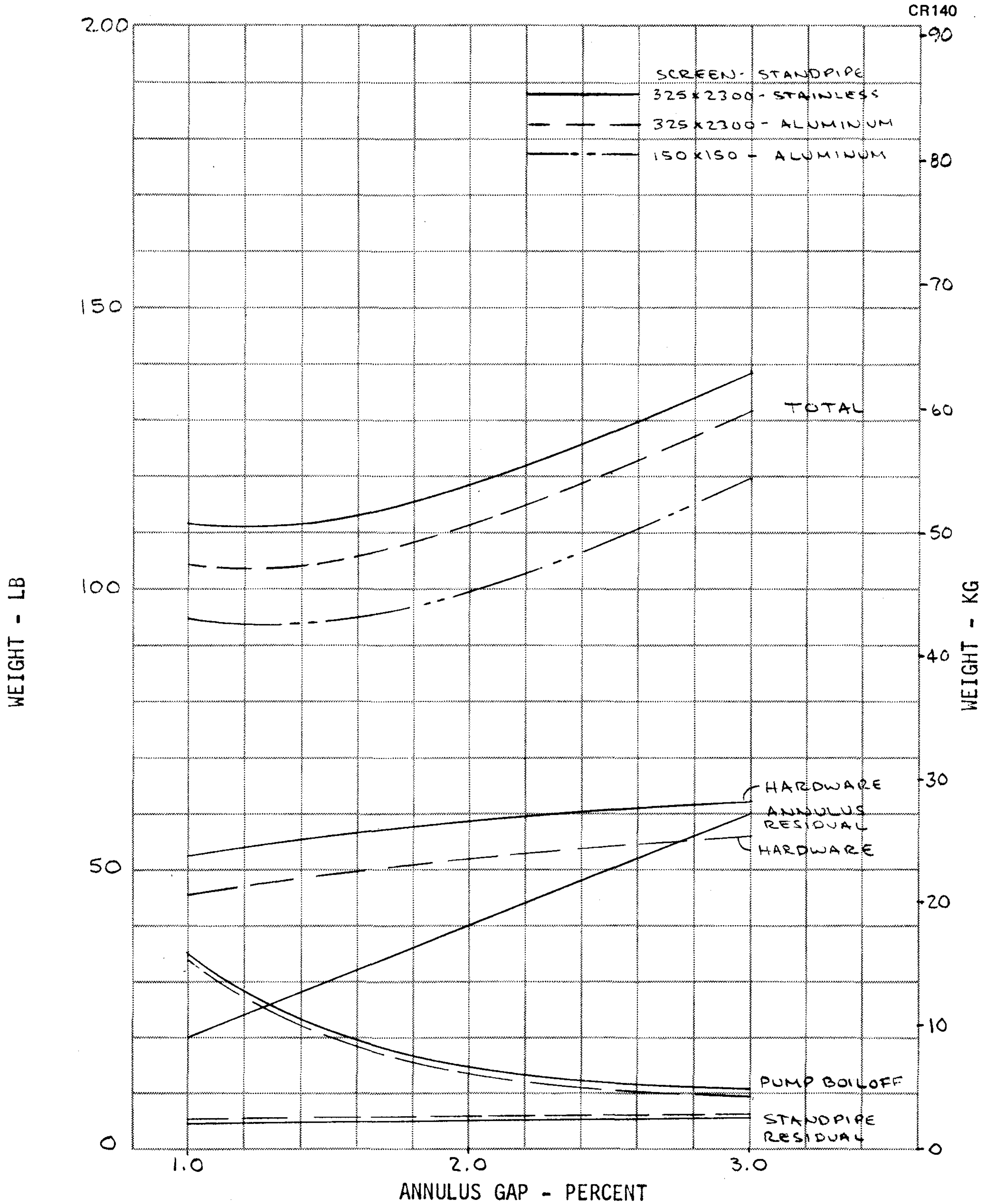

Figure 100. Weight Optimization for 500/1 Tank for 300-Day Mission

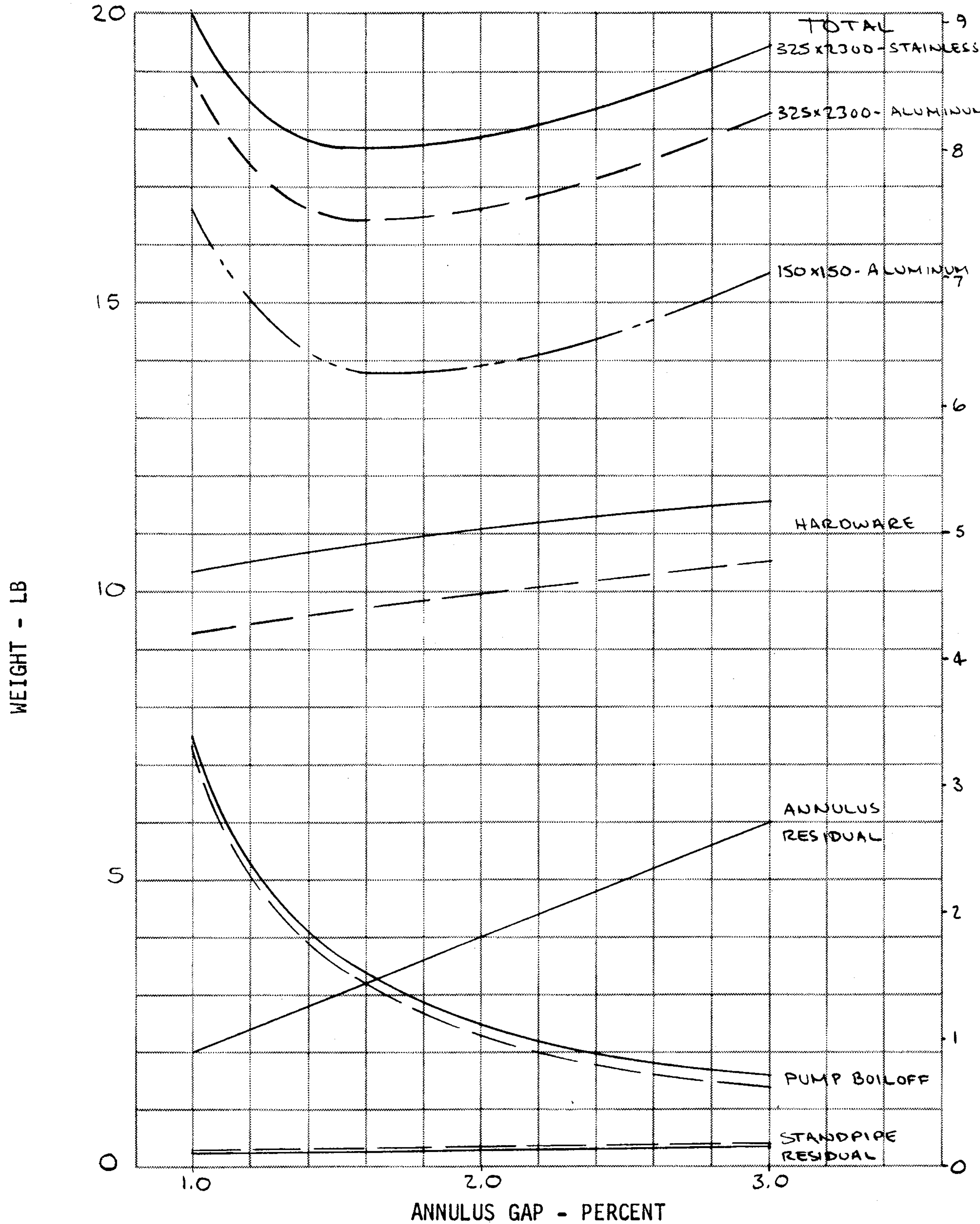

Figure 101. Weight Optimization for 50/2 Tank for 300-Day Mission

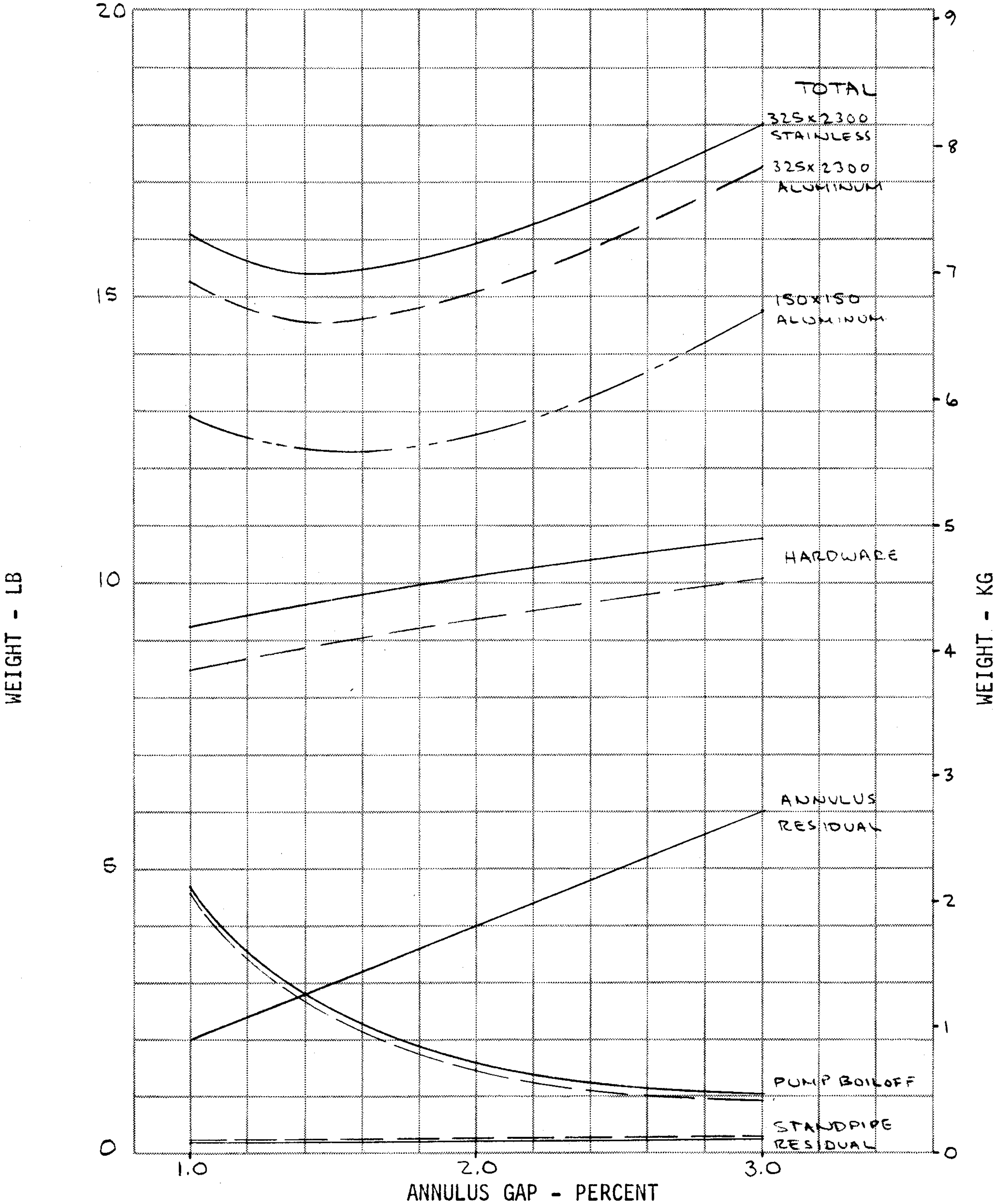

Figure 102. Weight Optimization for 50/1 Tank for 300-Day Mission

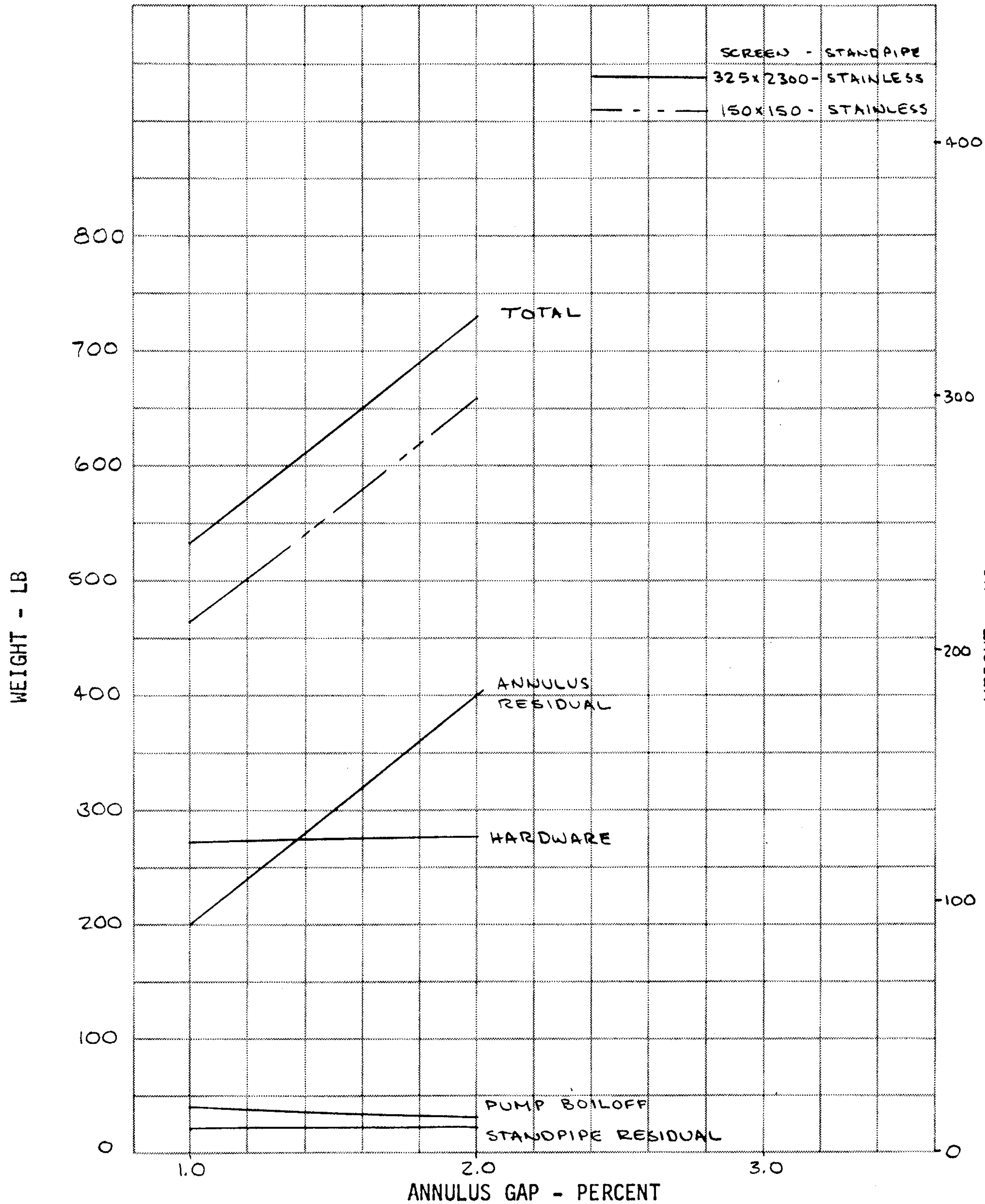

Figure 103. Weight Optimization for 5000/4 Tank for 300-Day Mission at 0.1% TVS Flow

However, for the 300-day mission, the pump boiloff became very important, as shown in Figures 97 through 102, so that an optimum annulus gap was found, at which minimum weight occurs. For the 5,000/4 and 500/4 tanks, this optimum was at about 2.0 to 2.2% annulus gap for both the 325 x 2,300 and the 150 x 150 screens. For the 500/2 and 50/2 tanks, the optimum gap was at about 1.6%, and for the 500/1 and 50/1 tanks the optimum was at an annulus gap of about 1.4 to 1.5%. In Figure 103, for the 5,000/4 tank at 0.1% tank volume/minute TVS flow, the optimum again occurred at the minimum annulus gap, as was the case for the other five tanks.

APPENDIX F

PROPELLANT HEATING FROM ELECTRIC PUMPS

Most of the power input to the electric motor/pump in the LH_2 tank is lost in electric motor inefficiency, principally windage losses and friction, which directly heat the LH_2. Some of the remaining power to the pump is lost as pump inefficiency, principally friction losses, with the remaining power being used as fluid power. However, nearly all of the fluid power is used to overcome flowing friction and only a relatively small fraction is stored in the LH_2 as fluid kinetic energy. All other power loss is essentially dissipated in the LH_2 as heat, leading to "boiloff."

To determine the maximum energy storage capability of the system, it can be assumed that over a long period of time the pump imparts momentum to not only the fluid in the annulus, but to all of the fluid in the tank by momentum exchange. The assumption that all of the fluid in the tank acquires the maximum velocity of the fluid in the annulus at the specified TVS flowrate gives the maximum energy storage capacity of the system. That energy is, for the 141.6 m^3 (5,000 ft^3) tank, simply the mass of liquid times the maximum dynamic head in the annulus at a TVS flowrate of 1% of tank volume/minute, or:

$$\text{K.E.} = V\rho H_d$$

$$= 141.6\ m^3\ (64.08\ kg/m^3)\ 0.0488\ m\ \ 9.807\ \frac{\text{watt-sec}}{\text{kg - m}}$$

$$= 4,335\ \text{watt-sec}$$

Compare this to the total energy entering the tank through the pump in 30 days:

9.75 watts x 2,592,000 sec = 25,250,000 watt-sec.

The ratio 4,335/25,250,000 = 0.017% of energy input remains stored as kinetic energy for a 30-day mission, or 99.983% is dissipated as heat to the LH_2. For the 300-day mission, 99.9978% is dissipated as heat to the LH_2. The results are similar for the other five tanks. Therefore, it is assumed that all of the energy input to the electric pump ends up heating the LH_2 and causing "boiloff."

APPENDIX G

TANKAGE INSULATION OPTIMIZATION AND TVS HEAT EXCHANGER DESIGN

For a given tank and mission, assuming constant tank pressure, the optimum insulation system can be determined by minimizing the combined weight of the multilayer insulation and the LH_2 "boiloff" due to external heat leak. First, the insulation effective conductivity must be determined. Based on extensive experimental work by MDAC (ref. 28), the performance of a typical high performance insulation, namely double-aluminized mylar with B4A dacron-net spacer, is characterized by the equation:

$$K_{eff} = 3.007 \times 10^{-25}\ \overline{N}^{8.6}\ \frac{(T_H + T_C)}{2}$$

$$+ \frac{8.333 \times 10^{-2}\ \sigma (T_H{}^2 + T_C{}^2)\ (T_H + T_C)\ N}{(N-1)\ (\frac{1}{\epsilon_1} + \frac{1}{\epsilon_2} - 1)\ \overline{N}} \qquad \text{(G-1)}$$

in English engineering units, where $\overline{N}$ is the layer density (assumed for our study at 100 layer-pairs/inch), N is the number of layer-pairs, σ is the Stefan-Boltzmann constant, 0.1714×10^{-8} Btu/hr-ft^2-°R^4, $T_H = 460$ °R, $T_C = 40$ °R, $\epsilon_1 = \epsilon_2 = 0.021$. Therefore, for $N > 100$

$$K_{eff} = 2.1 \text{ Joule/m-sec-°K} \qquad \text{(G-2)}$$

$$(1.351 \times 10^{-5} \text{ Btu/hr-ft-°R})$$

This value must be further degraded by 50% to account for heat leak through joints, fasteners, perforations, etc. The weight of this insulation in kg is

$$W = 0.0122 \frac{\text{kg}}{(\text{layer-pair})\ \text{m}^2} \times 3,937 \frac{\text{layer-pairs}}{\text{m}} \times \ell (A_I)\ (\text{m}^2)$$

$$+ 0.229 \left(\frac{\text{kg}}{\text{m}^2}\right)\ A_I\ (\text{m}^2) \qquad \text{(G-3)}$$

where ℓ is the insulation thickness, (m) and A_I the insulation area (m^2)

Thus, the total weight (boiloff plus insulation weight) is:

$$W = 1.5 \frac{(2.1)}{\ell} \frac{(255 - 22.2) \quad A_I \; t\,(sec)}{449,000 \text{ Joules/kg}} + 48\ell \; A_I + 0.229 \, A_I$$

$$+ \frac{\dot{q}_{HEAT\ SHORT} \; t}{449,000 \text{ Joules/kg}} \qquad \text{(G-4)}$$

Differentiating with respect to ℓ and equating to zero gives:

$$d \frac{W}{d\ell} = -1.64 \times 10^{-3} \frac{A_I \; t}{\ell^2} + 48 \, A_I = 0 \qquad \text{(G-5)}$$

or

$$\ell^2 = \frac{1.64 \times 10^{-3}}{48} \; t \quad , \qquad \text{(G-6)}$$

$$\ell = 5.84 \times 10^{-3} \; t^{1/2} \qquad \text{(G-7)}$$

Solving equation (G-7) for the insulation thickness (m) in terms of mission time (sec), t, the boiloff flowrate is:

$$\dot{W} = \frac{1.64 \times 10^{-3} \; A_I}{\ell} + \frac{(\dot{q}_{HEAT\ SHORT})}{449,000} \qquad \text{(G-8)}$$

This boiloff, together with that caused by pump/motor input power, gives the total vented flowrate through the TVS heat exchanger. By examining the heat transfer processes which occur, it will be possible to define the required heat transfer area and heat exchanger size.

Assuming the configuration shown in Figure 104 with a heat-exchanger coil bonded or brazed to the outside of the standpipe (so as not to affect flow or pressure-drop in the standpipe), the required length of coil and heat exchanger area will be defined by the overall heat-transfer coefficient.

The flow through the standpipe is being pumped by the TVS pump at 1% or 0.1% tank volume/minute; thus, the heat transfer coefficient on the inside of the standpipe, h_1, is governed by forced convection. Forced convection in a circular duct is described by the Dittus-Boelter equation:

$$\frac{h_1 \; D_s}{K} = 0.023 \left(\frac{4\dot{Q}\rho}{\pi \mu D_s}\right)^{0.8} \; Pr^{0.33} \qquad \text{(G-9)}$$

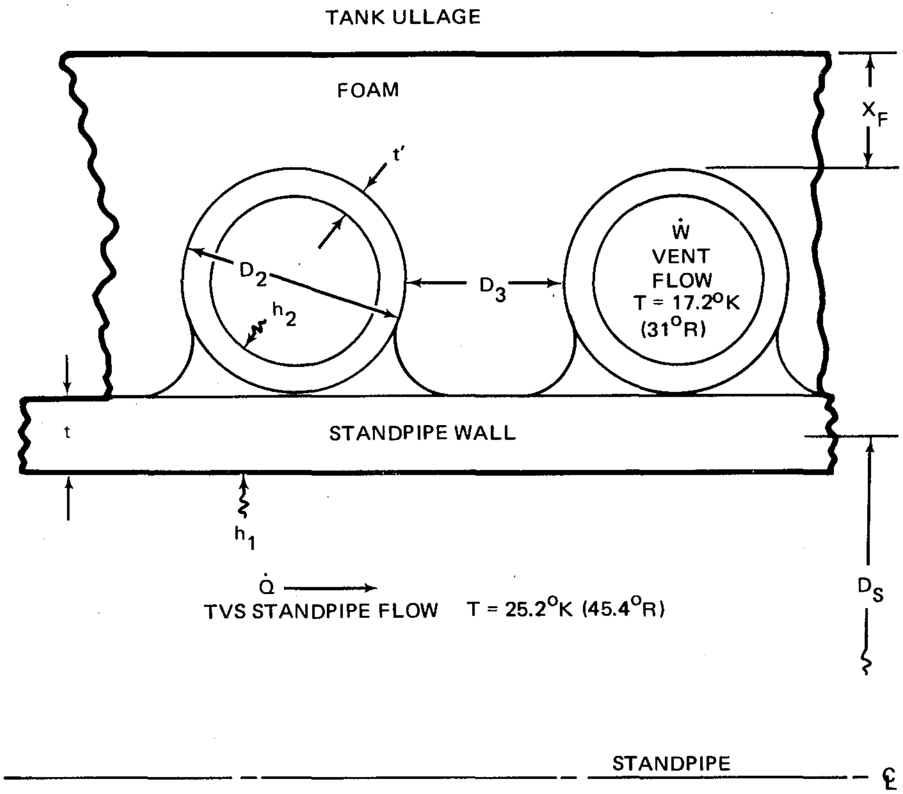

Figure 104. TVS Heat Exchanger Nomenclature

where $\dot{Q}$ is the TVS flowrate in m^3/sec, D_s is the standpipe diameter in m, and h_1 is in Joule/m^2-sec-°K with LH_2 properties evaluated at 29.2° K. Inside the heat exchanger tubing the heat transfer coefficient, h_2, is also governed by forced convection because of the vent flow, and the same equation applies:

$$\frac{h_2 D_{TUBE}}{K} = 0.023 \left(\frac{4\dot{W}}{\pi \mu D_{TUBE}}\right)^{0.8} Pr^{0.33} \qquad \text{(G-10)}$$

where $\dot{W}$ is the vent flow in kg/sec, D_{TUBE} is the heat exchanger tube diameter in m and h_2 is in Joules/m^2-sec-°K with LH_2 properties evaluated at a film temperature of 21.1° K.

Referring to Figure 104, assume that the tubing is spaced 0.318 cm (1/8 inch) apart, and only the half of the heat exchanger tubing in contact with the TVS flow is used for heat transfer to the flow in the tubing. The outside of the heat exchanger will be insulated with foam insulation to prevent condensation from the tank ullage which could use up all of the cooling capacity of the vent fluid. The foam insulation thickness will be sized to limit the condensing heat transfer from the ullage to 10% of that from the TVS flow. The heat flux required is that which will boil the vent flow, and equating this heat flux to the overall heat transfer coefficient, including the standpipe wall and tube resistance, K/X, gives:

$$(1.1)\ \dot{W}\ (449.000\ \text{Joules/kg}) = \frac{L\,(T_{H_2} - T_{HEX})}{\dfrac{1}{h_1 D_2} + \dfrac{X}{KD_2} + \dfrac{1}{h_2\ \pi(D_2-2t)/2}} \qquad \text{(G-11)}$$

where

$$X = \frac{(t + D_2/2)\ D_2}{D_2} - \frac{\pi(D_2 - 2t')^2}{8\ D_2}$$

or the heat exchanger length, L, is,

$$L = \frac{\dot{W}(449,000)\ (1.1)}{\left(T_{H_2} - T_{HEX}\right)} \left[\frac{1}{h_1 D_2} + \frac{(t + D_2/2 - \pi(D_2 - 2t')^2/8D_2}{K\ D_2} + \frac{2}{h_2\ \pi(D_2 - 2t)}\right] \qquad \text{(G-12)}$$

To minimize L, the smallest practical value of D_2 (tube diameter) should be used; however, the tube must be large enough to give a maximum pressure drop of about 1.38 N/cm^2 (2 psi) at the vent flow $\dot{W}$. The value of 1.38 N/cm^2 (2 psi) was chosen because it is assumed that the vent flow is expanded to T_{HEX} = 17.2 K (31° R), (T_{H2} = 25.2°K (45.4° R)) at 3.45 N/cm^2 (5 psia). With a pressure drop in the tube of only 1.38 N/cm^2 (2 psi), the vent flow will exit the system at about 2.07 N/cm^2 (3 psia), which is enough above the LH_2 triple-point pressure of 0.69 N/cm^2 (1 psia) to preclude premature freezing of the vent flow upon expansion to space.

The pressure drop in the tube is

$$\Delta P = f \frac{L}{D_2} \frac{\dot{W}^2}{2\ \rho g_c(\frac{\pi}{4} D_2{}^2)^2} \qquad \text{(G-13)}$$

The friction factor, f, can be evaluated for turbulent flow in a smooth tube from the Blasius correlation

$$f = \frac{0.316}{R^{0.25}} \tag{G-14}$$

where the Reynolds number, R, is that evaluated for the vent flow in equation (G-10)

The foam insulation thickness, X_F, can be determined from the heat flux criteria described above, and the equation:

$$0.1\,(\dot{W})\,449,000 = \frac{L\,(T_T - T_{HEX})}{\dfrac{X_F}{K_F\,(D_2 + D_3)} + \dfrac{2}{h_2\,\pi(D_2 - 2t')}} \tag{G-15}$$

The heat exchanger weight is found from:

$$W_{HEX} = \left[L\,D_2\,\pi\,t' + \left(\frac{D_2^{\,2}}{2} - \frac{\pi D_2^{\,2}}{8} \right) 2 \right] \rho_{HEX} \tag{G-16}$$

The heat exchanger length, tube diameter, weight, foam thickness and foam weight for each of the six tanks are shown in Table XIV. Since the thickness for the foam is too small for practical fabrication, 1.27-cm (1/2-inch) of foam was arbitrarily used. The foam weight shown is for the 1.27 cm (1/2-inch) thickness.

TABLE XIV. - TVS HEAT EXCHANGER DESIGN PARAMETERS

Tank ID	Tube diameter, cm (in.)	Tube wall thickness, cm (in.)	Tube length, m (ft)	Heat exchanger weight, kg (lb)	Foam thickness, [a] cm (in)	Foam weight [b], kg (lb)
5,000/4	0.635 (0.25)	0.0508 (0.02)	6.9 (22.6)	0.577 (1.275)	0.104 (0.041)	0.0385 (0.085)
500/4	0.318 (0.125)	0.0305 (0.012)	2.59 (8.5)	0.066 (0.145)	0.094 (0.037)	0.0109 (0.024)
500/2	0.318 (0.125)	0.0305 (0.012)	2.44 (8.0)	0.063 (0.140)	0.107 (0.042)	0.0104 (0.023)
500/1	0.318 (0.125)	0.0305 (0.012)	2.38 (7.8)	0.061 (0.135)	0.114 (0.045)	0.01 (0.022)
50/2	0.16 (0.063)	0.0152 (0.006)	0.915 (3.0)	0.00425 (0.0094)	0.140 (0.055)	0.00385 (0.0085)
50/1	0.16 (0.063)	0.0152 (0.006)	0.885 (2.9)	0.0040 (0.0089)	0.145 (0.057)	0.0037 (0.0082)

[a]Based on 10% of design heat flux through foam

[b]Based on 1.27-cm (0.5 in.) thickness

REFERENCES

1. K. L. Abdalla, et al: Liquid Transfer Demonstration On Board Apollo 14 During Transearth Coast, NASA TM X-2410, November 1971.

2. W. H. Sterbentz: Liquid Propellant Thermal Conditioning System. LMSC K-07-68-2, Lockheed Missiles and Space Company, NASA CR-72365, August 1968.

3. J. A. Stark and J. H. Blatt: Cryogenic Zero-Gravity Prototype Vent System. General Dynamics/Convair Report GDC-DD867-006, October 1967.

4. McDonnell Douglas Astronautics Company: Thermo and Hydrodynamic Experiment Research Module In-orbit. Final Report NAS 8-18053, MDAC 60594, March 1967.

5. W. C. Reynolds: Hydrodynamic Considerations for the Design of Systems for Very Low Gravity Environments. Technical Report LG-1, Stanford University, September 1961.

6. R. J. Corruccini: Surface Tensions of Normal and Para Hydrogen. NBS Technical Note 322, August 1965.

7. H. M. Roder and R. J. Goodwin: Extended Tables of Provisional Thermodynamic Functions of Para Hydrogen (British Units). NBS Report 7220, January 1962.

8. J. N. Castle: Cryogenic Bubble Point Testing of Selected Screens. MDAC Report MDC G2389, August 1971.

9. M. P. Hollister: Propellant Containment Utilizing Screen Mesh and Perforated Plate Surfaces. LMSC Report A665481, December 1964.

10. J. C. Armour and J. N. Cannon: Fluid Flow Through Woven Screens. AIChE Journal, May 1968, pp 415-420.

11. McDonnell Douglas Astronautics Company: Integration of Thermodynamic Vent and Screen Baffle for Orbital Storage and Transfer of Liquid Hydrogen, Volume 1, Technical Proposal, MDAC Report MDC G2916P, April 1972.

12. G. W. Burge: Study and Design of a Cryogenic Propellant Acquisition System. Third Quarterly Report, MDAC Report MDC G2940, 15 April 1972.

13. Kressilk Products: Metal Filter Cloth Technical and Performance Data, 23 June 1969.

14. Wintec Corporation: Cryogenic Fuel Filter Study, Contract NAS9-11264. Monthly Progress Report, March 1972.

15. General Dynamics Corporation: Low Gravity Propellant Control Using Capillary Devices in Large Scale Cryogenic Vehicles. Related IRAD Studies, General Dynamics/Convair Report GDC-DDB70-009, August 1970.

16. J. N. Castle: Viscous Flow Losses Associated with Wire Cloth Surface Tension Devices. MDAC Report DAC-62350, July 1968.

17. W. J. Hines, et al: Task 8, Capillary Acquisition and Transfer, Tests of Capillary Barrier Materials. North American Rockwell Internal Letter No. SII-193-603-71-093, 24 September 1971.

18. G. W. Burge: Study and Design of a Cryogenic Propellant Acquisition System. Fourth Quarterly Report, MDAC Report MDC G3695, 15 July 1972.

19. P. G. Morgan : Fluid Flow Through Screens of Low Solidity. Journal of the Royal Aeronautical Society, Volume 66, p. 54.

20. L. F. Moody: Friction Factors for Pipe Flow. ASME Transactions, Vol. 66, pp. 671-678, November 1944.

21. F. J. Edwards and N. Sheriff: The Heat Transfer and Friction Characteristics for Forced Convection Air Flow Over a Particular Type of Rough Surface. International Developments in Heat Transfer, ASME, 1961-62, pp. 415-425.

22. E. R. G. Eckert and T. F. Irvine: Incompressible Friction Factor, Transition and Hydrodynamic Entrance Length Studies of Ducts with Triangular and Rectangular Cross-Sections. WADC Technical Report 58-85 (ASTIA Document No. AD151027) April 1957.

23. H. Schlichting: Boundary Layer Theory, McGraw-Hill Book Company, 1960.

24. H. Blasius: The Law of Similarity Applied to Friction Phenomena. (German) Physik Zeit, Vol. 12, p. 1175, (1911).

25. L. J. Poth, et al: A Study of Cryogenic Propellant Mixing Techniques General Dynamics Report FZA-439-1, Final Report, Vol. 1, 1 Nov 1968.

26. G. H. Caine and A. V. Pradhan: Pumps or Fans for Destratification of Hydrogen Liquid and Gas. Advances in Cryogenic Engineering, Vol. 13, p. 728, Plenum Press, New York, 1968.

27. R. B. Bird, W. E. Stewart, and E. N. Lightfoot; Transport Phenomena. John Wiley and Sons, New York, 1960, p. 117.

28. G. O. Frederickson: Investigation of High Performance Insulation Application Problems. Final Report, MDC G4727, August 1973.

DISTRIBUTION LIST FOR FINAL REPORT - NAS3-15846

Name	No. of Copies
National Aeronautics & Space Administration Lewis Research Center 21000 Brookpark Road Cleveland, OH 44135	
Attn: J. Lerner, MS 500-313	1
E. A. Bourke, MS 500-205	5
Technical Utilization Office, MS 3-19	1
Technical Report Control Office, MS 5-5	1
AFSC Liaison Office, MS 501-3	2
Library, MS 60-3	2
Office of Reliability & Quality Assurance, MS 500-211	1
N. T. Musial, MS 500-113	1
J. C. Aydelott, Project Manager, MS 500-204	50
National Aeronautics & Space Administration Headquarters Washington, DC 20546	
Attn: RS/Director, Manned Space Technology	1
RP/Director, Space Propulsion & Power	1
KT/Director, Technology Utilization Division	1
National Aeronautics & Space Administration Ames Research Center Moffett Field, CA 94035	
Attn: Library	1
National Aeronautics & Space Administration Goddard Space Flight Center Greenbelt, MD 20771	
Attn: Library	1
National Aeronautics & Space Administration John F. Kennedy Space Center Cocoa Beach, FL 32931	
Attn: Library	1
DD-MDD-43/F. S. Howard	1
DD-SED-4/ W. H. Boggs	1

Name	No. of Copies
National Aeronautics & Space Administration Langley Research Center Hampton, VA 23365 Attn: Library	1
National Aeronautics & Space Administration Johnson Space Center Houston, TX 77001 Attn: Library	1
EP2/Z. D. Kirkland	1
National Aeronautics & Space Administration George C. Marshall Space Flight Center Huntsville, AL 35812 Attn: Library	1
ASTN-PF/A. L. Worlund	1
S&E-ASTN-PFA/L. Hastings	1
Jet Propulsion Laboratory 4800 Oak Grove Drive Pasadena, CA 91103 Attn: Library	1
NASA Scientific and Technical Information Facility P. O. Box 33 College Park, MD 20740 ATTN: NASA Representative	10
Defense Documentation Center Cameron Station - Bldg. 5 5010 Duke Street Alexandria, VA 22314 Attn: TISIA	1
National Aeronautics & Space Administration Flight Research Center P. O. Box 273 Edwards, CA 93523 Attn: Library	1

Name	No. of Copies
Aeronautical Systems Division Air Force Systems Command Wright-Patterson Air Force Base Dayton, OH Attn: Library	1
Air Force Office of Scientific Research Washington, DC 20333 Attn: Library	1
Aerospace Corporation 2400 E. El Segundo Blvd. Los Angeles, CA 90045 Attn: Library - Documents	1
Arthur D. Little, Inc. 20 Acorn Park Cambridge, MA 02140 Attn: Library	1
Beech Aircraft Corporation Boulder Facility Box 631 Boulder, CO Attn: Library	1
Bell Aerosystems, Inc. Box 1 Buffalo, NY 14240 Attn: Library	1
Boeing Company Space Division P. O. Box 868 Seattle, WA 98124 Attn: Library	1
Chrysler Corporation Space Division P. O. Box 29200 New Orleans, LA 70129 Attn: Library	1

Name	No. of Copies
General Dynamics/Convair P. O. Box 1128 San Diego, CA 92112 Attn: Library	1
R. Tatro	1
Missiles and Space Systems Center General Electric Company Valley Forge Space Technology Center P. O. Box 8555 Philadelphia, PA 19101 Attn: Library	1
Grumman Aircraft Engineering Corporation Bethpage, Long Island, NY Attn: Library	1
IIT Research Institute Technology Center Chicago, IL 60616 Attn: Library	1
Lockheed Missiles and Space Company P. O. Box 504 Sunnyvale, CA 94087 Attn: Library	1
G. D. Bizzell	1
Linde, Division of Union Carbide P. O. Box 44 Tonawanda, NY 11450 Attn: G. Nies	1
Denver Division Martin-Marietta Corporation P. O. Box 179 Denver, CO 80201 Attn: Library	1
H. L. Paynter	1
Space & Information Systems Division North American Rockwell 12214 Lakewood Blvd. Downey, CA Attn: Library	1
D. Gluck	1

5

Name	No. of Copies
Northrop Space Laboratories 3401 West Broadway Hawthorne, CA Attn: Library	1
TRW Systems, Inc. 1 Space Park Redondo Beach, CA 90278 Attn: Tech. Lib. Doc. Acquisitions	1
National Science Foundation, Engr. Div. 1800 G. Street, N.W. Washington, DC 20540 Attn: Library	1
Florida Institute of Technology Space Technology Dept. Melbourne, FL 32901 Attn: Dr. T. E. Bowman	1
Heat Transfer & Thermodynamic Laboratory University of Michigan Ann Arbor, MI 48107 Attn: Dr. John A. Clark	1
Dr. Edward B. Igenbergs 8000 Muchen 80 Rauchstrasse 3 Germany	1
Office National D'Etudes Et De Recherches Aerospatiales 29, Avenue de la Division LeClerc 92 Chatillon France Par Jean Maulard Michel Delattre	 1 1
RCA/AED P. O. Box 800 Princeton, NJ 08540 Attn: Mr. Daniel Balzer	1
4043 Cody Road Sherman Oaks, CA 91403 Attn: Dr. Marvin Adelberg	1

Name	No. of Copies
Southwest Research Institute Dept. of Mechanical Sciences P. O. Drawer 28510 San Antonio, TX 78284 Attn: H. Norman Abramson	1
Tufts University Mechanical Engineering Dept. Medford, MA 02155 Attn: Dr. Lloyd Trefethen	1
University of Tennessee Knoxville, TN 37916 Dept. of Mechanical & Aerospace Engineering Attn: Franklin T. Dodge	1